HYPOGENE KARST AND SUFLATE DIAGENESIS OF THE DELAWARE BASIN: SOUTHEASTERN NEW MEXICO AND FAR WEST TEXAS

By

Kevin Wayne Stafford

A dissertation
submitted to the faculty of
New Mexico Institute of Mining and Technology
in partial fulfillment of the requirements
for the Degree of Doctorate of Philosophy
in Geology
in the Department of Earth and Environmental Science

Socorro, New Mexico

May 2008

ABSTRACT

Hypogene speleogenesis is widespread throughout the Delaware Basin region as evidenced by intrastratal dissolution, hypogenic caves and suites of diagenetic minerals. The world famous carbonate caves of the Capitan reef facies of the Guadalupe Mountains have long been associated with sulfuric acid processes and recently have been associated with semi-confined, hypogene dissolution. However, evaporite karst within Permian backreef and basin-filling facies has been traditionally associated with surficial, epigene processes. On the eastern edge of the Delaware Basin cavernous porosity associated with oil reservoirs in Permian carbonates have been attributed to eogenetic karst processes.

Interbedded (evaporite / carbonate), backreef facies within the Seven Rivers Formation exhibit characteristics of hypogene dissolution associated with semi-confined dissolution controlled by the eastward migration and entrenchment of the Pecos River. Coffee Caves is a classic example of hypogene dissolution, forming a multi-storey, rectilinear maze with abundant morphologic features suites (i.e. risers, channels and cupolas) indicative of hypogene speleogenesis. Other caves within the Seven Rivers and Rustler Formations show similar patterns, yet often less developed.

Within the Delaware Basin, Castile Formation evaporites have been extensively modified by hypogene processes. Field mapping coupled with GIS analyses clearly shows karst development and evaporite calcitization are highly clustered throughout the

outcrop area. Individual caves commonly exhibit complex morphologies, including complete suites of morphologic features indicative of intrastratal dissolution. Clusters of hypogene caves are commonly associated with clusters of evaporite calcitization and often occurrences of secondary selenite bodies, suggesting all three are genetically related. Brecciated cores and associated native sulfur deposits indicate that calcitized occurrences are the result of semi-confined sulfate reduction in the presence of ascending hydrocarbons. Hypogene caves are currently being overprinted by epigene processes as surface denudation results in breaching of previously confined solutional conduits. However, castile buttes stand as resistant masses attesting to the widespread importance of hypogene processes within the Castile Formation.

On the Central Basin Platforms southern end, the spatial distribution of cavernous porosity, secondary mineralization and abundant karst fabrics within the carbonate strata of the Yates Field all provide convincing evidence that karst porosity, at least locally, within the San Andres and overlying Permian strata is the result of hypogene speleogenesis. Porosity development appears to have been enhanced by high geothermal gradients and the addition of sulfuric acid-rich fluids, reminiscent of the same processes that have been recently proposed for the extensive carbonate caves of the Guadalupe Mountains.

Recognition of the widespread occurrence of hypogene speleogenesis throughout the Delaware Basin region indicates that the regional diagenetic evolution has been significantly affected by confined fluid migration, including not only the development of porosity but also the emplacement of many secondary mineral deposits. This indicates that future natural resource management plans must consider the nature of hypogene karst

in site evaluations throughout the region in order to better predict geohazards, potential groundwater contamination and characterize mineral resources.

ACKNOWLEDGEMENTS

This author expresses his gratitude to the many people who have provided support and assistance through the course of this project. This project would not have been possible without the support of funding agencies. This includes grants from the American Association of Petroleum Geologist (Mimi Atwater Memorial Grant), Geological Society of America, New Mexico Geological Society and New Mexico Tech Graduate Student Association. Special thanks to the National Cave and Karst Research Institute for scholarship support for my graduate studies.

Thanks to all of the private land owners and ranchers in Texas that provided gracious access to their land throughout this study, including: Jack Blake, Draper Brantley, Stanley Jobe, Lane Sumner, and Clay Taylor.

Thanks to all of the individuals that assisted with fieldwork and the mapping of caves within the study area, including: Goshia Allison, Stan Allison, Paul Burger, Megan Curry, Jon Jasper, Jim Kennedy, Lucas Middleton, Laura Rosales-Lagarde, Charley Savvas, Pat Seiser, Bev Shade and Vickie Siegel.

Thanks to the Carlsbad Bureau of Land Management for their assistance with research within New Mexico, specifically the assistance of Dave Belski, Jim Goodbar, and Jon Jasper.

Thanks to Tim Hunt for his assistance and land access to University of Texas Lands within the study area.

Thanks to fellow graduate students Megan Curry and Laura Rosales-Lagarde for the many productive discussions we had over the course of our graduate studies.

Thanks to Gary Axen, Bruce Harrison, Lewis Land and Dana Ulmer-Scholle for their useful guidance and support throughout this project as committee members.

Thanks specifically to my advisor Penny Boston for her continued support of my research even though it falls outside of her primary fields of study. She has helped expand my realm of interests beyond purely terrestrial pursuits, opening up new avenues of research.

Special thanks to Ray Nance and Alexander Klimchouk. Ray Nance provided invaluable support throughout this research as we discussed ideas on countless trips to the field. Alexander Klimchouk of the Ukrainian Institute of Speleology provided invaluable mentoring throughout this project, fueling my interest in hypogene processes.

TABLE OF CONTENTS

Page

Page

Page

LIST OF FIGURES

Page

LIST OF TABLES

This dissertation is accepted on behalf of the
Faculty of the Institute by the following committee:

Advisor (Penelope Boston)

Gary Axen

Bruce Harrison

Lewis Land

Dana Ulmer-Scholle

Date

I release this document to the New Mexico Institute of Mining and Technology.

Student's Signature Date

PREFACE

Chapters II through VII of this dissertation are individual manuscripts which have been submitted for publication. Currently, chapters II through V have been accepted for publication.

Chapter II (Evaporite Speleogenesis of the Gypsum Plain: New Mexico and Far West Texas) is a requested manuscript that will be published in "The Caves and Karst of the USA" edited by Art and Peggy Palmer, which was co-authored by Ray Nance.

Chapter III (Hypogenic Speleogenesis within Seven Rivers Evaporites: Coffee Cave, Eddy County, New Mexico) was co-authored by Alexander Klimchouk and Lewis Land and was published in the December 2007 issue of the Journal of Cave and Karst Studies.

Chapter IV (Castile Evaporite Karst Potential Map of the Gypsum Plain, Eddy County, New Mexico and Culberson County, Texas: a GIS Methodological Comparison) was co-authored by Penny Boston and Laura Rosales-Lagarde was published in the December 2007 issue of the Journal of Cave and Karst Studies.

Chapter V (Gypsum karst manifestations of the Castile Formation: Eddy County, New Mexico and Culberson County, Texas, USA) was co-authored by Ray Nance, Laura Rosales-Lagarde and Penny Boston and has been accepted for publication in the International Journal of Speleology in 2008.

Chapter VI (Hypogene speleogenetic calcitization: Castile Buttes in the Western Delaware Basin) was co-authored by Dana Ulmer-Scholle and Laura Rosales-Lagarde and was submitted for publication in the Journal of Sedimentary Research in February 2008.

Chapter VII (New insights into Yates Field reservoir characterization: Hypogenetic cavernous porosity instead of eogenetic cavernous porosity) was co-authored by Fred Behnken, Alexander Klimchouk and Dana Ulmer-Scholle and was submitted for publication in American Association of Petroleum Geologists Bulletin in February 2008.

CHAPTER I:
INTRODUCTION

Cave and karst development within the greater Delaware Basin region of southeastern New Mexico and far west Texas (Fig. I.1) is widespread and diverse. Kunath and Smith (1968), Eaton (1987), Belski (1992), Elliott and Veni (1994), and Lee (1996) have documented numerous individual caves developed within gypsum facies in the area, but they did not attempt to characterize speleogenesis. Within the Guadalupe Mountains, numerous caves have been documented within the carbonate reef and back-reef facies that define the margins of the Delaware Basin (Hose and Pisarowicz, 2000). Hill (1990) concluded that these caves were formed in association with a falling water table in the presence of sulfuric acid waters. Recent advances in cave and karst research have shown that cavernous porosity within the Guadalupe Mountains is not associated with specific water table horizons, but instead is associated with rising fluids in a semi-confined system (Palmer, 2006; Klimchouk, 2007).

This study focuses largely on gypsum karst phenomenon within the Delaware Basin because speleogenesis within the evaporite facies of the region is poorly understood. Much of this study is specifically devoted to speleogenesis within the Castile Formation, because these strata are bounded within the Delaware Basin and therefore have been subjected to the same depositional, tectonic and diagenetic regimes. Throughout this

study, the evolution of cave and karst systems is evaluated and the implications of findings to the greater regions are discussed.

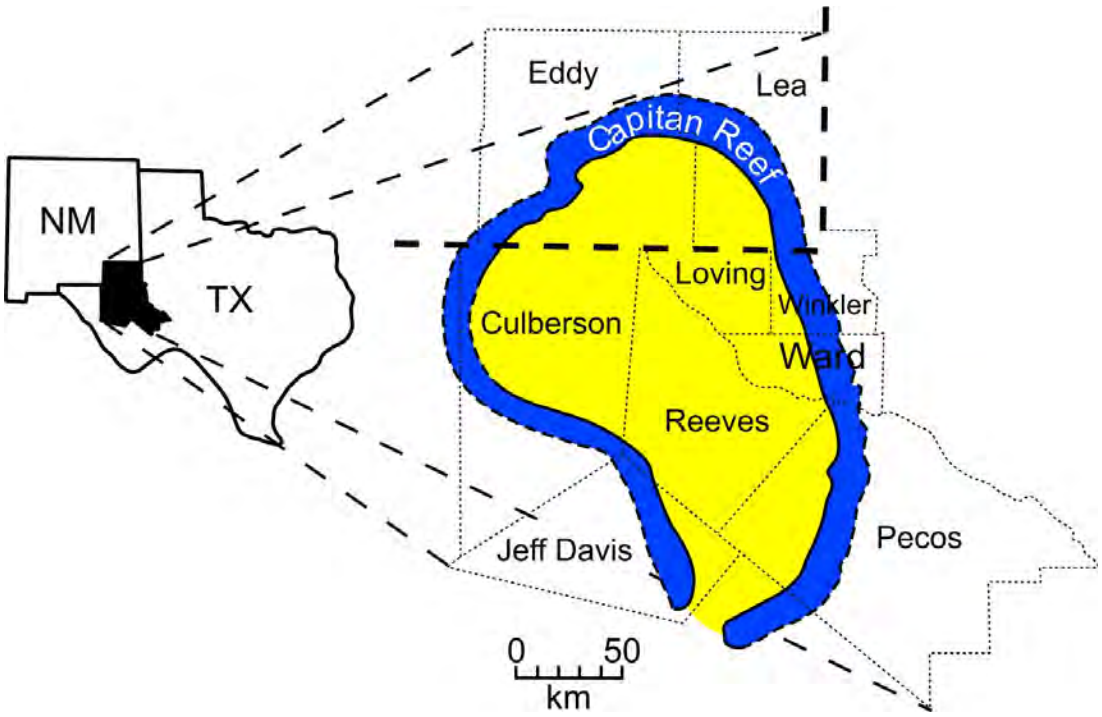

Fig. I.1. Map showing location of the Delaware Basin and extent of the Capitan Reef (blue) that defines the boundary of the basin (adapted from Hill, 1996).

DELAWARE BASIN

The Delaware Basin is located in southeastern New Mexico and west Texas, covers an area of ~33,500 km^2 (Hill, 1996) and represents one of the deepest intracratonic basins within the United States (Garber et al., 1989). Stratigraphic units within the Delaware Basin have been identified from the Precambrian to the present; however, 95% of the units exposed within the basin were formed in the Permian, including the Castile Formation (Kelley, 1971). The basin is delineated by the Permian Capitan Reef complex that forms a narrow carbonate belt 600 to 700 km long around the periphery of the basin (Fig. I.1), which crops out in the Guadalupe, Glass and Apache Mountains (Hill, 1996).

The Delaware Basin was part of the larger Tobosa Basin which formed in the latest Precambrian and lasted until the Late Mississippian with continuous deposition for almost 300 million years (Hill, 1996). No significant structural deformation occurred during this time, but slow subsidence allowed for the accumulation of thousands of meters of shallow platform sediments (Horak, 1985). This period of tectonic quiescence and constant deposition was interrupted by the major collision of Laurasia and Gondwana (Keller et al., 1980).

During the late Mississippian and early Pennsylvanian, collision of the North American and South American-African plates produced the Ouachita Orogeny and block faulting in the Tobosa Basin that separated it into the Delaware Basin, Central Basin Platform and Midland Basin (Fig. I.2) (Horak, 1985). Continued collision in the Pennsylvanian produced significant subsidence of the Delaware Basin that was further enhanced by high sediment loads, causing greater separation from the basin and Central Basin Platform (Hill, 1996). The collision phase continued throughout Wolfcampian time (~295-280 mya) of the Permian but had essentially ended by the beginning of Leonardian time (~280-270 mya) (Hill, 1996).

Beginning in the Leonardian and continuing into the Ochoan (~258-250 mya), the Delaware Basin entered a time of tectonic stability with continued subsidence from sediment load, resulting in ~3-5 km of sediment deposition in the basin and ~2 km of accumulation on the basin shelf (King, 1942). During this time, extensive deposits developed in the Delaware Basin, including sandstones, siltstones, evaporites and

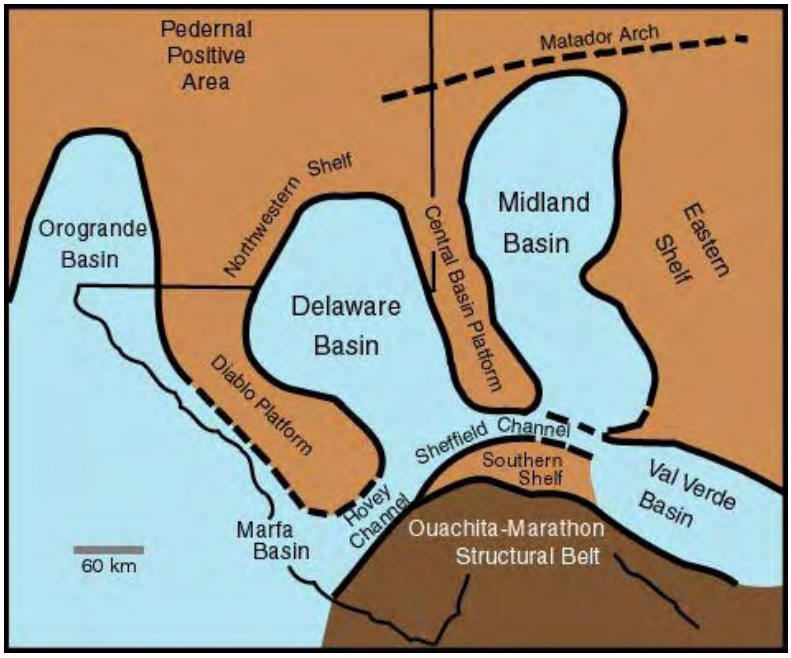

Fig. I.2. Map showing the configuration of the Delaware Basin, Midland Basin and Central Basin Platform during Guadalupian time (~270-259 mya) (from Scholle et al., 2004).

limestones of basinal, backreef and reef origin. However, toward the end of the Permian, during Ochoan time, the Hovey Channel that had once connected the Delaware Basin to open marine circulation closed (Adams, 1972). As a result of closing of the Hovey Channel, deposition in the basin switched from carbonate dominated sedimentation to evaporite sedimentation, which included the deposition of the Castile Formation, the unit of emphasis in this study, during the beginning of the Ochoan (Anderson et al., 1972). By the late Ochoan, differential uplift resulted in tilting of strata to the east (Hills, 1970).

In the early Triassic, during the final assemblage of Pangea, the Delaware Basin region was uplifted above sea level and throughout the Mesozoic the region was dominated by erosion and fluvial sedimentation (Dickenson, 1981). Near the end of the Cretaceous, the Laramide Orogeny began as the Farallon and North American Plates

collided (Dickenson, 1981). In the Delaware Basin this orogenic event produced up to 1.2 km of uplift, regional tilting to the east and broad anticlinal flexures (Horak, 1985). By the mid-Tertiary, the Laramide Orogeny had ceased with the development of volcanism that shifted Laramide compression to Basin and Range extension (Chapin and Cather, 1994).

In the late Oligocene to early Miocene, Basin and Range block-faulting resulted in the downdrop of the far western margin of the Delaware Basin which produced the Salt Basin and N-NW fracturing within the basin (Horak, 1985). From early Miocene to Pliocene, uplift dominated the region and a shift from N-NW extension to N-NE extension occurred, producing graben features within the basin (Hentz and Henry, 1989). By the Quaternary, Basin and Range extension decreased substantially.

SPELEOGENESIS

Speleogenesis can be subdived into three basic types, which are closely related to the diagenesis of soluble rocks (Fig. I.3): 1) syngenetic karst, 2) hypogenic karst, and 3) epigenic karst. While speleogenesis is commonly associated with cave development, it is more generally associated with the total porosity evolution within soluble rocks throughout eogenesis, mesogenesis and telogenesis.

Syngenetic karst, often referred to as island karst or eogenetic karst, forms penecontemporaneously with deposition in rocks that have not been removed from the effects of meteoric processes and retain there depositional porosity and permeability (Ford and Williams, 2007; Palmer, 2007). Syngenetic karst in evaporite rocks is generally limited to surficial karren development and ephemeral bypass caves that connect horizons

of differing elevation over short distances (Klimchouk, 2003; Yauro and Cooper, 1996). In carbonate settings, syngenetic karst is largely associated with the development of a freshwater lens in coastal and island settings (Mylroie and Carew, 1995). Dissolution is enhanced at the boundaries of the freshwater lens through the interaction of fresh and salt waters and the decay of organics trapped at density horizons.

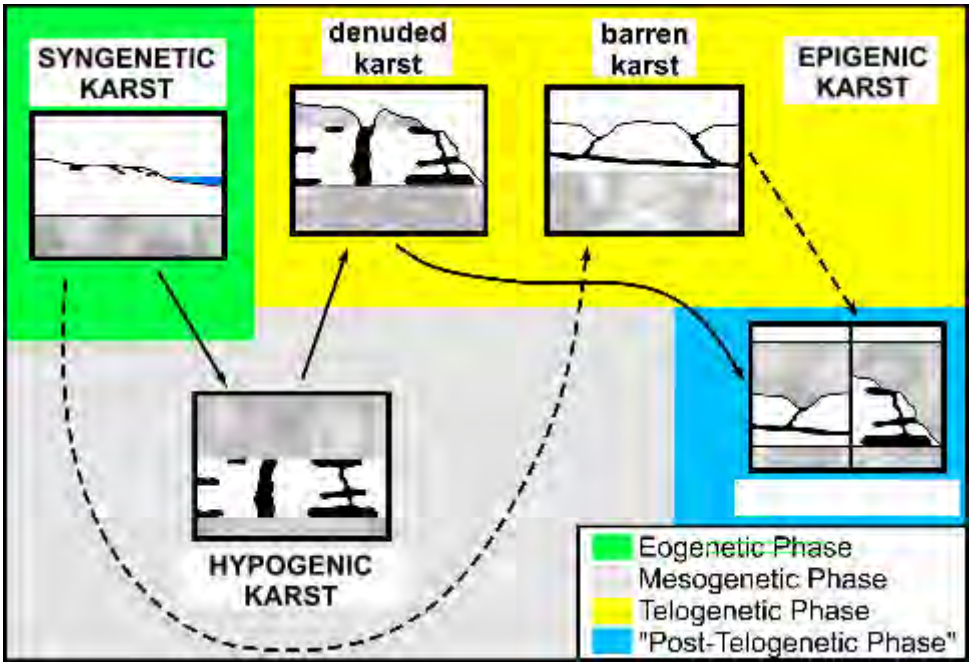

Fig. I.3. Speleogenesis in relation to burial diagenesis (adapted from Klimchouk, 1996).

Hypogenic or intrastratal karst forms as soluble rocks are removed from the direct effects of meteoric waters as strata are buried and compacted during mesogenesis (Ford and Williams, 2007). The development of hypogenic karst continues through mesogenesis and into the early stages of telogenesis as rocks are uplifted and exposed again to meteoric processes. Hypogene karst forms through the migration of soluble fluids within confined or semi-confined systems, such that dissolution is non-competitive but instead exploits all bedrock heterogeneities (Klimchouk, 2007). Hypogene systems

are characterized by mixed convection (free and forced) dissolution, where solutionally aggressive fluids are continuously delivered to the dissolution front because of density gradients associated with steep thermal or solute gradients (Tóth, 1999). Hypogene karst is often well developed in evaporite facies because the high solubilities of evaporite rocks (Klimchouk, 2000c), but is also extremely common in carbonate facies especially in regions were solutional agressivity is increased by the addition of sulfuric acids (Dublyansky, 2000).

Epigenic karst forms as soluble strata are returned to the earth surface and are once again exposed to the direct effects of meteoric processes (Palmer, 2007). Epigene karst commonly forms dendritic or branchwork cave systems reminiscent of surficial patterns formed by fluvial processes (Palmer, 1991). In the unsaturated zone, vadose karst development is driven by gravity as water attempts to reach the regional hydrologic base level through the most efficient path possible, which results in the convergence of cave passages with depth (Ford et al., 2006). In the saturated zone, phreatic karst development is driven by hydraulic potential groundwater attempts to discharge to the regional base level, generally a regional river or basin. As an open system, epigene karst responds rapidly to seasonal variations such that the boundary between the vadose and phreatic zones is constantly evolving in relation to changes in local base level (Palmer, 1991).

Speleogenesis includes the complete evolution of porosity throughout diagenesis. Therefore, porosity development in early diagenetic stages can be inherited in later stages, such that complex speleogenetic systems form as a result of subsequent overprinting of multiple episodes of dissolution.

CALCIUM SULFATE DIAGENESIS

Calcium sulfate rocks can be deposited in a wide range of depositional environments and may exhibit a complex diagenetic history as units pass through the primary stages of burial diagenesis: eogenetic (i.e. rocks have not been buried beyond the range of meteoric diagenesis), mesogenetic (i.e. rocks have undergone compaction and cementation associated with burial diagenesis) and telogenetic (i.e. rocks have undergone burial diagenesis and re-exposed to meteoric diagenesis near the Earth surface through uplift and/or surface denudation) (Fig. I.4) (Choquette and Pray, 1970). Gypsum and anhydrite are the hydrated and dehydrated forms of calcium sulfate respectively and represent reversible phases ($CaSO_4 \cdot 2H_20 \leftrightarrow CaSO_4 + 2H_2O$) (Klimchouk and Andrejchuk, 1996). Calcium sulfate rocks can exhibit a wide range of fabric textures, including: sucrosic, laminated, nodular, fibrous, radiate, and powdered (Machel and Burton, 1991; Demicco and Hardie, 1994).

In modern settings, primary deposits of calcium sulfate are generally associated with subaerial evaporation of marine brines in sabkha deposits or form subaqueously by the evaporation of inland basins in lagoon and salina deposits (Warren and Kendall, 1985). Continental settings may exhibit a combination of both subaerial and subaqueous deposition with layered composition resulting from variations in regional sediment source and precipitation (Selly, 1988). Modern examples of subaerial deposition occur throughout the Arabian Gulf, Baja California and western Australia where evaporite deposition, primarily displacive nodular masses, occurs in the shallow subsurface immediately above the water table (Schreiber et al., 1982). Modern examples of subaqueous deposition occur in evaporating basins in the Mediterranean, Mexico and

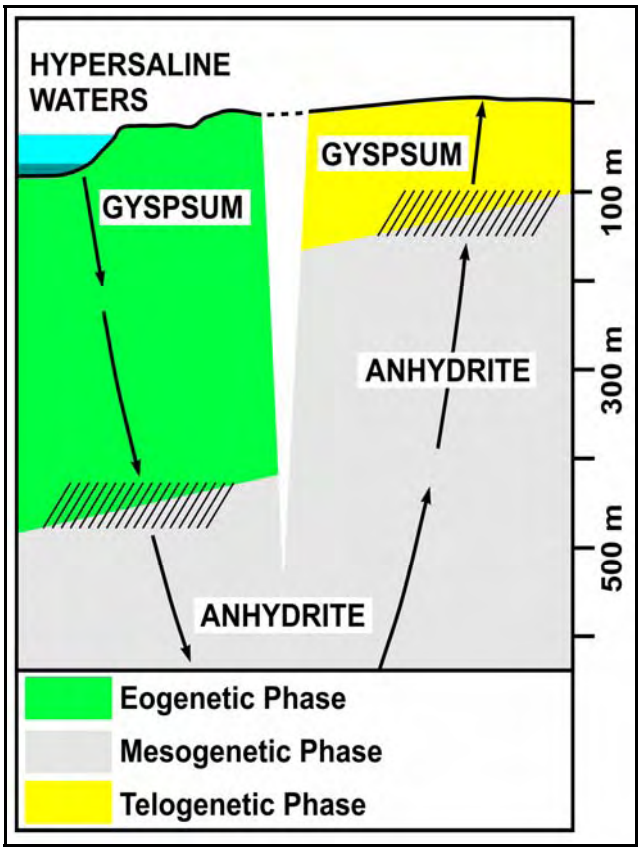

Fig. I.4. Calcium sulfate mineral conversion associated with diagenesis (modified from Murray, 1964).

Australia. In these basins, gypsum growth is primarily bottom nucleated, forming large selenite crystals that exhibit vertical aggradation; however, additional evaporite deposition can be produced by precipitation of gypsum rafts at the evaporating water surface which settle to the basin floor as their increased growth is no longer supported by surface tension (Dean and Anderson, 1982). Additionally, subaqueous gypsum deposits may exhibit laminated textures as seasonal influxes of marine or fresh water reduce the brine concentrations in the basins and promote the deposition of non-evaporite layers, usually calcium carbonates (Warren and Kendall, 1985). Continental calcium sulfate deposits have been primarily associated with intracratonic basins, often cover large areas

and were more common in the geologic past (Selly, 1988). Continental sequences frequently exhibit both subaqueous and subaerial deposition similar to modern salina and sabkha deposition, but often attain significant thicknesses and have abundant terrigenous input (Warren and Kendal, 1985).

Subsequent to deposition, calcium sulfate rocks are exposed to the effects of diagenesis, with the most common effect being mineral conversion between the hydrated and dehydrated states (Fig. I.1) (Klimchouk, 1996). Because gypsum and anhydrite have densities of 2.30 g/cm^3 and 2.98 g/cm^3 respectively, conversion results in a volume expansion / contraction of approximately 60%, which can induce structural deformation and destroy preexisting fabric textures that may only be preserved as ghost fabrics (Kasprzyk, 1995; Orti and Rosell, 2000). There is controversy over the exact mechanism of this mineral conversion, but it is believed that dehydration occurs through diffusion of water molecules from the crystal lattice while hydration occurs through the dissolution of anhydrite and precipitation of gypsum (Klimchouk, 1996). During deposition, gypsum can be dehydrated to anhydrite when surface temperatures exceed 45^{o}C, but it is usually hydrated during shallow burial where the rocks are still exposed to meteoric diagenesis (Klimchouk and Andrejchuk, 1996). As the rocks are buried, they are removed from the effects of meteoric diagenesis and exposed to higher temperatures and pressures, resulting in dehydration. The exact depth that dehydration occurs depends on the pressures and regional geothermal gradient, but Klimchouk (1996c) reports that this generally occurs at depths of 400 to 450 m. However, gypsum has been reported at depths of 1200 m (Sonnenfeld, 1984) and even below 3000 m (Ford and Williams, 2007). As anhydrite is brought back to the surface through uplift and/or surface denudation, it is

again exposed to the effects of meteoric diagenesis and lower temperatures, where hydration can occur (Klimchouk, 1996). Conservative estimates place hydration at depths of 100 to 150 m, which results in a net increase in rock volume that can induce deformation (Klimchouk, 1996), but it is possible that full expansion will not occur because of confining pressure (Zanbak and Arthur, 1986; James, 1992). Sonnenfeld (1984) found that 60-75 m of overlying rock would provide sufficient pressure to prevent full hydration. Because of the mineral conversion associated with burial diagenesis, it is believed that most calcium sulfate rocks exposed at the land surface have gone through several episodes of dehydration and rehydration (Klimchouk, 1996).

Evaporite rocks are known to undergo significant brittle and ductile deformation with ease (Schreiber et al., 1982). Brittle deformation can be the result of normal tectonic deformation or induced by mineral conversion in calcium sulfates. Tectonic deformation produces normal structural features such as faults, fractures and joints as might be observed in any sedimentary rock (Schreiber et al., 1982); however, hydration and dehydration can produce endokinetic fissuring as a result of rock expansion / contraction (Klimchouk and Andrejchuk, 1996). Endokinetic fissuring generally produces homogenously distributed, polygonal networks that are often limited to adjoining bedding planes, which differs from tectonic fissuring that usually is more isolated and generally cuts multiple bedding planes (Klimchouk and Andrejchuk, 1996). In addition to brittle deformation, calcium sulfates can deform and flow plastically when temperatures exceed 150^{o}C (Schreiber et al., 1982). In unconfined settings, calcium sulfates may even exhibit creep resulting in elastic deformation which produces swellings, waved structures and flow folding (Klimchouk and Andrejchuk, 1996).

Although solubilities of gypsum and anhydrite are very similar, the dissolution kinetics are significantly different. Molecular dissociation of gypsum is almost instantaneous and is controlled by diffusion across the boundary layer; therefore, gypsum dissolution reaches near-saturation in a short period of time depending on flow rates (Klimchouk, 1996). The dissolution of anhydrite is much slower and more uniform, because anhydrite is converted first to aqueous calcium sulfate before dissociation occurs (Klimchouk, 1996). The solubility of calcium sulfate is approximately four orders of magnitude greater than calcium carbonate in pure water (Drever, 1997). In the presence of CO_2, calcium sulfate dissolution is effectively unchanged, but calcium carbonate dissolution is greatly enhanced due to the increased acidity (i.e. the presence of carbonic acid). As a result, calcium sulfate solubility is generally only 10 to 30 times greater than calcium carbonate (Klimchouk, 1996). However, in the presence of dissolved salts, calcium sulfate solubility increases as a result of ion pairing which reduces the activity of the dissolved ions in solution (Klimchouk, 1996). Additionally, grain size and temperature can affect solubility, where smaller crystals exhibit higher solubilities and waters at 43^oC exhibit the highest solubility (Klimchouk, 1996). Dissolution of calcium sulfate can produce porosity with a wide range of scales, from moldic and vuggy porosity to cavernous porosity (Demicco and Hardie, 1994; Klimchouk, 1996).

OVERVIEW

The following chapters (II-VII) are a compilation of individual manuscripts which investigate karst phenomenon within the greater Delaware Basin, with an emphasis on evaporite karst primarily within the interior of the Delaware Basin. Throughout this work,

the widespread distribution of hypogene processes within the Delaware Basin region is illustrated and implications for the regional dominance of hypogene speleogenesis are discussed.

Chapter II provides an overview of evaporite karst within the greater region, encompassing all of New Mexico and far west Texas (Stafford and Nance, 2009). Chapter III is a detailed study on the mechanisms and characteristics of hypogene karst in the Seven Rivers Formation on the Northwestern Shelf of the Delaware Basin (Stafford et al., 2007a). Chapter IV utilizes GIS (Geographic Information Systems) to delineate the extent and distribution of karst development within the Castile Formation outcrop area in the interior of the Delaware Basin, while providing a critical evaluation of different GIS techniques used in karst studies (Stafford et al., 2007b). Chapter V investigates the diversity of karst development within the Castile Formation, including epigene and hypogene karst as it relates to the speleogenetic evolution of the Castile Formation (Stafford et al., 2008). Chapter VI evaluates the distribution and occurrence of evaporite calcitization within the Castile Formation outcrop area and details the correlation between evaporite calcitization, native sulfur occurrences, secondary selenite and hypogene karst within the region (Stafford et al., 200_a). Chapter VII evaluates karst development within the Central Basin Platform on the eastern edge of the Delaware Basin through a reevaluation of the speleogenetic origins of karst within the Yates Field Reservoir (Stafford et al., 200_b). The culminating chapter (VIII) discusses the greater significance of widespread hypogene speleogenesis within the Delaware Basin region and implication for future research.

CHAPTER II:
EVAPORITE SPELEOGENESIS OF THE GYPSUM PLAIN: NEW MEXICO AND FAR WEST TEXAS

ABSTRACT

Evaporite karst is widespread throughout New Mexico and far west Texas in strata ranging from Pennsylvanian to Quaternary age. Permian evaporite strata are the most widespread and contain the most developed cave systems within the region. Karst development within the Permian Yeso, San Andres, Seven Rivers, Castile and Rustler formation is dominated by hypogene processes, but commonly exhibit significant epigene overprinting as a result of surficial breaching. Jurassic deposits of the Todilto Formation show similar karst development, but are far less widespread. Other evaporite strata exhibit minimal karst development primarily limited to epigene processes except Quaternary deposits which develop ephermal, syngenetic karst. While evaporite karst in the region is dominated by porosity development, significant secondary mineral deposits have been documented in numerous individual caves, including gypsum stalactites, stalagmites, trays and flowers, as well as traditional calcite speleothems.

INTRODUCTION

New Mexico and Far West Texas contain the most extensive surficial exposures of evaporites in North America (Fig. II.1). Most karst development in the region occurs in

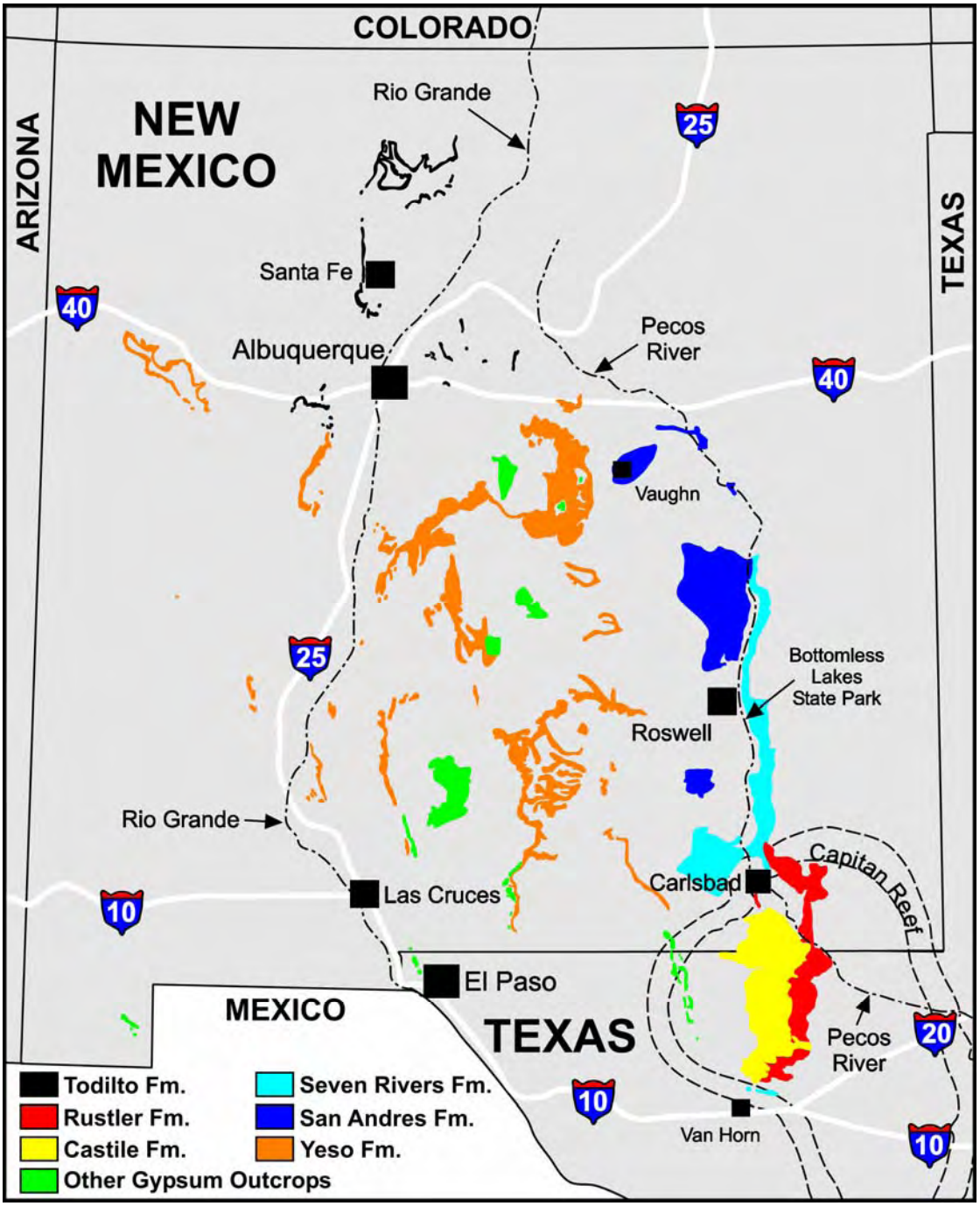

Fig. II.1: Map showing outcrop regions of gypsum formations in New Mexico and Far West Texas (adapted from Weber and Kottlowski, 1959 and Dietrich et al., 1995).

Permian rocks of the Gypsum Plain, which were deposited either contemporaneously or immediately subsequent to deposition of the Capitan Reef (Fig. II.1, II.2), famous for

Carlsbad Cavern, Lechuguilla Cave and other limestone caves. Because the Gypsum Plain is located near the Guadalupe Mountains caves, evaporite cave and karst development is often overlooked although extensive (Table II.1; Table II.2). Evaporite karst encompasses a wide range, producing a broad continuum from karren and sinkholes to complex, polygenetic caves exhibiting both epigenic and hypogenic phases of speleogenesis. In addition to the Gypsum Plain, other evaporite lithologies occur throughout New Mexico and Far West Texas, but documented karst in these regions is limited.

The gypsum plain is located in the semi-arid southwest, where precipitation and annual temperatures vary widely from eastern plains to northern mountains. Most precipitation occurs as monsoonal rains during late summer (July-September). Annual temperatures commonly exceed 40°C in the lowlands during summer months and frequently drop below -20°C in the mountains during winter. The Gypsum Plain is

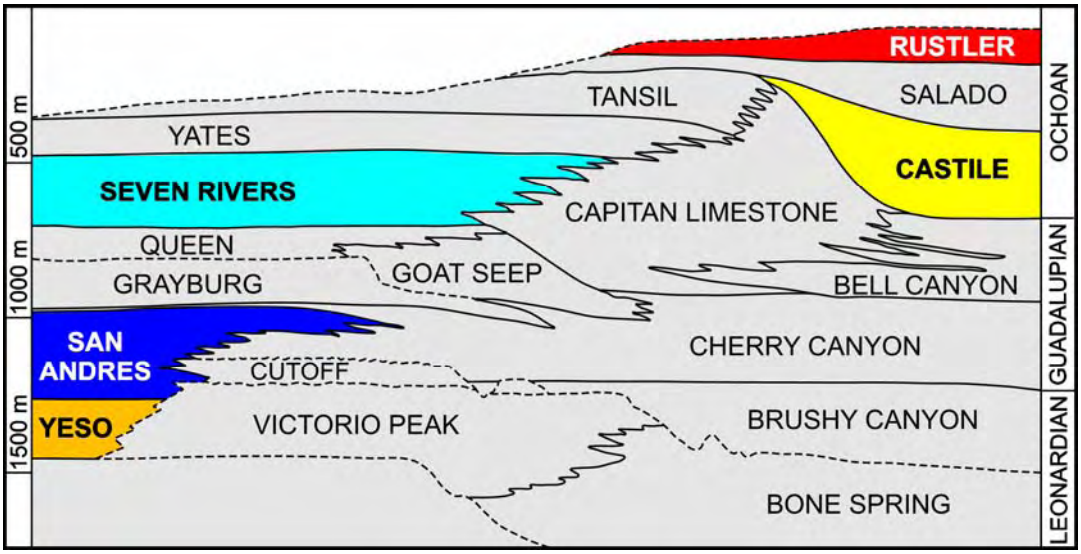

Fig. II.2: Diagrammatic representation of Permian formations (Leonardian through Ochoan) associated with the Guadalupe Mountains. Gypsum formations discussed are color-coded to the regional outcrop map (Fig. II.1) (adapted from Hill, 1996).

Cave	Formation	Depth (m)
Triple Engle Pit	San Andres	135
Millrace	Yeso	110
Harvey's	Yeso	107
Carcass	San Andres	102
Crystal Caverns	San Andres	101
Crystal Cave	Castile	93
Double Barrel Shot Gun	San Andres	88
Jansill / Driftwood	San Andres	71
Burro	San Andres	67
Montecito	San Andres	55

Table II.1: Ten deepest gypsum caves: New Mexico and Far West Texas (Belski, 2007 written communication).

Cave	Formation	Length (m)
Park's Ranch	Castile	6596
Crystal Caverns	San Andres	3776
Double Barrel Shot Gun	San Andres	3725
Scrooge	San Andres	3497
Carcass	San Andres	3165
Martin Cave System	San Andres	3023
Triple Engle Pit	San Andres	2486
Coffee (Eddy County)	Seven Rivers	2321
Hay's	San Andres	2037
Wayne's Womb	San Andres	1720
Jansill / Driftwood	San Andres	1710
Red Bluff	San Andres	1524
Burro	San Andres	1487
Alabaster	Todilto	1396
Fanning Ranch North	Seven Rivers	1393
Millrace	Yeso	1281
Great White Horned Owl	Castile	1205
County Line	San Andres	1190
Fanning Ranch South	Seven Rivers	1166
Crockett's	Yeso	1159

Table II.2: Twenty longest gypsum caves: New Mexico and Far West Texas (Belski, 2007 written communication).

located on the western edge of the Great Plains province and extends south into the northern edge of the Chihuahuan Dessert (Fenneman, 1931), where average annual temperature and precipitation is 17.3°C and 26.7 cm, respectively (Bryfonki, 1985).

Dissolution is more rapid in evaporites than in carbonates as a result of higher dissolution kinetics and solubilities. Gypsum solubility (2.53 g/L) is approximately three orders of magnitude greater than limestone (1.5 mg/L) in pure water and two orders of magnitude less than halite (360 g/L) (Klimchouk, 1996a). The rapid solution kinetics of evaporites encourages development of large sinks, incised arroyos and caves that are laterally limited with decreasing passage apertures away from insurgences. When epigenic caves in evaporites form bypass features connecting two points of different elevation, meteoric waters may pass from insurgence to resurgence without reaching saturation if flow velocity is sufficiently high. In hypogenic settings, steep fluid density gradients can be established that create convection cells for continued dissolution where rising or laterally migrating fluids maintain aggressiveness through the simultaneous sinking of saturated fluids and rising of undersaturated fluids (Anderson and Kirkland, 1980).

GypKaP (Gypsum Karst Project) documents and surveys gypsum caves within New Mexico (Eaton, 1987; Belski, 1992; Lee, 1996), while TSS (Texas Speleological Survey) documents cave regions in Texas (e.g. Redell and Feisler, 1977). These organizations focus on features large enough for human entry, biasing reports towards the largest features (Table II.1, II.2). These reports document some of the diverse nature of regional evaporite karst. Most caves are small, groundwater recharge features, but many exhibit morphologies indicative of hypogenic origins. Many caves contain maze-like regions

(Fig. II.3) that suggest hypogenic transverse speleogenesis where water has migrated vertically and laterally along preferential flow paths (Klimchouk, 2006). Maze-like patterns do not provide unequivocal evidence of hypogenic origin, but morphological feature suites in caves provide very strong evidence. These features include risers, half-tubes and cupolas where fluids move from locations of higher to lower gradient / pressure (Fig. II.4) (Klimchouk, 2007). Alone these features could be the result of various processes (e.g. back-flooding, sediment infilling, etc.) but when found together, they indicate fluid flow in confined conditions driven by free convection. These morphological features elucidate the previous hydrologic flow regimes which formed the cave, and do not depend on the overall cave morphology. Therefore, while cave patterns can provide insight into possible origins, observations of specific hydrologic features within caves is necessary to determine speleogenetic origins.

This paper systematically discusses each of the major evaporite karst regions of New Mexico and Far West Texas, specifically the Gypsum Plain, with subdivisions based on regional outcrops of specific geologic formations (Fig. II.1): 1) Northern Gypsum Plain: San Andres Fm; 2) Central Gypsum Plain: Seven Rivers Fm; 3) East Central Gypsum Plain: Rustler Fm; and 4) Southern Gypsum Plain: Castile Fm. Other gypsum regions, other evaporite karst manifestations and speleothems are discussed briefly. Examples of features will be discussed in relation to their speleogenetic evolution.

GEOLOGIC SETTING

New Mexico and Far West Texas host evaporite deposits ranging from Pennsylvanian age to the present; however, most were deposited in the Permian (Fig. II.1, II.2). The

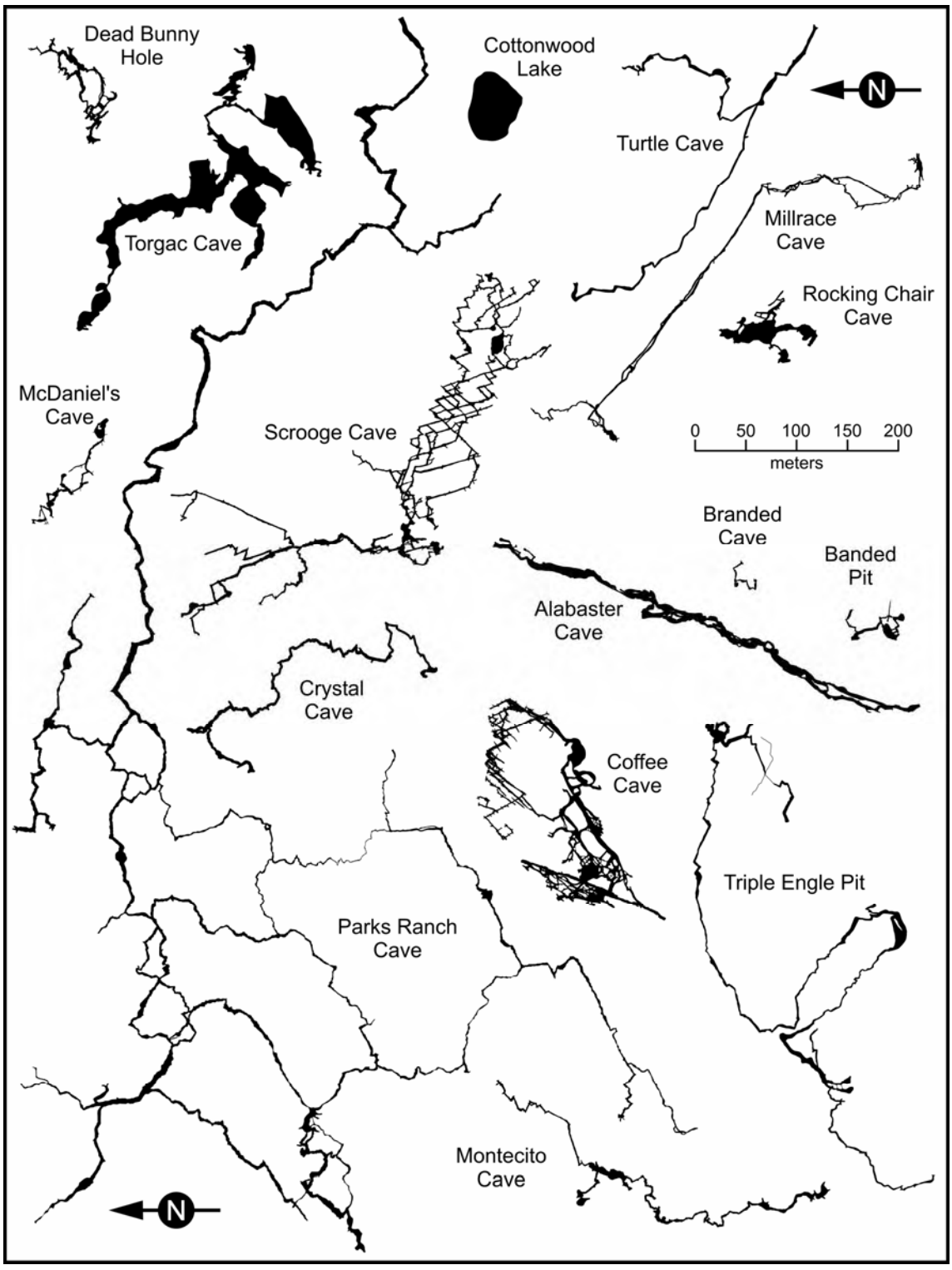

Fig. II.3: Scaled comparison of the 16 caves discussed in detail in the manuscript and a typical cenote at Bottomless Lakes State Park (Cottonwood Lake). Note the morphological diversity in cave passage patterns.

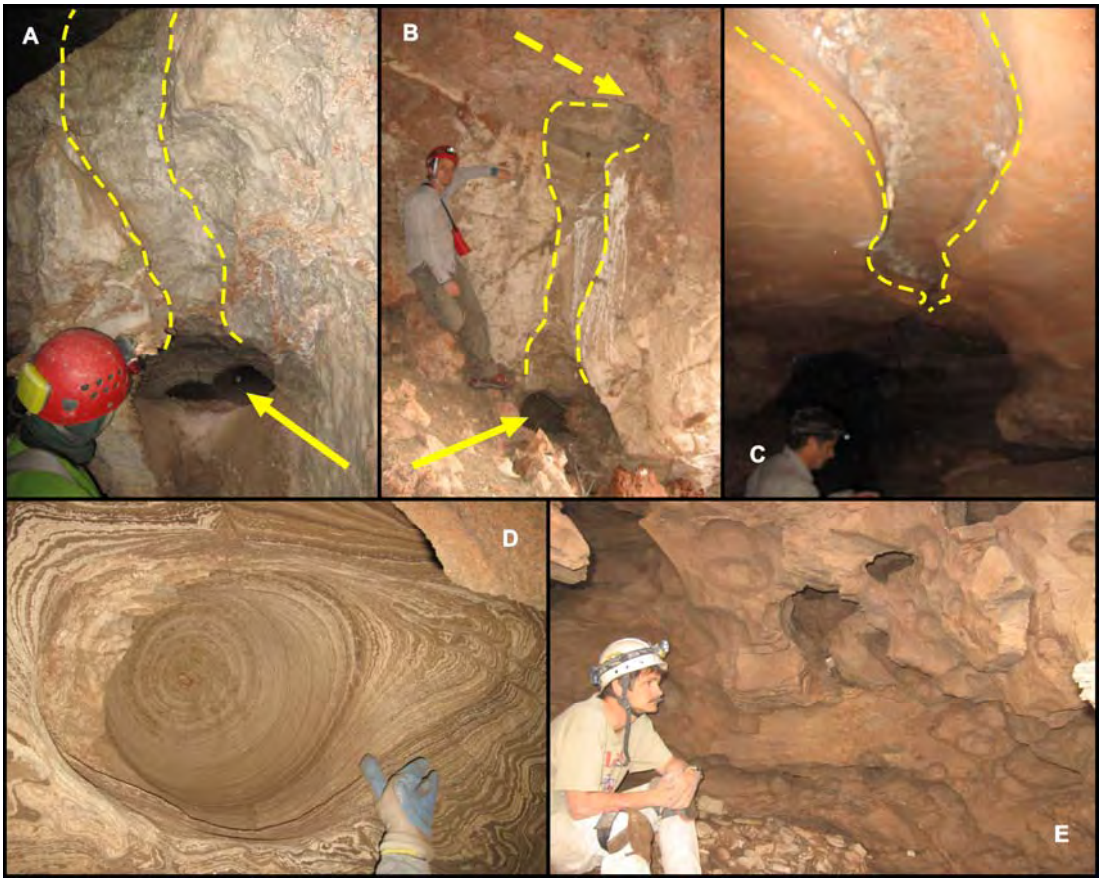

Fig. II.4: Suite of morphological features commonly associated with hypogenic speleogenesis. A) riser (arrow) and ascending wall half-tube (dashed lines) (Coffee Cave); B) complete hypogenic suite including riser (solid arrow), ascending half-tube (dashed lines), and outlet cupola (dashed arrow) (Banded Pit); C) well-defined ceiling channel (dashed lines) (Oasis Cave); D) typical closed cupola (Dead Bunny Hole); and E) complex hypogenic cluster in calcitized evaporites with several outlet cupolas and many small half-tubes (Dead Bunny Hole).

region is geologically complex resulting from its dynamic depositional and tectonic history. Beginning in the Mississippian and continuing into the Permian, collision of the North and South American plates (Ouachita Orogeny) produced significant regional block faulting that created several isolated basins optimal for evaporite deposition, including the extensive petroleum regions of the Permian and Orogrande Basins of Texas and New Mexico (Horak, 1985). These basins formed large, inland seas that enabled

deposition of shelf-facies (i.e. sabhka and salina facies) and deep-basin evaporites. Major north/south trending mountain ranges (e.g. Sacramento Mountains, San Mateo Mountains, etc.) formed during the Laramide Orogeny (Dickerson, 1985). Block faulting, during Basin and Range extension, further subdivided the region (Horak, 1985). Since the Permian, most of the Gypsum Plain has been exposed to surficial weathering, except during the Middle Cretaceous marine transgression. Karst processes have likely occurred continuously since deposition with a minor pause during the Cretaceous.

Gypsum deposits are widely distributed throughout New Mexico and Far West Texas (Fig. II.1) (Weber and Kottlowski, 1959; Kelley, 1971; Dietrich et al., 1995). Pennsylvanian gypsum is limited to the Organ Mountains near Las Cruces, NM. Lower Permian evaporites (Abo and Yeso Fm) occur widely throughout central New Mexico, from El Paso, TX to Albuquerque, NM, primarily near the Tularosa Basin and Estancia Valley. Middle Permian evaporites (San Andres and Seven Rivers Fm) are primarily limited to eastern New Mexico from Carlsbad to Vaughn, with extensive exposures along the Pecos River Valley. Late Permian evaporites (Castile and Rustler Fm) are limited to the extreme southeastern portion of New Mexico and adjoining Texas, from the Apache Mountains near Van Horn, TX to Carlsbad, NM. Jurassic gypsum (Todilto Fm) is limited to the northern New Mexico, cropping out in the Jemez and Sandia Mountains near Albuquerque. Cretaceous gypsum only crops out in the Big Hatchet Mountains in extreme southwest New Mexico. Tertiary gypsum occurs in a small outcrop just west of Las Cruces, NM. Quaternary gypsum deposits continue to form in the Estancia Valley and Tularosa Basin of central New Mexico.

Throughout deposition (eogenesis), burial (mesogenesis) and exposure (telogenesis), calcium sulfates can be altered extensively through mineral conversion, resulting in significant original fabric alteration. At the surface, calcium sulfate is primarily hydrated as gypsum ($CaSO_4 \cdot 2H_20$); however, at higher temperatures and pressures calcium sulfate dehydrates to anhydrite ($CaSO_4$). Gypsum dehydrates at 45^oC, which generally occurs at burial depths of 400 to 450 meters where geothermal gradients and rock pressures are high enough to induce dewatering (Klimchouk, 1996b). In contrast, anhydrite hydrates to gypsum as rocks return to the surface, overburden pressures diminish and unsaturated fluids are introduced, generally at depths of 100 to 150 meters. Mineral conversion has significant affects on sulfate diagenesis and volume changes during hydration/dehydration can produce endokinetic fissuring that can provide preferential flow paths (Klimchouk, 1996b).

NORTHERN GYPSUM PLAIN: San Andres Formation

The San Andres Formation crops out east and west of the Pecos River between Roswell and Vaughn in east-central New Mexico (Fig. II.1). Outcrops are found from the Glorieta Mesa, south of Santa Fe, to the Guadalupe Mountains near Carlsbad. The San Andres was deposited on a broad shelf as shoaling cycles during Late Leonardian – Guadalupian time (Fig. II.2) (Warren, 1989), resulting in thick and thin bedded carbonates, evaporites, and clastics. Along the western outcrop area, San Andres thickness ranges from 210 meters in the north to 400 meters in the south, near the Guadalupe Mountains. In the subsurface to the east, the thickness ranges from 275 meters

to nearly 520 meters, which Kelly (1971) attributes to faulting, erosion, and ground-water extraction.

The San Andres consists of four members, including in ascending order: Glorieta, Rio Bonito, Bonney Canyon, and Four Mile Draw members (Kelley, 1971). The Rio Bonito is noted for oil production to the east due to high porosity and permeability in thickly bedded dolomites (Pitt and Scott, 1981). Between Roswell and the Sacramento Mountains, the lower San Andres serves as the artesian aquifer forming the Roswell Artesian Basin (Havenor, 1968). Land (2006) describes the formation of Bottomless Lake sinks as the result of subsurface dissolution of evaporites by the upward leakage of groundwater from this karstic San Andres aquifer (Fig. II.5). Stafford and others (2007a) have described the formation of caves along the Macmillan Escarpment as a result of waters rising from the same aquifer. The Four Mile Draw Member contains interbedded carbonates and clastics, but is primarily evaporitic and is the unit in which caves of this study are located. Forbes and Nance (1997) described multiple gypsum textures in San Andres caves, including laminated, nodular, and massive.

Regional dip is to the east / southeast. Kelley (1971) mapped minor structures along the southern and western margins of the study area, but there has been very little study of the geologic structure within karsted regions. Locally, dip can vary in any direction due to localized folding and solution subsidence (Forbes and Nance, 1997). Passages develop intrastratally in gypsum and carbonates, where carbonates frequently form flat floors or ceilings.

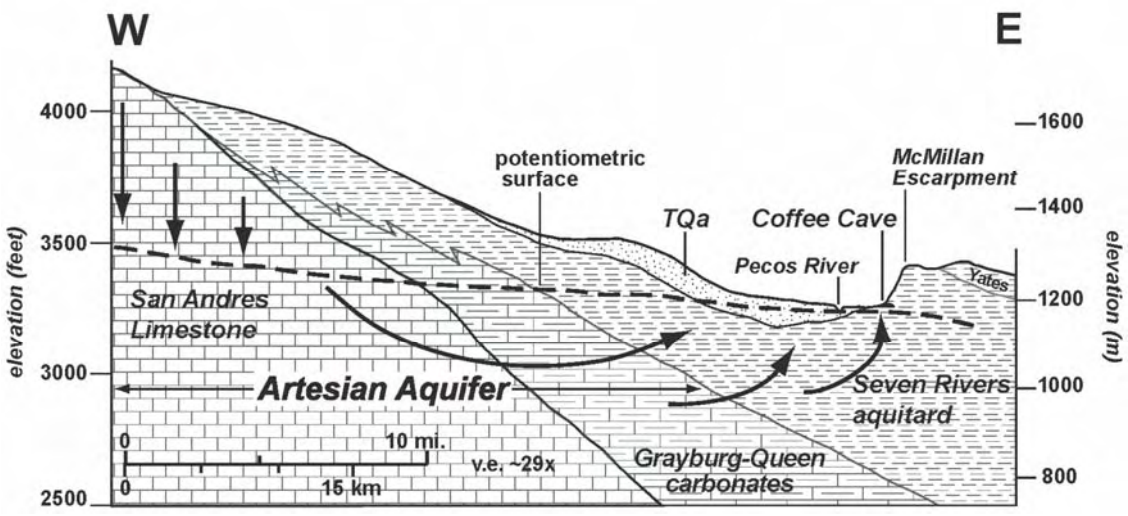

Fig. II.5: Schematic cross section of the southern Roswell Artesian Basin, showing hydrologic flow paths (arrows) and relationship to Coffee Cave (from Stafford et al., 2007a).

Caves in the study area are dominated by vadose water incised meandering passages through gypsum to carbonate beds beneath (Fig. II.6b). Belski (1992), Eaton (1987), Forbes and Nance (1997), and Lee (1996) described pits or large, stoping collapses intersected by passages, which continue at a lower stratigraphic level. Forbes and Nance (1997) described formation of these collapse structures when more resistant beds are undermined by dissolution of evaporites. They also described the effect of the sedimentary sequence variability on cave geometry and passage morphology. Though frequently less than 0.5 meters thick, carbonate beds act as resistant units and form the lips of pits and down climbs. The stairstep profile of these caves is consistent with speleogenesis in the vadose zone. Initial karst permeability of major caves in the area appears to be hypogenic, forming as a result of circulation along structural flowpaths during mesogenesis or telogenesis. Scrooge Cave (Fig. II.3) contains an extensive rectilinear maze exhibiting hypogenic characteristics described by Klimchouk (2000).

Fig. II.6: Bottomless Lakes State Park. A) Scarp failure along Seven Rivers Escarpment showing significant block rotation associated with slumping; B) Cottonwood Lake, one of the eight "cenotes" at the state park.

Montecito Cave (Fig. II.3) is the northernmost cave studied in the San Andres Formation. It is located 50 km. south of Vaughn, NM. It has only one known entrance and has been mapped to a length of nearly 600 meters and depth of 55 meters, but continues beyond the end of the last surveyed point. The first 160 meters of cave is a tight, joint controlled vadose passage, typically less than 0.6 meters wide, but over 10 meters tall, formed in nodular gypsum with thin interbedded dolostone stringers. The floor is a 0.6 meter thick unit of laminated dolostone that forms the lip of Classis Dome Pit. The dome pit extends another 7 meters above the lip and drops 15 meters to where it breeches an 8 meter thick dolostone unit. Passages lead from the pit to two suspected paleoentrances, both now blocked by breakdown. The main passage continues in a gypsum bed beneath the dolostone unit as a sinuous, incised canyon averaging 2 meters tall and 1 meter wide, similar to figure 7c. Overhead, smaller, elliptical tubes near the dolostone contact parallel the main passage. Beyond the last mapped point, the cave continues as a 1 meter tall stream passage. Nance (1996) described a region of rising tubes and an extensive room that had formed along the base of an overlying carbonate

Fig. II.7: Morphological diversity in passage development within gypsum karst. A) elliptical conduit (Parks Ranch Cave); B) canyon passage (Carcass Cave); C) keyhole passage formed from floor incision (Oasis Cave); D) multi-level passage with dolomite interbeds separating levels (Coffee Cave); E) complex vertical passage resulting from epigenic overprinting of large hypogenic riser (Plummet Cave); and F) shaft entrance developed along margin of collapse breccia.

unit and running parallel to the trend of the lower passage. The ceiling of the room is the 8 meter thick dolostone unit described previously and the floor is covered by a 5-7 cm thick silt layer and collapse blocks filled with drip tubes. The sides of the room slope toward low points in several areas, suggesting buried riser features. The morphology of

the room is indicative of hypogenic origin, while extensive vadose processes have likely overprinted the lower passages largely.

Triple Engle Pit (Fig. II.3) is currently the deepest gypsum cave in North America (Table II.1), with a length of 2486 meters and depth of 135 meters. Triple Engle Pit lies at the southern end of a northwest-southeast trend of large gypsum caves extending approximately 20 km; including Burro Cave, Crystal Cavern, Diamond Sink, Carcass Cave (Fig. II.7b), and Orange Feather Cave. Duchene and Belski (1992) proposed that the caves formed near the crest of an anticline; however, Forbes and Nance (1997) failed to find evidence of the anticline to the northwest, but did find evidence of a smaller anticline to the southeast. Triple Engle Pit is formed in interbedded evaporites, carbonates, and clastics (Forbes and Nance, 1997) with carbonate units frequently forming the ceiling or floor of passages. Triple Engle has 5 entrances draining a surface area of ~2-3 km^2. It is in a cluster of karst features, including Carcass Cave, Orange Feather Cave, Owl Cave, and Morris Sink. This cluster drains nearly 20 km^2. Owl Cave has been physically connected to the lower section of Triple Engle, but lacks a full survey due to flooding. The main upper passage of Triple Engle Pit forms an incised canyon up to 20 meters in height, exposing numerous gypsum textures. The cave becomes a series of low crawls, some ending at water filled sumps at their lowest point. Forbes and Nance (1997) described structural features, including three vertical faults and reverse-fault slippage along bedding planes, suggesting considerable compressional shear. Secondary gypsum crusts, flowstone (Polyak 1992), and gypsum flowers are found in several locations. The cave is an active epigenic recharge feature likely overprinted onto an existing hypogenic system that developed along vertical faults which enabled the

formation of this deep cave. Initial karst permeability likely formed during mesogenesis or telogenesis, developing preferential flowpaths for later shallow phreatic or vadose water.

Torgac cave (Fig. II.3) is located about 100 km northeast of the town of Capitan, NM. Because of its unique speleothems and use as a winter bat hibernaculum, entrance to the cave is strictly regulated by the Roswell office of the Bureau of Land Management (BLM). The surface topography forms a cold-air trap, funneling cold air into the entrance. Forbes (1998) measured temperatures during January and February 1995 ranging from 5.5ºC to 10.9ºC. Unlike the other caves described in the San Andres Formation, Torgac Cave is formed in thick dolostone units. The only exposed gypsum occurs at the entrance sinkholes and overlies most cave passages (Forbes, 1998). Jagnow (1998) described Torgac Cave as an inactive vadose cave with the main passage 30 m below the surface. Torgac Cave contains a variety of gypsum speleothems including gypsum rims, flowers, blisters and flowstone, as well as epsomite stalactites (Doran and Hill, 1998). Torgac Cave is best known for gypsum trays similar to those described in Rocking Chair Cave by Calaforra and Forti (1994).

CENTRAL GYPSUM PLAIN: Seven Rivers Formation

The Seven Rivers Formation crops out along a narrow strip bordering the eastern edge of the Pecos River Valley and in the Seven Rivers Embayment north of the Guadalupe Mountains (Fig. II.1). The outcrop regions cover an area of ~1300 km^2 ranging from Carlsbad, NM north to Interstate Highway 40. Eastward migration of the Pecos River throughout the Quaternary resulted in dissolution of the most of the Seven Rivers

Formation to the west (Welder, 1983), forming the Seven Rivers Escarpment. Intense dissolution along the escarpment has resulted in differential settling and intense fracturing causing bedding to locally dip steeply and chaotically (Fig. II.6a); however, the Seven Rivers Formation generally dips gently to the east away from the escarpment, reaching a maximum thickness of 50 meters with dolomite interbeds comprising about ten percent (Kelley, 1971).

The Seven Rivers Formation is part of the Artesia Group, the equivalent of the Whitehorse Group of north Texas and eastern Oklahoma. It is a backreef facies that grades into the Capitan Reef (Fig. II.2) (Scholle et al., 2004). Near the reef, the Seven Rivers Formation is interbedded dolomite and sandstone that grades northward into interbedded gypsum and dolomite, with a decreasing thickness in dolomite interbeds. The unit grades into siliciclastic facies in northeastern New Mexico. Lithologic fabric ranges from massive to nodular gypsum (chicken wire), with thin to medium-bedded, microcrystalline dolomite and gypsiferous, silty sandstone interbeds (Sarg, 1981).

Documented karst in the Seven Rivers Formation is largely limited to areas proximal to the Seven Rivers Escarpment (e.g. Bachman, 1987; Land, 2003, 2006) and the Sinkhole Flat in the Seven Rivers Embayment. Abundant epigenic karst features occur as bypass structures through scarp failure fissures in the Seven Rivers Escarpment. Hypogenic karst is common in the escarpment, as observed in active artesian springs (Fig. II.5) and complex, relict maze caves where dolomite interbeds create a vertically heterogeneous unit that favors multi-storey development. The caves of the Sinkhole Flat contain well developed hypogenic features (Fig. II.4c) with minimal epigenic

overprinting, as evidenced by a lack of scallops and abundant hypogenic features. Both hypogenic and epigenic karst is actively forming in the region today.

Bottomless Lakes State Park is located east of Roswell, NM. Eight, water-filled sinkholes or cenotes in the park are part of a series of sediment and water-filled sinkholes that extend several tens of kilometers north and south of Roswell along the Seven Rivers escarpment (Fig. II.6b). The “lakes” are fed by artesian waters from the underlying, karstic limestone of the San Andres Formation (Land, 2003, 2006), making them unique because they are sinkholes forming by rising fluids rather than sinking streams. These features act as localized discharge points for groundwater of the Roswell Artesian Basin (Fig. II.5). Groundwater recharge occurs to the east of Roswell along the slopes of the Sacramento Mountains in the unconfined San Andres Formation. Subsurface water flows down gradient to the east and south where it becomes confined beneath the Seven Rivers Formation (Welder 1983). Confined fluids migrate upwards through fissures, resulting in dissolution of Seven Rivers gypsum (Land 2003). Increased dissolution produces cavities that stope upwards to form cenotes. These cenotes suggest the importance of active hypogenic speleogenesis within the region.

Coffee Cave (Fig. II.3) provides one of the best examples of hypogenic speleogenesis within the entire Gypsum Plain. It is located on the eastern edge of the Pecos River Valley, along the southern edge of the Roswell Artesian Basin (Fig. II.5) (Hendrickson and Jones, 1952). The cave consists of four distinct storeys that decrease in size upwards and are separated by dolomite interbeds (Fig. II.7d), with potentially additional storeys below the water table. Most of the cave is a typical rectilinear maze, with levels connected along widened fractures and through point source risers. Most risers are

connected to wall channels that converge into ceiling channels and join at ceiling cupolas or risers to upper storeys, forming a complete inlet to outlet suite within individual storeys (Fig. II.4a). The maze-like pattern and entire morphological feature suite provide strong evidence of hypogenic speleogenesis (Stafford et al., 2007a). The cave was originally surveyed in the early 1970s and at that time interpreted as forming by back-flooding along the Pecos River and the construction of the now abandoned Lake McMillan in the early twentieth century. A resurvey of the cave was conducted in 2007 in order to specifically document the hypogenic origin (Stafford et al., 2007a).

Turtle Cave (Fig. II.3) provides a stark contrast from the Bottomless Lakes and Coffee Cave, although located along the same scarp and several kilometers north of Coffee Cave. Turtle Cave consists of two primary passages that converge to form a simple dendritic pattern with multiple entrances and 629 meters of surveyed passage (Belski, 1992). It is a typical bypass feature connecting insurgences above the scarp to a resurgence near the scarp base with well-developed scallops and significant allogenic sediments, suggesting large flow volumes. Throughout the cave, most ceilings are composed of dolomite or clay-rich gypsum providing relatively impermeable layers restricting dissolution and constraining passage development. Most passages are wider than tall with an increase in average passage diameter after feeder passages combine, suggesting breakthrough occurred early in cave development, enabling runoff to pass through the entire cave without reaching saturation. Turtle Cave illustrates significant epigenic speleogenesis in the Seven Rivers Formation.

EAST CENTRAL GYPSUM PLAIN: Rustler Formation

The Rustler Formation crops out over an area 8-20 km wide band from the Apache Mountains in Texas to east-central Eddy County, New Mexico (Fig. II.1) (Hill, 1996). North of the Delaware Basin, it is exposed on the east side of the Pecos River in a north-south band. Nearer the New Mexico-Texas state line, it is exposed to the west of the Pecos River in the Rustler Hills of Culberson County, TX. Smaller outcrops form topographic highs in the Yeso Hills of Eddy County, NM. The Rustler Formation is a post-Capitan Reef deposit (Fig. II.2), consisting of interbedded evaporites, carbonates, and clastics. The Rustler has been removed in much of the area west of the Pecos River, exposing the underlying Castile Formation. East of the Pecos, it has been studied in the subsurface near the Waste Isolation Pilot Plant (WIPP).

The Rustler Formation consists of five members; in ascending order: Virginia Draw (Unnamed) Member, Culebra Dolomite Member, Tamarisk Member, Magenta Dolomite Member, and Forty-niner Member (Hill, 1996). Bachman (1984), Hill (1996) and Kelley (1971) all describe the thickness of the Rustler as variable due to dissolution and differential deposition, ranging from 120 meters in the subsurface of eastern Eddy County, NM, to 200 meters in the south. Lorenz (2006) argued that other factors could also account for thinning of the Rustler in the area near WIPP (Waste Isolation Pilot Plant).

Most karst development in the Rustler occurs in the Forty-niner member. Karst development is extensive, though the formation of caves is minor. Breccia pipes have been documented in a number of locations, as well as large regions of solution subsidence, such as the San Simon Sink and Nash Draw (Hill, 1996). Evidence of

solution subsidence and collapse structures extend south of Malaga into the Rustler Hills (Kelley, 1971).

Caves in the Rustler Formation show evidence of hypogenic inception, where interbedded evaporites and permeable dolomites favor the development of hypogenic karst. Caves having features consistent with initial hypogenic development are clustered in widespread groups. Lorenz (2006) has shown that conduit flow within the Culebra and Magenta Members is unlikely in the region near WIPP, but none of the clusters showing evidence of hypogenic speleogenesis are in his study region. Burton Flats, approximately 30 km northeast of Carlsbad, NM contains two clusters evaluated during this study and a number of shallow epikarst features, including small caves that narrow rapidly. Along Nash Draw, epikarst features and small caves are found, which narrow rapidly beyond the insurgence, indicating epigenic origin. In extreme northern Nash Draw, linear soil piping over 100 meters in length appears as a surface expression of underlying lineaments. South of WIPP several small cave show evidence of hypogenic development. Hill (1996) described Remuda Basin, a closed depression in the south end of Nash Draw that drains a surface area of 1 km^2 into an open cave passage. Most Rustler cave development is in solutionally enlarged joints.

Rocking Chair Cave (Fig. II.3) is located in the Burton Flats area, near the northern limit of Rustler Formation outcrops. It is the largest of a cluster of ten caves and has as surface drainage less than 0.25 km^2, while adjacent basins cover areas exceeding 3 km^2. It is 488 meters long and almost 18 meters deep (Belski, 1992). Hypogenic flow developed initial karst permeability, as shown by infeeders and risers near the main entrance, with the most extensive riser observed above the intersection of the main shaft

and a passage leading to lower parts of the cave. Collapse into underlying voids resulted in development of a breakdown filled entrance shaft and formation of adjacent rooms along parted bedding planes. Rocking Chair Cave is noted for gypsum trays (Fig. II.9a) and other speleothems (Fig. II.9b) found in a 7 meter wide, 15 meter long room averaging 3-4 meters high, which Calaforra and Forti (1994) described. Directional stalactites in the room also indicate deflected growth in a preferential direction (Fig. II.9b).

Branded Cave and Banded Pit (Fig. II.3) are located in the Burton Flats area, within a group of wide, shallow depressions near the western edge of the Clayton Basin. The caves are 1 km apart and each one drains a surface area of ~1 km^2. Branded Cave's entrance is a tall, incised passage at the end of an incised arroyo. Thirty meters into the cave, small feeders join in a room 4 meters in diameter and 6-7 meters tall. Beyond, the passage is a low crawl terminating in a sediment fill after approximately 30 meters. The entrance of Banded Pit is also at the end of an incised arroyo, but the entrance room is a collapse feature in gypsiferous red clay. Infeeders, risers, and elliptical tubes occur in the entrance area (Fig. II.4b), including the two largest, which form the passages leading into the cave. Twenty meters into the cave is a room 4-5 meters in diameter and 6-7 meters tall. The floor is composed of large breakdown blocks, beneath which a 7 meter pit leads to a lower section of cave. Feeders and risers enter the room from multiple directions and levels. The total relief of the room is 14-15 meters, formed in intrastratal gypsum, carbonates, and clastic beds. The cave continues 40-50 meters in passage up to 2 meters wide and ends at a sump, well above the accepted water table for the area (Hendrickson and Jones, 1952). The morphology of both caves indicates hypogenic origins with epigenic overprinting, primarily allogenic sediment introduction and breakdown collapse.

England Cave is a short, unmapped cave west of highway 285 near the Delaware River in southern Eddy County, NM. The main cave entrance opens into a small closed basin that drains less than 1 km^2. Ten meters inside the cave is a skylight entrance 6 meters in diameter that continues into an entrance chamber 30 meters long, 8 meters wide and over 4 meters tall. In the back is an area of collapsed blocks filling a shallow shaft. An incised canyon, too tight for human passage, drains meteoric flow through clean-washed bedrock, indicating a non-obstructed drain. The cave is formed in interbedded gypsum, dolomite, and clastics and is capped by alluvial deposits of the Gatuna Formation. Risers occur in the collapse from multiple directions at several levels, commonly along the base of carbonate units. England Cave likely formed by epigenic processes along preferential flowpaths resulting from hypogenic development within the intrastratal evaporites of the Rustler Formation.

SOUTHERN GYPSUM PLAIN: Castile Formation

The Castile Formation crops out over an area of ~1800 km^2, the largest continuous exposure of a single gypsum unit within New Mexico and Far West Texas (Fig. II.1). Castile Formation evaporites were deposited within a deep, stratified, brine-filled basin during the Late Permian (early Ochoan) (Fig. II.2) as a result of the closing of the Delaware Basin (Kendall and Harwood, 1989). The unit is characterized as massive to laminated anhydrite/gypsum interbedded with halite (Kelley, 1971; Dietrich et al., 1995). The unit crops out in the western Delaware Basin along the Castile dissolution front, but descends into the subsurface to the east where it reaches a maximum thickness of 480 meters (Hill, 1996). Thinning of the unit to the east is attributed to dissolution subsidence

(primarily halite dissolution) and increased deposition to the east in the Ochoa Trough during the Permian (Anderson et al., 1972). The Castile Formation has experienced minimal tectonic deformation, limited to regional tilting (3 to 5 degrees) to the northeast, minor folding and abundant jointing (~N75^{o}E and ~N15^{o}W) (Hentz and Henry, 1989; Horak, 1985).

Although the Castile Formation is located in a tectonically quiescent area, sulfate rocks have been exposed to significant diagenesis. Original laminated gypsum often exhibits nodular and massive fabrics that are likely the result of plastic deformation associated with anhydrite/gypsum mineral conversion. Selenite can be locally abundant, forming lenticular masses, linear features and fracture fillings. Calcitized evaporites are common (often referred to as “castiles” or calcitized masses) (Fig. II.4e), generally forming clusters or linear trends of biogenic limestone associated with bacterial sulfate reduction (Kirkland and Evans, 1976). Sulfate reducing bacteria utilize rising hydrocarbons as a sources of energy. As a byproduct, $CaCO_3$, H_2S and H_2O are produced. H_2S commonly oxidizes into elemental sulfur, if it comes into contact with oxygenated waters, and generally filling vugs created during calcitization, but may form large, isolated masses (Hentz and Henry, 1989). Elemental sulfur can oxidize further, forming some selenite masses. Effectively, diagenetic calcite and the associated native sulfur and selenite (Hill, 1996) are hypogenic karst produced by fluid migration (both gaseous and liquid) through the Castile Formation, where waters recharged in the Delaware Mountains to the west descend down dip beneath the Castile Formation through the Bell Canyon Formation, while rising hydrocarbons migrate up dip through the Bell Canyon Formation. Both waters and hydrocarbons within the Bell Canyon Formation ascend

through fractures in the Castile Formation, resulting in evaporite calcitization of evaporites and subsequent oxidation of hydrogen sulfide. Associated increases in porosity provide preferential flow paths through which further dissolution can occur. Currently, many calcitized masses degas significant volumes of H_2S, indicating that hypogenic speleogenesis and bacterial sulfate reduction remain active processes within the region (Kirkland and Evans, 1976), suggesting that some current calcitization is occurring above elevations of oxygenated groundwater.

Karst development is extensive within the Castile Formation, with more than 200 caves known; however, more than 3000 individual features (sinkholes and sinking arroyos) have been identified using GIS (Geographic Information System). Surficial karst surveys in the area suggest that as many as 8,000 individual features may exist, but it is likely that less than 10% of the features are caves large enough to be humanly enterable (Stafford et al., 2007b). Caves are developed in all gypsum fabrics, as well as gypsite and biogenic limestone. Most known caves are small and function as groundwater recharge features with less than 50 meters of surveyable passage, exhibiting rapid aperture decreases from insurgences and appearing to represent epigenic speleogenesis (Stafford et al., 2008). However, many larger caves exhibit complex morphologies (Fig. II.7e) suggestive of polygenetic origins (Stafford et al., 2008).

Parks Ranch Cave (Fig. II.3) is the second longest gypsum cave in North America (6596 m long, 21 m deep) (Table II.2) and has 26 known entrances (Stafford, 2006). The Parks Ranch Cave area contains the densest documented gypsum karst development within New Mexico and West Texas (up to 50 features / km^2). The cave is primarily developed in sucrosic gypsum (Fig. II.7a); however, some lower regions are in laminated

fabrics. The cave alternates between regions of elliptical tubes (Fig. II.7a) and incised, meandering canyon passages, while passages converge in a complex anastomotic pattern. The cave is hydrologically dynamic, with rapid response to flash flood events that completely fill portions of the cave and introduce large quantities of detritus. Sares (1984) suggested that the cave developed as a fluvial bypass system in relation to lowering of surficial streams (i.e. Black River and Pecos River) during the late Pleistocene. However, many regions of the cave exhibit cupola, half-tube and riser suites, suggestive of confined speleogenesis. It is likely that hypogenic speleogenesis produced initial preferential flow paths; however, it appears that the majority of the cave is the result of epigenic speleogenesis as suggested by Sares (1984).

Dead Bunny Hole (Fig. II.3) was recently discovered through digital air photo analyses, which showed a small sinking arroyo with a limited watershed. The cave is developed in laminated gypsum (Fig. II.4d) with many passages oriented along small-scale folds axes, forming an irregular maze. Currently, the surveyed length and depth are 420 meters and 14 meters respectively; however, several unexplored passages remain. The cave trends towards the northeast in a series of three relatively horizontal levels, although folds trend southeast. The middle level is largely developed in calcitized evaporites with preserved original laminations (Fig. II.4e). Ceiling cupolas are common throughout the cave (Fig. II.4d), with occasional ceiling half-tubes connecting several cupolas. Most of the floor is composed of fine-grained sediments, large clasts or breakdown, which obscures original floor detail; however, several areas contain riser features, which are often filled with laminated clays. The combination of observed free convection features, the overall maze-like morphology and the presence of extensive

calcitization, an indication of rising fluids in the past which established transmissive zones, suggest that Dead Bunny Hole has a hypogenic origin that has been slightly overprinted by epigenic processes, primarily limited to the introduction of allogenic sediments.

Crystal Cave (Fig. II.3, II.8) is the deepest gypsum cave documented in Texas (93 meters deep, 669 meters long) (Table II.1) and terminates in a descending sump. The cave consists primarily of a single passage with numerous small infeeders that are not humanly passable. The majority of the cave is gently dipping with small, incised floor drops. Two pits occur in the cave, associated with major lithologic changes. Quarryman's Pit (8 m deep) is located ~70 meters from the entrance, while Glacier Bay II (15 m deep) is located near the terminal sump of the cave. Above Quarryman's Pit, the cave trends northeast along the regional dip and is developed in laminated gypsum with minor regions of nodular gypsum. Glacier Bay II and the lowest portions of the cave are developed entirely in selenite, where individual crystals average 0.5 to 1.0 meter. The region between the two pits generally trends southeast and is lithologically complex with alternating layers of laminated, massive and nodular gypsum, as well as selenite and calcitized evaporites. Brecciated zones and selenite deposits within zones exhibiting solutional truncation of laminated sulfates are common, suggesting significant hypogenic dissolution. Development through this lithologically complex region generally follows the strike of bedding with occasional passage drops into new lithologic suites. Although Crystal Cave is morphologically simple, well-developed ceiling tubes and significant amounts of selenite and calcitized evaporites suggest that the cave is the product of hypogenic speleogenesis, which established initial flow paths, that appears to be heavily

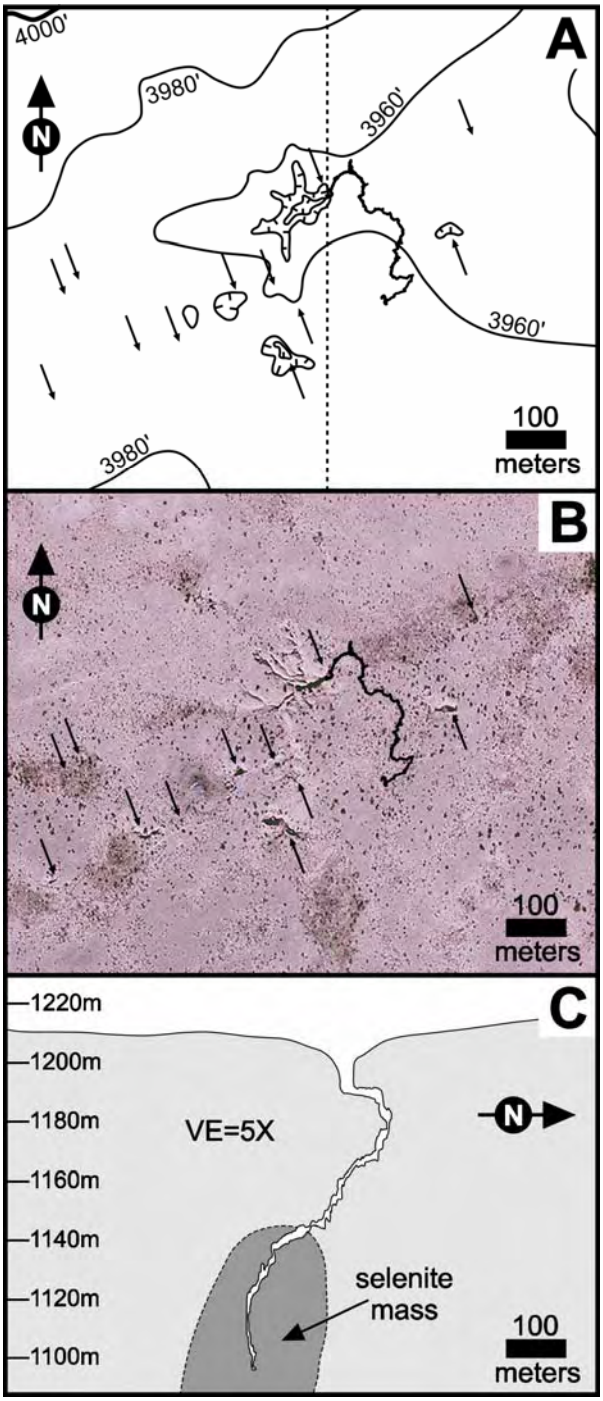

Fig. II.8: Crystal Cave, Castile Formation, Culberson County, Texas. Small arrows in A and B indicate locations of individual caves. A) topographic map of area surrounding Crystal Cave showing several large sinkholes and profile outline of Coffee Cave; B) digital air photo of area surrounding Crystal Cave showing geomorphic expression of karst and outline of Crystal Cave; C) north / south profile through Crystal Cave, showing the region of Crystal Cave completely developed in selenite.

overprinted by epigenic processes that occurred after surficial breaching, including passage entrenchment (keyhole passages) and speleothems deposition.

MINOR REGIONS WITHIN NEW MEXICO

Evaporite karst outside of the Gypsum Plain is poorly developed in New Mexico and Far West Texas. No significant karst is known in Pennsylvanian, Cretaceous, Tertiary or Quaternary evaporite deposits, or in the Permian Abo Formation. However, it is likely that minor surficial karst exists in all areas including syngenetic karst in modern deposits associated with playas, such as those that occur at White Sands National Monument. Outside of the Gypsum Plain, only the Jurassic Todilto Formation and the Permian Yeso Formation are know to host caves.

The Jurassic Todilto Formation (Fig. II.1) was deposited in a restricted lacustrine basin which is unconformably underlain and overlain by sands and shales respectively. Gypsum within the Todilto Formation is limited to the middle third of the formation where it consists of laminated gypsum with a thickness of 15 to 30 meters (Weber and Kottlowski, 1959). Alabaster Cave (Fig. II.3) is the only known significant cave in the Todilto Formation and is located on the southwestern edge of the Jemez Mountains. Alabaster Cave is 1396 meters long and located at the base of an erosional scarp. The cave contains a major trunk passage with smaller side passages. Half-tubes, risers and cupolas are common throughout suggesting a hypogenic origin; however, extensive breakdown and fine-grained allogenic sediments have heavily overprinted much of the cave during the epigenetic phase.

The Yeso Formation (Fig. II.1) was formed in the Early Permian as the shelf facies equivalent of Victorio Peak Formation during early Permian (Leonardian) (Fig. II.2) marine transgression (Hill, 1996). Yeso outcrops are widely distributed throughout the central portion of the study area, but are primarily limited to narrow outcrops. Composition varies from thin gypsum interbeds in dolomite and sandstone to massive and laminated gypsum facies, with formation thickness ranging from a few meters to more than 500 meters (Weber and Kottlowski, 1959). The only known karst development within the Yeso Formation is in the Chupadera Mesa region. Local groundwater recharge in this area likely serves as the source for sulfate-rich waters in spring-fed playas of the Tularosa Basin. Many of the known caves occur along the Carrizozo lava flow, which partially protects underlying gypsum and focuses allogenic recharge.

Caves within the Chupadera Mesa area include Millrace Cave and McDaniel's Cave. Millrace cave (Fig. II.3) is second deepest gypsum cave in North America, with a surveyed depth and length of 110 meters and 976 meters, respectively (SWR, 1976). It is located directly beneath the lava flow just west of Carrizozo in a 15 meter thick layer of laminated gypsum and developed along the eastern limb of a dipping anticline with bounding layers of limestone above and below (Davis, 1965). The cave is largely developed along a single major passage but contains several small sections of maze and numerous ceiling domes. Occasional risers and half-tubes are seen throughout the cave in feature suites, suggesting a hypogenic origin where fluids rose along the anticline limb; however, focused recharge along the western edge of the lava flow has resulted in extensive epigenic overprinting, primarily in the form of breakdown collapse and scalloping on the lower portions of passage walls.

In contrast to Millrace Cave, McDaniel's Cave (Fig. II.3) consists of two distinct levels with over 400 meters of surveyed passages, three entrances and only 15 meters depth. The upper level consists of isolated chambers in fissile dolomite, while the lower level is developed in laminated gypsum. Numerous vertical risers connecting levels, half-tubes and cupolas imply a hypogenic origin; however, the cave is currently an active recharge feature as evidenced by large accumulations of sediment, flood debris and extensive scalloping in lower passages. Recent exploration near Chupadera Mesa and other known caves, such as Crockett's and Harvey's, suggests extensive karst development exists in the region, forming a significant evaporite karst region outside the Gypsum Plain.

OTHER EVAPORITE KARST MANIFESTATIONS

In addition to caves, sinkholes, and karren, evaporite speleogenesis produces other significant manifestations within New Mexico and Far West Texas, including breccias, dissolution troughs and anthropogenically enhanced features. These are largely hypogenic features expressed as positive and negative relief structures at the surface and occur primarily within the Delaware Basin. Although halite does not occur at the surface within the study area, significant deposits occur in the subsurface. It is commonly associated with other karst development because of its extremely high solubility and susceptibility to dissolution.

Brecciation in the form of blanket breccias and breccia pipes has been well-documented in the region, primarily in the Castile, Salado and Rustler Formations (Fig. II.2) of the Delaware Basin. Blanket breccias occur in the Castile and Salado Formations

of the western Delaware Basin, where intrastratal halite dissolution from laterally migrating fluids has produced centimeter to decimeter-thick horizons of gypsum breccia (Anderson et al., 1972), which is often calcitized (Anderson et al., 1978). Breccia pipes have been documented along the eastern and northern edge of the Delaware Basin above the Capitan Reef in the Salado and Rustler Formations. Anderson and Kirkland (1980) proposed a brine density convection model for speleogenesis, where unsaturated fluids in the Capitan Reef aquifer dissolve overlying evaporites. In their model undersaturated, low density fluids rise and dissolve evaporites. As saturation increases, fluids become denser and subsequently sink such that undersaturated fluids are continually rejuvenated from below while saturated fluids simultaneously sink. As dissolutional void space increases, roof instability can result in collapses that stope upwards (Klimchouk and Andrejchuk, 1996). As stoping continues to the surface, large collapse features form creating breccia columns that may extend for hundreds of meters vertically. These features are now often represented as topographic highs through topographic inversion, where surface denudation has produced mounds or domes of more resistant brecciated material (Bachman, 1980). Breccia pipes, whether closed depressions, mounds or domes are widespread in the northern and eastern Delaware Basin. Similar vertical collapse structures have been observed in the Seven Rivers Embayment evaporites, where gypsum has been largely removed from the Seven Rivers Formation, residual dolomite has collapsed and pit caves have developed along the margins (Fig. II.7f).

Subsidence valleys, dissolution troughs and solution subsidence troughs are common along the Pecos River and within the Delaware Basin as a result of subsurface evaporite dissolution. The entire Pecos Valley is a large subsidence valley produced by dissolution

of evaporite facies within the San Andres Formation. It was formed largely by the eastward migration of the Pecos River in conjunction with groundwater recharge that has removed most evaporites (Welder, 1983). Large dissolution troughs filled with Quaternary sediments occur within the Delaware Basin (Toyah, Balmorhea-Loving and Big Sinks-Poker Lake Troughs) (Maley and Huffington, 1953). They have been attributed to deep-seated dissolution of Castile, Salado and Rustler evaporites (Anderson et al., 1978). Solution subsidence troughs are narrow linear structures in the Castile Formation of the western Delaware Basin, which formed by collapse of solutional voids formed along graben boundary faults, which are up to 75 meters deep (Anderson, 1982; Hentz and Henry, 1989). The lower limit of solution subsidence troughs is coincident with the upper limit of halite dissolution within the region, suggesting that they are associated with the formation of regional blanket breccias.

Anthropogenically induced evaporite karst has been well-documented in relation to petroleum extraction, including Jal, McCamey, San Simon, Wink and other sinks that formed catastrophically (e.g. Hill, 1996). These features are generally near-vertical collapse structures tens of meters wide and deep, which commonly reached their maximum size within days of initial appearance. They are often associated with petroleum wells in oil fields where production began in the 1920's (Baumgardner et al., 1982; Johnson et al., 2003); however, they occur along the eastern edge of Delaware Basin in a region where large dissolution troughs are also common (Hill, 1996). Because of the age of many of the oil wells, some were uncased or improperly cased, allowing confined fluids to easily rise into evaporite rocks and through brine density convection dissolve large voids around wells. Alternatively, when wells are not well-cased near the

surface, focused recharge down the edge of wells can increase epigenic dissolution or enhanced dissolution can occur from disposal injection of produced waters not saturated with respect to halite or sulfate into improperly cased wells (Powers, 2003). It is likely that other catastrophic collapses will occur in the region over the coming decades; however, these features have helped facilitate the development of improved well completion practices as petroleum extraction has evolved over the past century.

EVAPORITE KARST SPELEOTHEMS

Gypsum karst is not typically noted for speleothems; however, speleothems are commonly observed (Fig. II.9), including: flowstone (i.e. stalactites, stalagmites, draperies, and rimstone dams) (Fig. II.9b,c), gypsum balls, gypsum flowers (Fig. II.9f), crusts (Fig. II.9e), boxwork, and rims. Carbonate flowstone is found in Crystal Cave (Fig. II.9c), Plummet Cave, Parks Ranch Cave, and Skylight Cave in the Castile Formation to the south. Small carbonate stalactites were observed in Montecito Cave and throughout the Castile Formation. In northern caves, the most likely source of calcium carbonate would be overlying limestone or dolostone beds, while carbonate laminae provide source material in the varved Castile. The source of calcium carbonate is precipitation due to the common ion effect (Hill and Forti, 1997). Gypsum stalactites and stalagmites have been observed in numerous caves (Fig. II.9b). Gypsum balls, spheroids formed in areas of capillary seepage (Hill and Forti, 1997), were observed in Oasis Cave (Polyak and Colkendolpher, 1996) and in Rocking Chair Cave. Gypsum flowers and other fibrous speleothems were observed in several gypsum caves (Fig. II.9f), often on clay beds, but also on gypsum bedrock. They result from saturated water brought to the surface through

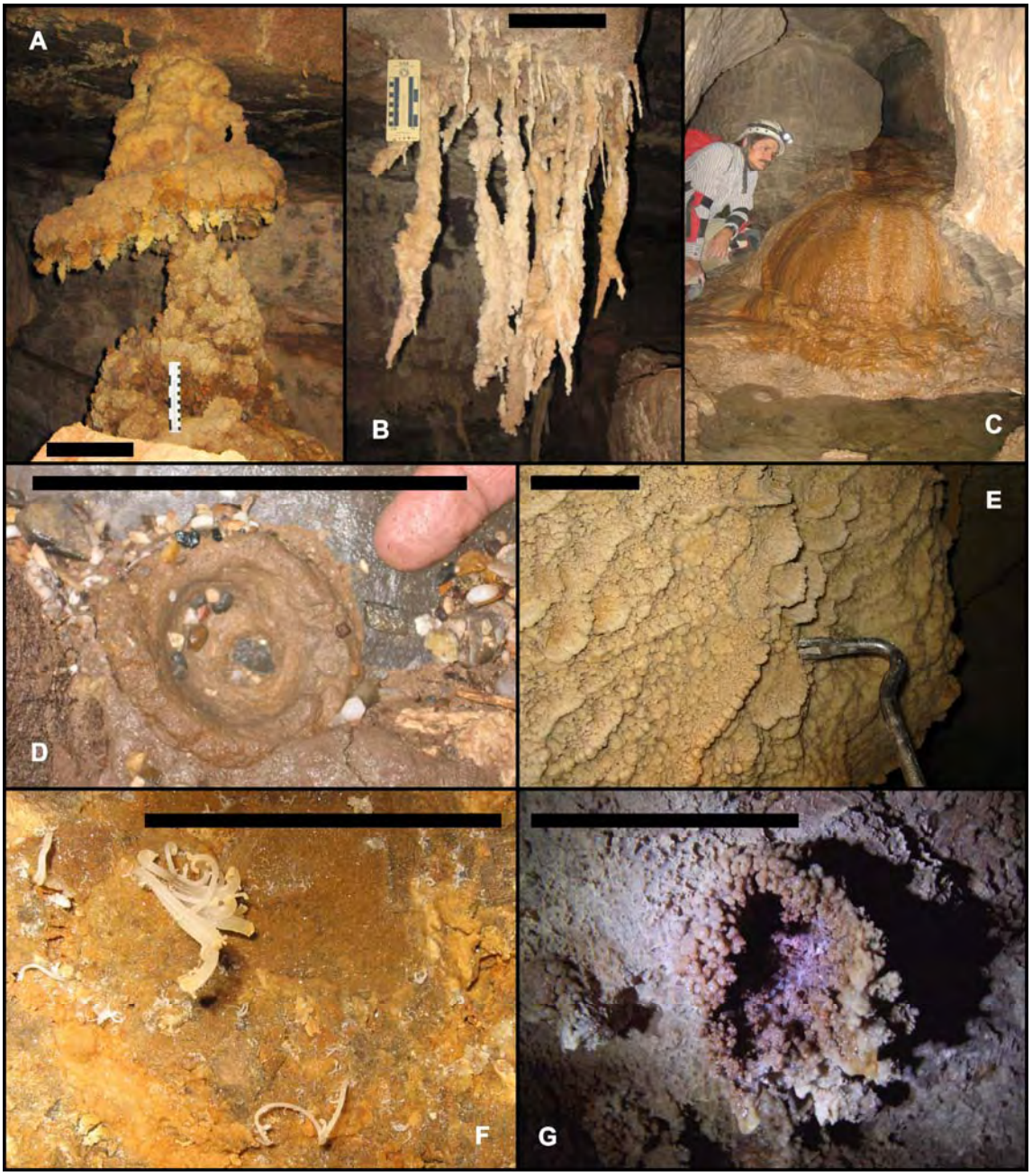

Fig. II.9: Speleothems in gypsum caves within the study area are extensive and diverse. A) gypsum trays (Rocking Chair Cave); B) gypsum stalagmites (Rocking Chair Cave); C) calcite flowstone mound (Crystal Cave); D) conulite (Crystal Cave); E) calcite wall coatings (Billy the Kid Cave); F) gypsum flowers (unnamed cave); and G) shower head (Whirlpool Cave). Note: all black scale bars are 20 cm long.

capillary action, where growth and persistence depends on the humidity, which can change seasonally (Hill and Forti, 1997). Crusts are abundant in the gypsum plains (Fig. II.9e) and often cover tens of square meters in sheet-like deposits. Others are linear, forming to either side of joints or seams. Crusts have been attributed to seepage of saturated water along cracks or seams (Hill and Forti, 1997). As in carbonate caves, boxwork forms where mineral precipitation from saturated water fills cracks that are later exposed as positive relief features due to removal of more soluble host rock. Gypsum and calcite rims and crusts (Fig. II.9e) with growth oriented toward nearby entrances were observed throughout the study area, where corrosion-translocation of condensation waters or capillary seepage move saturated water to an edge extending into a passage near an entrance. Dry air entering the cave enhances evaporation along the edge, resulting in directional rim deposits.

Gypsum trays, gypsum flour, a showerhead, and a conulite have also been observed in the gypsum plain. Gypsum trays are sprays or clusters of coralloids, popcorn, and frostwork ending in a flat, horizontal, tray-like surface (Hill and Forti, 1997). Trays are found in Torgac, Rocking Chair (Fig. II.9a), and Parks Ranch caves. Calaforra and Forti (1997) described simultaneous condensation and evaporation, a stable water supply, and a consistent airflow as conditions necessary for the unique morphology of trays. Gypsum flour was described by Calaforra and Forti (1997) as a deposit forming from the evaporation of saturated capillary water and subsequent precipitation of microscopic gypsum crystals on cave walls. In Whirlpool Cave a showerhead was observed (Fig. II.9g), which is an upside down cone, 15 cm in diameter and 10 cm in height. The walls are formed of corraloid deposits resulting from constant seepage of saturated waters

along the edges. A conulite, 5 cm wide and 4 cm deep, was observed near the lowest level of Crystal Cave. It formed from carbonate cementation of sediments in a sediment bank beneath a carbonate saturated drip. A portion of the sediment bank in which it formed has washed away, leaving it sitting on selenite bedrock.

SUMMARY

Evaporite karst development within New Mexico and Far West Texas is extensive and reflects a complex speleogenetic evolution for the entire region. Both hypogenic and epigenic caves are common throughout the region, including some of the most extensive gypsum caves known in the world, outside the Western Ukraine. Although this study reports many occurrences of hypogenic karst or epigenic overprinting on hypogenic caves, purely epigenic caves are extremely abundant. However, most of the epigenic caves are small, laterally limited features developing in equilibrium with the modern environment, hence they have not received the same attention by caving projects within the region. The survey bias towards larger, more complex caves, brecciation and collapse features (both natural and anthropogenic) inherently creates a database that is dominated by polygenetic karst features. Hypogenic speleogenesis is extremely important in the diagenetic evolution of the region, but the entire system should be viewed as a diagenetic continuum reflecting a constantly evolving hydrologic system. Observed karst development not only involves the complex interaction of hypogenic and epigenic hydrologic processes, but also the complete diagenetic history of the host rock as it has evolved since deposition.

Although only briefly mentioned in this study, reported evaporite karst is biologically diverse. Diverse assemblages of invertebrate species are observed in most caves suggesting that these systems are biologically rich habitats. Many vertebrate species commonly live in the entrance areas of the caves or frequently enter them in search of water in this arid climate. Numerous caves serve as winter hibernaculums and/or summer maternity roosts for bats. Tiger salamanders are commonly observed in caves throughout the entire region. Crayfish and amphipods have been observed in active stream caves, which may represent unique populations. Complex and diverse microbial communities have recently been recognized in many caves.

The complex speleogenesis in evaporite rocks within New Mexico and Far West Texas suggests that this region is vastly understudied and even underappreciated. The occurrence of abundant and often unique speleothems suggests a need for numerous secondary mineral studies. The diverse and complex cave systems suggest that many studies need to be conducted on the hydrologic and geologic controls on cave development within the region. Studies of the speleogenetic evolution of the entire region could provide substantial information on paleoclimate in what is now the arid southwest. The recent discovery of significant gypsum caves suggests that the opportunity to explore, map and study many new caves in the region is great. The evaporite karst of New Mexico and Far West Texas represents an understudied, complex speleogenetic system that continues to evolve.

CHAPTER III:
HYPOGENIC SPELEOGENESIS WITHIN SEVEN RIVERS EVAPORITES: COFFEE CAVE, EDDY COUNTY, NEW MEXICO

ABSTRACT

Coffee Cave, located in the lower Pecos region of southeastern New Mexico, illustrates processes of hypogenic speleogenesis in the middle Permian Seven Rivers Formation. Coffee Cave is a rectilinear gypsum maze cave with at least four stratigraphically-distinct horizons of development. Morphological features throughout the cave provide unequivocal evidence of hypogenic ascending speleogenesis in a confined aquifer system driven by mixed (forced and free) convection. Morphologic features in individual cave storeys include a complete suite that defines original rising flow paths, ranging from inlets for hypogenic fluids (feeders) through transitional forms (rising wall channels) to ceiling half-tube flow features and fluid outlets (cupolas and exposed overlying beds). Passage morphology does not support origins based on epigenic processes and lateral development, although the presence of fine-grained sediments in the cave suggests minimal overprinting by backflooding. Feeder distributions show a lateral shift in ascending fluids, with decreasing dissolutional development in upper storeys. It is likely that additional hypogenic karst phenomena are present in the vicinity of Coffee Cave because regional hydrologic conditions are optimum for confined speleogenesis, with artesian discharge still active in the region.

INTRODUCTION

Coffee Cave is located on the east side of the Pecos River valley, approximately 20 km north of Carlsbad, New Mexico at the base of the McMillan Escarpment. The cave is formed in the evaporite facies belt of the Seven Rivers Formation (Fig. III.1). Evaporite karst development is extensive throughout the lower Pecos region, not only in the Seven Rivers Formation, but also in other Permian evaporite facies of the Artesia Group (including the Seven Rivers), and the Yeso, San Andres, Castile, Salado and Rustler Formations. Numerous filled sinkholes and caves have been documented within a range that extends several km east and west of the Pecos River, and from Texas to as far north as Santa Rosa in east-central New Mexico. Most solutional openings are relatively small and not humanly enterable, but many features are extensive with complex morphologies, suggestive of multiple phases of speleogenesis. Cave patterns and abundant diagnostic morphologic features at meso-scale within individual caves appear to be the result of hypogenic, largely confined, speleogenesis, while cave sediments and minor entrenchment in some caves suggest a later phase of unconfined development. Although hypogenic features are seen in many caves within the region, this paper will focus on examples from Coffee Cave in relation to the current understanding of regional hydrology and speleogenesis in the Seven Rivers Formation.

Evaporite karst development within the Seven Rivers Formation, as with most evaporite karst phenomena in the United States, has not been thoroughly investigated. Most cave development within the Seven Rivers Formation has only been documented in anecdotal reports (Eaton, 1987; Belski, 1992; Lee, 1996), although evaporite karst has been recognized in association with regional aquifers (Hendrickson and Jones, 1952) and

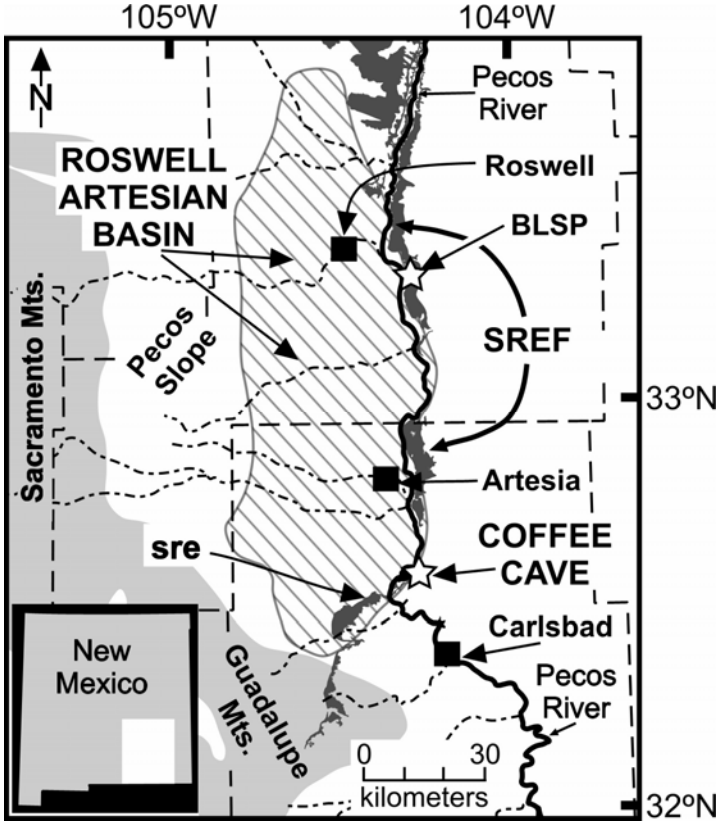

Fig. III.1: Regional map delineating the Roswell Artesian Basin, outcrop region of the Seven Rivers evaporite facies and location of Coffee Cave. SREF = Seven Rivers Evaporite Facies. sre = Seven Rivers Embayment. BLSP = Bottomless Lakes State Park (adapted from Kelley, 1971 and Land, 2003).

dam leakage along the Pecos River (Cox, 1967). The occurrence of large gypsum sinkholes at Bottomless Lakes State Park near Roswell dramatically illustrates the occurrence of artesian speleogenesis within the Seven Rivers Formation (Quinlan et al., 1987; Land, 2003; 2006). Although poorly documented within the United States, hypogenic evaporite karst has been extensively studied in the Western Ukraine, where large maze caves have developed in confined conditions and were later breached by surface denudation and fluvial entrenchment (e.g. Klimchouk, 1996a; 2000a). Other

examples of hypogenic gypsum karst are known from Germany, Russia, Spain and United Kingdom (Klimchouk et al., 1996).

GEOLOGIC SETTING

The Seven Rivers Formation, along with the other four members of the Artesia Group, represents the backreef facies equivalent of the Capitan Reef, which defined the shelf margin of the Delaware Basin during middle Permian (Guadalupian) time (Fig. III.2, III.3). The Seven Rivers Formation consists predominantly of dolomite in its near-backreef setting in the Guadalupe Mountains, but becomes increasingly evaporitic further to the north on the Northwestern Shelf (Fig. III.2), changing facies into interbedded gypsum and red mudstone (Scholle et al., 2004). Guadalupian rocks were later buried by extensive deposition of late Permian (Ochoan) evaporites that filled the basin and surrounding shelf areas (Fig. III.3) (Bachman, 1984). By the end of the Permian, marine sedimentation had effectively ceased (Dickenson, 1981). During the early Triassic the entire area was uplifted above sea level and the Laramide Orogeny produced regional deformation limited to uplift (1-2 km), tilting to the east and broad anticlinal flexures (Horak, 1985). By the mid-Tertiary, Laramide compression had ceased and shifted to Basin and Range extension (Chapin and Cather, 1994). As a result of tectonism, regional dip of Guadalupian strata in this part of southeastern New Mexico is ~ 1 to 2° to the east and southeast (Fig. III.4), with broad flexures and abundant high angle fractures and joints exhibiting minimal offset. Since the late Permian, southeastern New Mexico has been dominated by fluvial erosion, associated sedimentation, and karstic dissolution (Kelley, 1971).

Fig. III.2: Paleogeographic reconstruction of southeastern New Mexico during the middle Permian, showing the depositional relationship between the Delaware Basin and the Northwest Shelf where Seven Rivers evaporite facies were deposited (adapted from Scholle et al., 2004).

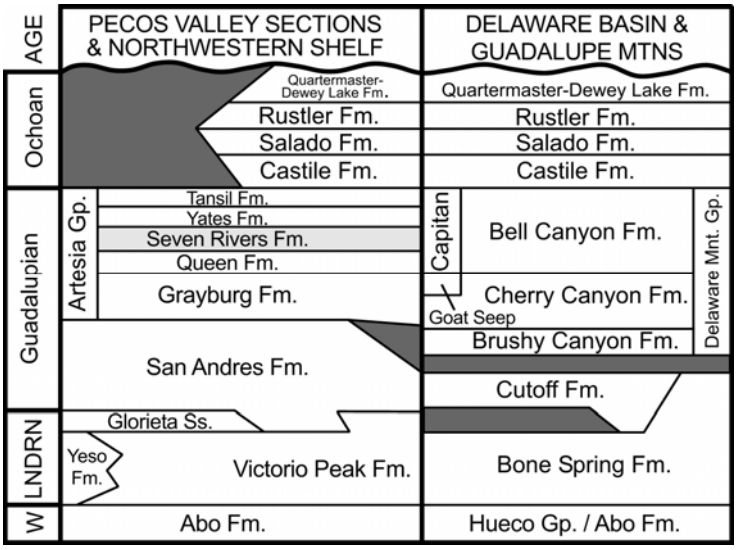

Fig. III.3: Stratigraphic chart of Permian facies in southeastern New Mexico with comparison of stratigraphic units within the Pecos Valley / Northwestern Shelf and the northern Delaware Basin / Guadalupe Mountains. Coffee Cave is developed in the Seven Rivers Formation (highlighted in gray). W = Wolfcampian; LNDRN = Leonardian (adapted from Zeigler, 2006).

The evaporite facies of the Seven Rivers Formation is up to 150 m thick in the study area, with anhydrite ($CaSO_4$) and bedded salt (NaCl) in the subsurface and gypsum ($CaSO_4 \cdot 2H_2O$) near the surface as a result of sulfate hydration (Kelley, 1971). Dolomite ($CaMg(CaCO_3)_2$) interbeds are common throughout the evaporite facies, forming laterally-continuous layers that thicken towards the reef and thin away from it. The entire gypsum sequence is capped by dolomite of the Azotea Tongue Member. Seven Rivers sulfates are generally white to grey, nodular to microcrystalline anhydrite/gypsum, forming individual beds ranging from centimeters to meters in thickness (Hill, 1996).

HYDROLOGIC SETTING

Coffee Cave is formed at the base of the McMillan Escarpment, which locally defines the eastern margin of the Pecos River Valley (Fig. III.4). The cave is located on the eastern shore of old Lake McMillan, an artificial impoundment that formerly stored water for the Carlsbad Irrigation District (CID). The original McMillan Dam was constructed in 1893, and the reservoir almost immediately began experiencing leakage problems through sinkholes formed in the lake bed. Water flowed through karstic conduits in the underlying Seven Rivers gypsum and returned to the Pecos River by discharge from springs downstream from the lake. Attempts to isolate the worst areas of sinkhole formation by construction of a dike along the eastern lake shore were only partially successful (Cox, 1967). McMillan Dam was breached in 1991 and the water allowed to flow into the newly constructed Brantley Reservoir, which is located in the dolomitic facies belt of the Seven Rivers Formation.

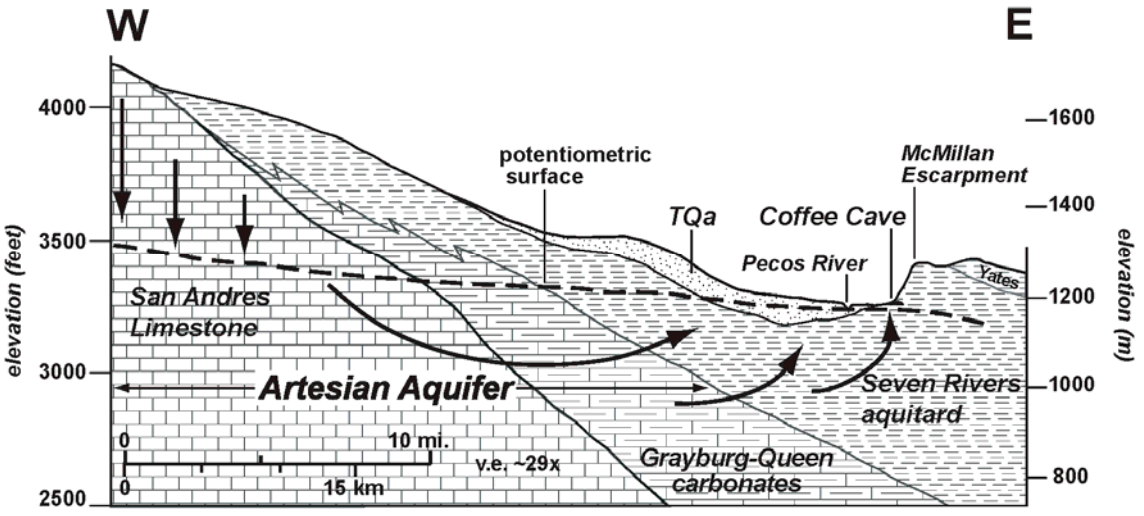

Fig. III.4: West-east hydrostratigraphic section across southern end of the Roswell Artesian Basin, showing relationship of Coffee Cave to the underlying artesian aquifer. The aquifer is recharged on the Pecos Slope to the west, where the San Andres and Artesia Group carbonates are exposed in outcrop. Groundwater flows downgradient toward the Pecos River and upward through Seven Rivers evaporites, which serve as a leaky confining unit for the aquifer. TQa = Tertiary and Quaternary alluvium, mostly floodplain deposits of the ancestral and modern Pecos River and lacustrine sediments in the bed of old Lake McMillan. Note vertical exaggeration is ~29X.

The Lake McMillan area lies near the southern end of the Roswell Basin, a karstic artesian aquifer system occupying several hundred square kilometers in the lower Pecos region of southeastern New Mexico (Fig. III.1). Groundwater in the Roswell Basin is stored in multiple highly porous and transmissive zones within Guadalupian carbonatesof the San Andres limestone and the overlying Grayburg and Queen Formations of the Artesia Group (Fig. III.4). Secondary porosity is developed in vuggy and cavernous limestones and intraformational solution-collapse breccias, the result of subsurface dissolution of evaporites. Recharge to the aquifer occurs on the Pecos Slope, a broad area east of the Sacramento Mountains where the San Andres limestone crops out. Redbeds

and gypsum of the Seven Rivers Formation serve as a leaky upper confining unit for the artesian aquifer (Fig. III.4) (Welder, 1983).

Water-bearing zones within the artesian aquifer system rise stratigraphically from north to south, occurring near the middle of the San Andres Formation in the northern Roswell Artesian Basin, and in carbonate rocks of the Grayburg Formation in the southern part of the Basin near Lake McMillan (Fig. III.4). The southern boundary of the Artesian Basin is not well-defined, but is usually located, somewhat arbitrarily, along the Seven Rivers Hills southwest of Lake McMillan.

The Seven Rivers confining unit is overlain by a shallow water table aquifer composed largely of Tertiary and Quaternary alluvial sediment. This material was deposited on the Pecos River floodplain as it migrated eastward due to uplift of the rising Sacramento Mountains to the west. A substantial percentage of recharge to the shallow aquifer is derived from upward flow through leaky confining beds from the underlying artesian aquifer (Welder, 1983). Very locally, in the vicinity of Lake McMillan, the Seven Rivers Formation makes up a large part of the shallow aquifer, probably as solution conduits in the Seven Rivers gypsum.

Since the inception of irrigated agriculture in the lower Pecos Valley in the early 20th century, most of the discharge from the artesian aquifer has been from irrigation wells. However, substantial natural discharge still occurs along the Pecos River, flowing upward through fractures and solution channels in the overlying Seven Rivers gypsum. This natural discharge has formed a complex of karst springs, sinkhole lakes, and extensive wetlands located along the west side of the Pecos River, east of the city of Roswell (Land, 2005). Along the eastern margin of the Pecos River valley southeast of

Roswell, discharge from the artesian aquifer has caused subsurface dissolution of gypsum and upward propagation of collapse chimneys, forming large gypsum cenotes at Bottomless Lakes State Park (Land, 2003; 2006).

In the early 20th century, many wells in the Artesian Basin flowed to the surface, with yields as high as 21,500 L/min (Welder, 1983). Although decades of intensive pumping have caused substantial declines in hydraulic head, many wells still display strong artesian flow (Land and Newton, 2007). As recently as the 1940s, wells in the vicinity of Lake McMillan flowed to the surface, with water levels reported up to 12 m above ground level (U.S. Geological Survey, 2007). Hydrologic conditions within the southern Artesian Basin thus continue to provide strong potential for hypogenic speleogenesis.

HYPOGENIC SPELEOGENESIS

Karst development is generally described in terms of geomorphology or hydrology, where dissolution is either hypogenic or epigenic (hypergenic). Epigenic speleogenesis, which is well-documented in karst literature, involves surficial features that act as insurgences for descending waters that may either recharge local groundwater or form integrated cave networks that function as subsurface bypass features for overland flow (e.g. Ford and Williams, 1989; White, 1988). Epigenic karst is well studied because it naturally forms numerous surface manifestations that are easily recognized and humanly accessible. In contrast, hypogenic speleogenesis is often overlooked because it forms without a direct surface connection, usually in confined or semi-confined settings. Hypogenic karst is often only exposed by surface denudation, and is often overprinted by epigenic processes (Palmer, 1991; Klimchouk, 1996a; 2000b). However, hypogenic

caves are occasionally intercepted during mining and drilling operations, where features show little or no overprinting (Kempe, 1996; Klimchouk, 2000b; 2003).

Hypogenic speleogenesis has been referred to broadly (e.g. deep-seated, confined, semi-confined, artesian, transverse) and is often attributed to specific fluid properties (e.g. sulfuric acid, hydrothermal), but in terms of hydrogeology, all types of hypogenic karst are similar. Hypogenic karst phenomena have been described in evaporitic and carbonate rocks. In evaporites, both maze caves (e.g. Klimchouk, 1996b; 2000a) and isolated voids (e.g. Kempe, 1996) are well-documented in Europe and have been attributed to confined speleogenesis. In mature carbonates, hypogenic karst has been associated with deep-seated processes involving acidic (e.g. Palmer, 1991; Lowe et al., 2000) and hydrothermal (e.g. Dublyansky, 2000) fluids. However, sulfuric acid and hydrothermal speleogenesis are simply special subsets where fluid chemistry and temperature, respectively, increase the solubility of host rock.

Following the suggestion of Ford (2006), we adopt the hydrogeological, rather than the geochemical, notion of hypogenic speleogenesis: "the formation of caves by water that recharges the soluble formation from underlying strata, driven by hydrostatic pressure or other sources of energy, independent of recharge from the overlying or immediately adjacent surface". Hypogenic karst can develop in any environment where fluids enter soluble host rock from below, being undersaturated with respect to the host rock or acquiring aggressiveness due to mixing with shallower flow systems (Klimchouk, 2000b; 2003). When the hydrogeologic framework is established for hypogenic transverse speleogenesis, dissolution may develop 3-D patterns with stratiform components, depending on the specific lithologic and structural host rock properties.

Pressurized fluids will attempt to migrate upward toward regions of lower pressure, often valleys or other topographic lows (Tóth, 1999), where the exact flow path depends on the permeability of local rock units and cross-formational fractures. Flow may be horizontal through relatively high permeability units, often sands or carbonates, or vertical through originally low permeability media, often soluble units (Klimchouk, 2000b; 2003).

Hypogenic processes may be the result of either forced or free convection of groundwater, or a combination of both. Forced convection is driven by differences in hydraulic head within an aquifer system. Free convection is driven by variability within fluid properties, which sets up density differences within the fluid. Lighter fluids rise and denser fluids sink, usually because of differences in salinity or temperature of the convecting fluids (e.g. Kohout, 1967; Kohout et al., 1988). Anderson and Kirkland (1980) physically modeled this process and showed that brine density convection could result in significant dissolution of soluble rocks, where undersaturated and saturated fluids simultaneously rise and sink, respectively, within a confined system. If limited connectivity occurs between source fluids and soluble rock, simultaneous flow can occur through the same pore throat, but in regions of greater connectivity separate flow paths for ascending and descending fluids may develop. Anderson and Kirkland (1980) considered brine density convection as the primary mechanism through which large vertical breccia pipes developed in the Delaware Basin, where fluids originating in a carbonate aquifer and undersaturated with respect to halite (NaCl) rose through overlying halite beds. As rising fluids dissolved halite, they became denser and subsequently sank back to the carbonate aquifer, thus undersaturated waters were continuously rejuvenated at the dissolution front. Kempe (1996) showed that speleogenesis driven by free

convection can create large cavities at the base of thick evaporitic formations with low fracture density. Klimchouk (2000a; 2000b) invoked mixed convection for early stages of confined transverse speleogenesis in fractured gypsum beds in the Western Ukraine, with free convection effects becoming increasingly important during subsequent stages, when head distribution within an aquifer system was homogenized due to increased hydraulic connectivity of aquiferous units.

Although maze caves have recently been shown to form in hypogenic confined settings (Klimchouk, 2003), traditional models involve epigenic speleogenesis. The classic mechanism of epigenic maze cave development was suggested by Palmer (1975; 2000), where water infiltrates from above through porous, insoluble rock. As the fluids descend they are evenly distributed through fractured soluble rock, such that individual passages enlarge at similar rates and converge to form maze patterns. Other epigenic models for maze cave development invoke epigenic fluids that are delivered laterally to fractured rock, primarily in the form of back flooding, with an associated shift from vadose to phreatic dissolution. Whether a maze cave is the result of hypogenic or epigenic speleogenesis, lithologic variability and fracturing dominate maze cave development.

Klimchouk (2000a; 2003) and Frumkin and Fischhendler (2005) have described specific morphological features that are indicative of hypogenic speleogenesis. The morphologic suite consists of feeders, master passages and outlets, which occur within individual storeys of hypogenic systems (Fig. III.5) (Klimchouk, 2003). Feeders, or risers, are the lowest elevation component within the suite and are characterized as vertical or near-vertical conduits through which undersaturated fluids rise from lower aquifers.

Feeders may form as isolated features or feature clusters. Master passages are the commonly explored portions of hypogenic caves, which are often extensive and form the largest passages because of the existence of laterally well-connected and extensive fracture networks encased within certain lithologic horizons. Outlets (i.e. cupolas and domes) occur at the highest elevations within a single storey of a hypogenic cave and form the discharge features for transverse flow to higher elevations / lower pressures. Isolated risers and outlets can converge through continued dissolution such that rift-like features may develop that connect storeys in a multi-storey, hypogenic system. Hypogenic caves form in sluggish flow conditions and show no evidence of fast-flowing fluids, but instead exhibit smooth walls with irregular solution pockets and residual pendants (Frumkin and Fischhendler, 2005), and various morphologic imprints of rising free convection circulation (Klimchouk, 2000b; 2003).

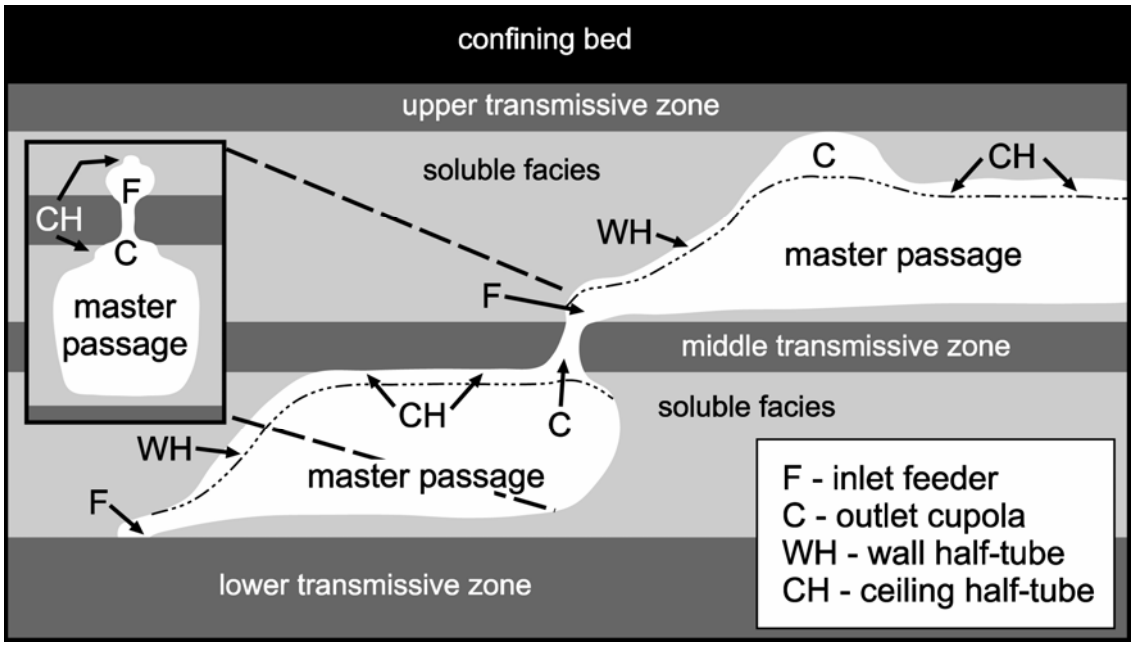

Fig. III.5: Diagrammatic representation of morphological feature suite indicative of hypogenic speleogenesis. Transmissive zones are dolomite and soluble beds are gypsum in Coffee Cave.

COFFEE CAVE

Recently, a resurvey of Coffee Cave was conducted in order to better document the cave's distribution and extent, lithologic variability and occurrence of morphological features indicative of hypogenic transverse speleogenesis. At present the lowermost storey, which comprises at least half of the known cave, based on the original survey (Belski, 1972), is flooded (Fig. III.6A).

Throughout most of the cave, fine-grained sediments and angular collapse blocks commonly cover the floor, obscuring much of the dissolutional floor morphology and displaying a bimodal distribution of allogenic sediment and autogenic breakdown. Passages proximal to the scarp edge have partially collapsed due to scarp retreat, creating large earth fissures on the land surface and a complex entrance network (Fig. III.7). The occurrence of abundant surface fissures beyond the known extent of Coffee Cave strongly suggests that numerous maze caves exist along the same erosional scarp, but most are largely blocked by breakdown. Several km to the east of Coffee Cave, clusters of caves occur within the Burton Flats area that exhibit similar morphologic features indicative of hypogenic transverse speleogenesis.

Most passages within the cave are roughly rectangular in cross-section with thin dolomite beds forming the ceiling, floors and intermittent ledges (Fig. III.6B, III.8). The cave is a three-dimensional maze with most passages oriented northwest and northeast, which probably represents a conjugate fracture set (Fig. III.6A). Most passages intercept at sharp angles, while many individual passages terminate in blind alcoves or narrow fractures, often recognized as feeders. Based on previous mapping, the lowermost storey appears to be the region of most intense lateral development (Fig. III.6A). Successively

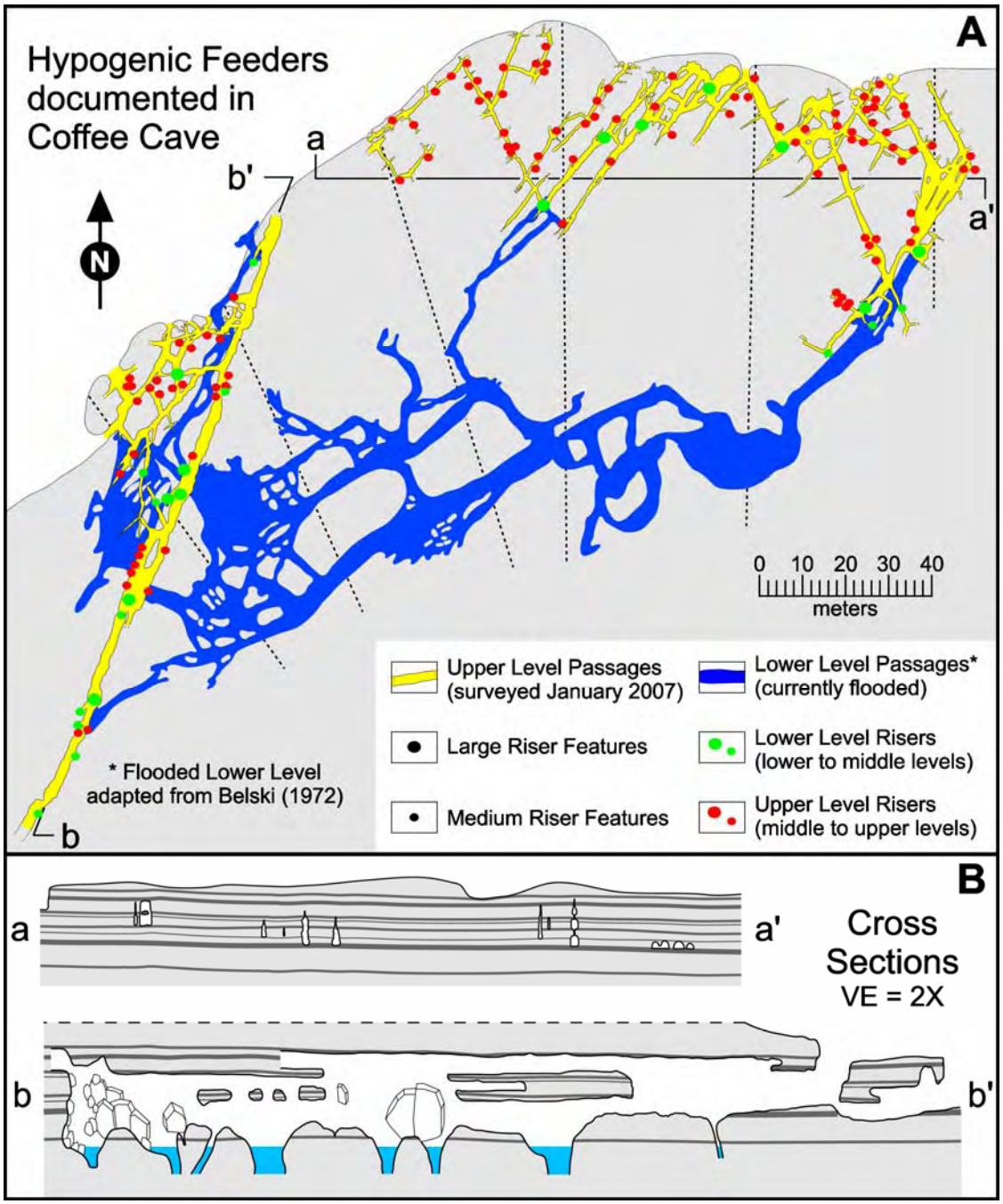

Fig. III.6: Geomorphic map of Coffee Cave. A) Plan view map of Coffee Cave showing maze passage morphology, hypogenic feeder distribution and delineation between lower flooded cave level and upper dry levels. The boundary between the gray and white regions along the northern edge of Coffee Cave represents the edge of the McMillan Escarpment.; B) Cross sections of Coffee Cave with 2X vertical exaggeration showing relationship of passage levels and dolomite interbeds (solid gray lines). Note that the dashed lines in Fig. III.6A delineate locations where passage width was measured perpendicular to the McMillan Escarpment for Fig. III.11.

Fig. III.7: McMillan escarpment showing large earth fissures (A) and complex entrance network (B).

higher storeys of the cave contain progressively smaller passages, creating at least four distinct cave storeys, although the two highest storeys are generally too small to be humanly accessed. In several regions, individual passages transect all four storeys forming major trunk passages, which are intermittently separated into distinct storeys (Fig. III.6B), while many regions contain upper storey passages that transect two or three storeys in limited areas. It should be emphasized that the designation of storeys within Coffee Cave refers only to distinct cave horizons that are lithologically separated and laterally extensive, which were formed concurrently under a constant, stable hydrologic regime. The term storey does not imply hydrologically distinct solutional events or levels related to changes in hydrologic conditions.

Most of the individual cave passages exhibit complex surficial sculpturing within individual gypsum beds and between different lithologies; however, no discernable patterns is common to epigenic caves with oriented scallops of similar shape and size were observed. Residual pendants are present throughout the cave. Additional morphological features indicative of rising transverse flow commonly occur on floors,

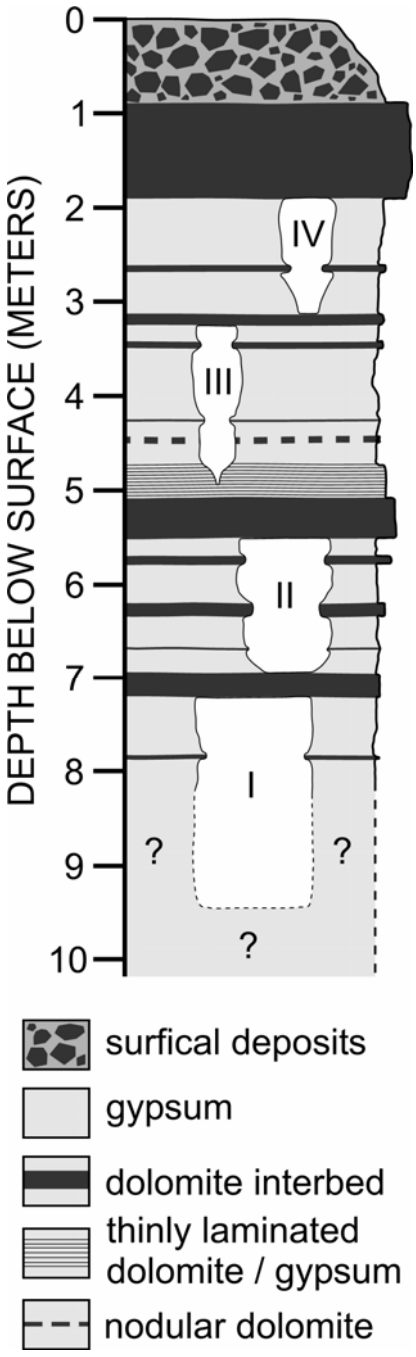

Fig. III.8: Composite lithologic section through Coffee Cave in relation to the four identified cave storeys (designated I – IV on diagram). Storeys II, III and IV represent the upper storeys that were resurveyed for this study. Storey I is currently flooded, hence lithology is unknown (presumably gypsum with dolomite interbeds). Passage cross-sections are average passage representations of distinct storeys and do not include connections between storeys.

walls and ceilings, including: 1) feeders, 2) rising wall channels, 3) cupolas, and 4) ceiling half-tubes. Generally, complex suites of features occur in a continuous series or in close proximity.

Feeders function as fluid inlet locations, either joining different storeys of a cave or terminating blindly in bedrock, generally transmissive dolomite layers. Throughout Coffee Cave, feeders commonly occur as point source (Fig. III.9A,B,D), dense clusters (Fig. III.9F) or linear fissure-like features (Fig. III.9E). Point source feeders are individual features that generally form along dolomite / gypsum contacts in walls (Fig. III.9B) or at the margins of floors (Fig. III.9A,C). They are crudely conical features exhibiting an increase in aperture width toward cave passages that generally includes minor doming proximal to the open passage (Fig. III.9A,B,C). Feeder clusters commonly exist as a dense occurrence of small- to medium-sized feeders within a limited area, but individual feeders within clusters are morphologically similar to point feeders. Linear feeders develop along the axis of passages, forming narrow fissures along fractures, and are often associated with passages that are triangular in cross section and broaden upwards (Fig. III.10E). Linear feeders are laterally extensive, as compared to point feeders.

Cupolas are well-documented in the speleogenetic literature as domal ceiling features (Osborne, 2004). However, for the purpose of this paper they are viewed in a broader sense that encompasses traditional cupolas as well as domes and similar outlet features that may either be closed or open, concave ceiling features. Cupolas are generally elliptical in plan view (Fig. III.10A), but may range from near-circular to lenticular. Cupola height ranges from centimeters to meters with inner walls that may vary from

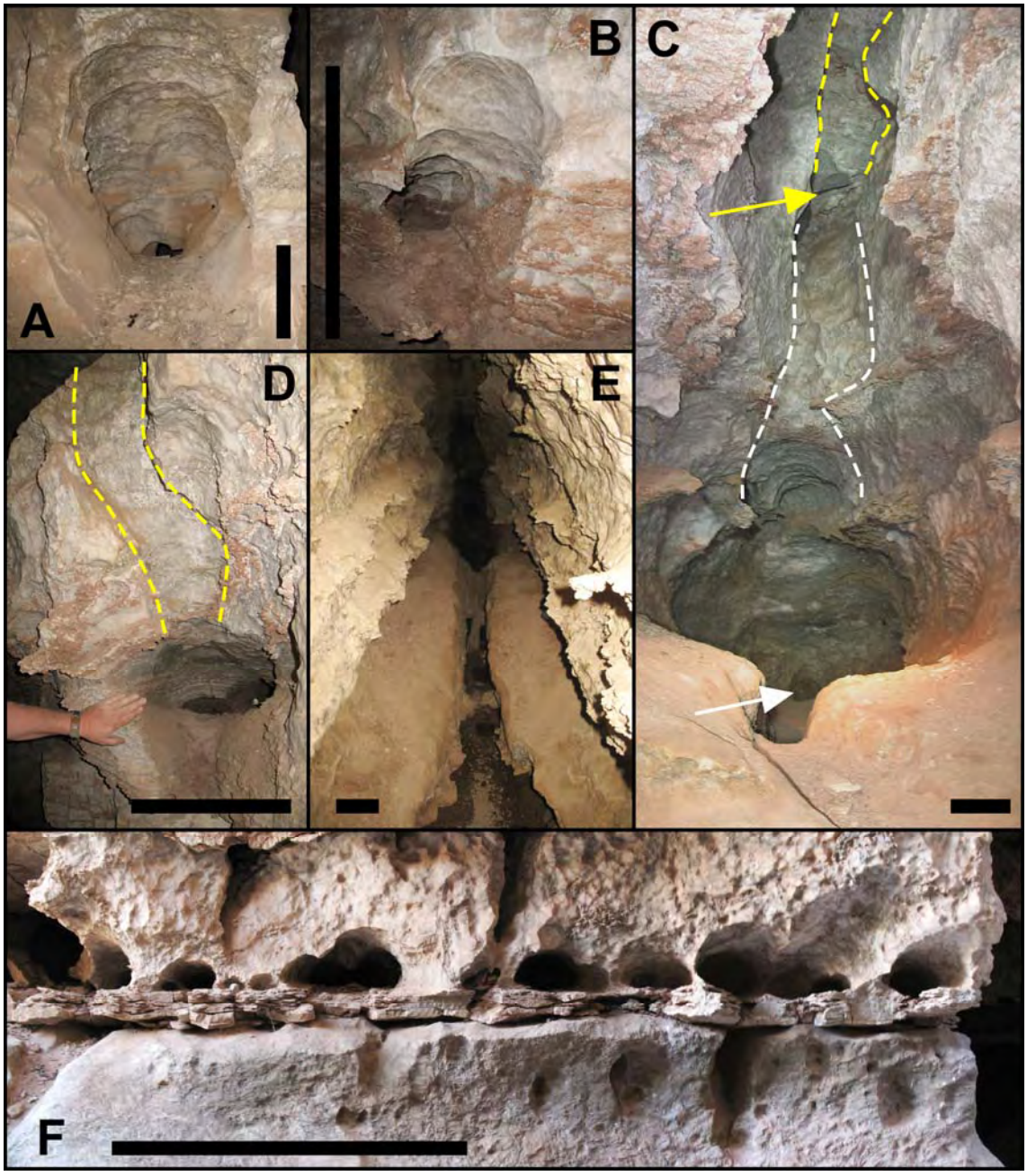

Fig. III.9: Feeder features in Coffee Cave. Black scale bars in figures are all approximately 0.5 m and camera angle is near-horizontal in all feeder features photos. A) point source feeder showing prominent doming morphology proximal to master passage ; B) typical feeder showing development at the top of a dolomitic interbed ; C) complete hypogenic morphologic suite showing riser (white arrow), wall channel (dashed white lines), ceiling channel (solid yellow lines) and outlet (yellow arrow); D) well developed wall riser with associated wall channel (dashed yellow lines); E) linear riser developed along axis of master passage; F) dense cluster of small feeders above dolomite interbed with minor vadose overprinting below dolomite interbed.

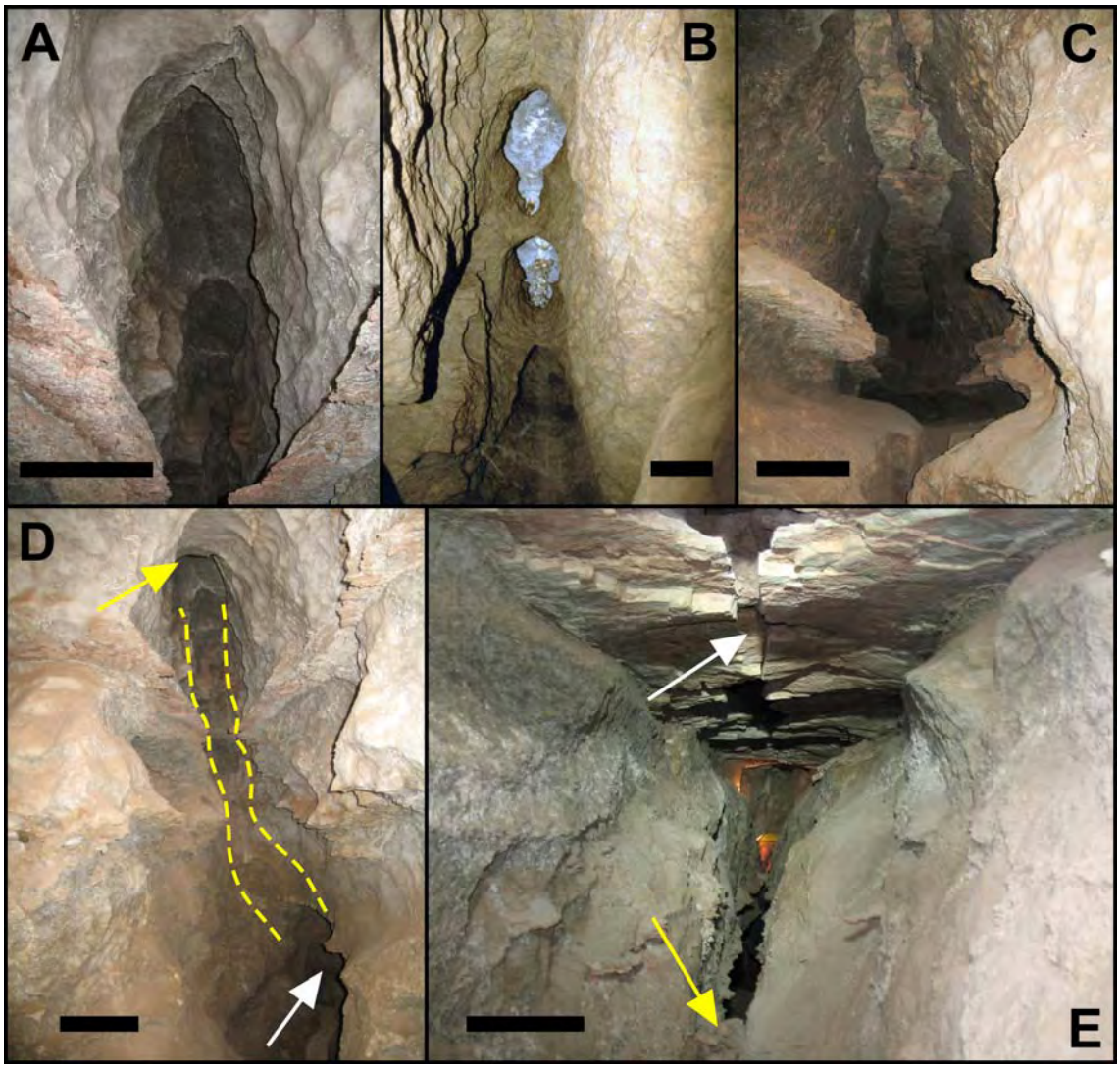

Fig. III.10: Outlet features in Coffee Cave. Black scale bars in figures are all approximately 0.5 m. A) series of typical ceiling cupolas (camera angle is ~60° up from horizontal, looking towards the ceiling); B) series of cupolas that are in the process of coalescing (camera angle is ~70° up from horizontal, looking toward the ceiling); C) ceiling channel formed by complete coalescing of serial cupolas (camera angle is ~30° up from horizontal, looking towards the ceiling); D) complete hypogenic morphologic suite showing riser (white arrow), wall channel (yellow dashed lines), and ceiling cupola (yellow arrow) (camera angle is roughly horizontal); E) rift-like passage showing linear feeder (yellow arrow), triangular passage and upper dolomite bed that has partially collapsed due to loss of buoyant support (white arrow) (camera angle is roughly horizontal). Fig. III.10B is from Fuchslabyrinth Cave, Baden-Würtenberg, Germany (developed in vertically heterogeneous beds of Triassic limestone showing lithologic variability between two distinct beds), instead of Coffee Cave, in order to better illustrate the intermediate stage of cupola coalescence.

gently sloping to near vertical. Closed cupolas, which fall within the traditional descriptions of cupolas and domes, are concave features where the entire inner surface is gypsum bedrock, with the upper surface commonly formed along the contact of transmissive dolomite interbeds (Fig. III.10C). In contrast, open cupolas have openings in upper surfaces, either in the center or offset to one side. Cupolas are recognizable in those passages where the ceiling is still within gypsum (Fig. III.10A,D). In many passages the next upper dolomite bed is continuously exposed at the ceiling but it is apparent that these exposures have formed by merging of closely spaced cupolas (Fig. III.10B,C).

Half-tubes (rising wall channels, ceiling channels) are elongate concave structures that occur on ceilings and walls and vary from shallow indentations to deep, incised channels, ranging in width from centimeters to meters with corresponding depths. Generally, half-tubes exhibit smooth rounded interior surfaces and abrupt, well-defined margins with adjacent walls or ceilings (Fig. III.9D, III.10C). Features on walls are generally vertically oriented, but may shift laterally from bottom to top (Fig. III.9D). Ceiling features are usually developed on the underside of dolomite layers and commonly display irregular margins resulting from the coalescing of serial cupolas (Fig. III.10B,C). When ceiling half-tubes do not form beneath dolomite beds, they gently slope up to an adjoining half-tube that contacts dolomite. All observed wall half-tubes join with feeders at lower elevations (Fig. III.9C,D) and converge with ceiling half-tubes at higher elevations (Fig. III.10D). Ceiling half-tubes join with cupolas, which when open form the lower surface of risers to the next higher cave storey; however, when cupolas are closed they appear as deeper concave structures within a continuous ceiling half-tube (Fig.

III.10A,B). Both wall and ceiling half-tubes commonly converge from smaller to larger features forming a complex network.

Cupolas, feeders and half-tubes form a composite suite of morphological features throughout Coffee Cave. Therefore, during the resurvey of Coffee Cave, feeders were mapped as a proxy for the distribution of this feature suite (Fig. III.6A). Small feeders (less than 10 cm wide) are abundant throughout the cave and could not be represented at the scale of mapping; therefore, mapping was limited to medium (0.1 to 1.0 m diameter) and large (>1.0 m diameter) features. During mapping of feeders, 25 features were identified that connect the lower flooded portion of the cave to the upper storeys, including 12 medium and 13 large feeders. In the upper storeys of the cave, 107 features were identified, all less than 1 m wide. It is probable that many more feeders exist, but they are either obscured by breakdown and sediments or are located in passages that were too small to be surveyed. Feeders are well distributed, but there appears to be a northward shift in feeder abundance from the lower storey to the upper storeys.

Observations within Coffee Cave during the first quarter of 2007 indicate that water levels in the cave have risen by at least 2 m in less than 3 months. This rise in water levels may be the result of an increase in hydraulic head in the artesian aquifer, or it may reflect a rise in water levels in the surficial aquifer. Both factors may be in play in the vicinity of the cave, since the water table aquifer is recharged to a large extent by upward leakage from the underlying artesian aquifer. Hydraulic head in the Artesian Basin has been rising since the late 1970s (Land and Newton, 2007), and flooding of the lower storeys of Coffee Cave may thus represent in part increased artesian flow from the underlying Grayburg Formation (Fig. III.4).

DISCUSSION

Coffee Cave is a classic rectilinear maze cave with at least four stratigraphic storeys of development and abundant morphologic features suggestive of hypogenic transverse origins with the pronounced role of free convection dissolution. Hydrologically, Coffee Cave is located at the southern end of the Roswell Artesian Basin (Fig. III.1), where artesian discharge from wells and springs is well-documented (e.g. Cox, 1967; Welder, 1983). Although water extraction for agricultural use has significantly lowered groundwater levels in the region over the previous century, artesian discharge is still active. Submerged springs in the gypsum cenotes at Bottomless Lakes State Park continue to discharge significant volumes of artesian waters (Land, 2003; 2006), while free-flowing wells in the Coffee Cave area have been reported as recently as the 1940s (U.S. Geological Survey, 2007). In addition to the hydrologic regime in which Coffee Cave is located, interbedded dolomite and gypsum (Fig. III.6B, 8), coupled with extensive tectonic fracturing in the Lake McMillan area, make the Seven Rivers Formation ideal for the development of multi-storey hypogenic maze caves. However, prior to this study, hypogenic origins for gypsum caves were not reported in this region.

It is instructive to emphasize the difference in the degree of karstification and slope geomorphology between the gypsiferous Seven Rivers outcrops within the Pecos River Valley and outcrops in the Seven Rivers Embayment (Fig. III.1) of the Guadalupe Mountains, west of the valley. In the Seven Rivers Embayment the Seven Rivers outcrops are extensive but largely intact with stable slopes, showing minimal signs of karstification, whereas within the Pecos River Valley and its vicinity the slopes are dramatically disturbed by gravitational processes with numerous collapse features,

apparently induced by the high degree of karst development in the subsurface. These morphologies indicate intense karstification within the Seven Rivers sequence beneath the migrating and incising valley, induced by rising artesian flow (Fig. III.1), in agreement with the general concept of speleogenesis in confined settings (Klimchouk, 2000b; 2003).

Coffee Cave has traditionally been characterized as a maze cave formed by back flooding along the Pecos River associated with the construction of Lake McMillan in the late 19th century. In this model, flooding produced dissolution along fractures proximal to the scarp. Reports of leakage from Lake McMillan through karst conduits within the Seven Rivers Formation (Cox, 1967) were used as evidence for the origin of Coffee Cave through epigenic, flooding processes (alternatively, this leakage can be perfectly explained by the presence of hypogenic conduit systems). Sediments and organic detritus within Coffee Cave were used as further evidence to support an origin through back flooding. Therefore, any new model for the proposed speleogenesis of Coffee Cave must consider previous, although unpublished, interpretations of cave origin.

Caves exhibiting maze patterns have been shown to form in both epigenic and hypogenic settings; however, the complete morphological feature suite, indicative of rising flow and the role of free convection, observed in Coffee Cave (i.e. feeders, half-tubes, and outlet cupolas) has only been reported from hypogenic caves (Klimchouk, 2003; Frumkin and Fischhendler, 2005). If Coffee Cave had formed by back flooding, as suggested by the presence of allogenic sediments, then the cave should exhibit an average decrease in passage aperture width away from McMillan Escarpment, because high gypsum solubility promotes increased dissolution proximal to the source in epigenic settings

(Klimchouk, 2000c). However, mapping in Coffee Cave has revealed that there is no systematic increase in passage width toward the scarp face. Analyses of passage width in relation to distance from the escarpment indicate that passage width actually increases with distance from the scarp (Fig. III.11). Because of presence of organic detritus in the cave, it is likely that waters derived from Lake McMillan have modified Coffee Cave to some extent, primarily through sediment infilling, but lake waters do not appear to have significantly modified the cave through dissolution. Most of the overprinting of Coffee Cave's hypogenic origin is the result of scarp failure and retreat, which has produced the complex collapse entrance area along the scarp face, including more than thirty documented entrances (Fig. III.6A).

The morphologic feature suite observed in Coffee Cave, as well as the presence of wall pendants and the absence of discernable scallop patterns, strongly supports a model of hypogenic speleogenesis driven by rising cross-formational flow as a significant part

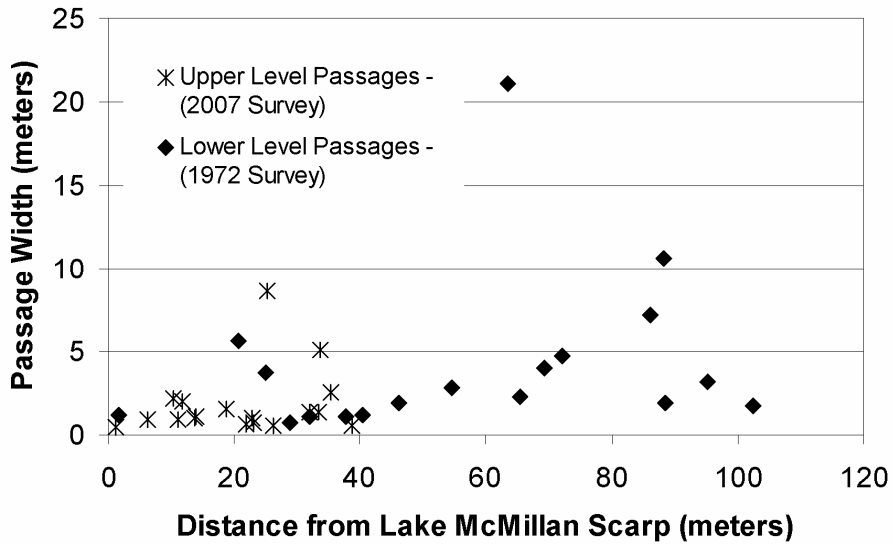

Fig. III.11: Plot showing relationship between passage width and distance from McMillan Escarpment. Note that the dashed lines in Fig. III.6A delineate locations where passage widths were measured perpendicular to the McMillan Escarpment.

of the evolution of karst features in the Lake McMillan area. It is suggested here that the cave was formed under confined conditions, when the floor of the Pecos Valley was at considerably higher elevations than at present. The distribution of feeders and the overall morphology of Coffee Cave are remarkably similar to well-documented hypogenic caves in Miocene gypsum deposits of the Western Ukraine, such as Ozerna Cave (Fig. III.12) (Klimchouk, 1991). Coffee Cave and the part of Ozerna Cave on the figure both show a lateral shift in passage development at adjacent storeys, where clusters of conduits at the lower storey served as a feeding subsystem and rising fluids have migrated laterally through the upper storey. Lateral migration results from discordance in distribution of water-bearing zones in the underlying (feeding) aquifer and preferential paths for discharge through the leaky confining units (argillaceous gypsum above the upper dolomite bed in Coffee Cave). In the sluggish flow conditions of the confined system, density differences readily developed when fluids rose from the dolomite beds through gypsum, so that free convection cells operated extensively. This is evidenced by characteristic morphologic imprints of rising buoyant currents (ear-like orifices of narrowing of feeders to depth due to shielding by sinking convection limbs. The feeders, rising wall channels, ceiling channels and cupolas) and characteristic similarity between Coffee Cave and well-documented hypogenic transverse caves elsewhere further supports the role of hypogene processes in the origin of Coffee Cave.

A conceptual model for the speleogenesis of Coffee Cave has been developed (Fig. III.13). Prior to karst development, evaporite facies in the Seven Rivers Formation near Lake McMillan provided a leaky seal for confined artesian fluids in the Roswell Basin aquifer (Fig. III.13A). Groundwater initially flowed downgradient through porous

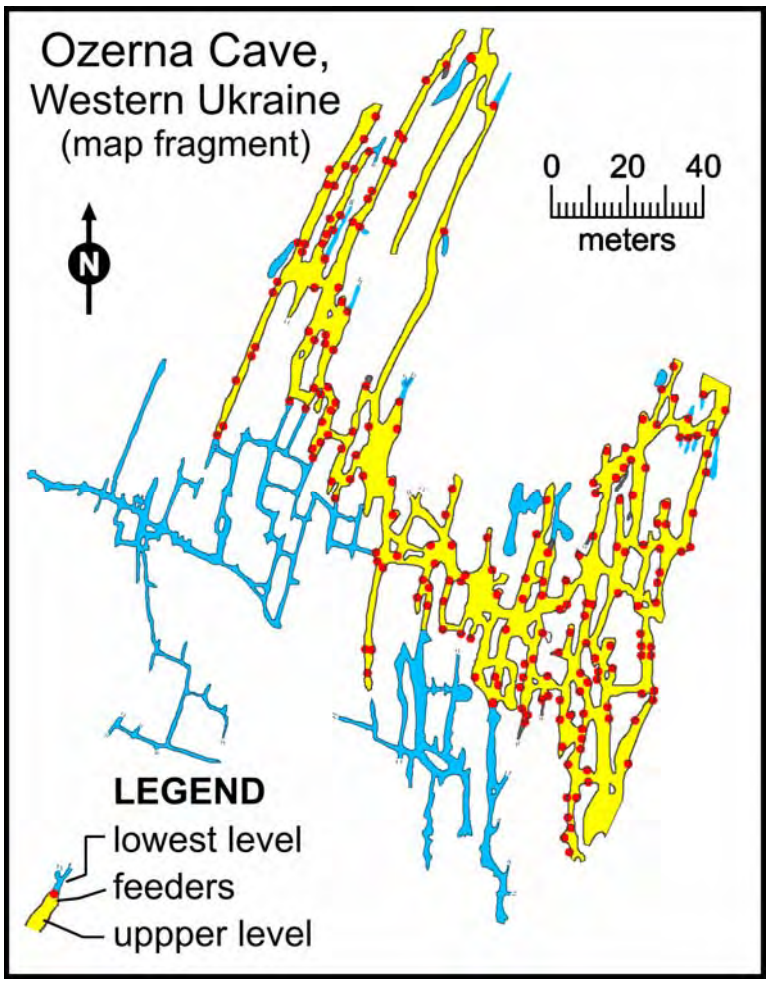

Fig. III.12: Map fragment from Ozerna Cave, Western Ukraine, showing cave morphology and feeder distribution (Klimchouk, 1991). Note the similarities with Coffee Cave depicted in Fig. III.6A.

carbonates of the Grayburg and San Andres Formations and rose toward the Pecos River valley. Beneath the valley, karst initiation began to develop vertical flow paths along fractures in the evaporite facies (Fig. III.13B). Highly fractured dolomite layers within the Seven Rivers Formation served as laterally transmissive units to distribute undersaturated, aggressive waters to available fissures in the vertically adjacent gypsum beds. Locally, rising conduits could have developed even without forced flow through guiding fractures in the gypsum, solely by buoyancy-driven dissolution. Controlled by

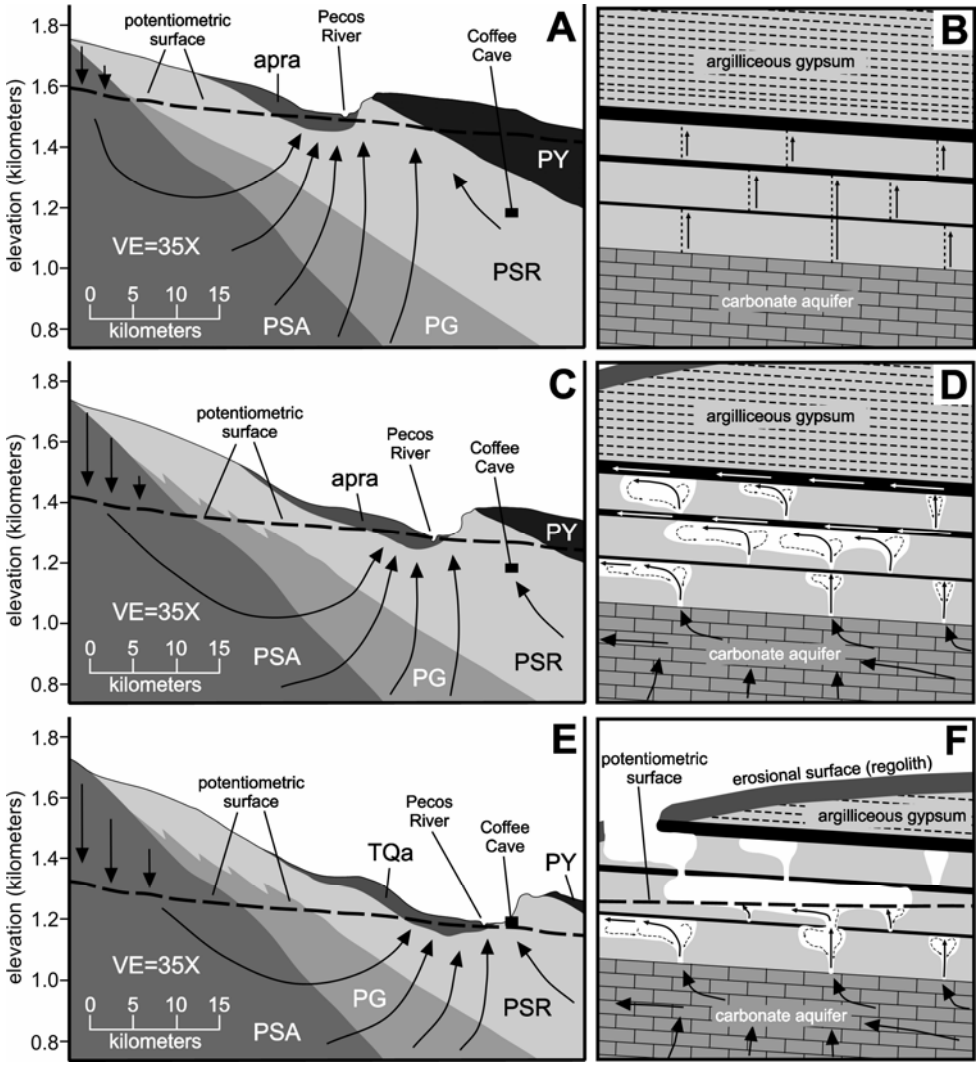

Fig. III.13: Conceptual model for the speleogenetic evolution of Coffee Cave in relation to the eastward migration of the Pecos River valley, associated surface denudation and evolving groundwater flow paths. A) regional conceptualization of groundwater circulation (solid black lines) in mid-to-late Tertiary time; B) local conceptualization of hydrology in Coffee Cave region, in relation to Fig. III.13A, showing forced flow (solid black lines) along vertical fractures in the Seven Rivers Formation; C) regional conceptualization of groundwater circulation in mid-to-late Quaternary when Coffee Cave was primarily forming; D) local conceptualization of Coffee Cave in relation to Fig. III.13C, showing forced convection (solid arrows) and free convection (dashed arrows) circulation involved in speleogenesis; E) current hydrologic regime in the lower Pecos River Valley; and F) conceptualization of the current hydrologic regime of Coffee Cave after surficial breaching, relating to Fig. III.13E. Note: Figures B, D and F are schematic illustratoins that are not drawn to scale, and do not represent the actual storeys of cave development, due to the resolution of the figure. PSA=Permian San Andres Fm; PG=Permian Grayburg Fm; PSR=Permian Seven Rivers Fm; PY=Permian Yates Fm; apra = ancestral Pecos River alluvium; TQa= Tertiary and Quaternary alluvium.

arrangement of fractures within a gypsum-dolomite intercalated sequence, the multi-storey maze cave developed (Fig. III.13C, D). Eventually, confinement was breached by the entrenching Pecos River Valley, and primary conduits were established for artesian discharge, most likely along a limited number of flow paths (Fig. III.13E, F). Base levels within the region lowered and the cave was exposed to epigenic processes. During this final phase, minor vadose overprinting and collapse of thin dolomite beds occurred due to loss of buoyant support (Fig. III.10E). Recently, in the 20th century, flooding of the cave through the construction of Lake McMillan introduced allogenic sediments. Today, continued scarp retreat has created a complex entrance network.

CONCLUSIONS

Coffee Cave provides direct evidence for hypogenic transverse speleogenesis driven by cross-formational flow and density convection within the Seven RiversFormation and more broadly in the Delaware Basin region of southeastern New Mexico. The complex, three-dimensional maze pattern of the cave is suggestive of hypogenic origin where non-competitive confined flow resulted in uniform dissolution along planes of brittle deformation. The complete suite of observed morphological features within the cave provides unequivocal evidence of hypogenic speleogenesis by rising mixed-convection flow, where smooth walls and concave morphologies delineate previous free convection cells. The presence of dolomite interbeds and regional fracturing makes the Seven Rivers Formation ideal for development of hypogenic caves; however, natural heterogeneities in most carbonate and sulfate rocks is sufficient for hypogenic speleogenesis in the proper hydrologic regime. The occurrence of abundant surface fissures beyond the known extent

of Coffee Cave suggests that numerous hypogenic, maze caves exist along the same erosional scarp, but most are largely blocked by breakdown. Moreover, clustered highly karstified fields exist beyond the scarp, although still within the broad limits of the Pecos Valley and within the evaporite facies of the Seven Rivers and Rustler Formations. These karstified fields (e.g. Burton Flats, Nash Draw) contain numerous caves lacking genetic relationships with the surface and are likely hypogenic systems that are currently being partially denuded. It is also feasible to assume that the leakage from Lake McMillan through karst conduits within the Seven Rivers Formation was related not to epigenic karst development but the presence of pre-existing hypogenic conduit systems beneath the valley.

Based on current and ongoing studies by the authors of karst development within the New Mexico / West Texas region, the significance of hypogenic speleogenesis appears to be poorly recognized. Karst development in other regional gypsum formations (i.e. Castile, Yeso, Rustler, and San Andres) includes numerous caves that are three dimensional mazes and/or contain complete suites of morphological features indicative of the role of density driven dissolution. However, these features are not limited to gypsum formations but have also been observed in carbonate karst within the region, including, but not limited to, the caves of the Guadalupe Mountains (e.g. Carlsbad Cavern, Lechuguilla Cave, McKittrick Hill caves). Although limestone caves of the Guadalupe Mountains have been attributed to sulfuric acid (H_2SO_4) speleogenesis, they are hypogenic caves not only by the source of acidity but first of all hydrologically. These caves are hypogenic transverse features containing morphologic suites indicative of rising flow and free convection effects. Therefore, the role of hypogenic speleogenesis is likely

to be extensive throughout the southwest United States, but is currently not recognized either because of extensive epigenic overprinting, misinterpretation, or because fluid chemistry (e.g. sulfuric acid) is proposed as the primary criterion for distinguishing hypogenic speleogenesis.

The identification of hypogenic speleogenesis within southeastern New Mexico, beyond the caves of the Guadalupe Mountains and breccia pipes within the Delaware Basin, suggests that more studies need to be conducted within the region, including re-evaluation of the origin of many individual caves and karst regions. The implications of an improved understanding of hypogenic speleogenesis within the region will have significant impacts on delineating areas of potential engineering geohazards, investigation of petroleum resources, mineral resources and groundwater behavior associated with karst. Ultimately, recognition of the importance of mixed convection processes related to hypogenic dissolution will enable the development of improved models for the speleogenetic evolution and basin diagenesis of the entire Delaware Basin region.

ACKNOWLEDGEMENTS

The authors wish to express their appreciation to the numerous individuals involved throughout this project. The resurvey of Coffee Cave was conducted by the authors with help from Stan Allison, Paul Burger, Jon Jasper, Lucas Middleton and Pat Seiser. Dave Belski, Jim Goodbar and Ray Nance provided essential information related to regional cave development and existing cave surveys within the area. Reviewers David Levy and

Paul Burger are thanked for their useful comments which helped to improve the manuscript.

CHAPTER IV:
CASTILE EVPORITE KARST POTENTIAL MAP OF THE GYPSUM PLAIN, EDDY COUNTY, NEW MEXICO AND CULBERSON COUNTY, TEXAS: A GIS METHODOLOGICAL COMPARISON

ABSTRACT

Castile Formation gypsum crops out over ~1,800 km^2 in the western Delaware Basin where it forms the majority of the Gypsum Plain. Karst development is well recognized in the Gypsum Plain (i.e. filled and open sinkholes with associated caves); however, the spatial occurrence has been poorly known. In order to evaluate the extent and distribution of karst development within the Castile portion of the Gypsum Plain, combined field and GIS (Geographic Information System) studies were conducted, which enable a first approximation of regional speleogenesis and delineate karst-related natural resources for management. Field studies included physical mapping of 50, 1-km^2 sites, including identification of karst features (sinkholes, caves and springs) and geomorphic mapping. GIS-based studies involved analyses of karst features based on public data, including DEM (Digital Elevation Model), DRG (Digital Raster Graphic) and DOQ (Digital Orthophoto Quad) formats. GIS analyses consistently underestimate the actual extent and density of karst development, based on karst features identified during field studies. However, DOQ analyses coupled with field studies appears to produce accurate models of karst development. As a result, a karst potential map of the Castile outcrop region was developed which reveals that karst development within the Castile Formation is highly

clustered. Approximately 40% of the region effectively exhibits no karst development (<1 feature/km^2). Two small regions (<3 km^2 each) display intense karst development (>40 features/km^2) located within the northern extent of the Gypsum Plain, while many regions of significant karst development (>15 features/km^2) are distributed more widely. The clustered distribution of karst development suggests that speleogenesis within the Castile Formation is dominated by hypogenic, transverse processes.

INTRODUCTION

The gypsum facies of the Castile Formation crops out over an area of ~1800 km^2 in Eddy County, New Mexico and Culberson County, Texas on the western edge of the Delaware Basin (Fig. IV.1). The region has traditionally been referred to as the Gypsum Plain (Hill, 1996), which covers an area of ~2800 km^2 and is composed of outcrops of the Castile and Rustler Formations (Fig. IV.2). The region is located in the semi-arid southwest on the northern edge of the Chihuahuan Desert, where annual precipitation averages 26.7 cm with the greatest rainfall occurring as monsoonal storms in late summer (July – September) (Sares, 1984). Annual temperature averages 17.3°C with an average annual minimum and maximum of 9.2°C and 25.2°C, respectively.

Throughout Castile outcrops, surficial karren occurs extensively in regions of exposed bedrock, including well-developed rillenkarren, spitzkarren, kamenitzas and tumuli. Sinkhole development is widespread, including both closed and open sinkholes ranging from near-circular features to laterally extensive, incised arroyo-like features. Cave development ranges widely, from small epigenic recharge features to large, complex polygenetic features (Stafford, 2006). The region hosts the second longest documented

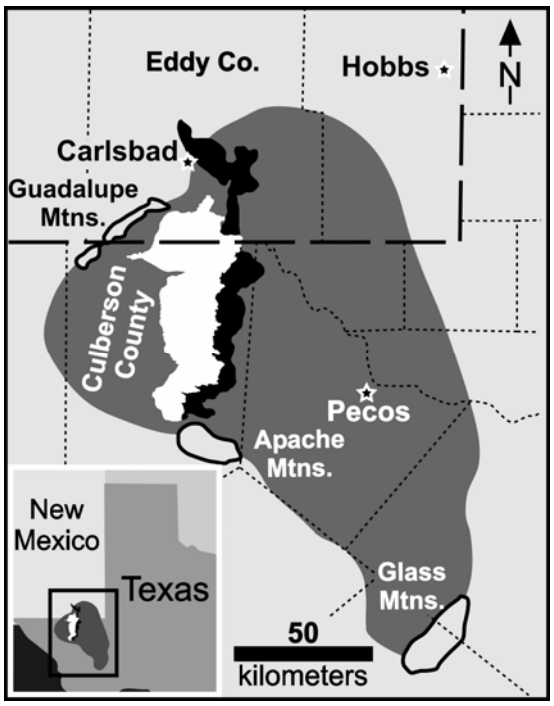

Fig. IV.1: Location map showing location of Gypsum Plain including outcrop areas of the Castile Formation (solid white) and the Rustler Formation (solid black) within the Delaware Basin (dark gray), Eddy County, NM and Culberson County, TX. Location of the Delaware Basin in relation to Texas and New Mexico is illustrated in bottom left corner, with the enlarged region outlined by the small black rectangle (adapted from Kelley, 1971, Dietrich et al., 1995 and Hill, 1996).

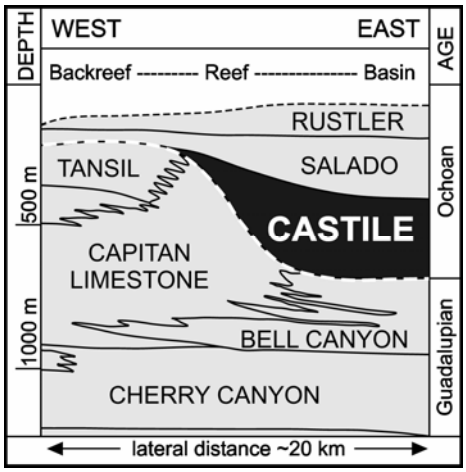

Fig. IV.2: Diagrammatic representation of late Permian (Guadalupian and Ochoan) deposits associated with the Guadalupe Mountains (left) and Delaware Basin (right). Note that the Castile Formation fills in the basin and marks the beginning of the Ochoan (dashed white line) (adapted from Hill, 1996).

gypsum cave in North America, Parks Ranch Cave, Eddy County, NM, with a surveyed length of 6596 m (Stafford, 2006). In addition, many other significant gypsum caves have been documented by the TSS (Texas Speleological Survey) (e.g. Redell and Feisler, 1977) and GYPKAP (GYpsum KArst Project) (Eaton, 1987; Belski, 1992; Lee, 1996). However, no systematic investigation has been conducted within the region with respect to karst development. Prior to this study, 246 karst features, primarily caves, were documented within the Castile outcrop region. The BLM (Bureau of Land Management) documented 45 of the total reported karst features (pers. com. John Jasper, 2006); while the TSS documented 201 of the total reported karst features (pers. com. Jim Kennedy, 2006).

The rapid solution kinetics and high solubility of gypsum promotes extensive karst development. Gypsum solubility (2.53 g/L) is approximately three orders of magnitude greater than limestone (1.5 mg/L) in pure water and two orders of magnitude less than halite (360 g/L) (Klimchouk, 1996). The high solubility and near-linear solution kinetics of evaporites encourages intense surface dissolution that often forms large sinkholes, incised arroyos and caves that are laterally limited with rapid decreases in passage aperture away from insurgences through epigenic speleogenesis (Klimchouk, 2000a). Additionally, the high solubilities of evaporites favor the development of hypogenic transverse speleogenesis driven by mixed convection (forced and free) (Klimchouk, 2000b). Forced convection is established by regional hydraulic gradients in confined settings, while free convection is generated where steep density gradients establish as fresh-waters are continuously supplied to the dissolution fronts (the upper levels) through the simultaneous sinking of saturated fluids by density differences (Anderson and

Kirkland, 1980). Therefore epigenic and hypogenic karstic features likely both exist in the study area, often superimposed on each other.

The work we report here focuses on delineating the extent and distribution of karst development within the outcrop region of the Castile Formation, in order to predict regions of intense versus minimal karst development, which can be used for karst resource management as well as a first approximation for understanding regional speleogenesis. A dual approach involving field and GIS analyses were utilized in order to define karst variability within the study area, including field mapping of 50, 1-km^2 regions (Fig. IV.3a) and GIS analyses, using ESRI ArcGIS 9.2 software, of public data (i.e. DEM: Digital Elevation Model; DRG: Digital Raster Graphic; and DOQ: Digital Orthophoto Quad) for the entire region. The combined results were used to develop a karst potential map of the Castile Formation outcrop region, while simultaneously evaluating different GIS-based techniques for karst analyses.

GEOLOGIC SETTING

The Castile Formation was deposited during the late Permian (early Ochoan), subsequent to deposition of the Guadalupian Capitan Reef (well-known for the caves it hosts in the Guadalupe Mountains; e.g. Hose and Pisarowicz, 2000). Castile evaporites represent deep-water deposits within a stratified, brine-filled basin (i.e. Delaware Basin) (Kendall and Harwood, 1989), bounded below by clastics of the Bell Canyon Formation, on the margins by Capitan Reef carbonates and above by additional evaporitic rocks of the Salado and Rustler Formations (Fig. IV.2) (Kelley, 1971). Castile evaporites crop out along their western dissolution front in the Gypsum Plain (Fig. IV.1), dip to the east

where they reach a maximum thickness of 480 m in the subsurface (Hill, 1996) and are characterized as massive to laminated sulfates (gypsum/anhydrite) interbedded with halite (Dietrich et al., 1995). Increased thickness in the east has been attributed to dissolution of intrastratal halite to the west and increased deposition to the east in the Ochoa Trough during the Permian (Anderson et al., 1972).

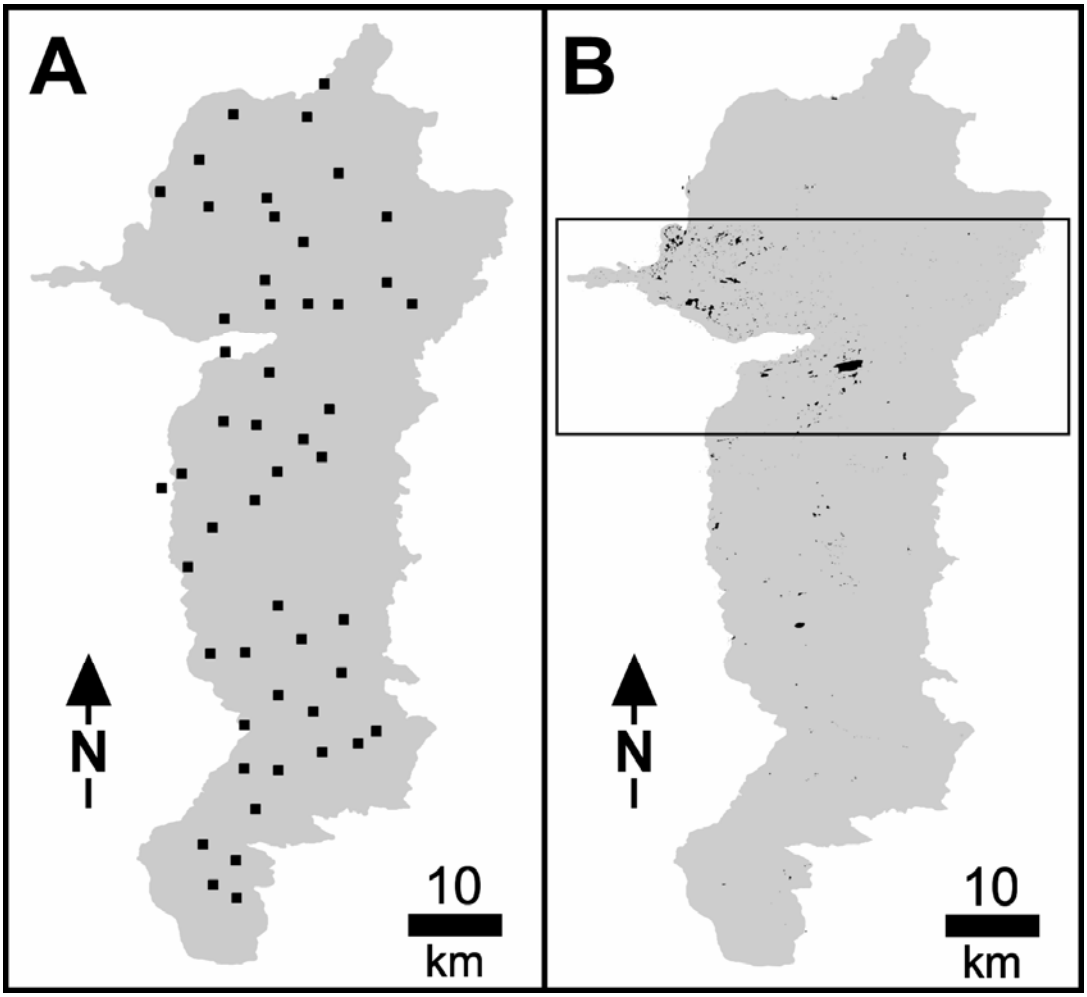

Fig. IV.3: Castile outcrop region. A) Castile outcrop region (gray) showing location of the 50 randomly selected 1 km^2 sites where field mapping was conducted; B) Castile outcrop region (gray) showing "sinks" (closed depressions) determined by DEM analysis (boxed area includes ~75% of the closed depressions identified through DEM analysis).

The Castile Formation, including outcrops in the Gypsum Plain, has experienced minimal tectonic deformation although located on the eastern edge of major tectonic events. Triassic and Laramide tectonism produced regional tilting to the northeast, broad flexures and fracturing with minimal offset within southeastern New Mexico and west Texas. The far western edge of the Delaware Basin has been down-dropped along the far eastern margin of Basin and Range block faulting; however, within the remaining Delaware Basin the effects are limited to near-vertical joints (Horak, 1985). As a result of tectonism, Castile evaporites currently dip 3 to 5 degrees to the northeast with abundant conjugate joint sets oriented at ~ N75°E and ~N15°W. Associated with joint sets along the western dissolution front, solution subsidence valleys have developed from subsurface dissolution of halite beds (Hentz and Henry, 1989).

In addition to tectonic deformation, some sulfate rocks have been exposed to significant diagenesis. Original laminated (varved) gypsum often exhibits massive and nodular fabrics that are likely the result of plastic deformation associated with anhydrite/gypsum mineral conversion (Machel and Burton, 1991). Calcitized evaporites are common (often referred to as “castiles” or calcitized masses), generally forming clusters or linear trends of biogenic limestone associated with bacterial sulfate reduction (Kirkland and Evans, 1976). Selenite is locally abundant, forming linear features and fracture fillings (likely associated with mineral conversion), as well as lenticular masses (probably associated with calcitization processes). Diagenetic fabric alteration within Castile evaporites probably has exerted significant influence on establishing preferential flow paths for karst development within the Gypsum Plain.

FIELD STUDIES

Field mapping was conducted at 50, 1-km^2 sites within the Castile outcrop area (Fig. IV.3A). Field sites were randomly selected using ESRI ArcGIS 9.2 software in order to obtain an accurate representation of karst development within the Castile outcrop region and minimize any human biases that might be introduced into site selection. Ten field mapping sites were shifted up to two kilometers away from GIS-defined locations, in order to avoid anthropogenic features (i.e. roads, houses, quarries), while two sites were shifted up to four kilometers to avoid regions where land access was not available.

Each field site was defined as a one kilometer square region. Transect surveys were conducted on 100-meter line spacing, such that ten, one kilometer long transects were traversed in each of the 50 field sites. Smaller line-spacing (40 m) for transect surveys was compared with 100-meter line spacing through independent surveys by two of the authors at five field sites, which identified less than 10% additional karst features (i.e. sinkholes and caves). Because of the results of sub-sampling and the location of the study region within the semi-arid southwest, where vegetation is sparse and does not commonly obscure karst features, 100-meter spaced traverse surveys were found to be sufficient to document more than 90% of surficial karst features. During field mapping, identified feature locations were recorded with a hand-held GPS (Global Positioning System) and individual features were characterized based on size (length, width, depth), geomorphic expression (closed sink, open sink [i.e. cave], spring) and geologic occurrence (laminated, massive and nodular gypsum; gypsite; calcitized evaporite).

Field mapping identified 389 individual karst features, including 236 open sinkholes with free drains (i.e. caves or smaller solutional conduits that connect directly to

sinkholes), 147 filled sinkholes, 4 caves with no associated sinkhole and 2 springs. However, of the 236 open sinkholes, only 39 contained caves that were large enough to be humanly enterable. Of the 50 field sites, 12 contained no karst features and 14 sites contained more than 10 features (Fig. IV.4). Only two sites contained more than 30 features, one with 31 and one with 48.

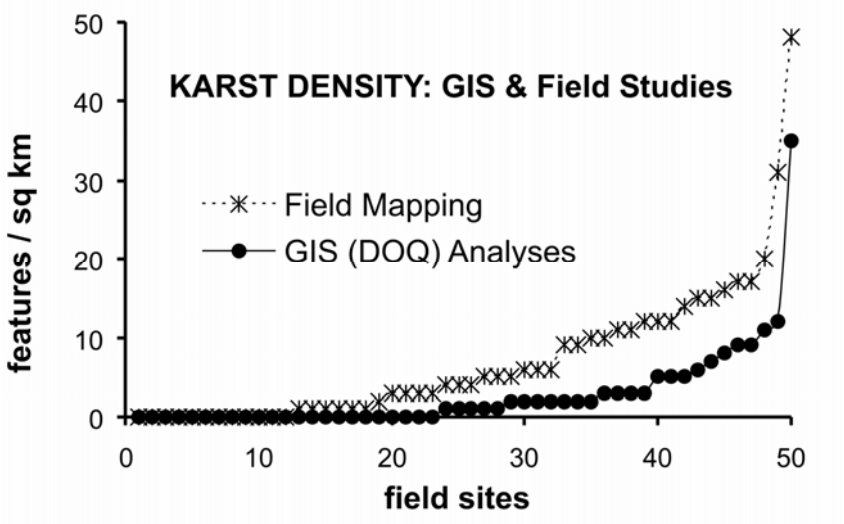

Fig. IV.4: Comparative plot showing karst features identified during field mapping compared with features identified through DOQ analyses for the 50, 1 km^2 field sites. Field mapping and DOQ analyses are only shown because most DEM and DRG analyses showed no features in the regions where field mapping was conducted. Note that DOQ analysis identified ~35% of features that were located during field mapping.

Features were found in a wide range of gypsum fabrics (Fig. IV.5). Caves are largely developed in laminated (~43% of features) (Fig. IV.5A) and massive fabrics (~26% of features) (Fig. IV.5B); however, numerous small surficial caves form in gypsite (~28% of features) (Fig. IV.5D). Caves were occasionally found in selenite (<2% of features) (Fig. IV.5C) and calcitized masses (<2% of features) (Fig. IV.5E). Filled sinkholes were generally found in gypsite or alluvium; however, this likely only represents surficial mantling over deeper features in most cases.

Sinkhole area and volume ranged widely within the surveyed sites. The average open sinkhole area was 1.99 x 10^3 m^2 (0.3 to 4.12 x 10^4 m^2) with an average volume of 1.73 x 10^3 m^3 (8.0 x 10^{-2} to 4.71 x 10^4 m^3). The average area of closed sinkholes was 1.01 x 10^3 m^2 (3.0 x 10^{-2} to 2.36 x 10^4 m^2) with an average volume 3.70 x 10^2 m^3 (5.0 x 10^{-3} to 6.54 x 10^3 m^3). Sinkhole area was calculated by treating features as simple ellipses based on the maximum width and length measured in the field, while sinkhole volume was calculated by treating features as conical ellipses based on elliptical area and sinkhole depth. Therefore, approximated sinkhole areas and volumes probably overestimate true values.

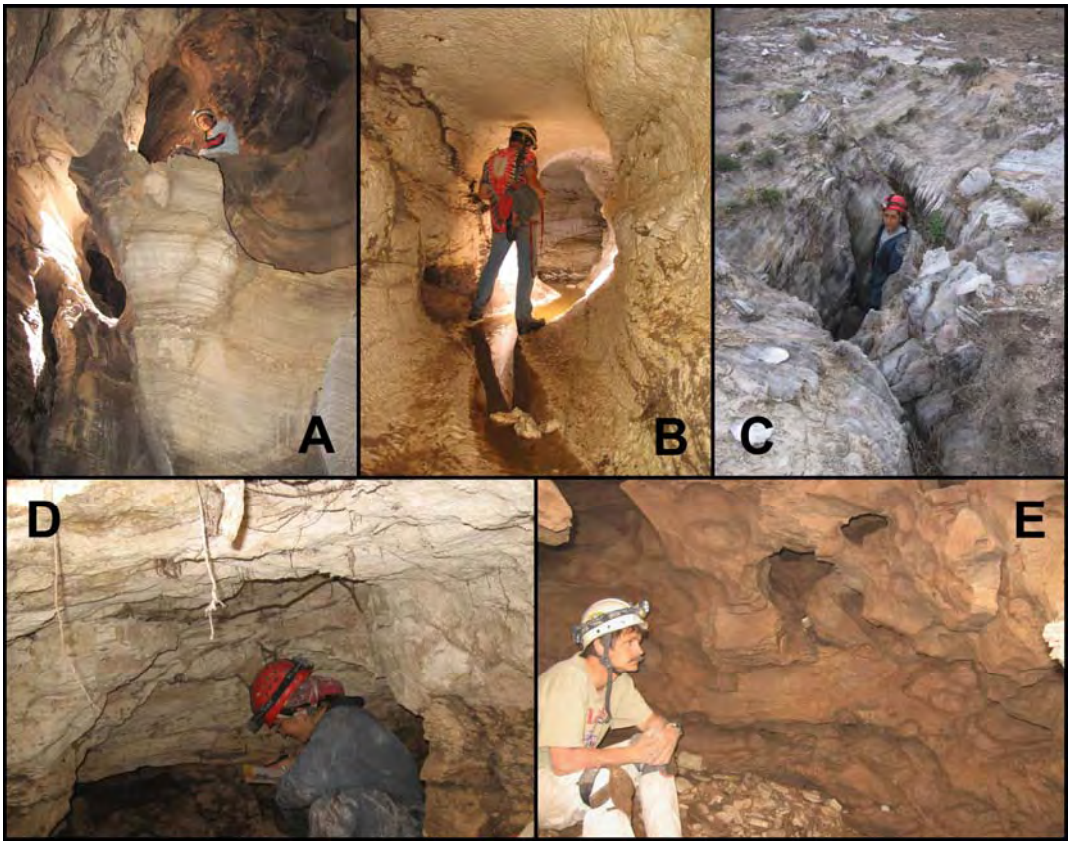

Fig. IV.5: Cave development in the Castile Formation occurs within a wide range of lithologic fabrics. A) Plummet Cave: laminated gypsum; B) Parks Ranch Cave: massive gypsum; C) Black Widow Hole: selenite; D) Pokey Cave: gypsite, and e) Dead Bunny Hole: biogenic limestone (calcitized evaporite).

GIS ANALYSES

In the last decade GIS has been recognized as a powerful tool for geographic analyses and has become a useful tool for cave and karst studies (e.g. Szukalski et al., 2002). Public data is available in multiple formats through government agencies, such as USGS (United States Geological Survey), NMBGMR (New Mexico Bureau of Geology and Mineral Resources), and TNRIS (Texas Natural Resource Inventory Service), which enables GIS analyses of large karst regions at zero cost.

GIS analyses of karst terrains have been used in various studies to delineate karst development. Florea et al. (2002) combined known point locations for karst features with digitized sinkholes from DRGs to develop karst potential maps in Kentucky, while Denizman (2003) conducted similar studies in Florida. Taylor et al. (2005) demonstrated the use of DEMs for delineating sinkholes in Kentucky. Hung et al. (2002) used an integrated approach involving analyses of multispectral imagery, aerial photography, and DEMs to evaluate relationships between lineaments and cave development.

Because most previous karst studies using GIS have focused on one or two techniques, multiple public data formats (DEM, DRG and DOQ) were compared and evaluated in this study, not only to characterize the extent of karst development but to also test the intercomparability of different methodologies. Physical mapping of karst features in the field, described in the previous section, was further compared with GIS techniques to fully evaluate the accuracy of GIS-based approaches. While field mapping identified the true occurrence of karst features within specific regions, the GIS analyses only represent approximations based on the geomorphic expression of karst features (Fig. IV.6, IV.7).

Digital elevation models (DEM) were analyzed to define closed depressions (i.e. "sinks") within the Castile outcrop region. Closed depressions were identified by creating a new DEM with "filled sinks" through GIS processing, which was compared with the original DEM to determine the difference between datasets (Fig. IV.3B, IV.6B) (Taylor et al., 2005). The resulting data included 554 individual sinkholes with an average area of

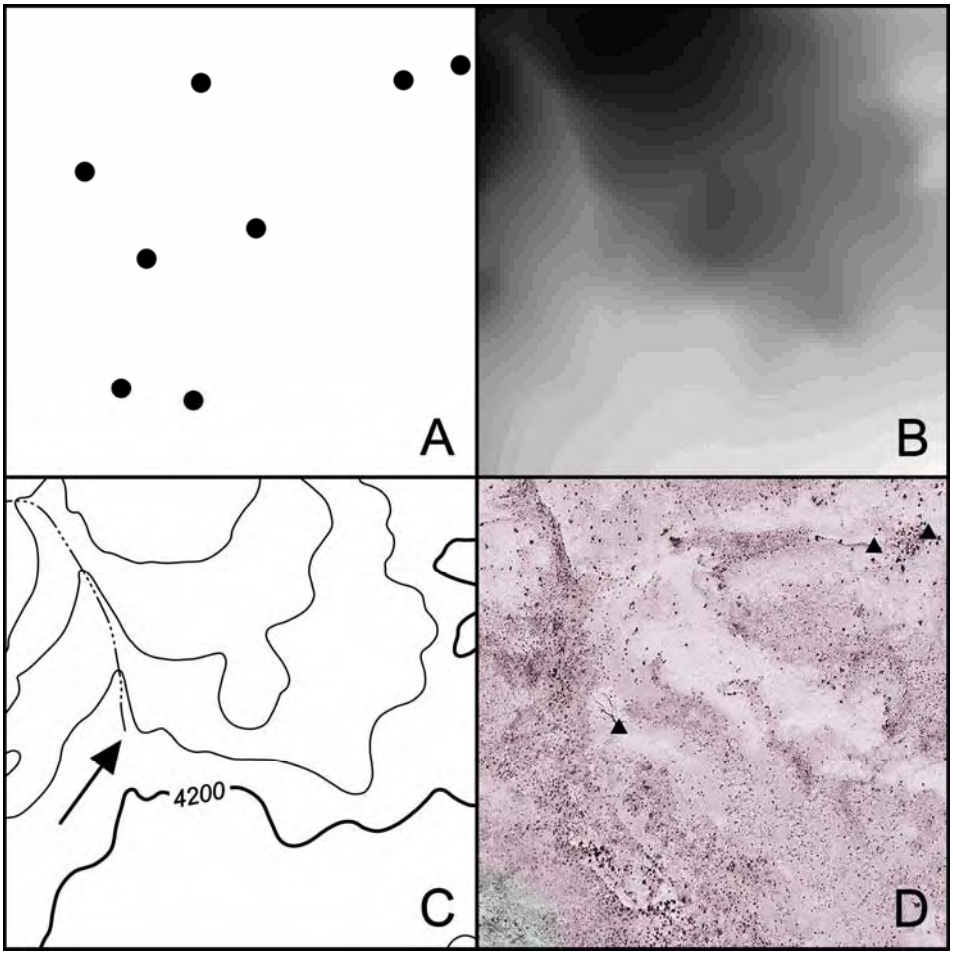

Fig. IV.6: Variability in karst identification through various methodologies within a representative 1 km^2 field site (each square region measures 1 km by 1 km). A) filled black circles represent eight karst features documented through physical mapping of field site; B) original DEM of field site from which no karst features (closed depressions) were identified during GIS analysis (note darker shading in upper left is the highest elevations); C) DRG of field site showing no closed depressions, but a blind-terminated, ephemeral stream suggest sink point (arrow); and D) DOQ of field site showing geomorphic variability and the location of three features (black triangles) which could be resolved through DOQ analysis.

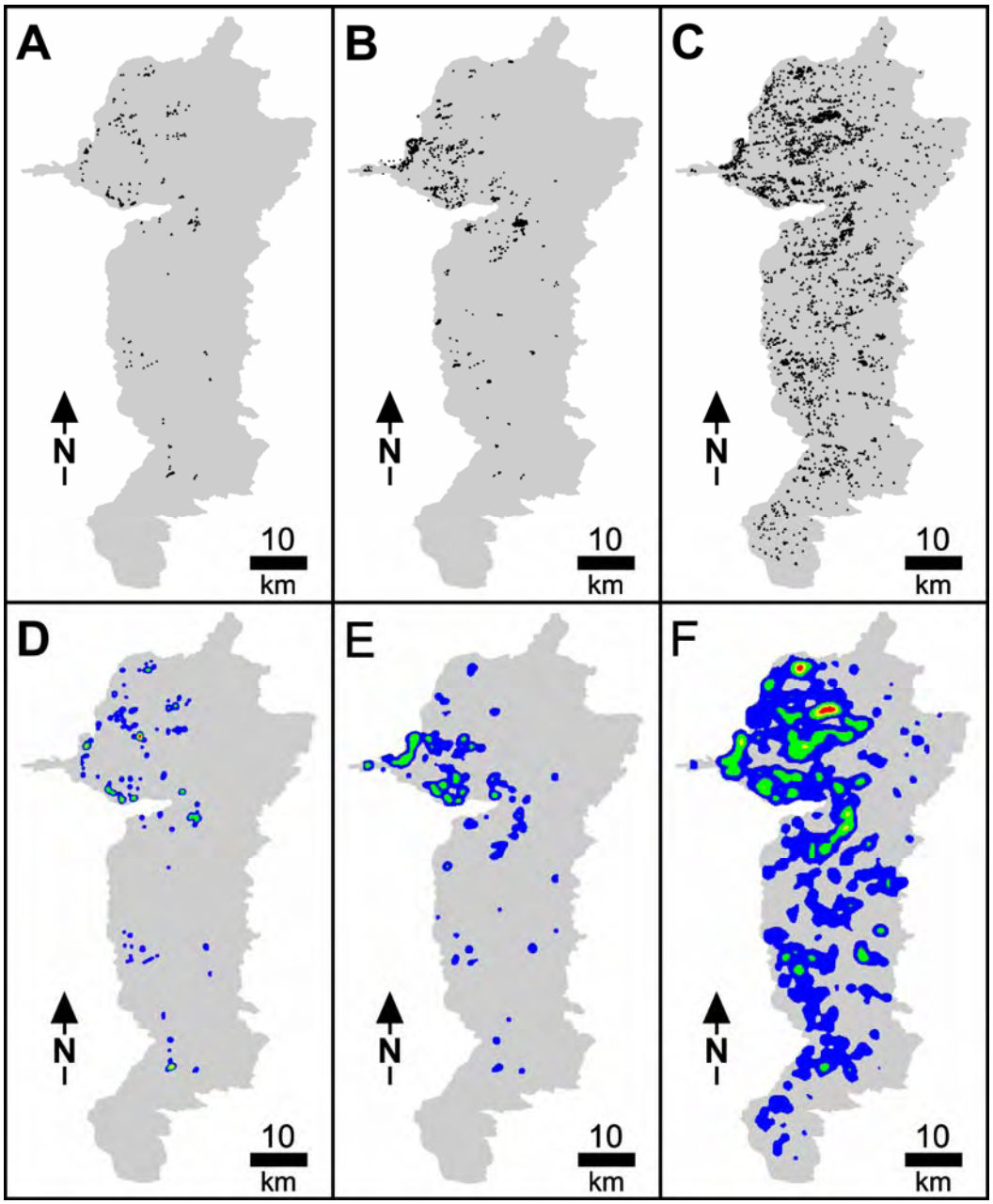

Fig. IV.7: Comparison of data used for density analyses within the Castile outcrop region (grey). A) point data for individual karst features previously documented by the TSS and BLM; B) closed depressions digitized from DRGs; C) point data for individual karst features identified through DOQ analysis; D) karst feature density map based on previously documented karst features in Fig. IV.6A; E) karst feature density map based on distribution of individual closed depressions digitized from DRGs shown in Fig. IV.6B; and F) karst density map based on features identified through DOQ analysis shown in Fig. IV.6C. Color shading in karst density maps represent the number of karst features / km^2, where: gray = <1 feature/km^2; blue = 1-5 features/km^2; green = 5-10 features/km^2; yellow = 10-15 features/km^2; and red = > 15 features/km^2.

2.57×10^4 m^2 (6.0×10^2 to 8.70×10^5 m^2); however, approximately 80 % of the identified features occurred within a 26 km (16 mile) wide strip immediately south of the New Mexico / Texas state line. Less than 5% of the features occurred north of the strip of abundant closed depressions, while the remainder was distributed south of the strip (Fig. IV.6B). Although all public data used for DEM analyses had 10-meter postings, the resulting sinkhole map suggests that there is significant variability in the source material used to create these DEMs. The region of sinkhole abundance appears to represent well the actual closed depressions within the study area, while regions outside this area appear to significantly underestimate feature abundance.

Digital raster graphics (DRG) of 1:24,000 USGS topographic maps were analyzed for the study area and all closed depressions were digitized as indicators of individual karst features (Fig. IV.6C, IV.7B); however, it is likely that multiple karst features exist within some large, closed depressions. From DRGs, 552 individual closed depressions were identified (Fig. IV.7B), with an average area of 1.54×10^4 m^2 (53 m^2 to 1.74×10^6 m^2), based on GIS spatial analyses. Because topographic maps of this region are based on 20 foot (6.1 m) contour intervals, numerous small sinkholes, including most of the features documented during field mapping, are not represented. However, most of the karst features documented by the BLM and TSS are represented as sinkholes on DRGs because topographic maps have traditionally been used for locating and identifying karst features.

Digital orthophoto quads (DOQ) within the study region have a resolution of one meter. DOQ analyses were conducted by visually picking probable karst features (Fig. IV.6D) at a resolution of 1:4,000. Features were identified based on geomorphic expression through comparison with known cave and karst features either documented by

the BLM in New Mexico and the TSS in Texas or features documented during field mapping. Based on comparison with known features, 3,237 individual features were identified within the Castile outcrop region (Fig. IV.7C).

Spatial analyses of feature densities were performed in order to delineate karst development within the study area. Three sets of data were processed separately to evaluate karst density, including: 1) known caves documented by the TSS and BLM (Fig. IV.7D); 2) DRG defined sinks (Fig. IV.7E); and 3) features identified through DOQ analyses (Fig. IV.7F). Density analyses of features identified from DEM data was not conducted because of the apparent high degree of variability in quality of these public data sets. All density analyses indicate intense karst development within the northwestern portion of the study area and a general decrease in feature abundance towards the east.

DISCUSSION

Studies conducted to determine the extent and distribution of karst development vary widely (Veni, 2002), but GIS-based studies have enabled significant advances in geographic analyses within the last decade. Analyses of known karst distributions and features identified through GIS within the Castile outcrop region all show similar trends for areas of significant karst development. However, the degree of resolution of various public data used in GIS analyses produces substantial differences in evaluation of karst development throughout the entire region (Fig. IV.8), suggesting that field studies should always be coupled with any GIS-based studies. Sinkholes identified through DEM analyses were not used to develop karst density maps because of the apparent variability

within the original data used to develop the DEMs. However, the DEM variability illustrates an important point, in that public data must be interpreted with caution.

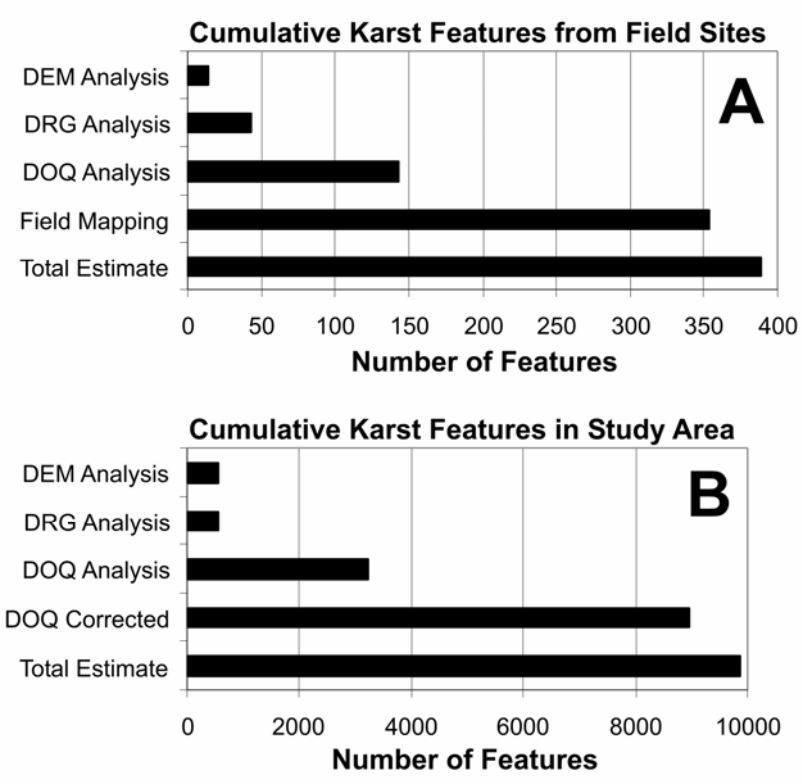

Fig. IV.8: Comparative graphs of the results from various methodologies used to evaluate karst development within the Castile outcrop region. Note that "Total Estimate" refers to the 10% additional karst features expected based on field tests of smaller transect survey line spacing. A) Cumulative methodology results from the 50, 1-km^2 sites that were physically mapped during field studies. B) Cumulative karst features for the entire Castile outcrop region based on different methodologies, where "DOQ Corrected" represents the weighting DOQ-defined features by a factor of 2.77 based on the ratio of true features documented during field mapping with those identified through DOQ analysis.

Analysis of previously documented cave and karst features within the Castile outcrop region indicate small clusters of caves, focused in the northwestern region of the study area, largely along the dissolutional margin of the Castile Formation; however, only minor regions of karst development are observed scattered throughout the rest of the study area (Fig. IV.7D). Based on previously documented features, approximately 95%

of the study area effectively exhibits no karst development (<1 feature/km^2). Studies based on documented karst features inherently create biased results that may not accurately depict the complete distribution of karst development. Biases are introduced by variable access to portions of a karst region, such as regions where landowner access is not available or regions that are remote with poor road access.

Analysis of closed depressions depicted on DRGs (Fig. IV.7E) shows similar patterns of karst development as documented karst distributions (Fig. IV.7D), but do not show any regions with densities greater than 10 features/km^2. DRG analyses shows greater distributions of karst features than documented cave analyses, expanding the predicted boundaries of karst development; however, the majority of the study area (~90%) still appears to have minimal karst development (<1 feature/km^2). As with analyses of documented caves, DRGs appear to underestimate the actual extent of karst development because the contour interval of DRGs prevents distinguishable representation of small closed depressions and narrow, incised karst arroyos.

Analysis of karst features identified on DOQs indicates a significantly greater degree of karst development density and distribution (Fig. IV.7F) as opposed to other GIS-based analyses. Regions of minimal karst development were reduced to approximately 50% and several regions with karst feature densities greater than 15 features/km^2 were identified. Intense karst development still appears concentrated within the northwestern portion of the study area; however, regions of extensive karst development are identified throughout the entire western half of the Castile outcrop area, as well as several smaller regions closer to the eastern margin of the study area. Although DOQ analysis shows more extensive karst development, it is inherently biased because features were visually picked

based on comparison with the geomorphic expression of known features. Comparison of karst features physically documented during field studies with features identified through DOQ analysis, within the boundaries of field sites mapped, indicates that DOQ analysis consistently underestimates the total number of karst features present (Fig. IV.4). This underestimation is likely the result of the 1-meter resolution of the DOQ public data.

DOQ analysis appears to best represent karst development within the outcrop region of the Castile Formation; however, all GIS-based analyses appear to under represent the extent of actual karst development as compared to physical karst surveys conducted in the field (Fig. IV.8). DOQ analyses generally identify 36% of the features documented during field studies (Fig. IV.4, IV.6, IV.7, IV.8), while other GIS analyses commonly identify less than 5% of the features documented during field studies. Therefore, DOQ density analysis was weighted by a factor of 2.77 using Spatial Analyst, in order to adjust the densities calculated through GIS as compared to densities documented during field studies. As a result, a karst potential map was developed for the entire outcrop region of the Castile Formation (Fig. IV.9), which indicates that less than 40% of the outcrop region contains effectively no karst development (<1 feature/km^2), while two small regions (<3 km^2 each) within New Mexico exhibit intense karst development (>40 features/km^2). Comparative tests of line spacing used in transect-based field mapping, suggests that the actual density of karst features may be at least 10% greater (Fig. IV.8). The karst potential map likely represents karst development relatively accurately within the study area, but a complete physical survey of the entire 1,800 km^2 region would probably show discrepancies.

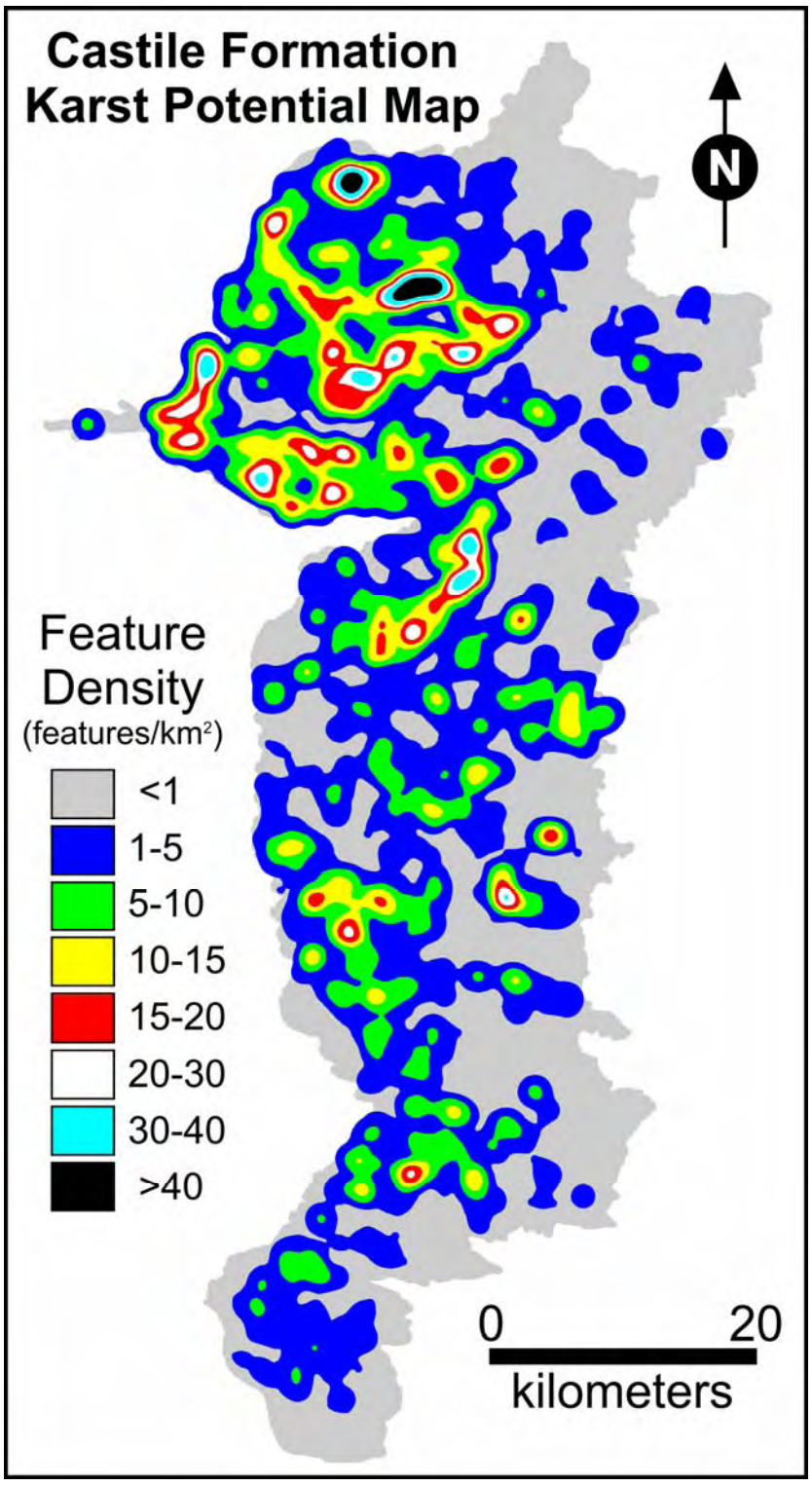

Fig. IV.9: Karst potential map of the Castile Formation outcrop region defined in this study. Note the two dense areas of karst development within the northern portion of the study area with densities greater than 40 features/km^2.

CONCLUSIONS

The development of a karst potential map for the Castile Formation shows that karst development is distinctly clustered within the Gypsum Plain (Fig. IV.9). Visual interpretation of the clustering distribution of karst features within the Castile outcrop region was confirmed through GIS-based nearest neighbor analyses (Ford and Williams, 1989), which yielded a nearest neighbor index of 0.439. A nearest neighbor index of 1 is classified as random while values greater than 1 approach a regular, evenly spaced pattern while values less than 1 approach greater clustering (Ford and Williams, 1989). A nearest neighbor index of 0.439 indicates significant clustering. Large regions exhibit minimal surficial karst expressions, primarily along the southern and eastern edges of the Castile outcrop area.

The densest regions occur in the northwestern portion of the outcrop area, and commonly contain more than 20 features/km^2 (Fig. IV.9), with more than 40 features/km^2 locally. The northern of the two densest regions contains the second longest known gypsum cave in North America, Parks Ranch Cave, and is largely included within a BLM critical resource area that does not allow surface occupancy, thus protecting the extensive karst development within this area. However, the second dense karst region should be evaluated through more intense field studies to determine if it should also be protected as a critical resource area.

GIS-based analyses have become an important tool for karst studies. DOQ analysis coupled with field studies has been shown to be the most effective method for delineating the actual extent and intensity of karst development within the Castile outcrop area, because of the sparse vegetation associated with the semi-arid southwestern United States.

However, this may not be the most effective technique in other regions where vegetation is denser. Although commonly used in many karst regions, DRG analysis within the study area proved to poorly represent the actual extent of karst development within the region because of the low resolution of contour intervals, including significantly underestimating the actual abundance of karst features within the two densest regions. DEM analysis proved to be of little use within the study area, because apparent variability in original data from which DEMs were constructed does not consistently represent the same resolution.

Although DEM and DRG analyses proved ineffective in the study area, it is likely that these methodologies could be effective for delineating karst development in other regions where higher resolution DEM or DRG data is available. Ultimately the scale of karst features within regions being evaluated with GIS methodologies must be compared with the resolution of available GIS data, in order to determine the effectiveness of GIS-based studies. Therefore, caution must be taken when conducting GIS-based karst analyses, which should always be coupled with field studies for verification, not only in densely karsted areas but also in regions that appear to have minimal karst development.

The distinct clustering pattern of karst provides some insight into the nature of speleogenesis within the region (Fig. IV.7, IV.9). Klimchouk (2003) and Frumkin and Fischhendler (2005) suggest that hypogenic karst tends to form in dense clusters separated by regions of minimal karst development because heterogeneities within soluble strata promote transverse speleogenesis in regions where rising fluids become focused along favorable flow paths. In contrast, epigenic karst is generally expressed as more widely distributed features where descending meteoric waters attempt to utilize all

available irregularities near the surface and converge with depth. Because convergence occurs with depth in epigenic karst, surficial expressions tend to be less clustered in epigenic dominated karst as opposed to hypogenic karst where convergence occurs near the surface.

Current studies of karst development within the Castile Formation by the authors have found significant morphological evidence within individual caves that supports the interpretation of speleogenesis dominated by hypogene processes. These include the diagnostic suite of hypogenic features (e.g. risers, channels and cupolas) reported by Klimchouk (2007), as well as the widespread occurrence of blanket breccias (Anderson et al., 1978), breccia pipes (Anderson and Kirkland, 1980), evaporite calcitization (Kirkland and Evans, 1976) and native sulfur deposits (Hentz and Henry, 1989) previously reported within the region. Current research is focusing on interpreting the speleogenetic evolution of the Castile Formation, including the diagenetic alteration of calcium sulfate rocks and the development of cavernous porosity. However, this is beyond the scope of this manuscript and will be reported separately in the near-future. While GIS-based analyses provide insight into the speleogenetic processes of the region, detailed field studies of specific features will be required in order to interpret the speleogenetic evolution of the region.

While the karst potential map of the Castile Formation outcrop region alone can only provide limited insight into regional speleogenesis, it can provide an effective tool for land management within Eddy County, New Mexico and Culberson County, Texas. Delineation of karst intense regions can be used in land management planning for road construction and oilfield well and pipeline placements in order to not only avoid regions

of potential geohazards associated with collapse but also to protect regions of significant groundwater recharge. Whether Castile karst is primarily the result of hypogenic or epigenic speleogenesis, most exposed features currently act as groundwater recharge features, thus the delineation of dense karst regions is crucial for the sustained management of sparse water resources within this portion of the semi-arid southwest. Ultimately, karst potential maps can be used to delineate sensitive regions for karst resource management.

ACKNOWLEDGEMENTS

The authors are indebted to Jack Blake, Draper Brantley, Stanley Jobe, Lane Sumner and Clay Taylor for their generous access to private ranches in Texas throughout this study. Tim Hunt provided useful information and assistance with University Land in Texas. John Jasper and Jim Goodbar provided essential information about known gypsum karst development within New Mexico. Jim Kennedy provided essential information about know gypsum karst development within Texas. The authors are thankful for the useful comments provided by an anonymous reviewer and Amos Frumkin helped to improve this manuscript. This research was partially funded through grants from the New Mexico Geological Society and the New Mexico Tech Graduate Student Association and support from the National Cave and Karst Research Institute (NCKRI).

CHAPTER V:
EPIGENE AND HYPOGENE GYPSUM KARST MANIFESTATIONS OF THE CASTILE FORMATION: EDDY COUNTY, NEW MEXICO AND CULBERSON COUNTY, TEXAS, USA

ABSTRACT

Permian evaporites of the Castile Formation crop out over ~1,800 km^2 in the western Delaware Basin (Eddy County, New Mexico and Culberson County, Texas, USA) with abundant and diverse karst manifestations. Epigene karst occurs as well-developed karren on exposed bedrock, while sinkholes dominate the erosional landscape, including both solutional and collapse forms. Sinkhole analyses suggest that more than half of all sinks are the result of upward stoping of subsurface voids, while many solutional sinks are commonly the result of overprinting of collapsed forms. Epigene caves are laterally limited with rapid aperture decreases away from insurgence, with passages developed along fractures and anticline fold axes. Hypogene karst occurs as diverse manifestations, forming the deepest and longest caves within the region as well as abundant zones of brecciation. Hypogene caves exhibit a wide range of morphologies from complex maze and anastomotic patterns to simple, steeply dipping patterns, but all hypogene caves exhibit morphologic features (i.e. risers, outlet cupolas and half-tubes) that provide a definitive suite of evidence of dissolution within a mixed convection (forced and free convection) hydrologic system. Extensive blanket breccias, abundant breccia pipes and numerous occurrences of calcitized evaporites indicate widespread hypogene

speleogenesis throughout the entire Castile Formation. Although most cave and karst development within the Castile outcrop region appears to have hypogene origins, epigene processes are actively overprinting features, creating a complex speleogenetic evolution within the Castile Formation.

INTRODUCTION

Southeastern New Mexico and Far West Texas are well known internationally for the carbonate caves of the Guadalupe Mountains (e.g. Carlsbad Cavern, Lechuguilla Cave) (e.g. Hose and Pisarowicz, 2000). However, extensive evaporite karst regions occur to the north, south and east of this region (Fig. V.1), but they have remained largely underappreciated and understudied in karst science. The famous carbonate caves of the Guadalupe Mountains are developed in the Permian reef facies (Capitan Formation) and near backreef facies (Yates and Tansil Formations) of the Delaware Basin, while evaporite caves are developed in the contemporaneous far backreef facies (Artesia Group), as well as in subsequent basin filling evaporite facies (Castile Formation) and overlying units that covered the Permian Reef (Salado and Rustler Formations) during late Permian (Fig. V.2) (Scholle et al.., 2004). Limited studies on specific caves or local karst regions have been conducted within the evaporite facies of the Permian Basin, including karst studies in the San Andres Formation (Forbes and Nance, 1997) and Seven Rivers Formation (Stafford et al., 2007a; Land, 2006) of the Artesia Group, the Castile Formation (Sares, 1984; Nance, 1993), and the Salado and Rustler Formations (Hill, 1996). However, no studies have been conducted to evaluate the full range of cave and karst development within any of the evaporitic units of the region. Cave exploration has

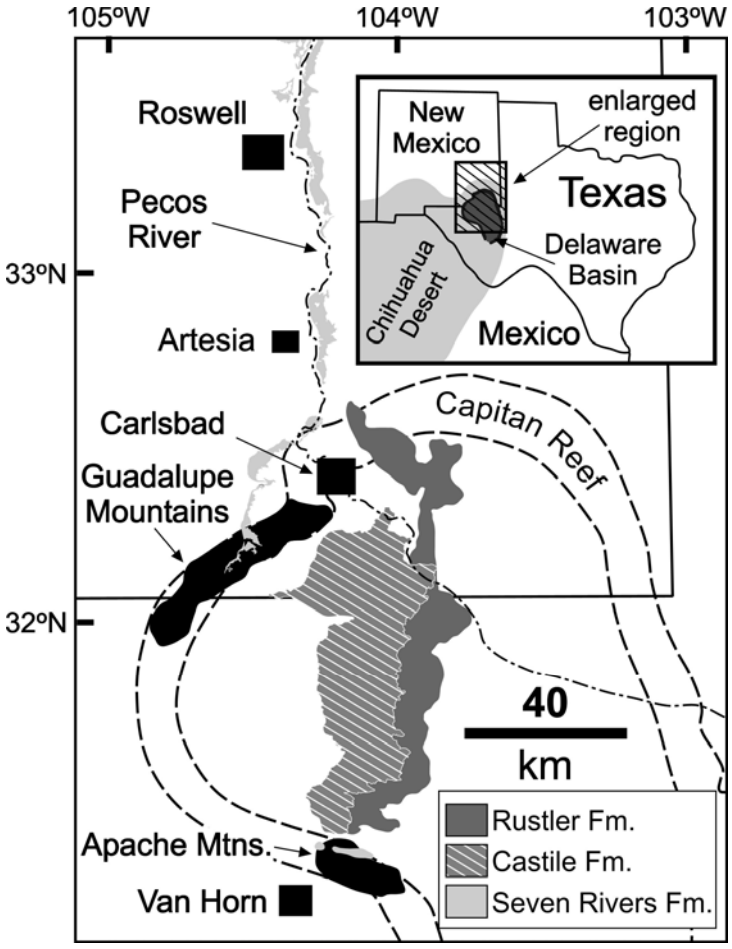

Fig. V.1: Regional map showing major outcrops of Permian evaporite facies in southeastern New Mexico and far west Texas (Rustler, Castile, and Seven Rivers Formations). Hatched area delineates the Castile Formation outcrop region, the primary study region of this manuscript. The Capitan Reef, the reef facies of the Capitan Formation, delineates the margin of the Delaware Basin and forms the Guadalupe Mountains on the northwest and the Apache Mountains to the southwest, where it crops out at the surface. Inset box in upper right delineates the location of the enlarged area within Texas and New Mexico and the spatial extent of the Delaware Basin. (Adapted from Kelley, 1971 and Dietrich et al., 1995).

been conducted by the Gypsum Karst Project (GYPKAP) of the National Speleological Society throughout the evaporite karst regions of New Mexico (Eaton, 1987; Belski, 1992; Lee, 1996). Documentation of evaporite karst regions within Texas has been conducted by the Texas Speleological Survey (TSS) (e.g. Redell and Fiesler, 1977).

Although all of the evaporite facies of the region deserve comprehensive study, it is beyond the scope of a single study; therefore, this research focuses specifically on karst development in one evaporitic unit, the Castile Formation because it is the largest continuous outcrop of a single evaporite formation in the Permian Basin. This study is part of a larger ongoing study to evaluate the regional speleogenetic evolution of the Delaware Basin, throughout southeastern New Mexico and far west Texas.

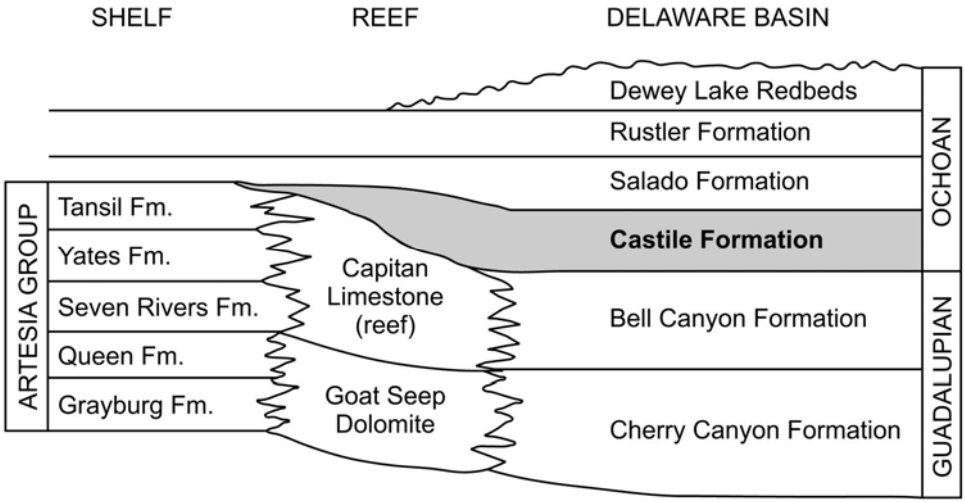

Fig. V.2: Diagram of Permian formations associated with the Guadalupe Mountains, including the shelf, reef and basin facies. Note the stratigraphic position of the Castile Formation (shaded area) discussed throughout this study (adapted from Scholle et al., 2004).

Because of the high solubility of evaporite rocks, dramatic karst landscapes can develop in them. The near linear solution kinetics of evaporites encourages the development of large sinks, incised arroyos (i.e. incised stream beds that experience high flow during flash flood events but remain dry the majority of the year), and caves that are laterally limited in epigene settings (Klimchouk, 2000a). Similarly, in hypogene settings steep fluid density gradients can be established in calcium sulfates, which create free

convection cells that have the potential to dissolve significant volumes of void space (e.g. Anderson and Kirkland, 1980; Kempe, 1996; Klimchouk, 2007). Whether speleogenesis is epigene or hypogene, the high solubility of evaporites enables the development of extensive karst much more rapidly in calcium sulfates (gypsum/anhydrite) than in carbonate rocks. In the United States, calcium sulfate rocks (gypsum and anhydrite) underlie 35-40% of the continental land surface (Johnson, 2002). However, most studies of karst in these evaporitic rocks of the United States have focused primarily on risk assessment and avoidance associated with gypsum karst geohazards (e.g. Johnson and Neal, 2003; Trzhtsinsky, 2002; Klimchouk and Andrejchuk, 1996; Yauro and Cooper, 2002). In contrast, gypsum karst in other regions of the world has been the focus of significant speleogenetic studies. The giant gypsum maze caves of the western Ukraine, developed in highly fractured, Miocene gypsum, have been studied extensively, providing the basis for much of the modern understanding of hypogenic speleogenesis (e.g. Klimchouk, 1996b, 2000b). Similarly, large, isolated voids, termed Schlotten, developed in the Permian gypsum of Germany have provided greater insight into hypogene processes in regions where little structural deformation of rocks has occurred (Kempe, 1996). In contrast, extensive studies of epigene karst have been conducted in Spain (e.g. Calaforra et al., 2002; Calaforra and Pulido-Bosch, 1996) and Italy (e.g. Sauro, 1996), where gypsum karst forms dramatic landscapes consisting of extensive solutional doline fields and abundant small caves.

Cave and karst development within the Castile Formation is extensive. Within the Castile outcrop area of the western Delaware Basin (Eddy County, New Mexico and Culberson County, Texas), surficial karren, sinkholes and associated caves dominate the

landscape (Stafford, 2006; Stafford et al., 2006, 2007b). Throughout the entire Delaware Basin, evidence of subsurface dissolution through hypogene speleogenesis occurs in the Castile Formation as evidenced by the widespread distribution of collapse structures and cross-formational brecciation (Anderson and Kirkland, 1980). Here we will systematically discuss the different karst manifestations observed within the Castile Formation (surficial forms, epigene caves, hypogene caves, and intrastratal breccias) with representative examples provided. The Castile Formation offers a unique opportunity to study karst development within an entire formation because it was deposited as a basin-filling sequence that isolated deposition to a restricted region which has subsequently experienced the same tectonic history throughout.

STUDY AREA

The Castile Formation crops out over approximately 1800 km^2 (~12-40 km wide from east to west and ~90 km long from north to south) in the western Delaware Basin (Fig. V.1) (Hill, 1996). The outcrop region is bounded on the north by the Guadalupe Mountains, on the south by the Apache Mountains, on the west by the dissolution front of the Castile Formation and on the east by outcrops of the Rustler Formation where the Castile Formation dips into the subsurface (Bachman, 1984; Stafford et al., 2007b). The study area is located on the northern edge of the Chihuahuan Desert where annual precipitation averages 26.7 cm and occurs primarily as intense, short duration monsoonal storm events during late summer (Sares, 1984). Annual temperature averages 17.3°C, with an average minimum and maximum of 9.2°C and 25.2°C, respectively.

The Castile Formation was deposited during the late Permian, subsequent to deposition of the Capitan Formation (Scholle et al., 2004), which forms the bounding reef margin of the Delaware Basin (Fig. V.2). Castile evaporites represent deep-water deposits within a stratified, brine-filled basin (Kendall and Harwood, 1989), bounded below by clastic deposits of the Bell Canyon Formation. Castile evaporites filled the Delaware Basin during deposition and were subsequently covered by Permian evaporites of the Salado and Rustler Formations (Fig. V.2) (Kelley, 1971).

The Castile Formation is classically defined as laminated to massive anhydrite / gypsum, interbedded with halite (Dietrich et al., 1995), where laminated portions represent seasonal variations in basin salinity during deposition. Because of the extremely high solubility of halite, it does not crop out at the surface within the study area and has been completely removed in the subsurface by intrastratal dissolution within the Castile outcrop region. However, four zones of halite interbeds have been documented within the eastern Delaware Basin, which directly correlate with intrastratal breccia zones in the western Delaware Basin. Thin calcite laminae were deposited during less saline, wetter climates and gypsum / anhydrite laminae were deposited during more saline, dryer climatic periods (Anderson et al., 1972). However, diagenetic alteration since deposition has produced additional variability in lithologic texture, such that laminated, massive, nodular and tabular (selenite) fabrics, as well as calcitized evaporites, commonly occur (Machel and Burton, 1991, Stafford et al., 2007b). Most fabric alteration is the product of gypsum / anhydrite mineral conversion associated with hydration / dehydration processes during burial and exposure (Dean et al., 1975). Mineral conversion also induces brittle deformation related to mineral conversion associated with hydration and dehydration,

resulting in endokinetic fissuring (Klimchouk and Andrejchuk, 1996). Calcitization of evaporites is widespread, where sulfate reducing bacteria in the presence of ascending hydrocarbons have reduced calcium sulfates, enabling the replacement of calcium sulfates with calcium carbonates, often termed biogenic limestone, as well as the byproduct hydrogen sulfide (Kirkland and Evans, 1976). Oxidation of hydrogen sulfide commonly produces native sulfur, which has formed several economic sulfur bodies within the region (Hentz and Henry, 1989).

In addition to diagenetic sulfate alteration within the Castile Formation, the region has experienced some tectonic deformation. Compressional tectonism in the Triassic and Laramide (late Cretaceous to mid-Tertiary) produced regional tilting to the northeast, broad anticlinal flexures and fracturing with minimal offsets within southeastern New Mexico and far West Texas (Dickenson, 1981). The far western edge of the Delaware Basin has been down-dropped along the far eastern margin of Basin and Range extensional block faulting in the mid-Tertiary; however, within the remaining portion of the Delaware Basin the effects are limited to near-vertical joints (Horak, 1985). As a result of the tectonic history of the region, Castile evaporites currently dip 3 to 5 degrees to the northeast (Fig. V.3), where they reach a maximum of 480 meters in the subsurface (Hill, 1996) and gradually thin to several meters on the far western edge of the Castile outcrop region where surface denudation has been the greatest. Tectonic fissuring has produced abundant conjugate joint sets oriented at ~N75°E and ~N15°W (Nance, 1993).

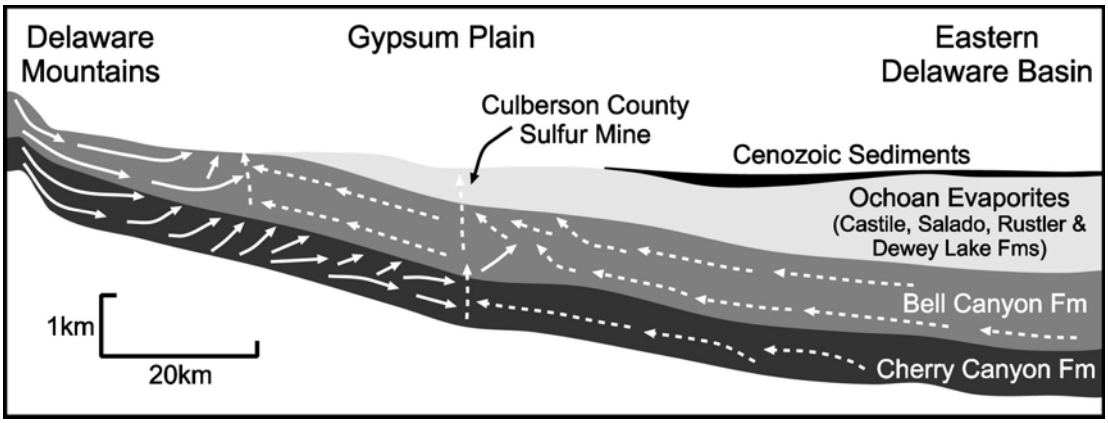

Fig. V.3: Simplified paleohydrology of the Castile Formation showing the uplifted Delaware Mountains to the west and the interior of the Delaware Basin to the east where the Castile Formation is completely buried in the subsurface (adapted from Lee and Williams, 2000). Solid white arrows depict meteoric waters recharged into the Bell Canyon and Cherry Canyon Formations to the west of the Castile Formation outcrop area. Dashed arrows depict ascending basinal fluids and hydrocarbons that have migrated up dip through the Delaware Basin. Both oxic meteoric waters and anoxic basinal waters migrate vertically through the overlying Castile Formation resulting in the formation of hypogene caves and calcitization of evaporites with emplacement of secondary native sulfur. As surface denudation continues to the east, oxic hypogene fluids replace anoxic hypogene fluids, which further enhance hypogene dissolution and can oxidize native sulfur in calcitized regions. As surface denudation continues to the east, fluid confinement is breached and epigene processes begin overprinting previously established hypogene flow paths.

CASTILE KARST

Karst development within the Castile outcrop region is diverse and widespread. Stafford et al. (2007b) reported approximately 10,000 surficial karst features (i.e. sinkholes and caves) for the entire Castile outcrop region by coupling field mapping and GIS techniques. They pointed out that feature distribution was highly clustered (Fig. V.4) and suggested that this indicate that most karst development was associated withhypogene speleogenesis. Approximately 40% of the region exhibits effectively no karst development, while two small regions, each less than 10 km^2, contain more than 40 caves

or sinkholes per square kilometer (Fig. V.4) (Stafford et al., 2007b). Karst development is most intense in the northwestern portion of the Castile outcrop region, but numerous clusters of significant karst development occur throughout the entire study area. In addition to sinkholes and caves, extensive karren is present on exposed rock surfaces, as well as karstic breccias. Closed depressions are often filled with sediments, making it difficult to determine their speleogenetic origin, whether collapse of hypogenic or epigenic voids or incised from epigene processes (e.g. Ford and Williams, 2007; White, 1988). The study of individual caves within the region indicates that both hypogene and epigene karst phenomena are widespread.

Fifty randomly selected 1 km^2 regions were physically mapped, including characterization of karst features, throughout the 1,800 km^2 study area (Stafford et al., 2007b). Mapped sites were randomly selected using GIS (Geographic Information System) in order to avoid any human biases that could be introduced into field studies and to enable a more accurate representation of total karst development within the region, not just regions containing abundant karst features. Field mapping identified 196 open sinkholes with associated caves and 139 filled sinkholes; however, only 102 of the open sinkholes included associated caves large enough to be entered by humans. Time constraints limited cave mapping to a representative sample of 32 previously undocumented caves which were chosen to demonstrate the diversity of cave development within the Castile Formation. These newly surveyed caves were subsequently used as the primary database for evaluation of Castile karst development because they were mapped with the same level of accuracy, while previously mapped features were surveyed by a wide range of individuals with varying levels of detail and

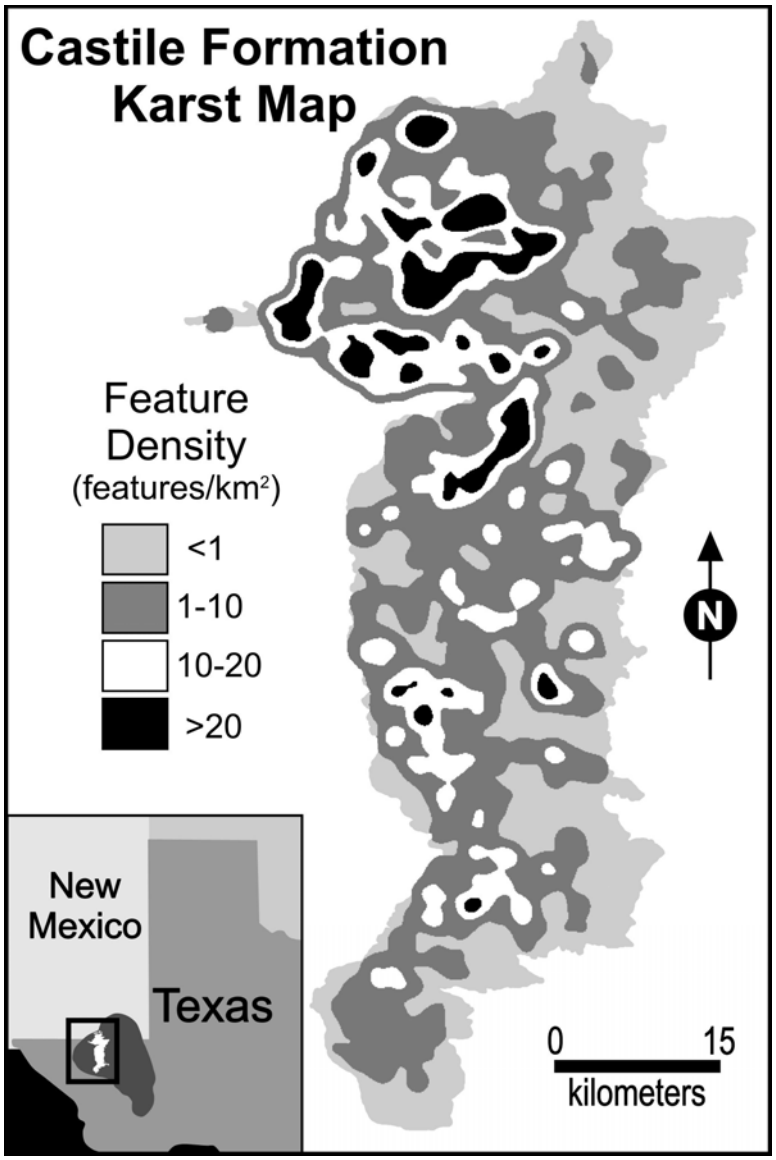

Fig. V.4: Simplified karst feature distribution and density map of the Castile Formation outcrop region (adapted from Stafford et al., 2007b). Note the clustering pattern of denser karst regions shown in black.

accuracy (e.g. Redell and Feisler, 1977; Eaton, 1987; Belski, 1992; Lee, 1996). In order to confirm observations made in newly documented features in this study, several previously known and mapped caves were visited for comparison.

Analysis of this database and previous studies (e.g. Redell and Feisler, 1977; Lee, 1996) indicates that caves and karst in Castile evaporites are developed in a wide range of lithologic fabrics and do not appear to be associated with any specific gypsum fabric. Most caves are developed in laminated or massive gypsum, which directly corresponds to the relative abundance of these fabrics. Many caves are hosted in the surficial gypsite deposits, which are often developed at the interface of the gypsic soils and the underlying bedrock. Gypsite is composed of fine-grained aeolian particles (primarily clay and silt), residual insoluble material derived from solution of underlying bedrock and precipitated secondary gypsum which binds sediment and creates a poorly consolidated soil (Cantón et al., 2003). Caves have been observed within tabular (selenite) and nodular gypsum as well as calcitized evaporites, but more commonly, karst development is observed within these fabrics when they are transected within portions of larger caves primarily developed in laminated or massive fabrics. However, caves and karst appear to develop largely independently of the local gypsum fabric. Instead, karst development appears to be primarily related to the local and regional geologic and hydrologic regime with only minor variations in passage wall morphology and surficial geomorphology associated with local variations in lithologic fabric.

Caves within the Castile Formation are usually developed along regions of structural deformation, both ductile and brittle, which is consistent with observations made within other evaporite karst regions of the world (Klimchouk et al., 1996; Johnson and Neal, 2003). Because of the low permeability of gypsum and anhydrite, fractures and bedding partings are crucial for enabling fluids to migrate through sulfate rocks promoting the development of dissolutional conduits (Klimchouk, 1996a). Most individual passages

within the Castile Formation are developed either along joints (Fig. V.5A,B) with no apparent offset or other fractures with minimal offset (Fig. V.5C). These guiding fractures are most easily recognized in epigene caves (Fig. V.5A), but are also commonly observed in major passages in hypogene caves (Fig. V.5B,C). In regions where folding has occurred, individual passages are frequently developed along the axis of anticlines (Fig. V.5D,E), where compressional forces have produced small-scale bedrock partings. Previous studies on cave development have used analyses of passage orientations as a proxy for determining regional structural deformation, especially in regions where vegetation or surficial mantling obscures bedrock (Nelson, 1991; Barlow and Ogden, 1992). Because gypsum weathers easily and often forms hydration crusts that significantly distort surficial rock exposures, a similar study was conducted using the caves that were mapped during this study. Of the 32 caves mapped, 4 are developed in surficial gypsite; therefore, these caves were not included in analyses because they are not developed within bedrock and did not show any definitive evidence of structural control. In order to apply greater significance to larger or longer passages, the passage orientations were weighted according to passage length. Each five meter segment of passage was considered as a separate orientation measurement (e.g. a 15 meter long passage oriented at 35° azimuth is counted as three separate orientation measurements of 35°) (Stafford et al., 2005). Passages less than 2.5 meters long were not included in analyses. Because cave maps are oriented according to magnetic north, passage orientation measurements were corrected for local magnetic declination, which ranges from 7°20’ E on the northern edge of the study area to 8°30’ E on the southern edge of the study area (Hill, 1996).

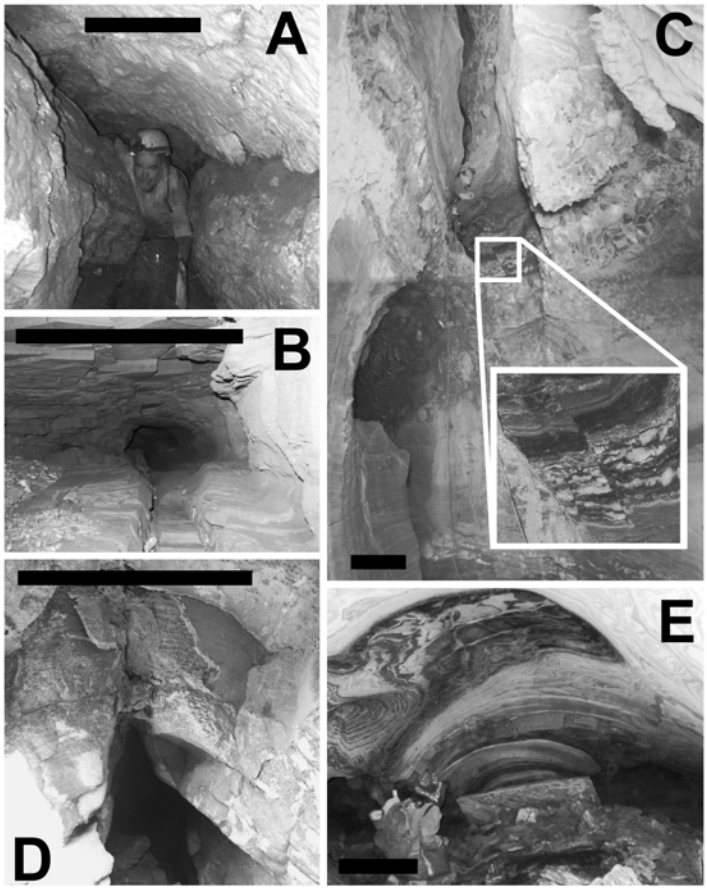

Fig. V.5: Brittle and ductile structural controls on gypsum karst development within the Castile Formation. Black scale bars are ~0.5 m long. A) Fracture controlled passage in an epigene cave (Zombie Cave, Eddy Co., New Mexico); B) Fracture controlled passage in a hypogene cave (Dead Bunny Hole, Culberson Co., Texas); C) Fracture controlled passage in a hypogene cave with inset showing ~10 cm of vertical offset al.ong fracture (Crystal Cave, Culberson Co., New Mexico); D) Epigene cave developed along an anticline fold axis (Dead East Cave, Culberson Co., Texas); E) Hypogene cave development along an anticline fold axis (Dead Bunny Hole, Culberson Co., Texas).

Passage orientation analyses (Fig. V.6) indicate a wide range of fracture orientations associated with cave development. One dominant orientation trend of ~N40°W and two secondary orientation trends of ~N10°W and ~N45°E are present within the data, which probably represent tectonic deformation within the region. Only the N10°W trend of these orientations is similar to the tectonic fissuring reported by Nance (1993). Epigene

cave passages and most hypogene cave passages show direct correlation with fractures in the field, but the complexity of total passage orientations suggests that many of these are not tectonic fractures. Instead, it is likely that many of the fracture controlled passages are developed along endokinetic fissures that have been induced through mineral conversion, while the dominant passage orientations likely represent major structural deformation within the region. Hypogenic caves develop within a non-competitive, uniform hydrologic regime where all bedrock heterogeneities are exploited equally; therefore, we expect that the complexity in evaluating regional tectonic deformation based on analyses including hypogene caves will inherently increase compared to cave development in purely epigene settings. Bedrock heterogeneities include fractures, as well as minor variations in rock permeability, porosity and composition, which result from the depositional and diagenetic history of the region.

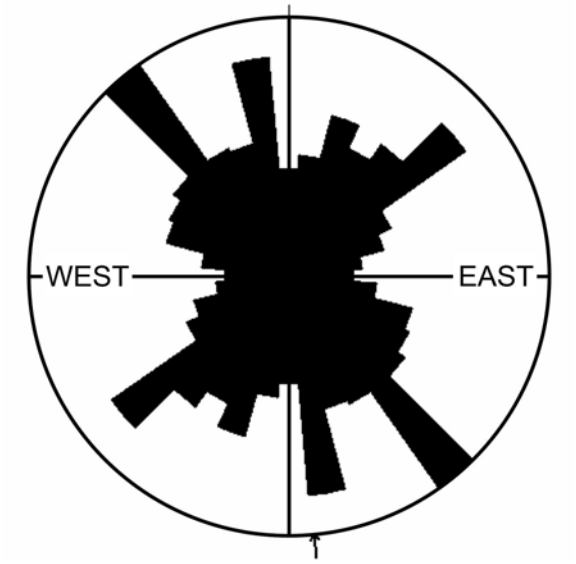

Fig. V.6: Rose diagram showing cave passage orientations from 28 caves surveyed within the Castile outcrop area during this study (N=556 passage segments). Note the three dominant passage orientations (~N40°W, ~N45°E and ~N10°W), which likely represent major tectonic fissuring within the western Delaware Basin.

Within the study area, karst manifestations occur in four primary forms: 1) surficial karst, 2) epigene caves, 3) hypogene caves, and 4) intrastratal brecciation. There is significant overlap between each of the individual forms due to multiple formational episodes and varied genetic origins of speleogenesis within the Castile Formation. The following sections systematically discuss each of the primary types of karst manifestation.

SURFICIAL KARST

Karst development within the Castile outcrop region has abundant surficial manifestations, ranging from sinkholes to karren and surficial precipitates. Approximately 8% (138 km^2) of the outcrop region is composed of exposed bedrock. Most exposed bedrock is covered with a thin gypsum crust; however, bedrock regions that are not covered by crust generally exhibit extensive karren. Throughout the entire, 1,800 km^2 outcrop region, sinkholes or closed depressions are abundant, including both open and filled forms.

Sinks (i.e. sinkholes or closed depressions) are the dominant karst geomorphic manifestation throughout the Castile outcrop region; however, their geomorphic expression is varied. Sinkholes appear as both filled and open forms, where open sinkholes are connected directly to solutional conduits. Sinkholes, in general, form by two basic mechanisms, solutional incision of descending waters or collapse of upward stoping subsurface voids (e.g. Ford and Williams, 2007; White, 1988). Incised sinkholes generally exhibit lateral elongation and often have several, well-developed arroyos that converge towards a central drain. Collapse sinks tend to be expressed as near-circular or elliptical features with steep walls; however, sink morphology is often obscured because

of sediment infilling. Because collapse sinks tend to be near-circular and solutional sinks tend to be elongate (Ford and Williams, 2007; White, 1988), analyses of sink width to length ratios can be used to proxy for predicting sink origin when surficial expression is subdued by sediment filling. However, this is only an approximation because significant overprinting of collapse sinks by surficial processes can modify original morphology. Therefore, sinks with a width to length ratio of greater than 0.5 are elliptical or near-circular, hence these features likely represent collapse sinks, while features with a width to length ratio less than 0.5 likely represent solutional sinks or collapse sinks that have been heavily overprinted by surficial processes. Based on width to length analyses of 335 sinks identified during field mapping, 55% of the features are the result of collapse (Fig. V.7). It is likely that most of the remaining 45% of features are solutional sinks, but it is probable that many of these are collapse features that have been overprinted by solutional incision from meteoric processes. Each of the sinkholes used in this analysis was visually inspected in the field. Elliptical sinks observed in the field often contained large collapse blocks and appeared to be the result of subsidence collapse, while elongate sinks were deeply incised and showed clear evidence of significant solutional enlargement.

Solutional karren is well-developed on exposed rock surfaces and exhibits a wide-range of morphological forms. On near-vertical rock surfaces, deeply incised rillenkarren forms decimeter to meter long solutional flutes with centimeter-scale widths and depths (Fig. V.8A). On moderately inclined surfaces, rillenkarren are less-developed, generally forming shorter solution flutes that commonly converge in the down slope direction, creating complex, small-scale, dendritic channel networks (Fig. V.8B). On near horizontal surfaces, spitzkarren and kamenitzas are observed. Spitzkarren occurs as

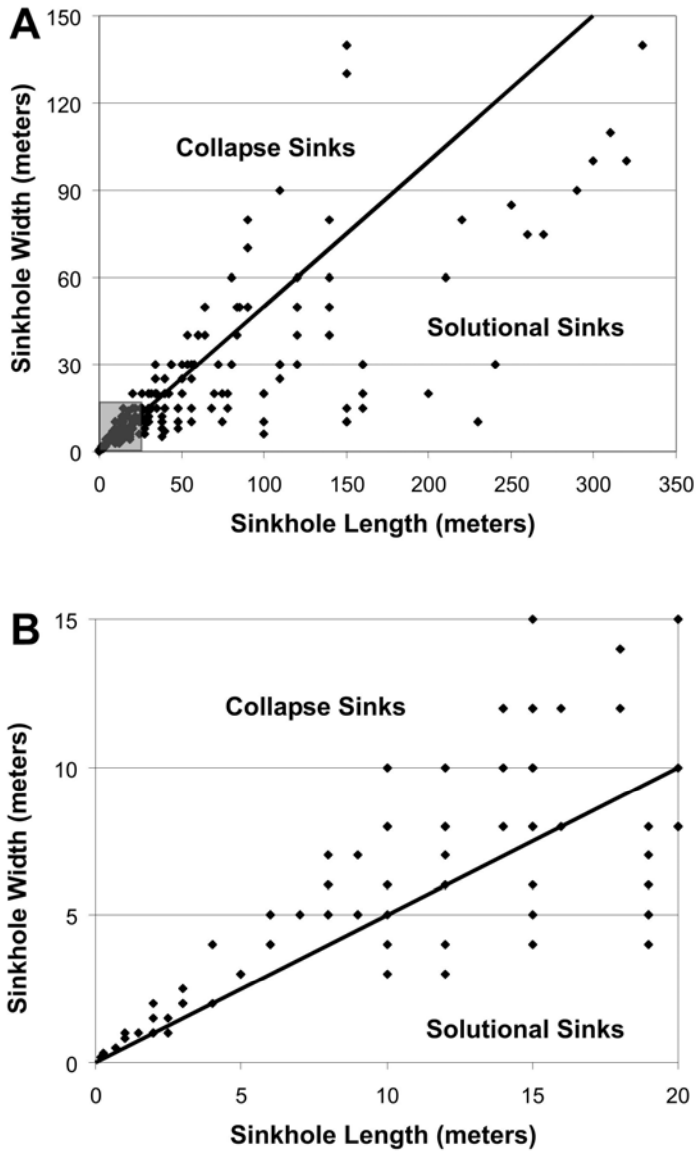

Fig. V.7: Plots comparing length to width of sinkholes identified in the field within the Castile outcrop region. Diamonds represent sinkhole length/width while the solid line represents sinkhole length/width = 2. Features that plot above and to the left of this line are interpreted as collapse sinks, while features that plot below and to the right are interpreted as solutional sinks. A) Composite plot showing the 335 individual sinkholes studied in the field, which gives the impression that sinkholes are primarily solution; however, 55% of sinks are interpreted as collapse features because many collapse sinks are less than five meters wide. B) Enlarged view of shaded area in Fig. V.7A showing that a many of the collapse sinks are small features that are not easily recognized in a plot of the entire data set. Observations in the field were consistent with interpretation of sinkhole origin basin on length to width analyses.

centimeter scale karst pinnacles (Fig. V.8C) on gently sloping surfaces that generally converge with rillenkarren where surface slope increases. Kamenitzas or solution pans form shallow, depressions floored with microbial mats on level surfaces, with depths up to several decimeters and widths ranging from decimeters to meters. In addition to traditional karren forms, unique karren are observed in the region. Where selenite is exposed at the surface, blade-like karren is formed (Fig 8D) and microkarren forms through preferential dissolution of individual crystals within selenite masses.

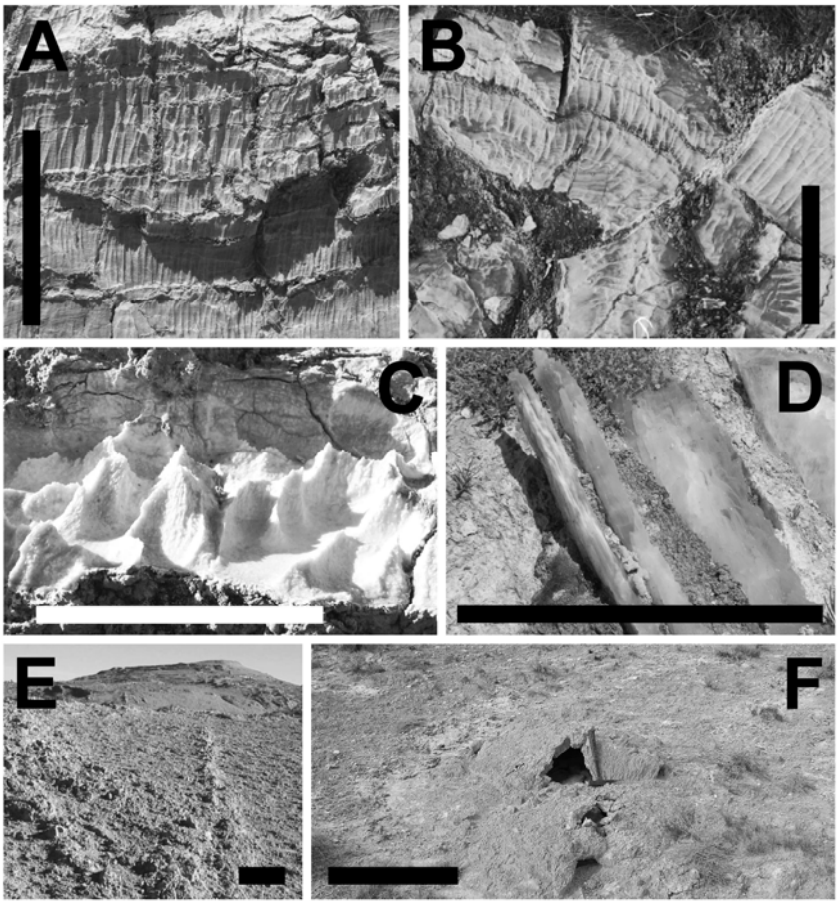

Fig. V.8: Surficial karst manifestations within the Castile outcrop region. Black scale bars are ~50 cm long. White scale bar is ~20 cm long. A) Incised rillenkarren on vertical surfaces; B) Complex rillenkarren on moderately inclined surfaces (~30º); C) Spitzkarren developed on near-horizontal surfaces; D) Blade-like karren developed on exposed tabular (selenite) gypsum surfaces; E) Extensive gypsum crusts developed on large bedrock exposures; F) Domal tumuli forming small hollow surface cavities.

On most exposed gypsum bedrock surfaces a thin, millimeter to centimeter crust develops that is largely devoid of macro flora (Fig. V.8E). The crusts form as a result of dissolution of the uppermost, exposed bedrock producing saturated fluids that subsequently precipitate a highly porous crust. This occurs because the lack of confinement does not constrict crystal growth (Cantón et al., 2003; Macaluso and Sauro, 1996). Although macroflora is uncommon, abundant lichens and microbial colonies are present on crust surfaces, which likely contribute to crust formation by retaining saturated fluids on exposed surfaces instead of allowing them to be removed by surface runoff. In addition to crusts, tumuli or gypsum blister caves commonly develop (Fig. V.8F). Tumuli form hollow, domed structures from gypsum precipitation in areas where crystal growth is laterally confined and results in surficial buckling (Calaforra and Pulido-Bosch, 1999). Although neither crusts nor tumuli are classic surficial karst manifestations in carbonate terrains, they are common features in gypsic terrains (Macaluso and Sauro, 1996).

EPIGENE CAVES

Epigene caves are widespread within the Castile outcrop region, but primarily occur as isolated features associated with well-developed, solutional closed depressions. Because of the high solubility of calcium sulfate, dissolution occurs rapidly in response to the modern environment. The near-linear solution kinetics of gypsum encourages greater epigenic dissolution at the surface proximal to the source of meteoric waters. This often forms large, incised sinkholes connected to small solution conduits (Klimchouk, 2000a). Epigene caves in the study area have been identified in laminated, massive, nodular and tabular (selenite) gypsum fabrics as well as in surficial gypsite deposits. All epigene

caves studied contain well-developed, small-scale scallops on walls, ceiling and floors, indicating that epigene caves transmit significant volumes of water at high velocities (White, 1988), most likely during intense, monsoonal precipitation events.

Although it is often impossible to definitively determine the origin of solution conduits that are too small to be entered by cavers, it is logical to assume that most small, solutional sinkhole drains in the study area are the result of epigene speleogenesis, which is consistent with solution kinetics of calcium sulfate (Klimchouk, 2000a). Where dissolution has been sufficient to create epigenic caves, they are generally limited laterally and form shallow groundwater recharge features. In these cases, the average passage aperture rapidly decreases away from insurgences, where the most intense dissolution occurs at the land surface and first few tens of meters in the subsurface (Fig. V.9). Beyond this, descending fluids are likely close to saturation and unable to dissolve additional bedrock (Klimchouk, 1996a; Jeschke et al., 2001). Occasionally, epigenic caves form shallow subsurface bypass features connecting points of differing elevation at the land surface and do not exhibit the typical passage aperture decrease. This may be the result of waters passing directly through these features without reaching complete saturation (Stafford et al., 2006).

Zombie Cave is one of the largest epigenic caves identified within the Castile Formation, with a 43 meter surveyed length and depth of 3 meters (Fig. V.10A). It isdeveloped in laminated gypsum, but the characteristics it exhibits are also typical of all observed epigenic caves found either in laminated, massive or nodular gypsum. The cave is developed along two distinct joint sets (Fig. V.5A) that intersect at acute angles, with the primary solutional conduit descending gently into the subsurface, forming a

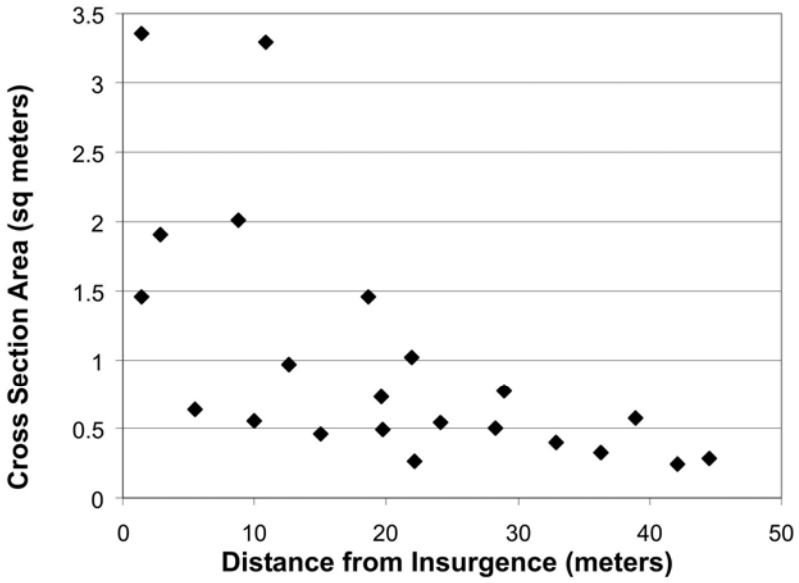

Fig. V.9: Plot showing cave passage cross-sectional area compared to distance from cave insurgence for five epigene caves (Cave of the Room, Dead East Cave, Lightening Cave, White Centipede Cave, and Zombie Cave) surveyed during this study in laminated and massive gypsum within Castile outcrop region. Note the rapid passage aperture decrease away from the insurgences as a result of the high solution kinetics of calcium sulfate.

branchwork cave pattern. Passage aperture decreases consistently away from the insurgence until it becomes too small to be humanly passable (Fig. V.10A). Throughout, several small infeeders converge along fractures that intersect the main conduit at various angles, which has probably enabled significant solutional enlargement to continue over greater distances than generally observed in epigenic caves within the Castile Formation. Although most observed epigenic caves in bedrock are laterally limited with development along joint sets, occasionally epigenic caves develop along the fold axis of anticlines where rock compression has produced fractures along the fold axis (Fig. V.5D), as is seen in Dead East Cave (Fig. V.10B). Epigene caves that have formed along folds are generally linear features consisting of a single main conduit, which exhibits minimal convergence from secondary infeeder passages.

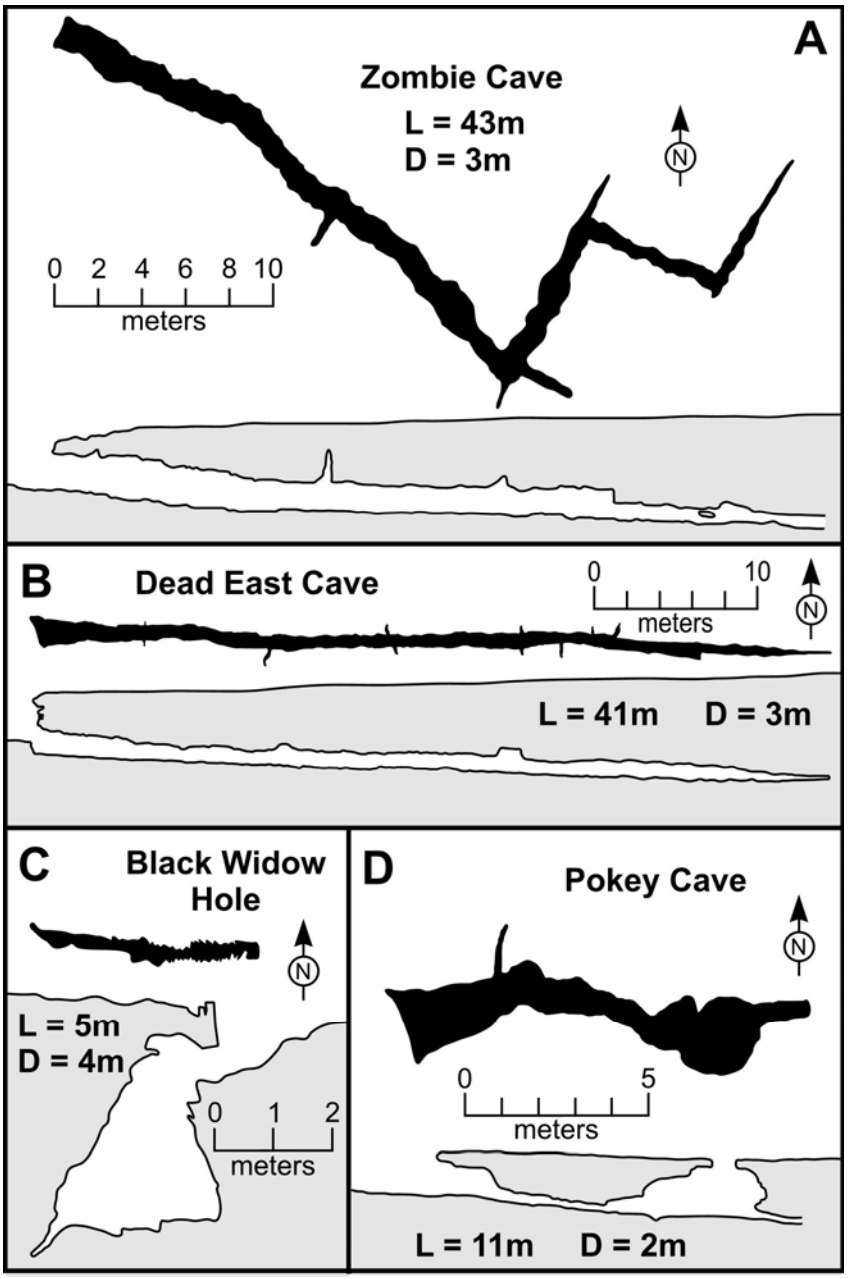

Fig. V.10: Simplified maps of representative epigene caves surveyed during this study in the Castile Formation, including plan view (solid black) and profile (gray outline) views. Note that "L" refers to surveyed length and "D" refers to surveyed depth on individual maps. A) Zombie Cave is developed along well-defined fractures (Eddy Co., New Mexico); B) Dead east Cave is developed along the fold axis of an anticline (Culberson Co., Texas); C) Black Widow Hole is developed in tabular (selenite) gypsum (Culberson Co., Texas); D) Pokey Cave is developed in gypsite near the contact with gypsum bedrock (Culberson Co., Texas). Note that all north arrows indicate magnetic north. At the time of survey, Fall 2006, magnetic declination was ~8° east.

Epigene caves developed in tabular gypsum (selenite) exhibit similar characteristics with those developed in other gypsum fabrics. These caves are the least common type of epigenic cave, which is directly related to the limited areas where selenite is exposed at the land surface. They are small and laterally limited, similar to other epigenic caves, but cave development is controlled by the inherent selenite crystal structure (Fig. V.11A), where partings between large tabular crystals provide preferential flow paths for solutional enlargement. Passage configuration and wall morphology directly reflect changes in crystal orientation and intersection, instead of exhibiting solutional control related to structural deformation. Caves developed in selenite demonstrate well the critical role of bedrock partings, whether fractures, bedding or individual crystal partings, for epigene solutional development in gypsum. Black Widow Hole (Fig. V.10C) represents a typical epigene cave in selenite, where the solutional passage is oriented along crystal faces, descending steeply into the subsurface where it rapidly becomes too small for human exploration.

In surficial gypsite deposits (i.e. gypsic soils), epigene caves are common where they frequently develop along the contact with underlying gypsum bedrock. Although gypsite is a surficial mantling within the study area and not actually bedrock of the Castile Formation, cave development within surficial deposits and underlying bedrock appears related. Most epigene gypsite caves are small, laterally limited and appear largely ephemeral. Many contain several collapse entrances connected in series, where dissolution of secondary gypsum cements has enabled suffusion of insoluble soil components (Fig. V.10D, V.11B). Generally gypsite caves become too small to be enterable or plugged with sediment within a few tens of meters of their insurgence.

However, in rare occurrences epigene gypsite caves can connect directly to caves in gypsum bedrock, suggesting that the occurrence of gypsite caves is related to bedrock caves by providing preferential flow paths for descending waters.

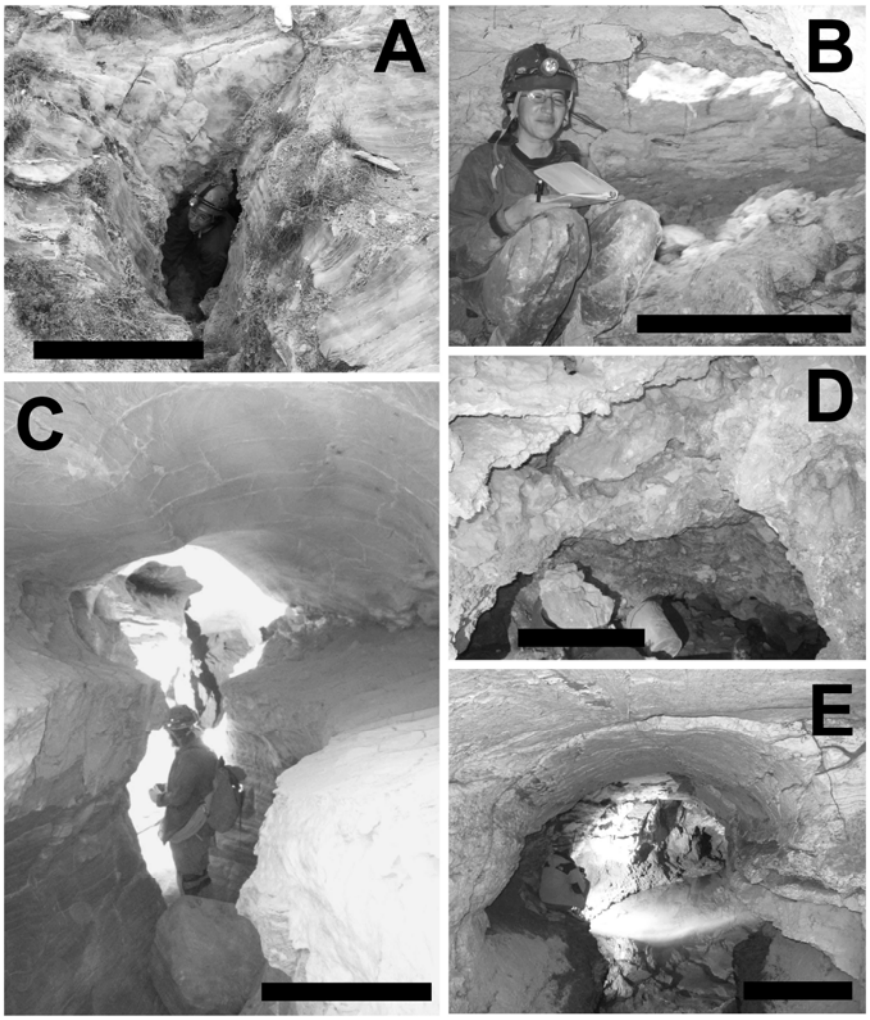

Fig. V.11: Caves of the Castile Formation. Black scale bar are ~1 m long. A) Black Widow Hole (Culberson Co., TX) is an epigene cave developed entirely in tabular (selenite) gypsum ; B) Pokey Cave (Culberson Co., TX) shows typical characteristics of gypsite caves including collapse regions through the thin gypsic soils; C) Epigene overprinting of hypogene conduits commonly produces passages with well-defined floor trenches and elliptical ceiling tubes (Crystal Cave, Culberson Co., TX); D) Isolated hypogene voids occur within calcitized masses (China Mine, Culberson Co., TX); E) Brantley Stream Cave (Culberson Co., TX) is one of several hydrologically active caves that exhibit hypogene morphologies and continuously discharge spring water through the year.

HYPOGENE CAVES

In contrast to epigene speleogenesis, which includes both epigene caves and most surficial karst manifestations, hypogene caves do not form with a direct connection to surface meteoric processes. Instead, hypogene speleogenesis is associated with dissolution from rising fluids that are delivered from undersaturated reservoirs beneath soluble rock units (Ford, 2006). In hypogenic systems, including both carbonate and evaporitic lithologies, dissolution is driven by a mixed convection hydrologic system, composed of components of both forced and free convection (Klimchouk, 2000c, 2007; Anderson and Kirkland, 1980; Kohout et al., 1988). Forced convection is driven by differences in hydraulic potential across the region. Fluids from lower, pressurized aquifers or transmissive zones rise towards upper, lower hydraulic pressure regions, often the regional base level (Tóth, 1999). In order for pressurized (artesian) aquifers to develop, they must be confined or semi-confined such that pressure gradients can develop (Klimchouk, 2007). In the study area, the gypsum and anhydrite rocks of the Castile Formation act as leaky seals for the lower clastic Bell Canyon Formation (Fig. V.3) (Lee and Williams, 2000). Here, fluid is directed vertically through fractures within the Castile evaporites. These fractures rarely cross the entire formation, but instead are composed of discontinuous fracture sets that limit cross-formational connectivity (Hill, 1996), which induces both vertical and horizontal flow between fractured regions (Klimchouk, 2007). Such limited connectivity results in sluggish flow driven by forced convection until breakthrough can be achieved, hence free convection becomes an important component of the dissolution process (Klimchouk, 2000b,c, 2007). Through free convection, aggressive waters are continuously delivered to the dissolution front through the

simultaneous rising of less dense, undersaturated fluids and the sinking of more dense, saturated fluids (Anderson and Kirkland, 1980; Klimchouk, 2007). Rising, undersaturated fluids are supplied by the lower transmissive zone, while descending, saturated fluids are removed down gradient through the same lower aquifer. Although the effects of speleogenesis can be observed in any type of soluble host rock (e.g. limestone, dolomite), they are particularly well pronounced in calcium sulfate rocks (i.e. gypsum / anhydrite) where high solubility enables the development of steep density gradients through free convection (Klimchouk, 2007; Anderson and Kirkland, 1980).

Traditionally, hypogenic speleogenesis has been associated with multi-storey maze caves (Klimchouk, 1996, 2000b, 2000c) and isolated subsurface voids (Kempe, 1996). However, recent studies have shown that a diagnostic suite of morphological features observed in caves provides evidence of dissolution driven by a mixed convection system that is independent of cave patterns (Klimchouk, 2000b, 2003, 2007; Frumkin and Fischhendler, 2005; Stafford et al., 2007a). This morphological suite of features includes: 1) risers, 2) outlets, and 3) half-tubes. Risers or feeders are cuspate wall and floor features (Fig. V.12A,D) that indicate preferential flow paths that connect transmissive zones to soluble zones. This is where ascending, undersaturated fluids are delivered to soluble rock and saturated fluids are returned to transmissive zones. Outlets or cupolas are domal structures formed along ceilings (Fig. V.12C,D) where ascending fluids move toward higher elevations and lower pressures (including upper transmissive zone and ultimately base level) through dissolution of soluble host rock. Half-tubes are developed on ceilings and walls where undersaturated fluids migrate from risers to outlets, forming concave, semi-circular channels vertically along walls (Fig. V.12D) or horizontally along the axis

of ceiling passages (Fig. V.12B). Although any of the features alone can be formed by various speleogenetic processes, when found together in composite morphologic suites, they provide unequivocal evidence of hypogene speleogenesis (Klimchouk, 2007; Stafford et al., 2007a).

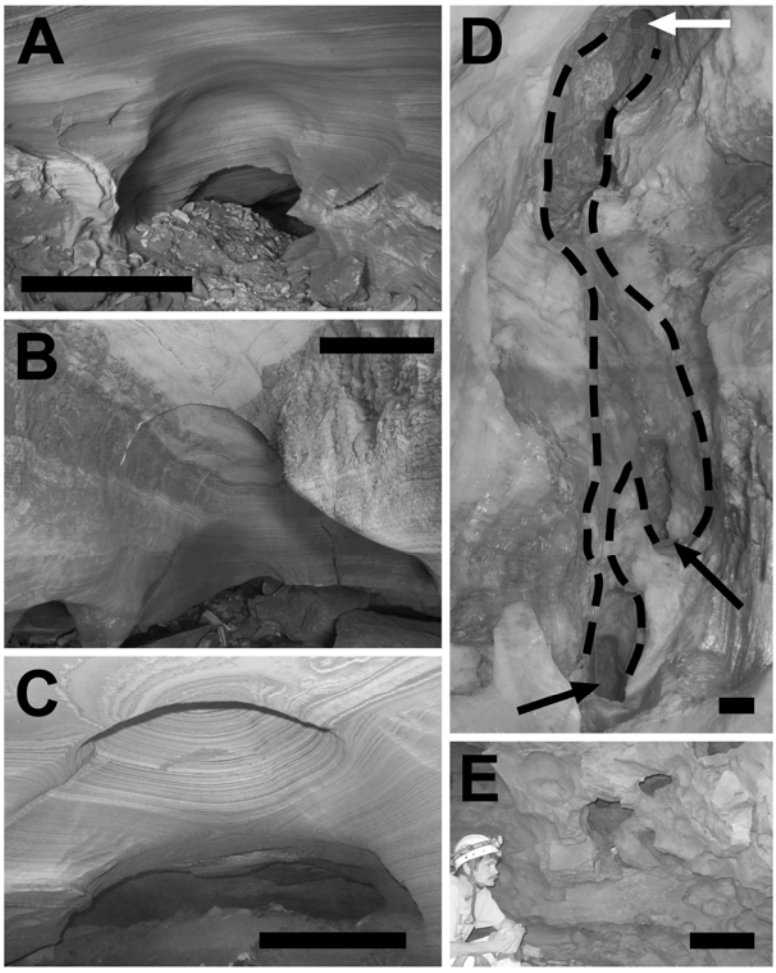

Fig. V.12: Morphologic cave features indicative of hypogene speleogenesis within the Castile Formation. Black scale bars are ~0.5 m long. A) Typical riser feature intersecting primary cave passage (Dead Bunny Hole, Culberson Co., TX); B) Well-developed ceiling half-tube (Dead Bunny Hole, Culberson Co., TX); C) Typical ceiling cupola or outlet in a series of domal ceiling features (Dead Bunny Hole, Culberson Co., TX); D) Complete morphologic suite of hypogene features developed in selenite: dashed lines delineate wall half-tubes, black arrows indicate separate risers and the white arrow indicates outlet cupola (Crystal Cave, Culberson Co., TX); E) Typical region of solutional boneyard morphology (Dead Bunny Hole, Culberson Co., TX).

Dense clusters of caves and sinkholes within the Castile outcrop region (Fig. V.4) suggest that karst development is dominated by hypogene speleogenesis in the western Delaware Basin (Stafford et al., 2007b). Caves interpreted in the study area as having formed through hypogene processes inherently contain an epigenic component because surface denudation has breached them, enabling human entry and study. Therefore, overprinting by epigene processes complicates speleogenetic interpretations. However, overall cave morphology and suites of morphological features provide strong evidence for hypogene speleogenetic origins. Many caves exhibit extensive and complex spatial patterns with cave development that is not supported by their limited surficial drainage areas had they formed by epigene processes. Most caves show evidence of hypogene origins, supporting regional speleogenetic interpretations based on clustering of the surface expression of caves and sinkholes (Stafford et al., 2007b). However, hypogene caves within the Castile Formation are diverse, as shown below. They demonstrate well the continual evolution of speleogenetic systems where caves that have formed by confined ascending fluids are subsequently being overprinted by surficial, epigene processes.

Rectilinear maze caves, commonly attributed to hypogenesis, are uncommon within the Castile outcrop region, most likely because the Castile Formation is not composed of distinctly interbedded lithologies which promote rectilinear maze development. However, many caves exhibit ramiform, maze-like regions or complex patterns composed of ramiform, spongework and anastomotic passage configurations. Parks Ranch Cave is the largest cave documented within the Castile Formation, with 6596 m of surveyed passage, forming a complex anastomotic pattern (Fig. V.13) (Stafford, 2006). However, Dead

Bunny Hole (Fig. V.14B) is the most complex maze cave documented within the study area, although it has a surficial drainage area of less than one square kilometer. It is developed in both laminated gypsum and calcitized evaporites, with a current surveyed length and depth of 439 meters and 14 meters, respectively. The cave is developed in three offset storeys that decrease in depth towards the northwest, which largely correspond to lithologic variations in bedrock. The upper and lower levels are developed in laminated gypsum, while the middle level occurs in calcitized evaporites. The southwestern portion of the cave is primarily developed along the fold axes of anticlines (Fig. V.5E), while the central and northeastern portions of the cave follow along fractures. Throughout the cave, the floor is mantled with extensive breakdown and allogenic sediments; however, abundant risers (Fig. V.12A), outlets or cupolas (Fig. V.12C) and half-tubes (Fig. V.12B) are distributed throughout, as well as regions of highly porous,

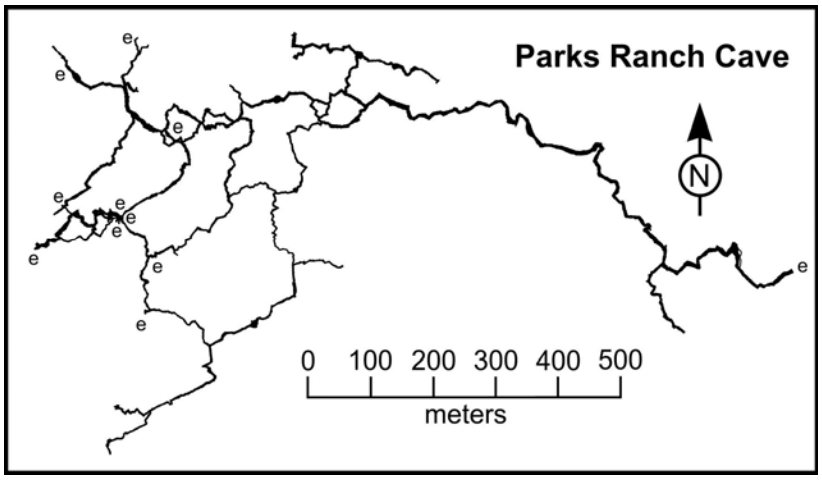

Fig. V.13: Plan view map of Parks Ranch Cave which exhibits a complex anastomotic cave pattern (adapted from Stafford, 2006). Parks Ranch Cave is the longest, currently documented cave within the Castile Formation, with a surveyed length of 6596 m. This cave contains significant features indicative of hypogene origins that have been heavily overprinted by epigene processes. The overprinting features show the continuous speleogenetic evolution of karst within the study area. Major entrances are labeled with the letter “e”.

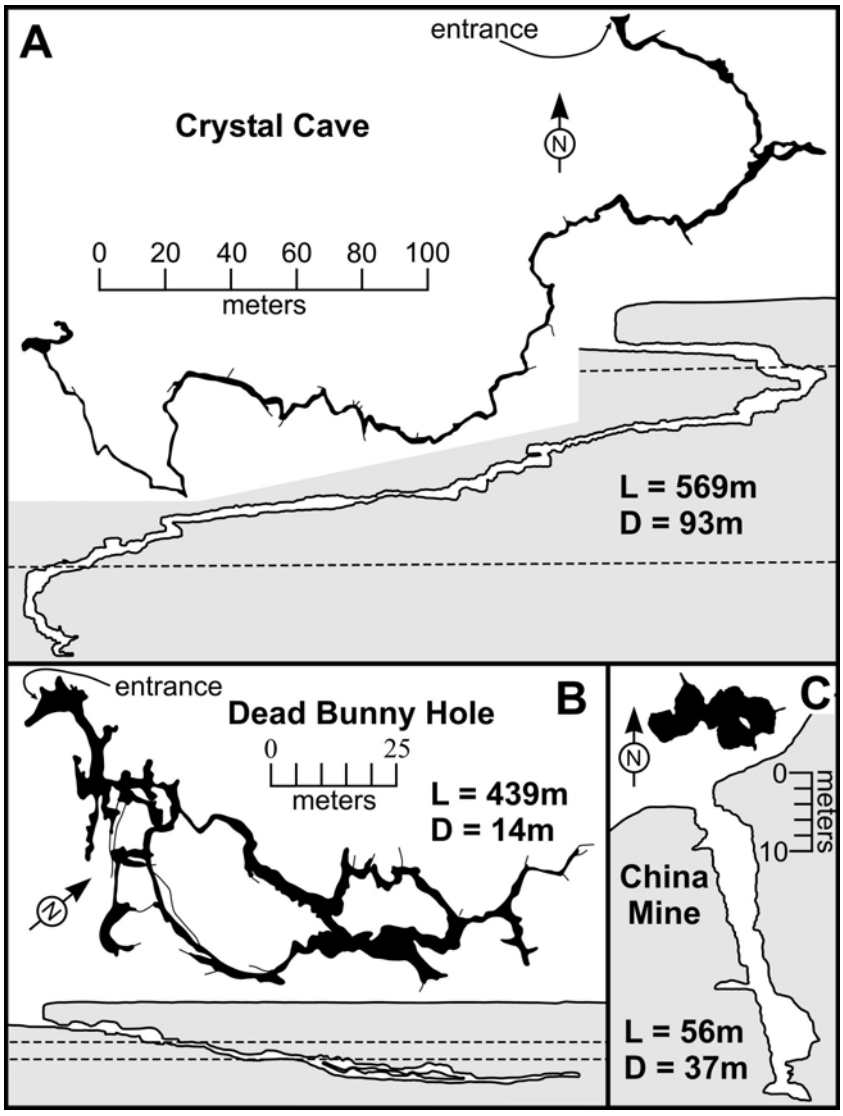

Fig. V.14: Simplified maps of representative hypogene caves surveyed during this study in the Castile Formation, including plan view (solid black) and profile (gray outline) views. Note that "L" refers to surveyed length and "D" refers to surveyed depth on individual maps. A) Crystal Cave represents a large single riser system and is developed in a wide range of gypsum fabrics (Culberson Co., Texas) (Dashed line in profile view delineates the approximate boundaries between major changes in lithologic fabric); B) Dead Bunny Hole is a complex cave consisting of anastomotic and maze-like passages within laminated gypsum and calcitized gypsum (Culberson Co., Texas) (Dashed lines in profile view delineate approximate boundaries between cave storeys); C) China Mine is an anthropogenic feature excavated in calcitized gypsum that intersects several isolated hypogene voids (Culberson Co., Texas). Note that all north arrows indicate magnetic north. At the time of survey (Fall 2006) magnetic declination was ~8° east.

boneyard morphology (Fig. V.12E). Few scallops, indicative of significant epigene processes, were observed in the cave. The complex cave pattern and associated morphological suite indicate that the cave was originally formed under confined conditions where non-competitive, mixed convection hydrologic flow simultaneously produced solutional conduits along all available fractures and anticlines. Currently, the cave is being overprinted by epigene process, but because of the limited surficial drainage area, much of the original hypogene morphology is preserved.

Many of the hypogene caves of the Castile Formation do not exhibit traditional patterns, but instead occur primarily as single ascending passages, forming the largest and deepest caves within the study area. Crystal Cave (Fig. V.14A) is the deepest cave yet identified in the Castile outcrop region, with a length and depth of 569 meters and 93 meters, respectively. From the sinkhole entrance, the cave descends gently, with only two major pits and many small drops. The cave alternates between elliptical passages and tall domal passages, with a small incised canyon along the axis of the floor that is well-developed near the entrance (Fig. V.11C) and intermittently throughout the cave. Scallops are only observed on the walls and floor of the incised canyon, suggesting that this portion of the cave was formed by epigene overprinting of the original hypogene morphology. The upper portion of the cave, before the first pit, is developed largely in laminated gypsum. The lowest portion of the cave, the second pit and below, is developed entirely in tabular gypsum (selenite) (Fig. V.12D) forming a steeply descending series of small drops beginning at the base of the second pit. The middle portion is developed in a complex suite of gypsum fabrics that alternate between laminated, massive, and nodular tabular fabrics, as well as calcitized evaporites; however,

the majority of the middle portion appears to have developed in association with a zone of secondary tabular gypsum (selenite). Cave passage and the associated selenite zone commonly cut across gypsum fabrics at acute angles suggesting that lithologic variability exerted little control on cave development, as would be expected if the cave had formed by descending, meteoric waters; instead, the cave passage development appears genetically related to the occurrence of secondary selenite. Through the majority of the cave, a well-developed ceiling channel is observed along with many small to large cupolas, creating an irregular ceiling profile. The lowest portion of the cave is completely flooded and beyond exploration, but the sump area appears very similar to a large-scale, isolated riser feature. Based on cave morphology and passage development that appears largely associated with secondary tabular gypsum, Crystal Cave was formed as a large, single rising column of water where dissolution was dominated by mixed convection driven by variations in the density of ascending and descending fluids along limited fractures with poor hydraulic connectivity.

Isolated chambers are also observed in most calcitized evaporite masses. These are usually meter-scale ovoid chambers that show no relation to the modern geomorphic landscape, but are developed within highly porous biogenic limestone. Associated with many subsurface calcitized masses are significant accumulations of native sulfur (Hentz and Henry, 1989). However, minimal native sulfur is observed at surficial exposures of calcitized masses. Therefore, it is logical to assume that the isolated voids found within some calcitized masses are related to sulfuric acid dissolution of the biogenic limestone, where native sulfur in the presence of oxic waters has produced aggressive, sulfuric acid-rich waters (Fig. V.3). Of the hypogenic caves formed in calcitized masses, one was

previously reported in association with late 19th century mining activity (Phillips, 1917). China Mine (Fig. V.14C), also known as Sulfur Mine Cave or Sulphuretted Hydrogen Cave (Hill, 1996; Smith and Elliott, 1994), is a vertical mine shaft that descends to a depth of 37 meters. Hill (1996) reported this feature as a natural pit cave that had been modified by sulfur mining activity. During this study, the feature was mapped and determined to largely represent an anthropogenic mine shaft that had been excavated along a fracture containing minimal sulfur accumulations. However, five small (less than 10 m^3 each), previously undocumented, natural voids were identified (Fig. V.11D) at three separate depths. Although the entire feature was originally misinterpreted as a natural cave, the recently documented natural voids which were intercepted during original mining show direct evidence of hypogene speleogenesis within calcitized masses.

The examples above exemplify the diversity of the hypogene caves that are developed within the Castile Formation, by providing end member examples of a maze cave (Fig. V.14A) and a cave consisting of a single major riser feature (Fig. V.14B). Isolated voids within calcitized masses indicate that this is not a phenomenon limited to the gypsum facies, but instead occurs throughout the entire Castile Formation. Although space does not allow, numerous other examples exist within the Castile outcrop region, including several features that contain hydrologically active spring discharge, yet contain clear evidence of hypogene origins (Fig. V.11E). Based on abundant aquatic fauna in these caves, the hydrologically active stream caves do not appear to be directly related to seasonal, monsoonal precipitation events. It is more likely that they are related to artesian discharge derived from lower transmissive zones. Future studies on regional hydrology are planned to elucidate the source and flow paths of these hydrologically active features.

INTRASTRATAL BRECCIA

Throughout the study area and the entire Castile Formation, zones of brecciation are common; however, the manifestations are varied. Vertical breccia pipe structures are widespread and can extend through the entire thickness of the Castile Formation (Hill, 1996). In contrast to vertical breccia structures, laterally extensive blanket breccias frequently occur over wide regions. Commonly, blanket breccias and breccia pipes are manifested as solution subsidence valleys, dissolution troughs and collapse pits. However, all breccia occurrences are genetically related because they form from intrastratal dissolution of evaporites through hypogene speleogenesis, where void space created in the subsurface subsequently collapsed.

Breccia pipes have been documented throughout the Delaware Basin, not only related to the Castile Formation but also the Salado and Rustler Formations (Anderson and Kirkland, 1980). Large breccia pipes are developed along the northern and eastern margin of the Delaware Basin above the Capitan Reef and extend vertically for hundreds of meters through the Castile and Salado Formations. These breccia pipes are either expressed as negative topographic features where collapse has occurred or as positive relief features where past collapse formed resistant breccias that are now expressed as mounds through topographic inversion related to surface denudation (Bachman, 1980). Anderson and Kirkland (1980) proposed a brine density convection model for breccia pipe development where undersaturated fluids from the Capitan Reef aquifer dissolve overlying evaporites. In their model, undersaturated, low density fluids rise and dissolve overlying evaporites until fluids become saturated. Saturated, high density fluids subsequently sink back to the lower aquifer along the margins of upward stoping solution

pipes. Therefore, aggressive waters are continuously delivered to the top of an upward stoping collapse column, while sinking, saturated waters prohibit lateral dissolution along the margins of the collapse structure. Upward stoping and hypogene dissolution continue until surficial breaching occurs, which results in a shift from dissolution dominated brine density convection (i.e. free convection) to dissolution dominated by forced convection with an established outlet for ascending, artesian fluids (Klimchouk and Andrejchuk, 1996).

Blanket breccias (Fig. V.15B) are widespread within the Castile Formation and have been largely associated with dissolution of halite interbeds (Anderson et al., 1972). Halite interbeds were deposited throughout the Castile Formation; however, they have largely been removed from the entire western Delaware Basin through subsurface dissolution resulting in thinning of the Castile Formation to the west and the development of laterally extensive breccia horizons. Most blanket breccias are centimeters to decimeters thick and are believed to have formed by laterally migrating fluids, undersaturated with respect to halite (NaCl), which dissolve salt interbeds such that overlying calcium sulfate beds were no longer supported and collapsed (Anderson et al., 1972). Associated with the solution of halite, increased calcium sulfate dissolution is expected as a result of solute ion pairing (Klimchouk, 1996a), such that brecciation is further enhanced by dissolution of calcium sulfate proximal to dissolved halite interbeds. Solution subsidence valleys, narrow linear topographic lows, occur along the western edge of the Castile outcrop area. They have been shown to form along graben boundary faults up to 75 meters deep, where the lower fault limit is coincident with the upper limit of halite dissolution (Hentz and Henry, 1989). Larger dissolution troughs occur within the central Delaware Basin, which have been

attributed to similar processes in the Castile, Salado and Rustler Formations (Anderson et al., 1978). Many of these larger features have been subsequently filled with thick sequences of Quaternary alluvium (Bachman, 1980).

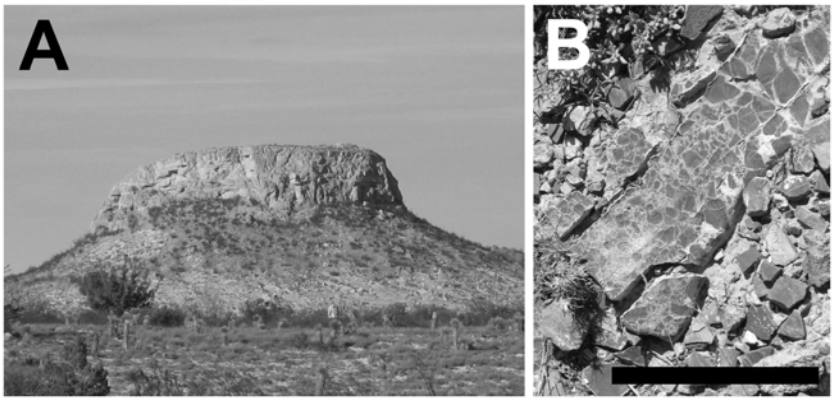

Fig. V.15: Intrastratal brecciation and calcitization in the Castile Formation. A) Typical calcitized butte, which forms a residual hill ~40 m taller than the surrounding gypsum landscape and contains a breccia pipe core; B) Surficial exposure of blanket breccia that is likely the result of intrastratal dissolution of halite and subsequent collapse that has been calcitized. Black scale bar is ~0.5 m long.

Throughout the Castile outcrop region, breccia pipes and blanket breccias are common. This region is not underlain by the Capitan Reef aquifer as occurs in the northern and eastern Delaware Basin; however, the evaporites of the central Delaware Basin, including those of the outcrop area, are underlain by the clastic Bell Canyon aquifer which provided the source fluids for hypogene dissolution and formation of brecciated zones (Lee and Williams, 2000). Many of these brecciated zones are also associated with calcitization where both vertical (Fig. V.15A) and laterally extensive calcitized, breccia zones (Fig. V.15B) have developed (Kirkland and Evans, 1976; Hentz and Henry, 1989). Whether calcitization was contemporaneous with or subsequent to brecciation is unclear. However, the same transmissive and soluble zones that enabled

hypogene dissolution and brecciation also have provided many of the preferential flow paths for ascending hydrocarbons that provided the energy source for sulfur reducing bacteria associated with evaporite calcitization (Fig. V.3). Therefore, both brecciation and calcitization provide direct evidence of the widespread occurrence of hypogene speleogenesis within the Castile Formation and the entire Delaware Basin.

DISCUSSION and CONCLUSIONS

Cave and karst development within the Castile Formation is widespread and diverse, ranging from surficial to intrastratal manifestations associated with both epigene and hypogene speleogenesis. The surficial landscape is dominated by epigenic karst, as is expected for highly soluble, exposed, evaporite rocks. However, cave development and subsurface transmissive zones (e.g. brecciated zones) are dominated by hypogene processes as predicted by cluster analyses of karst feature distribution (Stafford et al., 2007b). Most caves exhibit hypogene origins. More than 55% of sinkholes are collapse features and the widespread occurrence of calcification and brecciation all suggest that the greater abundance of hypogene karst manifestations observed along the western margin of the Castile outcrop region may be the result of a sampling bias created by surface denudation, because hypogene features inherently form without a direct surface connection. With greater surficial denudation towards the west (Fig. V.3), it is probable that a greater proportion of hypogene features will be breached and exposed at the land surface in this region, accounting for the greater abundance of caves within the western portion of the outcrop region. It is probable that numerous other hypogene caves exist in the subsurface to the east, where surface denudation has yet to breach them. By extension

of the theory of hypogene speleogenetic dominance in the region, it is likely that hypogene processes continue to actively form solutional conduits and affect calcium sulfate diagenesis in regions where the Castile Formation remains buried in the subsurface to the east. Therefore, as surface denudation continues to strip away overlying strata and the dissolution front of the Castile Formation moves eastward, it is expected that more hypogene caves will be breached to the east, in the down dip direction of the Castile Formation. This eastward shift in denudation will result in continual breaching of hypogene caves that have formed by ascending fluids originating from the underlying Bell Canyon aquifer.

Although karst development appears to be dominated by hypogene processes, epigene processes can significantly overprint evidence of hypogenic origins. Parks Ranch Cave (Fig. V.13) is the only cave within the study area that was formally studied prior to current research (Sares, 1984; Nance, 1993). It is a complex, anastomotic cave system with 6,596 meters of surveyed passage (Stafford, 2006), which was interpreted as an epigenic cave formed as a subsurface bypass feature that developed in association with the Black River, an ephemeral spring fed stream located a few kilometers to the north (Sares, 1984). However, extensive evidence of hypogene origins is common throughout the cave, including regions which contain diagnostic morphological features (i.e. risers, cupolas and half-tubes). Although the evidence is extensive, numerous regions of the cave have been heavily overprinted by epigene processes. This indicates that it is necessary to study entire caves instead of only the most accessible portions before interpreting speleogenetic origins. Because hypogene karst develops in confined or semi-confined settings, evidence of hypogene processes in caves must predate epigenic

development that is forming in equilibrium with the modern climatic regime. Therefore, hypogene speleogenesis formed the initial conduit porosity of Parks Ranch Cave while the region was still in confinement, but epigene processes have utilized these preexisting flow paths and are currently overprinting the original cave system heavily, such that it is difficult to determine the relative importance of epigene and hypogene processes on the formation of this specific cave. Further study of Parks Ranch Cave should reveal interesting details on the local speleogenetic evolution of this small area of the Castile Formation, but it provides little information on the large, basin-scale picture of speleogenesis within the Castile Formation.

Evaporite karst and hypogene speleogenesis are generally underappreciated in North American karst research; however, this investigation has shown that both deserve greater attention in order to better evaluate regional speleogenetic patterns. Hypogene caves and intrastratal breccias within the Castile Formation provide significant insight into basin evolution and previous fluid migration paths within the Delaware Basin. This has implications for not only modern groundwater behavior but also regional hydrocarbon maturation and migration, as associated with evaporite calcitization. The high solution kinetics of calcium sulfate rocks of the Castile Formation results in a landscape that rapidly responds to the modern environment, such that the speleogenetic evolution of the region is preserved to varying degrees. Most caves show extensive evidence of hypogene origins, including complete suites of diagnostic morphologic features. However, hypogene caves exhibit variable degrees of epigenetic overprinting because of surficial breaching, ranging from minor floor entrenchment to significant solutional overprinting and large introductions of allogenic sediments. Karst development in the Castile

Formation demonstrates that speleogenetic systems need to be viewed from an evolutionary standpoint, because the modern environment only reflects the current stage of development and may not represent the origins of cave and karst features within the region.

ACKNOWLEDGEMENTS

The authors are grateful to the numerous individuals who made this study possible. Generous land access was provided to private ranches in Texas by Jack Blake, Draper Brantley, Stanley Jobe, Lane Sumner, and Clay Taylor. John Jasper and Jim Goodbar provided assistance with cave and karst studies on BLM (Bureau of Land Management) public land within New Mexico. Volunteer cavers assisted with cave surveys, including: Jim Kennedy, Lucas Middleton, Charley Savvas, Beverly Shade, and Vickie Siegel. Alexander Klimchouk provided many useful discussions on hypogene processes. Research was partially funded by grants from the New Mexico Geological Society (NMGS) and the New Mexico Tech Graduate Student association, with support from the National Cave and Karst Research Institute (NCKRI). The authors are grateful to Jo De Waele, Ph. Audra and an anonymous reviewer for their insightful review comments, which improved this manuscript.

CHAPTER VI:
HYPOGENE SPELEOGENETIC CALCITIZATION:
LIMESTONE BUTTES OF THE CASTILE FORMATION, DELAWARE BASIN

ABSTRACT

Evaporite calcitization within Castile Formation of the Delaware Basin is more widespread and diverse than originally recognized. Coupled field and GIS studies have identified more than 1000 individual occurrences of calcitization within the Castile Formation outcrop area, which includes both calcitized masses (e.g. limestone buttes) and laterally extensive calcitized horizons (e.g. limestone sheets). Both limestone buttes and sheets commonly contain a central brecciated zone that we attribute to hypogene dissolution. Lithologic fabric of calcitized zones ranges from little alteration of original varved laminae to fabrics showing extensive laminae distortion as well as extensive vuggy and open cavernous porosity. Calcitization is most abundant in the western portion of the Castile outcrop region where surface denudation has been greatest. Calcitization often forms linear trends indicating fluid migration along fractures but also occurs as dense clusters indicating focused, ascending, hydrocarbon-rich fluids. Native sulfur, secondary tabular gypsum (e.g. selenite) and hypogene caves are commonly associated with clusters of calcitization. This assemblage suggests that calcium sulfate diagenesis within the Castile Formation is dominated by hypogene speleogenesis.

INTRODUCTION

Calcitization of evaporite minerals is a common occurrence and has been described in numerous settings associated with either bacterial sulfate reduction (BSR), thermal sulfate reduction (TSR) or infiltration of meteoric waters. Adams (1944) originally documented the occurrence of “castiles” within the Ochoan (Lopingian) (Fig. VI.1) rocks of the western Delaware Basin (Fig. VI.2A). Kirkland and Evans (1976) recognized these features as calcitized evaporites, which they termed “limestone buttes”, and associated them with BSR and near-surface, methane seeps. Originally, calcitization within the Delaware Basin was only associated with isolated masses within the Castile and Salado Formations, including 71 limestone buttes physically documented (Fig. VI.2B) and over 100 estimated (Kirkland and Evans, 1976). However, this study, in conjunction with cave and karst studies in the region, has found that the occurrence of calcitization within the Castile Formation is far more extensive, including not only numerous, newly documented isolated masses but also laterally extensive calcitized zones. Additional calcitized evaporites occur in the carbonate facies on the margins of the Delaware Basin were anhydrite nodules have been replaced by calcite spar as gravity driven meteoric waters passed downdip to the east through the Capitan Reef complex (Scholle et al., 1992).

Most previous studies of the Castile Formation have focused on its Permian deposition (e.g. Adams, 1944, 1972; Anderson et al., 1972; Hill, 1996), while occurrences of calcitization have long been noted to be associated with native sulfur deposits, including several ore bodies that have been mined economically (e.g. Wessel and Wimberly, 1992). Recently calcitization has also been found to be associated with occurrences of hypogene karst (i.e. cavernous porosity formed by ascending fluids within

a confined or semi-confined system) (Stafford et al., 2007b, 2008) and selenite masses (Lock et al., 2004) within the Castile Formation.

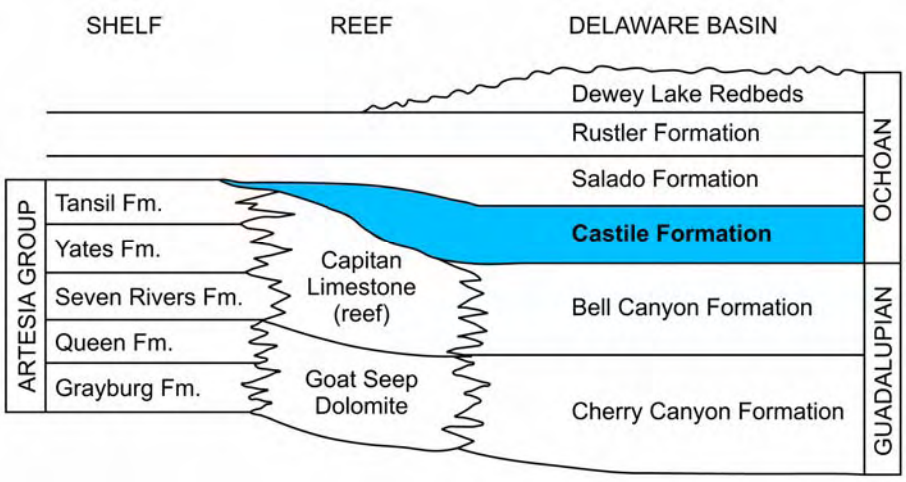

Fig. VI.1. Stratigraphic north (Shelf) to south (Delaware Basin) section of significant lithologic units within the study area. Note the relationship between the Castile Formation (blue) and adjacent formations (adapted from Scholle et al., 2004).

Studies in Miocene gypsum deposits of the western Ukraine have found similar diagenetic assemblages of calcitized evaporites, native sulfur, selenite and extensive cave systems (Klimchouk, 1997). These Miocene diagenetic assemblages have been attributed to hypogene speleogenetic processes similar to those observed in Mississippi Valley Type deposits. Salt dome caprock studies within the Gulf of Mexico contain complex diagenetic assemblages of anhydrite, calcitized evaporites, sulfur and abundant vuggy porosity, suggesting a similar diagenetic environment to that of Castile buttes (Lock et al., 2004).

Current research by the authors within the Castile Formation focuses on the diagenetic evolution of calcium sulfate rocks, with specific emphasis on the relationship between calcitized evaporites, native sulfur, secondary tabular gypsum (i.e. selenite),

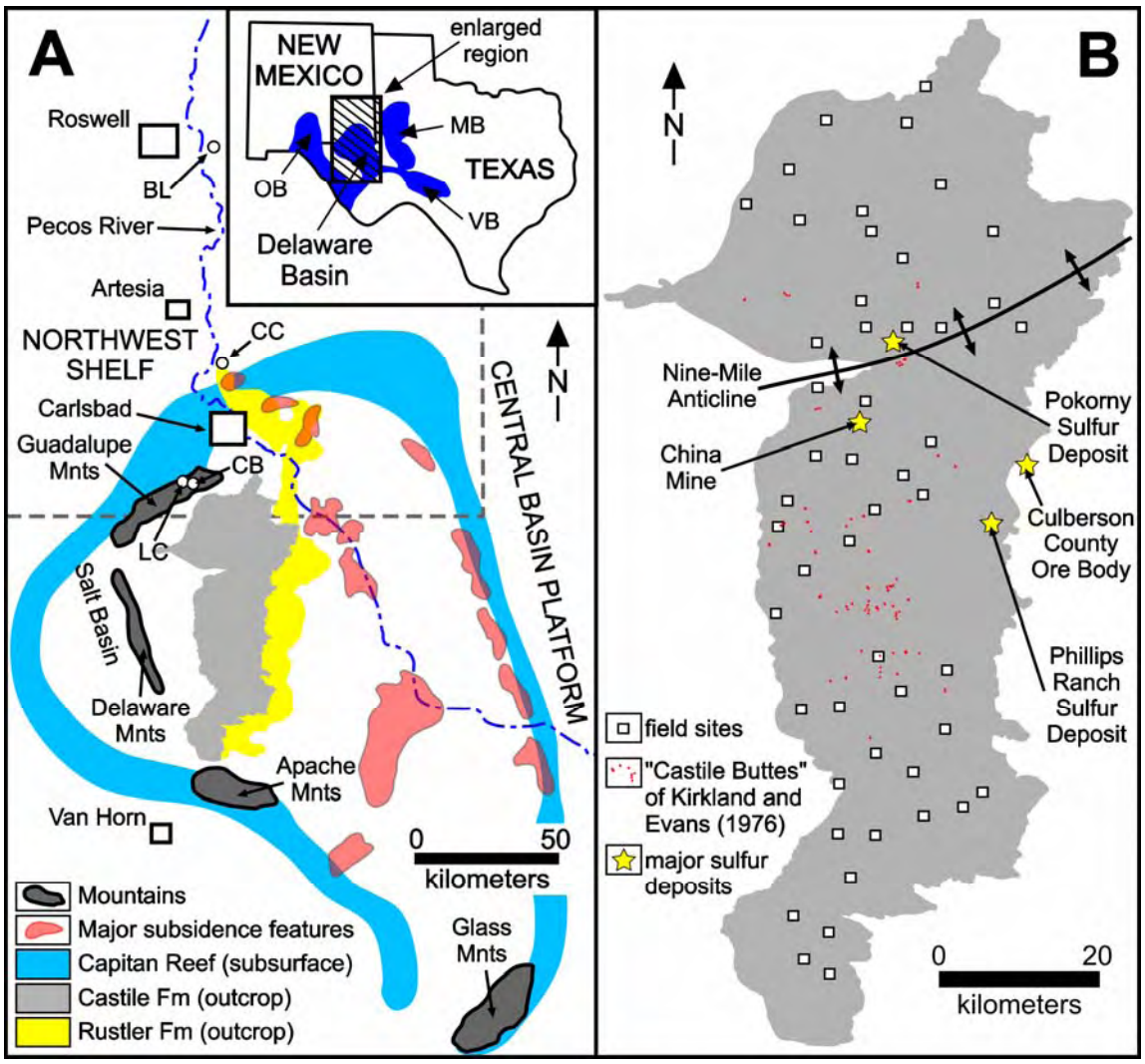

Fig. VI.2. Castile Formation outcrop area. A) Regional overview of Castile Formation outcrop area (grey) in relation to the Delaware Basin, which is defined by the boundary of the Capitan Reef (light blue) and Gypsum Plain (Castile and Rustler Formation outcrops). Features of interest include: BL – Bottomless Lakes; CC – Coffee Cave; CB – Carlsbad Cavern; and LC – Lechuguilla Cave. Inset shows location of expanded region and the Delaware Basin in relation to other major seas of the Permian, including: OB – Orogrande Basin; VB – Val Verde Basin; and MB – Midland Basin (adapted from Hill, 1996; Klimchouk, 2007; Scholle et al., 2004; and Stafford et al., 2007 a,b,c).; B) Enlarged Castile outcrop region showing the Nine-Mile Anticline, location of physically mapped field sites, “Castile Buttes” identified by Kirkland and Evans (1976) and major sulfur deposits (adapted from Hill, 1996; Kirkland and Evans, 1976; Stafford et al., 2007c; and Wessel and Wimberly, 1992).

which consistently occur in clustered associations within the Castile outcrop area. Initial research focuses on the distribution and occurrence of calcitization within the Castile Formation, which is far more diverse and widespread than originally reported by previous investigators.

GEOLOGIC SETTING

The Castile Formation crops out over ~1,800 km^2 (Fig. VI.2) within the western Delaware Basin extending from the Castile dissolution front on the west, to the east where it descends into the subsurface beneath the Salado and Rustler Formations (Kelley, 1971). The Castile Formation reaches a maximum thickness of 480 m in the subsurface, while it gradually decreases in thickness from east to west through the Gypsum Plain, until only a few meters of the lower Castile Formation remain on the western dissolution front (Kelley, 1971). The outcrop area is part of the larger Gypsum Plain, a physiographic province located on the northern edge of the Chihuahuan Desert that includes extensive outcrops of the Castile and Rustler Formations, but only minor residual outcrops of the Salado Formation (Fig. VI.1).

At the time of deposition, the Delaware Basin was located within 5-10° of the equator on the western edge of Pangea (Lottes and Rowley, 1990). Collision of the North American and South American-African plates during the Pennsylvanian produced the Ouachita Orogeny and block faulting within the Permian Basin, forming the Delaware Basin, Central Basin Platform and Midland Basin (Ross, 1986). Throughout the Permian, high rates of sedimentation and subsidence dominated the Delaware Basin, with deposition of 3-5 km of strata (King, 1942). Early to middle Permian (Wolfcampian to

Guadalupian) strata include thick siliciclastic and carbonate sequences. Late Permian (Ochoan / Lopingian) evaporite strata were deposited as open marine circulation in the Delaware Basin ceased with the closing of the Hovey Channel (Adams, 1972).

The Castile Formation was deposited during the early Ochoan (Lopingian) after the closing of the Delaware Basin at the end of Guadalupian time (Adams, 1972). The Castile Formation is bounded below by clastic deposits of the Bell Canyon Formation (Guadalupian), on the margins by carbonates of the Capitan Reef (Guadalupian) and above by the largely evaporitic Salado and Rustler Formations (mid to late Ochoan / Lopingian) (Fig. VI.1) (Kelley, 1971).

Castile evaporites were deposited as deep-water deposits within a density-stratified, closed basin, which filled the entire Delaware Basin (Kendall and Harwood, 1989). Castile sulfates have been traditionally defined as laminated to massive (Fig. VI.3), where laminae consist of mm to cm thick alternating layers of gypsum / anhydrite and calcite, including more than 260,000 individual laminae couplets, which have been correlated over distances up to 113 kilometers (Anderson and Kirkland, 1966). These laminations have been widely studied and are believed to represent annual varve sequences reflecting seasonal variations of basin salinity during deposition, where sulfate laminae represent dry periods and calcite laminae represent wetter periods (Anderson et al., 1972), similar to dry and monsoonal seasons seen in many semi-arid regions today.

Subsequent to the Permian sedimentation in the Delaware Basin, the region has remained largely tectonically quiescent. Early Triassic, Laramide and Basin and Range tectonism resulted in uplift and regional tilting towards the east-northeast (Horak, 1985). Broad anticlinal flexures oriented roughly east-west occur throughout the region in

association with Laramide compression, beginning in the late Cretaceous (Dickenson, 1981; Hentz and Henry, 1989). Basin and Range (mid-Tertiary) extension affected the far western Delaware Basin, where the salt basin was down dropped at least 500 meters (Friedman, 1966); however, throughout the majority of the Delaware Basin this was limited to high angle fracturing, primarily represented by minimally offset joint sets oriented at ~N75°E and ~N15°W (Nance, 1992). Since Permian time, the Delaware Basin region has been largely exposed to surficial processes, except during a brief period of marine inundation during middle Cretaceous deposition (Hill, 1996).

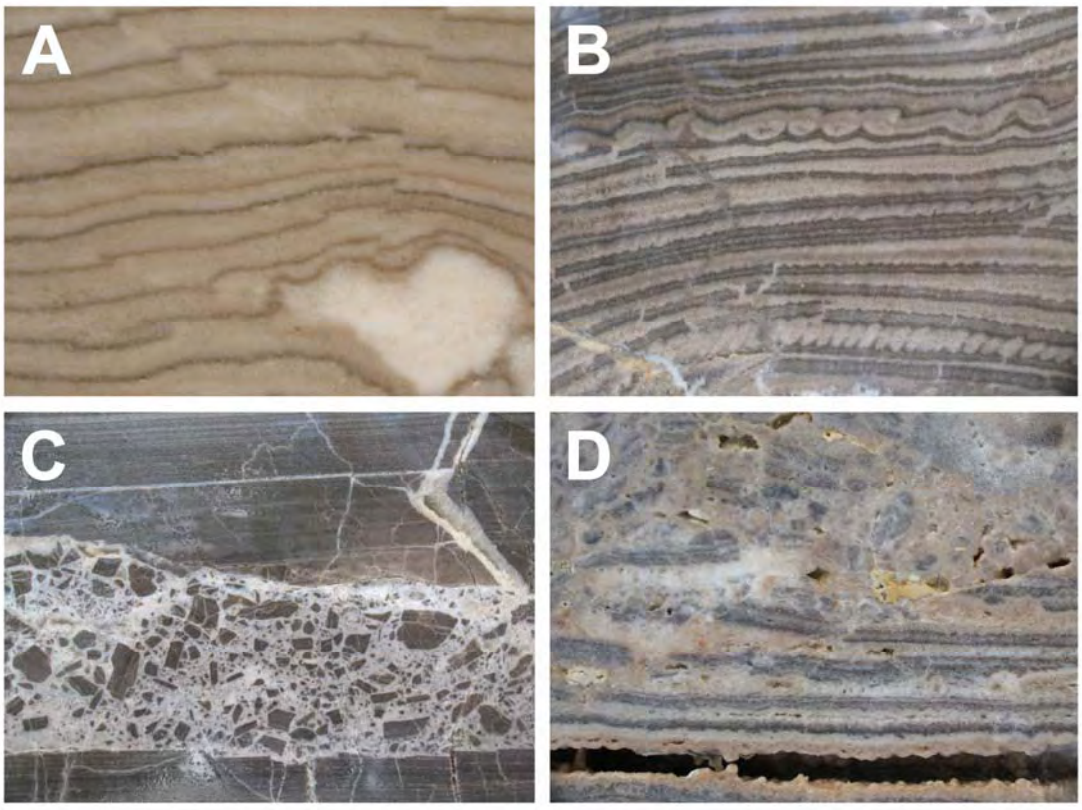

Fig. VI.3. Slabs of Castile Formation bedrock. Image widths are ~10 cm. A) laminated and nodular gypsum; B) calcitization with preserved laminae including minor microfolding; C) calcitization showing a central zone of brecciation; and D) calcitization with vuggy porosity, laminae distortion and minor native sulfur.

Although structural deformation appears to be minimal within the Castile Formation, diagenetic alteration is widespread. Calcitization is extremely common, resulting from the reduction of calcium sulfate in the presence of rising hydrocarbons that has been associated with BSR (Kirkland and Evans, 1976). Associated with calcitization, native sulfur deposits occur from the oxidation of hydrogen sulfide, a calcitization byproduct (Klemmick, 1992). Similarly, large selenite masses have been suggested as further oxidation of native sulfur into sulfuric acid, which reacted with calcium carbonate to produce secondary gypsum (Hill, 1996). Alternately, large selenite masses have been attributed to hydrothermal origins (Lock et al., 2004). In addition to diagenetic alteration associated with calcitization, originally laminated sulfate fabrics are commonly distorted or destroyed during dehydration / hydration processes of anhydrite / gypsum mineral conversion (Klimchouk, 1996). Massive fabrics, showing no evidence of laminations, commonly cover large regions, while diagenetic nodular fabrics with some semblance of original laminations are found in many localized regions (Dean et al., 1975).

In addition to tectonic and diagentic alteration of Castile evaporites, dissolution processes have extensively modified the region. Surface denudation and karst development has created a geomorphic landscape that is dominated by regions of intense sinkhole development and large subsidence valleys (Bachman, 1984; Hill, 1996; Stafford, 2006; Stafford et al., 2007b, 2008). Subsurface dissolution of halite interbeds has produced laterally extensive blanket breccias throughout much of the western Delaware Basin (Anderson et al., 1978), which form laterally extensive, highly transmissive zones. Vertical breccia pipes form highly transmissive, cross-formational flow paths throughout the entire Delaware Basin. These features formed by mixed convection (free and forced

convection) dissolution of large, intrastratal voids that stoped towards the surface as large subsidence features (Fig. VI.2A) (Anderson and Kirkland, 1980). Numerous individual caves and clusters of caves within the Castile outcrop region suggest that most karst development within the study area is the result of hypogene speleogenesis associated with rising fluids (Stafford et al., 2007b, 2008).

EVAPORITE CALCITIZATION

Calcitization of gypsum / anhydrite occurs primarily through three main processes, Bacterial Sulfate Reduction (BSR), Thermochemical Sulfate Reduction (TSR) and meteoric calcitization. Meteoric calcitization is commonly associated with dedolomitization where dolomites are converted to calcites through the simultaneous dissolution of dolomite and calcium sulfates and the precipitation of calcite (Back et al., 1983). Meteoric calcitization can also result solely from the dissolution of evaporite nodules and the precipitation of replacive calcite minerals. Unlike meteoric calcitization, both BSR and TSR require the presence of sulfate rocks and an organic carbon source (e.g. hydrocarbons) (Machel, 1992). Sulfate is reduced and in the process hydrogen sulfide and calcite saturated fluids are formed, which either contemporaneously or subsequently precipitate as native sulfur and secondary calcite (Machel, 1992). BSR occurs in a wide range of low temperature, sedimentary environments, including shallow groundwater aquifers, in the presence of low molecular weight organic compounds (Machel, 1987). Because sulfate reducing bacteria provide catalysts for sulfate reduction, environmental parameters including the availability of nutrients, the ability to remove waste products (H_2S) and thermal regime (0 to ~80°C) limit BSR (Ehrlich, 1990). TSR

generally occurs in higher temperature regimes (~100 to 180°C), as an inorganic processes (Machel, 1998); however, thermodynamically TSR is possible at temperatures as low as 25°C (Worden and Smalley, 1996). As with BSR, TSR will proceed as long as sulfate and organic compounds are present, but TSR does not require the active involvement of microbial organisms. Therefore, TSR can proceed in confined systems without the complete removal of hydrogen sulfide byproducts, which can become toxic for sulfur reducing bacteria (Machel, 1992).

Kirkland and Evans (1976) identified calcitization in the Ochoan (Lopingian) evaporite facies of the Delaware Basin and noted that localized occurrences formed resistant “limestone buttes” that retained the lithologic texture of the original calcium sulfates that had been replaced (Fig. VI.3A,B). In the subsurface, many of these calcitized masses contain significant amounts of native sulfur, often forming vug-filling ore deposits. However, the presence of associated sulfur near the surface is limited to a few isolated occurrences because native sulfur rapidly oxidizes in the presence of meteoric waters. Based on their analyses of $\delta^{34}S$ and $\delta^{13}C$, they concluded that the occurrence of evaporite calcitization within the Delaware Basin was the result of BSR. Their $\delta^{34}S$ (CDT) values for anhydrite in the Castile Formation range from +9.6 ‰ to +11.5 ‰, while their $\delta^{34}S$ (CDT) values for native sulfur range from -15.1 ‰ to +9.2 ‰. Although the native sulfur values show a wider range of variability in $\delta^{34}S$ (CDT) values, samples were consistently depleted with respect to the anhydrite of the Castile Formation. They suggest this is consistent with normal variability in sulfate reducing bacteria processes (Kirkland and Evans, 1976). Their $\delta^{13}C$ (PDB) values for depositional calcite laminae within the Castile Formation range from +5.0 ‰ to +6.7 ‰, which is consistent with

marine deposition, while their $\delta^{13}C$ (PDB) values for calcitized evaporites range from -3.1 ‰ to -29.2 ‰ (mean is -23.5 ‰), which shows significant $\delta^{13}C$ depletion. This $\delta^{13}C$ depletion was attributed to ascending hydrocarbons, most likely methane, from the Bell Canyon and other formations of the Delaware Mountain Group. Therefore, Kirkland and Evans (1976) concluded that the limestone buttes of the Castile Formation were the byproduct of BSR in the presence of ascending methane.

Although, Kirkland and Evans (1976) suggest that calcitization in the Castile Formation is the result of BSR, their isotope data does not provide unequivocal proof. The observed $\delta^{34}S$ and $\delta^{13}C$ patterns could also result from TSR, although this is generally ruled out because evaporite rocks have not been buried to sufficient depths within the Delaware Basin to have induced TSR under normal geothermal gradients. Tertiary igneous dikes (Calzia and Hiss, 1978) have been documented within the northern Delaware Basin which suggests significantly higher geothermal gradients in the past; however, calcitized occurrences occur throughout the entire western portion of the Castile outcrop area. Some occurrences of secondary selenite have also been attributed to hydrothermal origins (Lock et al., 2004), which frequently crop out over sever hundred square meters proximal to calcitized masses forming bodies that appear comparable in size to the more resistant limestone buttes (Stafford et al., 2008).Although, Tertiary dikes are limited to the northwestern margin of the study area, Barker and Pawlewicz (1987) report that geothermal gradients within the entire region were as high as 40-50°C/km during the late Oligocene to middle Miocene during the initiation of Basin and Range extension, which is above the lower temperatures limits where TSR is thermodynamically possible (Worden and Smalley, 1996).

Native sulfur bodies are commonly associated with calcitized masses within the Ochoan (Lopingian) evaporites of the western Delaware Basin. Sulfur deposits are formed as either vug-fillings within calcitized masses or within breccias (e.g. breccia pipes and blanket breccias) primarily in the Castile and Salado Formations (Wessel and Wimberly, 1992). Of these ore bodies, all have been associated with ascending fluid processes and calcitization, while several have been economically mined through Frasch processes where sulfur is extracted through the injection of super-heated waters, which melt sulfur so that it can be pumped to the surface. Major sulfur deposits within the Castile Formation include the Culberson Ore Body, the Pokorny Sulfur Deposit, and Phillips Ranch Sulfur Deposit (Fig. VI.2B) (Wessel and Wimberly, 1992). The Culberson Ore Body is the largest sulfur ore body documented within the Delaware Basin with sulfur occurring as crystals lining vugs and filling fractures and vugs (Wallace and Crawford, 1992). Most of the Culberson Ore Body is developed in the Salado Formation within solutional breccias developed along high angle faults (Fig. VI.4), which contain clasts of the Permian Rustler and Cretaceous Cox Formations and is associated with calcitization within the Salado and underlying Castile Formations (Wallace and Crawford, 1992). Lee and Williams (2000) modeled hydrocarbon migration and ore genesis associated with Culberson County Ore Body and showed that the paleohydrogeology associated with sulfur mineralization and calcitization was a mixed hydrologic system dominated by basinal fluids derived from the Bell Canyon Formation and meteoric fluids migrating down gradient through the Cherry Canyon Formation (Fig. VI.5).

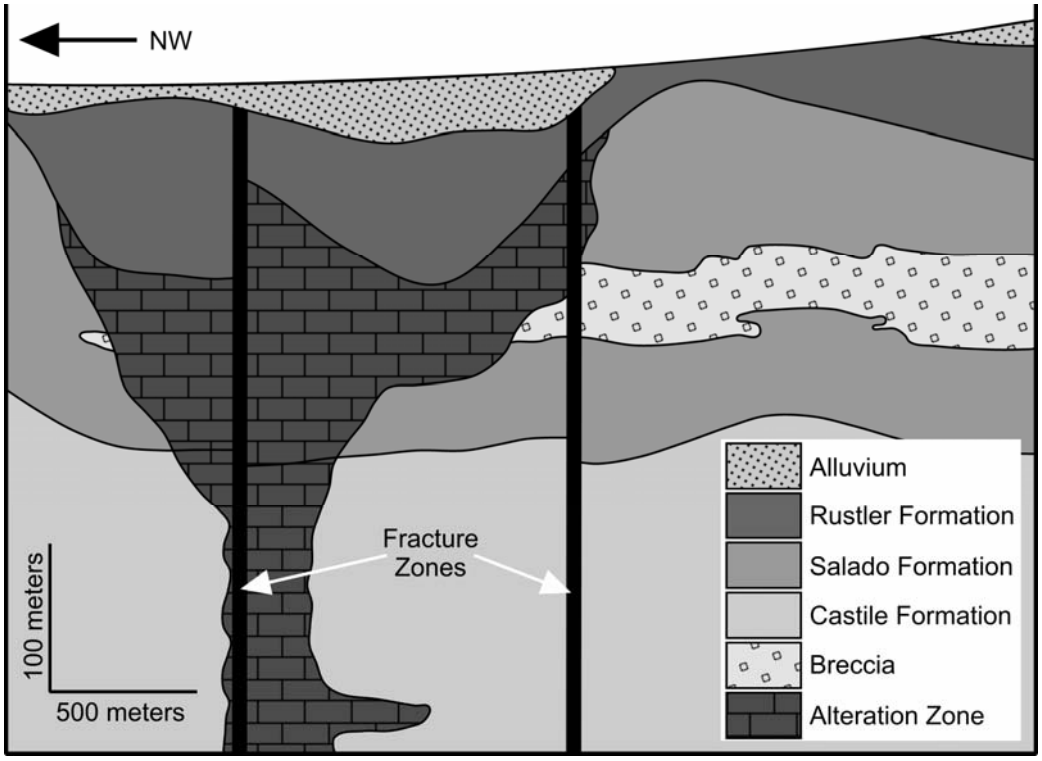

Fig. VI.4. Simplified schematic diagram of the Culberson Ore Body showing the configuration of the "Alteration Zone", which contains native sulfur within calcitized evaporites (adapted from Wallace and Crawford, 1992). Note the relationships between the "Alteration Zone", fracture zone, intrastratal breccia and different strata.

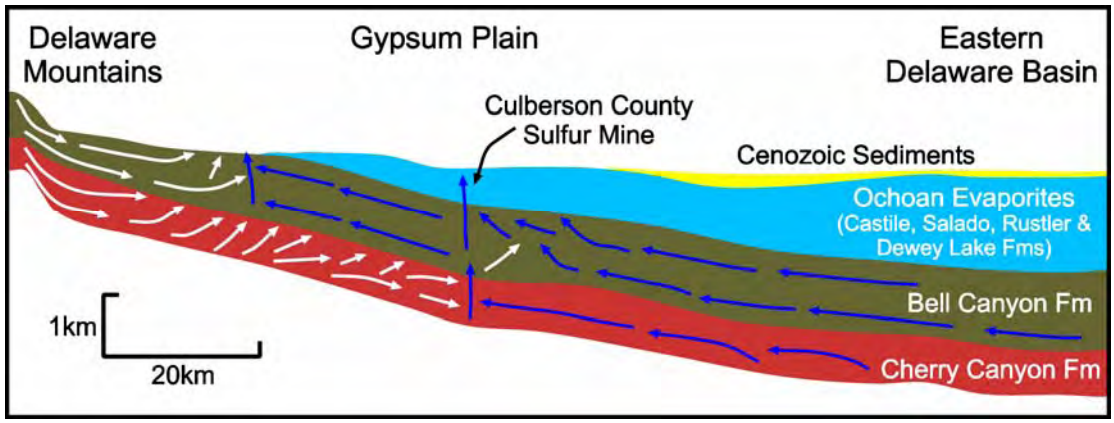

Fig. VI.5. Simplified paleohydrology associated with calcitization and sulfur deposition of the Culberson County Ore Body. White arrows indicate flow paths of meteoric waters originating as groundwater recharge in the Delaware Mountains Paleohydrology. Blue arrows indicate flow paths of basinal waters and associated hydrocarbons (adapted from Lee and Williams, 2000).

The Pokorny Sulfur Deposit (Fig. VI.2B) is completely developed within the Castile Formation within a calcitized mass, which is largely developed along three horizontal zones of brecciation (e.g. blanket breccias formed by halite dissolution and collapse) and bounded on the margins by high angle faults (Klemmick, 1992). As with the Pokorny Sulfur Deposit, the Phillips Ranch Sulfur Deposit is developed entirely in the Castile Formation; however, the Phillips Ranch Sulfur Deposit (Fig. VI.2B) occurs directly above the Bell Canyon Formation along the contact with the Castile Formation in association with calcitization (Guilinger and Nestlerode, 1992). Although not economically mined using Frasch processes, numerous exploration pits have been mined throughout the Castile outcrop area, some dating back to the late 19th century (e.g. China Mine, aka Hydrogenated Sulfur Mine) (Hill, 1996). All occurrences of native sulfur within the Castile and Salado Formations have been associated with calcitization that occurred along solutionally enhanced transmissive zones (Wessel and Wimberly, 1992), suggesting that hypogene speleogenesis is directly involved in sulfur mineralization, which has been validated by modeling of paleohydrology (Lee and Williams, 2000).

Although, Kirkland and Evans (1976) reported evaporite calcitization within the Castile and Salado Formation, all of the calcitized masses that they documented occur within the outcrop area of the Castile Formation (Fig. VI.2B). Calcitization has been documented in the Salado Formation associated with native sulfur deposits (Wallace and Crawford, 1992), while Kirkland and Evans (1976) speculated on surficial exposure of Salado calcitization based on one limestone butte, their butte number 3, which did not exhibit laminated fabric. However, massive, sucrosic gypsum is common in the Castile Formation as a result of diagenetic alteration or depositional soft sediment deformation

(Dean et al., 1975); therefore, calcitized rocks of the Castile Formation do not have to show preserved laminations. No unequivocal evidence of surface exposures of calcitized Salado evaporites have been documented, and all surficial limestone buttes reported by previous studies occur within the Castile outcrop region; therefore, this study focuses on calcitization of Castile evaporites within the outcrop region. The surficial expression of limestone buttes within the Castile outcrop region is used as a proxy for evaluating the spatial distribution of calcitization processes.

CALCITIZATION OCCURRENCES IN THE CASTILE FORMATION

In order to evaluate the spatial distribution and occurrence of evaporite calcitization, a coupled field and GIS (Geographic Information System) based approach was undertaken as part of a larger study investigating speleogenesis and sulfate diagenesis within the Castile Formation. Fifty randomly selected, 1-km^2 regions where physically mapped within the Castile outcrop region (Fig. VI.2B), including characterization of individual karst features, geologic features and geomorphic surfaces (Stafford et al., 2007b). Based on field mapping, digital air photos (DOQs - digital orthophoto quads) with a pixel resolution of one-meter were visually evaluated for the entire ~1,800 km^2 Castile outcrop region. Calcitized areas were identified based on their geomorphic expression, including topographic relief, low reflectance and lack of gypsofile vegetation, as compared with features physically documented during field mapping. A total of 1020 individual calcitized occurrences were documented (Fig. VI.6A), with an average surface area exposure of 2,296 m^2. Field checks of approximately 150 individual calcitized occurrences identified through GIS analyses confirmed the techniques validity. Because

of the one-meter resolution of air photos, only regions covering an area greater than one meter wide and more than ten square meters in total area were identifiable. This includes most exposed calcitized masses and calcitized sheets at least 30 centimeters thick, which become exposed as low relief ridges more than one meter wide, due to the gentle regional dip.

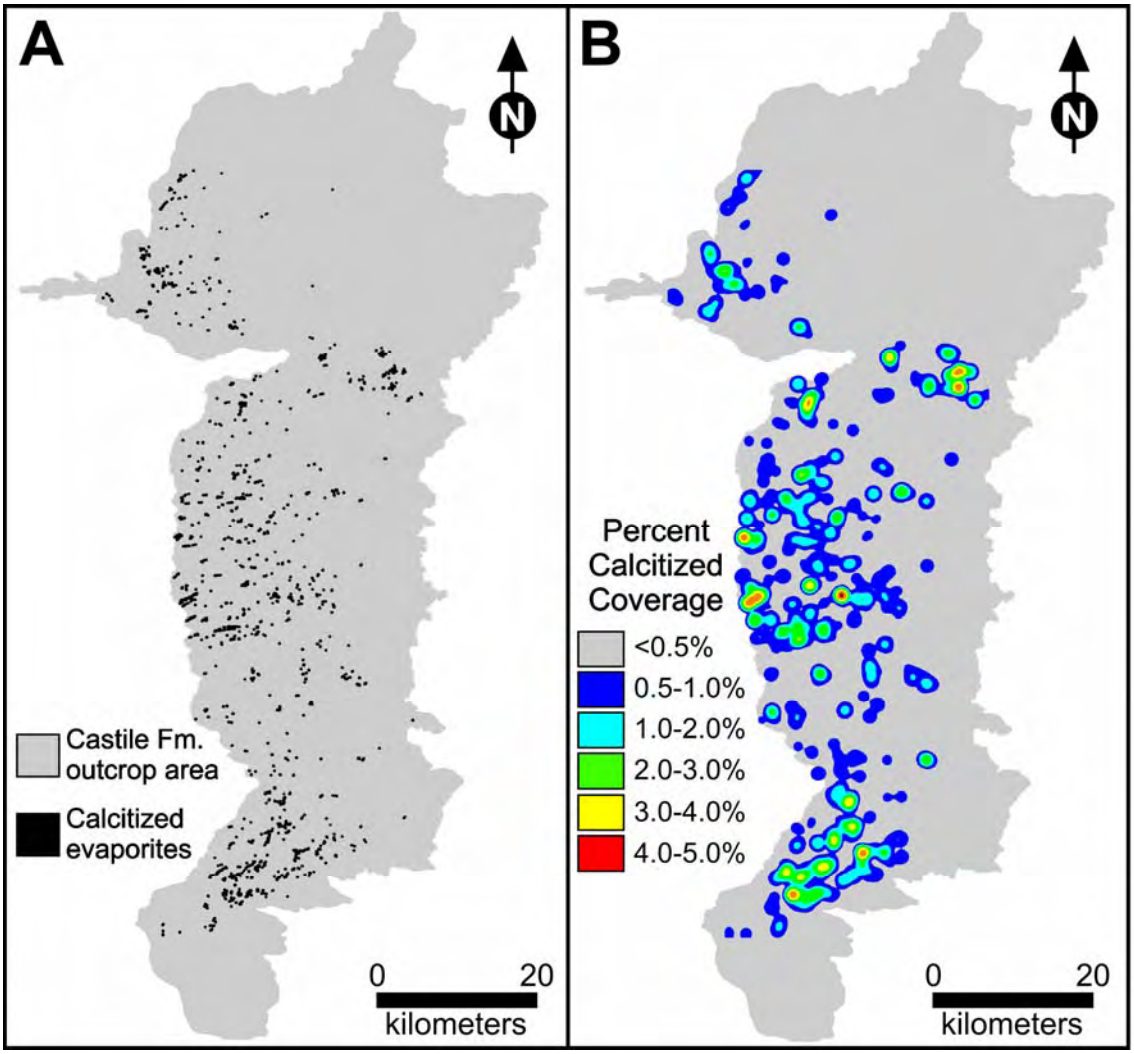

Fig VI.6. Distribution of calcitization within the Castile outcrop region (grey). A) Spatial distribution of occurrences of calcitization (black) identified through couple field mapping and GIS analyses of DOQs; B) Spatial analyses of calcitized occurrences showing clustered distribution of calcitization as a function of outcrop coverage. GIS analyses performed using ArcGIS 9.2.

GIS analyses clearly show that calcitization is widespread in the western portion of the Castile outcrop area with a general decrease in calcitization abundance in the northern portion of the study area (Fig. VI.6A). The extreme northern and southern portions of the study area are effectively devoid of calcitization, while minor regions of calcitization occur scattered throughout the eastern portion of the Castile outcrop area. Spatial analyses of calcitization coverage throughout the study area indicate that the overall pattern of calcitization is highly clustered (Fig. VI.6B). Local calcitized occurrences are generally developed along linear trends oriented primarily at ~N70°E and ~N15°W; however, secondary linear trends of calcitization occur along orientations of ~N25°E, ~N55°E and ~N40°W (Fig. VI.6A). The linear trends of calcitization indicate mineral alteration along fractures within the Castile Formation (Hentz and Henry, 1989), while the clustered nature of calcitization suggests focused diagenetic alteration within specific regions.

Based on field mapping, calcitized evaporites within the Castile outcrop area occur primarily in two distinct forms: 1) massive limestone buttes or “castiles” (Fig. VI.7) and 2) laterally extensive limestone sheets (Fig. VI.8). Lithologic fabric associated with calcitization can vary significantly. Most commonly, calcitization results in little fabric alteration, such that original fabrics (Fig. VI.3A), usually laminated but also massive and nodular fabrics, are preserved (Fig. VI.3B). Original fabric is often highly distorted where calcitized masses have developed extensive vuggy-like porosity, where laminations are observable but highly distorted (Fig. VI.3D). In addition to surface exposures, numerous calcitized zones have been identified within caves in the area (Fig. VI.9). In some cases,

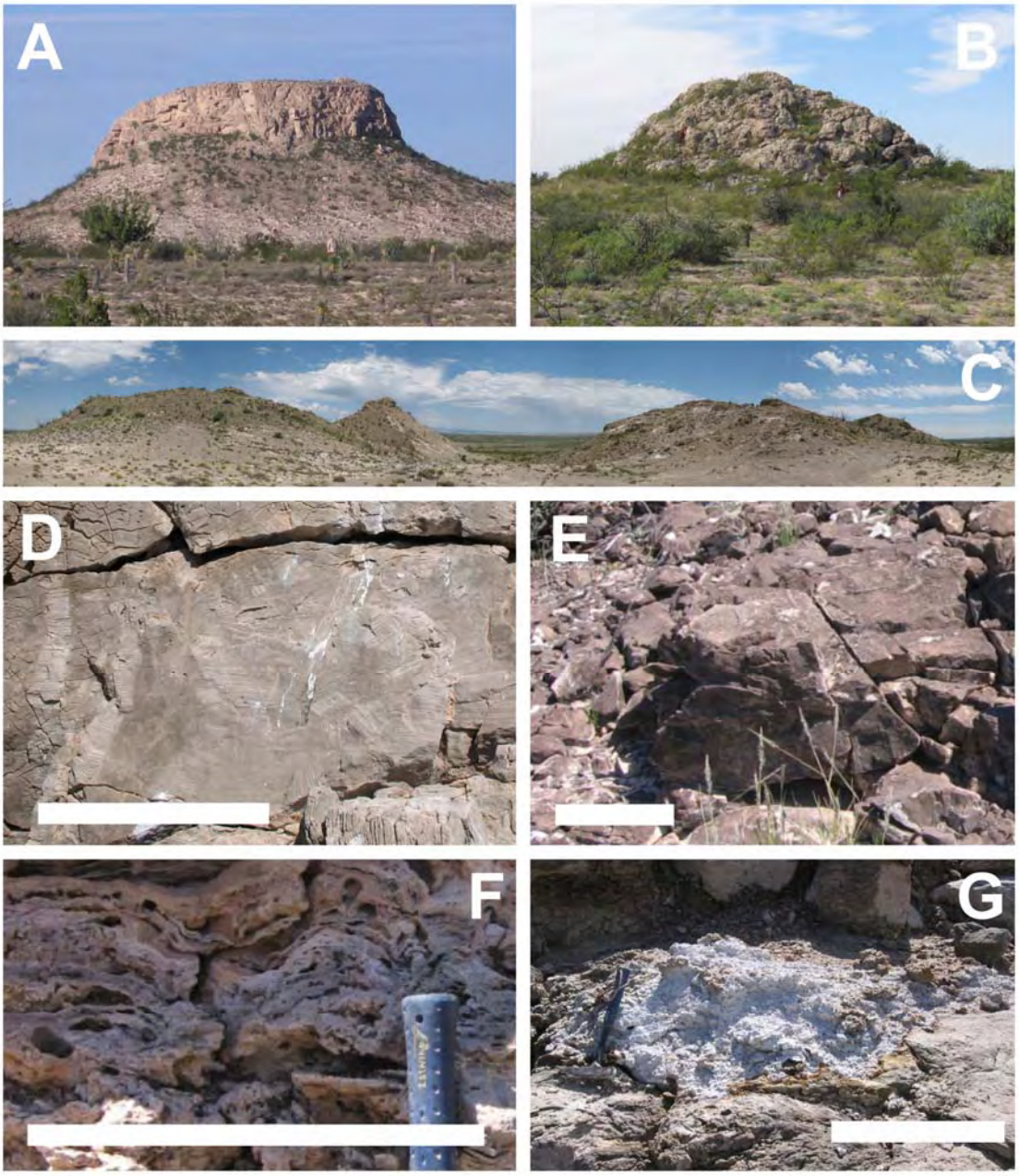

Fig. VI.7. Calcitized masses or limestone buttes. White scale bars are ~25 cm long. A) large limestone butte ~40 m tall (note person in foreground for scale); B) typical limestone butte ~10 m tall (note person for scale); C) cluster of limestone buttes including three distinct calcitized masses that are ~20 m tall; D) typical brecciated core of calcitized masses; E) typical calcitization with preservation of original laminae distal to calcitized masses; F) typical calcitization with vuggy porosity proximal to calcitized masses; G) typical active vent and secondary gypsum powder associated with calcitized masses actively degassing hydrogen sulfide.

calcitization boundaries have been preserved between the calcitized and uncalcitized rocks showing direct lateral relationships.

Massive limestone buttes occur throughout the Castile outcrop region forming resistant topographic highs up to 40 meters higher than surrounding topography (Fig. VI.7A), although commonly less than 10 meters (Fig. VI.7B). Surficial expression of individual limestone buttes ranges from a few square meters (minimum documented coverage of 36 m^2) to several tens of thousands of square meters (maximum documented coverage of 40,687 m^2). They frequently occur in groups of several limestone buttes (Fig. VI.7C), either clusters covering several square kilometers or linear trends up to ten kilometers long, suggesting concentrated migration of hydrocarbons through these regions. Most individual limestone buttes contain a central core of highly brecciated calcitization (Fig. VI.7D), but the periphery usually shows little alteration of original fabric beyond mineral replacement (Fig. VI.3B; 7E). Occasionally, limestone buttes also contain a highly porous intermediate zone (Fig. VI.3D; 7F) between the breccia core and the largely unaltered periphery fabrics. The highly porous zone commonly shows evidence of original laminations, but laminae are highly distorted with abundant vuggy (Fig. VI.7F) to cavernous porosity (Fig. VI.9A), up to several hundred cubic meters. Several limestone buttes continue to actively degas hydrogen sulfide based on odor and the presence of highly porous, secondary gypsum precipitates at vent areas (Fig. VI.7G). This suggests that calcitization processes are still occurring in the subsurface or residual hydrogen sulfide from previous calcitization episodes have been trapped within the Castile Formation and are now degassing as surficial denudation provides preferential flow paths for releasing trapped gas (Lock et al., 2004). Many of these degassing

limestone buttes have been continually producing hydrogen sulfide for at least a century (Richardson, 1905).

Laterally extensive limestone sheets are common throughout the study area, but generally occur within a 1-2 km radius of limestone buttes, suggesting that they are genetically related. Limestone sheets are generally decimeters thick, but have been observed up to 2 m thick. They commonly outcrop over large areas as residual clasts coating the ground surface (Fig. VI.8A) where overlying and underlying gypsum have been removed by dissolution; however, intact sheets are observed where calcitized zones dip into the subsurface, often forming linear or sinuous features that can be observed on aerial photos when they are at least 30 centimeters thick and several meters long. Usually, limestone sheets contain a central zone of brecciated material (Fig. VI.3C; 8B), such that the brecciated region and several decimeters above and below this zone are calcitized. Calcitized sheets have been identified at the base of the Castile Formation at the contact with the underlying Bell Canyon Formation (Fig. VI.8C). Although the Castile Formation has been traditionally characterized as having a depositional basal carbonate unit (Anderson et al., 1972), field observations at the contact suggest that this basal zone may actually be the result of calcitization. These calcitized regions are laminated, contain vuggy porosity (Fig. VI.8D) similar to that observed in many limestone buttes (Fig. VI.7D), contain significant levels of hydrocarbons as evidenced by a strong fetid odor, and native sulfur deposits with associated calcitization have been mined at the Bell Canyon / Castile contact (Guilinger and Nestlerode, 1992).

Calcitization associated with cave and karst development is widespread within the Castile Formation, suggesting that the two are genetically related. Dense clusters of caves

Fig. VI.8. Calcitized sheets. White scale bars are ~0.5 m long. A) linear ridge of calcitization where calcitized sheet dips into the subsurface; B) central brecciated core of calcitized sheet; C) calcitization of immediately above the Bell Canyon, Castile Formation contact (dashed line delineates contact); D) vuggy porosity and laminae distortion of calcitization at Bell Canyon / Castile Formation contact (dashed line delineates contact).

are commonly found proximal to limestone buttes, with complete or partial solutional development within calcitized zones (Stafford et al., 2008). Caves developed entirely in limestone buttes form small elliptical chambers (Fig. VI.9A) that are effectively large-scale vugs. Within many sinkholes and associated caves, thin, centimeter- to meter-thick lenses of calcitization are abundant, which are bisected by solutional cave passages (Fig. VI.9B) or incised karst arroyos (Fig. VI.9C). Portions of some larger caves are completely developed in limestone sheets, such that different levels of the caves are

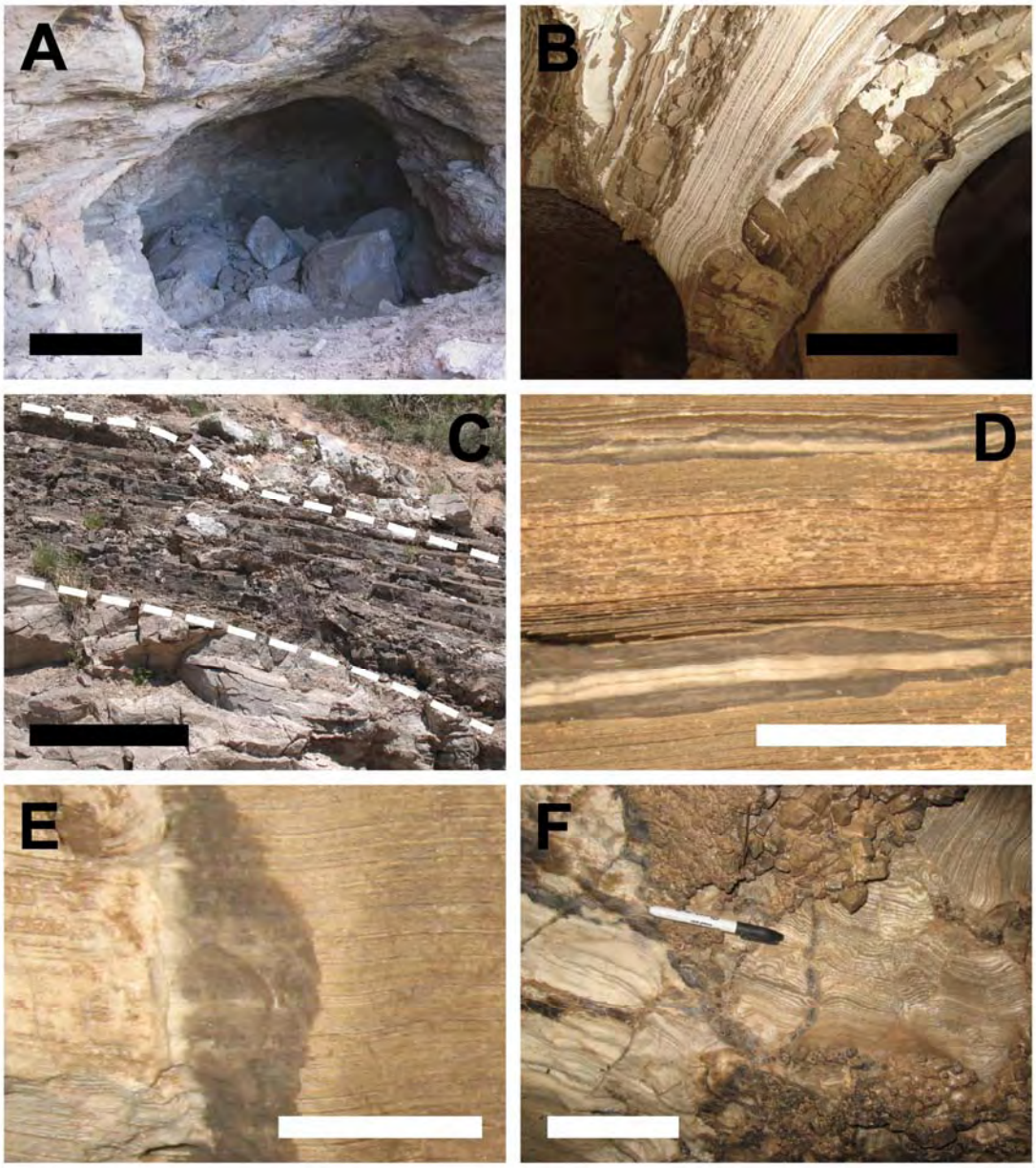

Fig. VI.9. Calcitization associated with karst development. Black scale bars are ~1 m long. White scale bars are ~10 cm long. A) elliptical cave developed entirely within a calcitized mass; B) solutional cave passage containing calcitized sheets developed within folds; C) limestone sheet (bounded by dashed lines) dissected by solution entrenchment of karst arroyo; D) parallel contact between calcitization (tan) and original gypsum (white) showing alteration zone (grey); E) perpendicular contact between calcitization (tan) and original gypsum (white) showing alteration zone (grey); F) acute angular contacts between calcitized breccia (tan) and laminated gypsum (white).

developed in alternating zones of gypsum and calcitized sulfate. Although caves intersecting the calcitized zones show similar textural patterns as surficial exposures, contact boundaries between original gypsum and calcitized zones are often preserved in passage walls. Preserved diagenetic boundaries include boundaries that are both parallel (Fig. VI.9D) and perpendicular (Fig. VI.9E) to laminations, as well as boundaries that cross laminae at acute angles (Fig. VI.9F). Commonly, these boundaries include a transitional zone of alteration averaging 1 cm wide (Fig. VI.9D,E). Kirkland and Evans (1976) noted no transitional boundaries between calcium sulfate and calcitization in the Castile Formation. This may be due to the fact that they looked only at surface exposures and the transition zones have only been observed in caves.

The 1020 identified occurrences of calcitization within the Castile outcrop region are highly clustered (Fig. VI.6B), although forming linear trends (Fig. VI.6A), with the greatest abundance of calcitization occurring along the western edge of the study area. The only major exception to this pattern is a dense cluster of calcitization that occurs along US HWY 652 in northern Culberson County, Texas, where limestone buttes are present on the eastern margin of the study area; however, these occurrences are also located along the axis of the structural high formed by the Nine-Mile Anticline (Fig. VI.2B) (Hill, 1996). Because the regional dip of the Castile Formation and underlying Permian units is to the east-northeast, surficial denudation is greatest on the western edge of the Castile outcrop region and along the Nine-Mile Anticline where the base of the Castile Formation is at a higher elevation than in the northern and southern portions of the study area. The distribution of surficial exposures of calcitization is coincident with the degree of surficial denudation of the Castile Formation, indicating that calcitization is

most intense proximal to the contact with the underlying Bell Canyon Formation, which has been proposed as the transmissive source region through which hydrocarbons were delivered to the Castile Formation.

SPELEOGENESIS IN THE DELAWARE BASIN

Speleogenesis has been traditionally associated with caves and karst; however, speleogenesis is not limited to the development of cavernous porosity. Instead, speleogenesis is simply part of the genetic evolution of soluble rocks, where void space ranging from sub-millimeter intragranular porosity to vuggy and cavernous porosity is created by dissolution, which may be subsequently filled by secondary deposits. Speleogenesis occurs in three basic diagenetic settings, based on the characteristics of the soluble fluids: 1) coastal, 2) epigene, and 3) hypogene (e.g. Ford and Williams, 2007; White, 1988). However, geologic systems are constantly evolving through time such that multiple episodes of different types of speleogenesis may occur within any system (e.g. Klimchouk et al., 2000).

Coastal speleogenesis is largely associated with the interaction of fresh and marine waters in coastal and island settings (Mylroie and Carew, 1995). At the top of the fresh-water lens, dissolution is enhanced by the decay of organics, while at the margin and base of the fresh-water lens, dissolution is enhanced by the mixing of fresh and saline waters (Back et al., 1984). Epigene speleogenesis occurs in unconfined settings and is directly associated with meteoric precipitation (Palmer, 1991). Dissolution is driven by gravity in the unsaturated, vadose zone and by hydraulic potential in the saturated, phreatic zone. Epigene secondary deposits may form either subaerially in the vadose zone, most

commonly due to variations in void microclimate, or subaqueously in the phreatic zone, generally associated with changes in water chemistry (Ford and Williams, 2007). Hypogene speleogenesis occurs in confined or semi-confined settings where dissolution is driven by a mixed hydrologic flow system, including significant components of both free and forced convection (Klimchouk, 2007), where soluble fluids are delivered from underlying or adjacent transmissive zones. Hypogene systems do not form direct connections with surface process, but instead are associated with regional and basin-scale fluid movement where waters are delivered from deep sources or distal meteoric recharge areas. Hypogene speleogenesis is most commonly associated with hydrothermal or sulfuric acid systems, but in a broader context includes most geologic systems where fluids originating from lower depths or distal margins migrate vertically and laterally through overlying or adjacent soluble rocks, often not only forming complex solution features but also extensive, economic secondary mineral deposits (e.g. Mississippi Valley Type deposits) (Ford and Williams, 2007).

In the greater Delaware Basin hypogene processes appear to dominate the speleogenetic evolution of the area (e.g. Klimchouk, 2007; Palmer, 2006; Stafford, 2007a,b, 2008). The famous caves of the Guadalupe Mountains (Fig. VI.2A) (e.g. Carlsbad Cavern, Lechuguilla Cave) are developed in the Guadalupian reef (Capitan Formation) and near-backreef facies (Artesia Group). These massive caves and the extensive associated cavernous porosity in the Guadalupe Mountains, has been attributed to sulfuric acid dissolution, where rising anoxic fluids saturated with hydrogen sulfide mixed with shallower oxic fluids to produce aggressive, sulfuric acid-rich waters (Hill, 1990; Palmer, 2006). In the Guadalupian backreef facies (Artesia Group), numerous

hypogene caves occur where pressurized fluids rise through interbedded carbonate and evaporite rocks (e.g. Bottomless Lakes) (Fig. VI.2A) (Land, 2006). Because the rising fluids originate from lower carbonate aquifers, they are likely undersaturated with respect to calcium sulfate, such that significant dissolution occurs as fluids pass into gypsum / anhydrite interbeds. As a result, complex, three-dimensional, maze caves have formed within the interbedded evaporite sequences of the Artesia Group (e.g. Coffee Cave) (Fig. VI.2A; Stafford et al., 2007a). Within the Delaware Basin, numerous breccia pipes, subsidence troughs (Fig. VI.2A) and blanket breccias have been described in association with rising fluids through the Ochoan (Lopingian), basin-filling, evaporite sequences (e.g. Hill, 1996). Anderson and Kirkland (1980) attributed the large, vertical breccia pipes to brine density convection, where fluids originating from lower carbonate units rose through overlying evaporite units. As the less dense, undersaturated water rose and dissolved overlying evaporitic beds, the resulting saturated / denser fluids simultaneously sank back to the lower carbonate aquifer, such that aggressive waters were continuously delivered to the upper solution front. With increasing void size, eventually ceiling collapse began stoping towards the surface such that large breccia columns were formed (Anderson and Kirkland, 1980). Similarly, solution troughs and extensive blanket breccias have been described within these same Ochoan (Lopingian) rocks, where laterally migrating fluids dissolved halite interbeds, leaving behind residual blanket breccias from the simultaneous collapse of overlying beds (Anderson et al., 1978). Numerous examples of the dominance of hypogene speleogenesis occur throughout the greater Delaware Basin region, although the specific composition of the fluids and host rocks may differ.

Within the Castile outcrop region, evidence of both epigene and hypogene speleogenetic processes is extensive. Widespread epigene karst and caves occur within the study area in relation to modern surficial processes (Bachman, 1980). However, hypogene processes appear to dominate the speleogenetic evolution of the Castile Formation (Stafford et al., 2008). Recent work (Stafford et al., 2007b) has shown that cave development within the Castile Formation is highly clustered, suggesting that speleogenetic origin is largely associated with rising fluids, while surface expression is simply the result of breaching. Hence, more intense clustering of caves occurs along the western side of the Castile outcrop area where surface denudation has been the most extensive, similar to the patterns seen in calcitization distribution (Fig. VI.6B). Additionally, morphometric features (i.e. inlet risers, wall channels, ceiling half tubes and outlet cupolas) present within many of the clustered caves show unequivocally evidence of dissolution driven by mixed convection from rising fluids (Stafford et al., 2008). In general, clusters of hypogene caves, calcitized occurrences and selenite bodies are found in grouped associations suggesting that they are all genetically related. Within the study area and throughout the Delaware Basin, breccia pipes and blanket breccias have been documented within the Castile Formation adding greater credence to the importance of hypogene processes within Castile evaporites.

DISCUSSION AND CONCLUSIONS

Evaporite calcitization within the Delaware Basin and specifically within the Castile Formation is far more extensive and widespread than was originally recognized by Adams (1944) and Kirkland and Evans (1976). Analyses of the occurrence and

distribution of calcitization in the Castile outcrop area has identified numerous previously undocumented limestone buttes, as well as identification of the occurrence of abundant limestone sheets. Calcitization is most intense in the western portion of the study area where surface denudation has removed a greater portion of the upper Castile Formation and other overlying Ochoan (Lopingian) evaporites. Field observations of the Castile / Bell Canyon contact indicate extensive calcitization at the base of the Castile Formation. Numerous clusters of hypogene caves and masses of selenite are commonly associated with the clustering of surficial exposures of calcitization within the study area. The occurrence of clusters of calcitized masses and sheets with selenite masses and hypogenic caves indicates that ascending hypogene fluids have dominated the diagenetic evolution of the Castile Formation, which is supported by paleohydrology modeling within the Delaware Basin (Fig. VI.5) (Lee and Williams, 2000). While the exact mechanism of sulfate reduction remains unclear, either BSR or TSR, ascending, hypogene waters and hydrocarbons is consistent with most diagenetic processes observed within the Castile Formation.

This study, coupled with previous research on karst (Stafford et al., 2007b, 2008), native sulfur deposits (e.g. Wallace and Crawford, 1992; Davis and Kirkland, 1970) and limestone buttes (e.g. Kirkland and Evans, 1976; Lock et al., 2004) within the Castile Formation indicates that calcitization within the Ochoan (Lopingian) evaporites of the Delaware Basin represents part of a complex speleogenetic evolution in the region. Ascending fluids established initial flow paths largely along fractures and bedding planes, through solution and brecciation (e.g. breccia pipes and blanket breccias). Because many calcitized masses and sheets contain central breccia zones, these initial transmissive flow

paths established by ascending fluids were subsequently or simultaneously used by ascending hydrocarbons. Ascending hydrocarbons fueled sulfate reduction, resulting in calcite replacement of original calcium sulfate deposits along with the production of hydrogen sulfide. Calcitized rocks that show little original fabric alteration were likely well-connected to adjacent transmissive zones, such that hydrogen sulfide byproducts could be removed from the system easily. In contrast, calcitized rocks that show significant fabric alteration (i.e. laminae distortion and extensive vuggy porosity) probably had poor connectivity and could not remove hydrogen sulfide from the system easily or were zones of enhanced mixing between hydrocarbon-rich and hydrogen sulfide-rich waters. Hydrogen sulfide that did not completely escape the system was oxidized into native sulfur in many instances, which formed economic mineral deposits associated with calcitized masses. Although the origins of large selenite masses is still unclear, it is reasonable to assume that some selenite masses are the result of further oxidation of native sulfur, while others may be the result of ascending hydrothermal fluids or simply the solution and reprecipitation of original gypsum.

The widespread distribution of calcitization within the Castile Formation indicates that hypogene speleogenesis has significantly affected the diagenetic evolution of the region. Much of the hydrogen sulfide produced during calcitization appears to have been oxidized to either native sulfur or secondary gypsum (selenite) within the region. Current theories on the origin of hypogene caves of the Guadalupe Mountains attribute calcitization within the Castile Formation as the source of the hydrogen sulfide that produced the sulfuric acid waters involved in speleogenesis (Hill, 1990). However, minimal calcitization occurs proximal to the Guadalupe Mountains, while most

calcitization occurs primarily in northern Culberson County, Texas. This distribution of calcitization suggests that the diagenetic hydrogen sulfide of the Castile Formation is not likely the primary source for hypogenic, sulfuric acid speleogenesis in the Guadalupe Mountains. Future research needs to evaluate other possible sources of hydrogen sulfide generation in the greater Delaware Basin region or demonstrate geologically feasible mechanisms for delivering hydrogen sulfide from the known calcitized regions of the Castile Formation to the Guadalupe Mountains. Evaporite units of the backreef facies associated with either the Capitan or Victorio Peak reef masses appear to be more probable source areas for hydrogen sulfide associated with Guadalupe Mountain karst development.

Calcitization within the Castile Formation is far more extensive and diverse than originally recognized. Research is currently being conducted to better constrain the geochemical relationships between evaporite calcitization, native sulfur, selenite bodies and hypogenic karst within the Castile Formation through isotopic and petrographic studies of closely related field occurrences. Detailed studies are being conducted on the transitional boundaries observed within caves, which will hopefully provide significant insight into the diagenetic alterations associated with calcitized evaporites, native sulfur and selenite within the Castile Formation.

ACKNOWLEDGEMENTS

The authors are indebted to Jack Blake, Draper Brantley, Stanley Jobe, Lane Sumner and Clay Taylor for their generous access to private ranches in Texas throughout this study. This research was partially funded through grants from the New Mexico

Geological Society (NMGS), the American Association of Petroleum Geologists (AAPG), the Geological Society of America (GSA), and the New Mexico Tech Graduate Student Association, with support from the National Cave and Karst Research Institute (NCKRI).

CHAPTER VII:
NEW INSIGHTS INTO YATES FIELD RESERVOIR CHARACTERIZATION: HYPOGENIC ORIGIN FOR CAVERNOUS POROSITY

ABSTRACT

Karstic porosity in Guadalupian strata of the Yates Field of eastern Pecos County, Texas, has been recognized for over 80 years, since the first well was completed. Early characterization of Yates Field karst development attributed cavernous porosity to eogenetic, island speleogenesis contemporaneous with San Andres deposition. However, significant advances in karst science in recent decades suggest that the dominant karst development within the Yates Field is the result of hypogene speleogenesis. Support for the dominance of hypogene processes is widespread throughout the entire Permian Basin, including relict caves that have been exposed by surface denudation and extensive brecciation and mineral deposition in the subsurface. Specifically within the Yates Field, strong evidence supports hypogene speleogenetic origins based on the spatial distribution of cavernous zones and secondary mineralization. Yates Field karst is focused along tectonic fractures, permeability boundaries and the crest of the dominant fold within the area, which creates a classic pattern of hypogene dissolution reminiscent of three dimensional mazes in other hypogene settings. Intrastratal brecciation and infiltration of residual clasts into underlying strata is another common result of hypogene speleogenesis. The precipitation of non-meteoric, subaqueous speleothems and calcite

spar attest to mineralization within a confined system. While early theories of karst development associated with San Andres island complexes were intriguing, our new hypogene speleogenetic model for karst development within the Yates Field provides a simpler conceptual model that better accounts for the variability of karst development documented throughout the study area.

INTRODUCTION

The Yates Field is located in eastern Pecos County, Texas on the southeastern tip of the Central Basin Platform within the Permian Basin (Fig. VII.1). The Yates Field produces from Guadalupian strata, while the superjacent and overlapping Toborg Field produces from the overlying uppermost Triassic and Cretaceous units (Fig. VII.2, VII.3) (Franklin, 1966). Although this work focuses on the Yates Field, the less studied Toborg Field provides important clues into the speleogenetic evolution of the entire region. Cavernous porosity within the carbonate units of the Toborg Field is likely genetically related to the karst development within the Yates Field.

The Yates Field was discovered in 1926 when the first well was drilled to a depth of 990 feet (302 m) and produced 540 bopd, although oil had been suspected in the region a decade earlier because of oil seeps along the Pecos River (Marathon, 1973) and a water well that was drilled in the area which rapidly developed a thick film of oil on it (Levine et al., 2002). By 1929, more than 200 producing wells had been completed within the Yates Field, (Levine et al., 2002). The top of the San Andres is a horseshoe shaped anticline whose relief has been enhanced by post San Andres erosion. In 1929, oil production peaked at 41 million barrels, while attempts were made to preserve

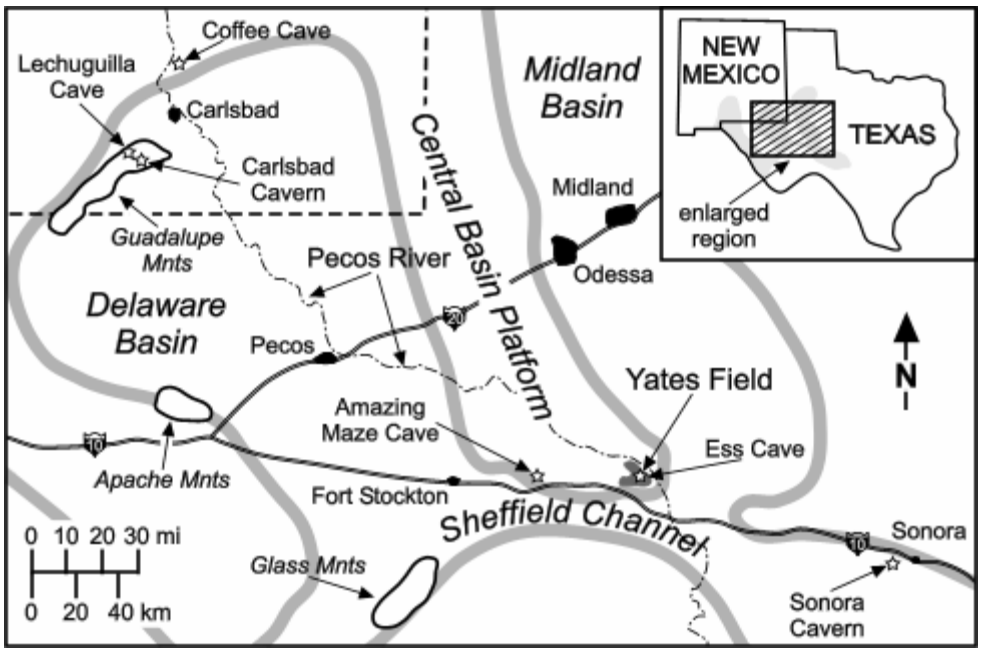

Fig. VII.1: Location of Field, showing relationship to the Central Basin Platform, Delaware Basin, Midland Basin and Sheffield Channel. Other important features shown include the location of Amazing Maze Cave, Carlsbad Cavern, Coffee Cave, Ess Cave, Lechuguilla Cave, Sonora Cavern and the Pecos River (adapted from Klimchouk, 2007 and Hill, 1996).

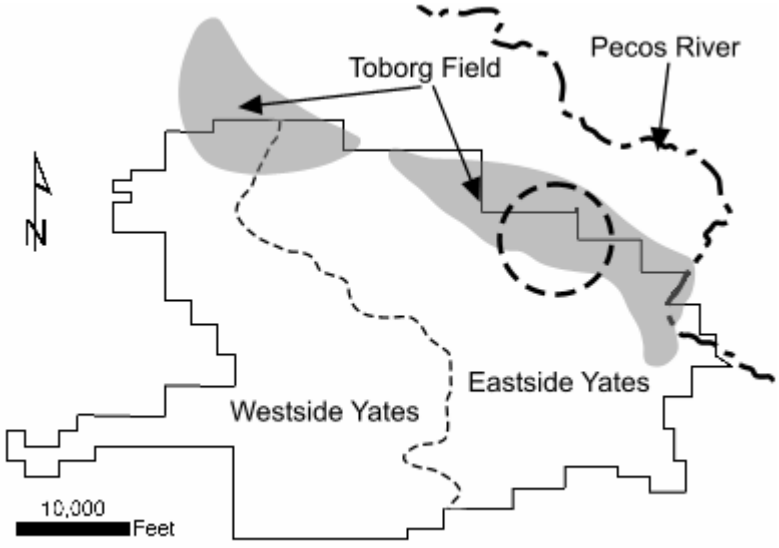

Fig. VII.2: Map of the Yates Field area showing the boundary between eastside and westside Yates, as well as the relationship of the Toborg Field and Pecos River. Dashed circle shows approximate location of Ess Cave (adapted from Franklin, 1966 and Kunath and Smith, 1968).

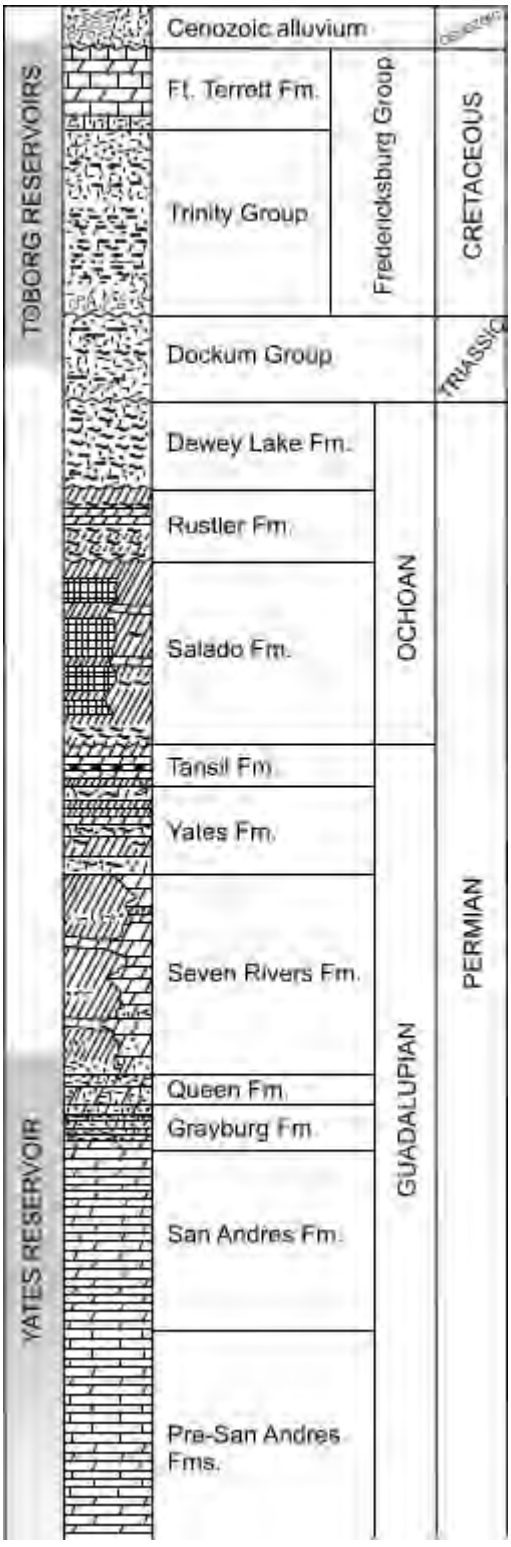

Fig. VII.3: Simplified stratigraphic section of the Yates Field area including delineation of the stratigraphic position of the Yates and Toborg Reservoirs (adapted from Franklin, 1966 and Wessel, 2002a).

the reservoir integrity by limiting drilling to the upper 225 feet (69 m) of the San Andres Formation. Just when operators thought that all of the big wells had been drilled, the Transcontinental-Mid-Kansas Oil Co. I. G. Yates Well #30A came in at world record producing 204,672 bopd in 1930. By 1941 annual oil production dropped to 6 million barrels, but because of wartime fuel needs increased drilling raised oil production to 18 million barrels in 1948 (Levine et al., 2002).

The San Andres here is comprised of series of successively vertically stacked progradational shelf carbonates resulting in 540 ft of closure at the crest of the structure. The east and southeastern portions of the San Andres are seaward margins and have the highest carbonate grain packing, with the western and leeward side of the San Andres being predominantly more carbonate mud rich with evaporites. These depositional lithofacies significantly impact the production characteristics over the 26,000 acre field so that Western and Eastern parts of the unit have been designated for over 40 years. Multiple dolomitization of the San Andres with karsting and collapse karst fabrics, with fracturing have enhanced the reservoir deliverability to the reservoir. The San Andres Formation reservoir in the Yates Field Unit is characterized by remarkably high porosity and permeability in the Eastern portion. Core derived porosities and permeabilities range as high as 35% and 3,000 mD, respectively.

The field was on primary depletion until unitization in 1976 in order to better manage water encroachment and conserve reservoir pressure with Marathon Oil becoming the field operator. Soon after, secondary oil recovery was begun (Levine et al., 2002). The high reservoir connectivity of the eastern side of the field led Marathon to develop a secondary recovery strategy using gravity drainage. The field initially had no observable

gas cap so that oil saturation in the present gas cap within the uppermost San Andres was initially high, thereby, making gravity drainage the most appropriate recovery strategy. Nitrogen and produced gas were injected in the gas cap to maintain reservoir pressure while the oil-water contact was lowered by exporting produced water offsite. The gas injection and prodigious water export resulted in the development of a relatively thin 25-80 ft (7-25 m) thick oil column over the oil – water contact at approximately an elevation of +1020 ft (+311 m). The gas – oil contact was at approximately 1060 ft (323 m) above sea level. At the time that Kinder Morgan acquired the field, a total of 1,766 wells had been drilled in the unit and average oil column thickness was approximately 35 ft (11m) with field wide variance from 15 to 80 ft (5-25 m). Air separation units were installed in the field to provide the nitrogen for injection, with a brief six year experiment injecting carbon dioxide. At that time CO_2 was considered too expensive and nitrogen injection was resumed.

Kinder Morgan acquired Marathon Oil Company's operational interest in the Yates Field Unit in November, 2003. At that time production was approximately 19,000 barrels of oil a day from 362 active wells. Injection of nitrogen from air separation units ceased immediately after the acquisition. In March 2004, when Kinder Morgan initiated injection of carbon dioxide gas at a rate of 40 million cubic feet per day, the daily production had fallen to approximately 17,000 bopd. Reservoir pressure of 632 psi is currently being maintained by immiscible CO_2 injection and injection of produced gas into the gas cap, with water injection and export of water out of the field balanced to maintain a stable oil-water contact.

At the end of December 2007, 521 wells produced an average 27,655 bopd (barrel of oil per day) + 510,749 bwpd (barrels of water per day) + 214,131 MCFPD (million cubic feet per day) with most of the production from the Eastern portion of the field. The average daily CO_2 injection was 103,565 MCFPD. Almost 41,000 bwpd were exported and approximately 470,000 bwpd were reinjected. The median gas-oil contact is at 1039 ft (317 m) above sea level and the median oil – water contact is at 1016.5 ft (310 m) above sea level.

The Yates Field is well known as a karstic reservoir, which was recognized early in the production history of the field (Hennen and Metcalf, 1929; Adams, 1930). Over the past 80 years, wells drilled have continuously intercepted cavernous porosity, often recognized by bit drops and sustained very high oil flow rates, while coring efforts since the 1970s have documented numerous zones of vuggy to cavernous porosity, extensive secondary mineralization including both speleothem and spar fabrics, and voids containing sediment fills. Craig (1988), Tinker and Mruk (1995) and Tinker et al. (1995) characterized the karst development as paleokarst associated with eogenetic, coastal speleogenesis because karst appears to be focused beneath major changes in San Andres lithology, which they interpreted to represent subaerial exposures of San Andres island complexes during deposition. However, much of the support which they gave for subaerial exposure was based on the presence of cavernous porosity at these boundary zones and through reciprocal reasoning they concluded that cavernous porosity must have formed through subaerial exposure and freshwater / saltwater mixing, which implies that the San Andres was subaerially exposed during deposition and developed a freshwater lens. While this was a compelling speleogenetic model during the late 20th century,

significant advancements in karst science in the last two decades provided sound alternatives. Therefore, this manuscript proposes a new model for karst development within the Yates Field involving hypogene speleogenesis while reviewing previous work and demonstrating how evidence provided by earlier researchers supports this new interpretation.

SPELEOGENESIS: Three Basic Models

Cave and karst development occurs throughout the diagenetic evolution of sedimentary rocks; therefore, it is necessary to review the basic speleogenetic processes as they are currently understood in order to evaluate past and current theories on karst development within the Yates Field. Although often considered a special type of porosity, cavernous porosity is effectively large-scale, vuggy porosity, which often forms a hydrologically connected system. Cavernous porosity can develop during the eogenetic, mesogenetic or telogenetic phases of diagenesis, through syngenetic, hypogenic or epigenic speleogenesis, respectively (e.g. Klimchouk et al., 2000; Klimchouk and Ford, 2000; Ford and Williams, 2007; Palmer, 2007). Because speleogenesis is directly related to diagenetic evolution, karst systems are constantly evolving in relation to changes in local and regional hydrogeology, often inheriting components of previous phases of speleogenesis in subsequent phases. However, specific speleogenetic processes often dominate systems and can be easily characterized based on spatial and morphological patterns and regional paleohydrogeological analysis. Below are summaries of the three basic processes of speleogenesis, each of which must be considered as a possible mechanism for cavernous porosity development within karst reservoirs.

Syngenetic Karst: Eogenesis

Syngenetic karst, often called eogenetic or island karst, forms in diagenetically immature rocks (i.e. eogenetic rocks) that are poorly cemented and retain high primary porosities and permeabilities (Vacher and Mylroie, 2002). Eogenetic rocks have not been removed from the affects of meteoric processes and have not undergone burial compaction and cementation (Choquette and Pray, 1970). Most commonly, eogenetic karst is associated with coastal regions, either continental or island, where the mixing of fresh and saline waters at the margin of the fresh-water lens increases dissolution. Eogenetic island karst is characterized predominantly by the presence of flank-margin caves, which form elliptical to globular chambered features at the periphery of the freshwater lens (Fig. VII.4a), often exposed as a horizontal series of caves along coastlines when they have been breached by wave erosion and/or surface denudation (Mylroie and Carew, 1995). Isolated features can develop at the top of the lens, termed banana holes, but these features are generally spatially limited (Harris et al., 1995). Although theorized, no unequivocal proof of cavernous porosity development at the bottom of the fresh-water lens (e.g. halocline caves) has been documented (Stafford et al., 2005). Most eogenetic coastal karst exhibits well-developed epikarst. Along coastlines, littoral eogenetic karren forms regions of jagged, pinnacle karst as a result of the interaction of meteoric water, salt spray, and biology (Taborosi et al., 2004). Away from coastlines, the development of soils promotes the dissolution of extensive vadose epikarst, including “pit caves”. Syngentic karst has also been documented in modern evaporite deposits where seasonal precipitation fluctuations produce surficial, solutional sculpturing on recently deposited evaporite sequences (Yauro and Cooper, 1996);

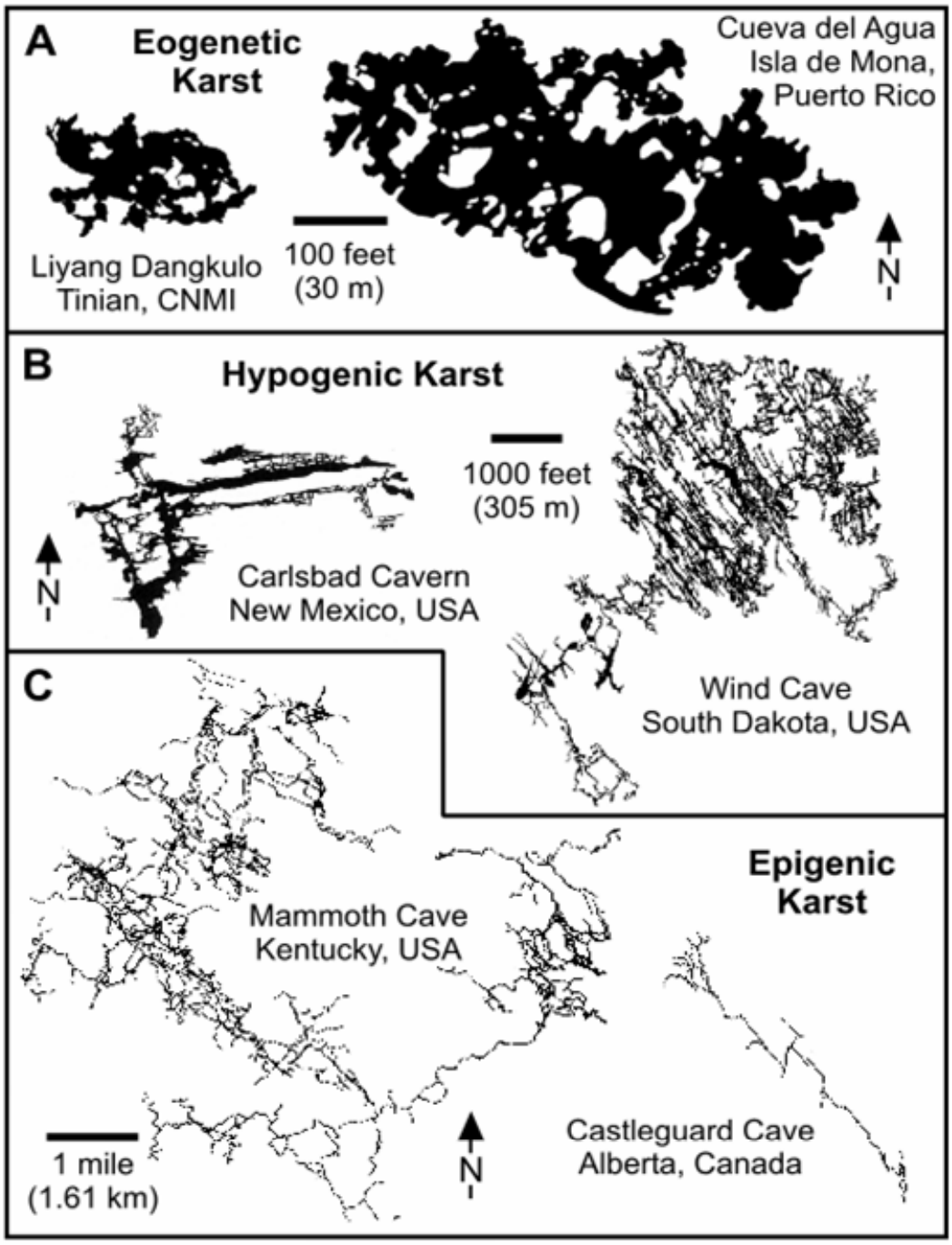

Fig. VII.4: Plan view maps of large caves developed by different speleogenetic processes. Note the significant difference is scale for each of the different classes of caves. a) Eogenetic caves formed in Quaternary Limestone; b) Hypogenic caves formed in Permian Limestone (Carlsbad Cavern) and Mississippian Limestone (Wind Cave); c) Epigene caves formed in Mississippian Limestone (Mammoth Cave) and Cambrian carbonates (Castleguard Cave) (adapted from Klimchouk et al., 2000 and Klimchouk, 2007).

however, eogenetic karst is most common and widespread in immature, coastal carbonates.

Although eogenetic karst development can occur throughout island and coastal settings, flank-margin cave development (Fig. VII.4a) is the most common and extensive type of karst development (Mylroie and Jenson, 2002). Flank margin caves develop largely independently of lithologic variability, but instead develop in direct association with the position of the fresh-water lens (Mylroie and Carew, 1995). Although the mixing of two fluids saturated with respect to calcite will produce a solution undersaturated with respect to calcite that enables increased dissolution, perhaps even more important are the affects of organic acids at the top and margin of the fresh-water lens created by the decay of organic material trapped at density boundaries (Mylroie and Jenson, 2002). Recent research has suggested that aragonite to calcite mineral inversion may be an important component of flank-margin cave development (Moore et al., 2007), which implies that eogenetic karst would be less common in the calcite seas of the Paleozoic. Ultimately, the volume of water and flow rate through the margin of the lens, as fresh-water is discharged to sea-level, will control the extent of eogenetic, coastal karst development; which directly relates to climate, freshwater lens thickness and total recharge area (i.e. island size).

In most modern carbonate islands, sea-level fluctuations resulting from glacio-eustacy, tectonic uplift and subsidence have produced multiple freshwater lens horizons and associated levels of flank-margin cave development. Modern examples of eogenetic coastal karst (Fig. VII.4a) have been well documented throughout the Bahamas (e.g.

Mylroie et al., 1995) and Mariana Islands (Jenson et al., 2006), as well as other coastal regions around the world. In these modern environments, rings of flank margin caves delineate previous sea-level still stands, which can often be seen in exposed cliff and terrace faces. Fracture control on island karst development is generally limited because eogenetic rocks have not been subjected to deep-burial diagenesis. However, on scarped coastlines fractures do develop roughly parallel to coastlines as a result of coastal undercutting of erosion notches (Stafford et al., 2005). Tectonic fissuring has only been widely documented on carbonate islands in volcanic regions where differential uplift creates partitioning of the freshwater lens (Jenson et al., 2006). Although fractures distort the fresh-water lens by providing preferential fast flow paths, even in tectonically active regions like the Mariana Islands eogenetic karst development is still dominated by flank margin caves (Stafford et al., 2005).

Hypogenic Karst: Mesogenesis and Early Telogenesis

As sedimentary rocks are buried beyond the affects of meteoric diagenesis, they enter the mesogenetic phase of diagenesis, where overburden pressure and increased temperatures results in compaction and cementation, removing much of the original, depositional porosity and permeability (Choquette and Pray, 1970). As burial diagenesis continues, differential compaction and regional tectonic deformation induce brittle deformation, ranging from intragranular fracturing, to jointing isolated within individual beds, to large-scale fault offsets. With cementation and compaction removing most of the original porosity, a shift from the dominance of intergranular permeability to fracture / bedding plane permeability occurs (Choquette and Pray, 1970). Mesogenesis continues as

buried rocks are returned to the surface through tectonic uplift and surface denudation, until buried rocks are once again exposed to the direct affects of meteoric diagenesis. Throughout mesogenesis and early telogenesis, speleogenesis is dominated by hypogene processes, which is the formation of solution-enlarged permeability structures by fluids ascending to a cave-forming zone from below in leaky confined conditions, where deeper groundwaters in regional or intermediate flow systems interact with shallower and more local groundwater flow systems. This upward groundwater movement can be driven by hydraulic gradients, or other sources of energy. While hypogenic karst exploits all bedrock heterogeneities as flow paths, pressurized fluids predominantly migrate along fractures, attempting to reach lower pressure, regional base levels such as incised rivers and closed basins where overburden confinement is thinner and/or disrupted (Klimchouk, 2007). Previous studies have shown that groundwater convergence towards incised river valleys affects regional groundwater flow more than kilometer deep (Klimchouk, 2007).

Hypogenic karst is potentially the most extensive type of karst development, because it develops throughout mesogenesis and early telogenesis. Although many people attempt to classify sulfuric-acid, hydrothermal and artesian karst as unique types of cavernous porosity development, they are all hypogenic karst where dissolution is hydrologically driven by ascending fluids originating from greater depths or distal recharge regions (Klimchouk, 2007). Because hypogenic karst develops in confined or semi-confined settings, dissolution is often driven by a mixed convection system including components of both free and forced convection (Klimchouk, 2007). Forced convection is induced by regional or basinal hydrologic patterns as ascending fluids attempt to reach local base-levels, while free convection is driven by density variations, either thermal or solute. Free

convection occurs as ascending waters either cool or become saturated through rock dissolution, which results in the sinking of the denser fluids within the confined system as less dense fluids rise towards the solution front (Kohout et al., 1988). Free convection flow patterns form in both regional and local (cave system) scales. Forced convection ultimately directs upward migrating fluids towards the regional base-levels (Tóth, 1999). As a result of rising flow pattern, unique suites of morphometric features occur within hypogene caves, including feeders which delivered solutionally aggressive fluids from lower transmissive zones and outlet cupolas which discharged soluble fluids into upper transmissive zones, as well as wall and ceiling channels that commonly connect feeders to cupolas (Klimchouk, 2007; Stafford et al., 2007a).

Hypogenic karst development ranges from large isolated chambers in poorly fractured rock (Kempe, 1996) to extensive, multi-storey maze caves in well-fractured and interbedded rock sequences (Fig. VII.4b) (Klimchouk, 2000). Hypogene fluids exploit all bedrock heterogeneities in a soluble unit because flow through it is limited by the conductivity of the least permeable adjacent formation, and hence speleogenetic competition is subdued. Those horizons that had greater and hydrologically better connected initial porosity will preferentially develop greater karstic porosity (Klimchouk, 2007). In thick-bedded, homogeneous units, hypogene dissolution is dominated by vertically exaggerated solution pipes along fractures, where free convection continues to deliver aggressive fluids to the upper solution front (Anderson and Kirkland, 1980). In heterogeneously bedded sequences (e.g. dolomite and anhydrite; sandstone and limestone; packstone and wackestone facies), multi-storey caves develop along both fractures and bedding planes (Klimchouk, 2007). Initially more permeable beds (e.g.

dolomite, sandstone, packstone) serve as laterally transmissive zones while less permeable beds served as leaky aquicludes (e.g. anhydrite, limestone, wackestone). As fluids attempt to migrate vertically towards upper transmissive zones, solutional development in the original aquicludes results in a hydrologic shift, such that the solutionally enlarged regions become more permeable (Klimchouk, 2007). As solution continues, extensive regions of stratiform brecciation commonly develop as a result of collapse along these zones of intense dissolution (Anderson et al., 1978; Klimchouk and Andrejchuk, 1996). Although these processes are most pronounced in carbonate / evaporite sequences due to the high solubility of anhydrite and halite, they commonly occur in heterogeneous carbonate sequences especially when solution agressivity is increased by the addition of organic acids (e.g. sulfuric acid) (Lowe et al., 2000) or thermal gradients (Dublyansky, 2000).

Recently, hypogenic speleogenesis has begun to receive more attention in North American karst research, although its specific variants have been long recognized as an important speleogenetic mechanism in European karst science. Various styles of hypogenic speleogenesis that were previously considered unrelated, specific either to certain lithologies (e.g. western Ukrainian giant gypsum mazes) or chemical mechanisms (e.g. sulfuric acid caves or hydrothermal caves), are shown to share common hydrogeologic genetic backgrounds (Klimchouk, 2007). Where proper structural pre-requisites exist, hypogene karst processes form dense networks (Fig. VII.4b), often exhibiting a highly clustered regional pattern with areas of intense solutional development, surrounded by regions of minimal karst development, resulting from the regional hydrogeology, stratigraphy and structural deformation (Klimchouk, 2007). Some

of the best known examples of hypogene multi-storey, maze caves occur throughout the western Ukraine (e.g. Optimistikaya, Ozerna and other maze caves in gypsum) and the Black Hills of North and South Dakota, USA (Fig. VII.4b) (e.g. Wind Cave, Jewel Cave), as well as the famous caves of the Guadalupe Mountains of southeastern New Mexico and far west Texas (Fig. VII.4b) (e.g. Carlsbad Cavern and Lechuguilla Cave), which are vertically exaggerated caves with complex 3D patterns (Klimchouk, 2007).

Epigenic Karst: Late Telogenesis

Epigenic karst develops as rocks are returned to the earth surface through tectonic uplift and surface denudation and once again exposed to the affects of meteoric processes during telogenesis (Klimchouk and Ford, 2000). Because telogenetic rocks have been buried and compacted, they commonly have low matrix porosity such that planer bedrock heterogeneities provide the majority of total rock permeability (Choquette and Pray, 1970). Therefore, it is not surprising that most epigenic karst development is strongly controlled by bedding planes, fractures and other structural deformation to the bedrock (e.g. folding and tilting) (Palmer, 2007). Epigenic karst is often viewed as the dominant karst type because it develops in direct relationship to modern surficial process where undersaturated meteoric waters descend into the subsurface, which inevitably creates a greater abundance of epigene karst features that are exposed at the land surface. Although it cannot be definitively proven that epigene karst is the dominant speleogenetic process, there is a distinct sample bias towards studies of karst development in epigene settings simply because they are the most accessible karst type for direct study. Therefore, greater abundance of physically documented epigene caves and karst features simply indicates

that these are more easily studied and does not confirm that epigene speleogenesis is the dominant process of cave and karst development.

Epigene karst features can be subdivided into two basic categories (e.g. vadose and phreatic) based on the hydrogeologic conditions associated with formation. Dendritic or branchwork cave systems are most common for epigene karst (Palmer, 2007). Vadose, epigene karst develops in the unsaturated zone above the local water table and is commonly characterized by extensive epikarst and solutional sinkholes at the land surface, which commonly converge in a dendritic pattern with increasing depth or distance from meteoric recharge (Fig. VII.4c) (Palmer, 2007). Vadose development is driven by gravity as water rapidly attempts to reach the local groundwater table, forming caves that are essentially horizontal with development along bedding planes in low-relief areas (Palmer, 2000) and vertically exaggerated caves developed along fractures or dipping bedding planes in high-relief, alpine areas (Hose, 2000). In contrast to vadose caves, phreatic caves develop in the saturated zone or beneath the water table. Here cave development is driven by a combination of hydraulic potential and gravity as groundwater attempts to reach the local base level, often regional rivers or basins (Ford and Williams, 2007). Because epigene karst is unconfined, the water table fluctuates in response to variations in precipitation and local base level, such that the boundary between the phreatic and vadose zone is constantly evolving. During intense recharge events, the water table may rise rapidly, increasing hydraulic potential and ultimately the rate of flow through the system, similarly during periods of minimal recharge the water table may lower which results in lower hydraulic potential and flow rates (Ford and Williams, 2007). Because epigenic karst is directly connected to surface processes, river

incision will cause downward incision of epigene systems, often forming a multi-level cave system where upper levels developed in relation to previous river elevations, but are now abandoned as more recently developed lower levels form in relation to the modern river position (Palmer, 2000). While multiple levels can develop in epigene caves as result of regional lowering of the water table, this should not be confused with the multiple storeys that can develop simultaneously in hypogene caves. In epigene settings, speleogenesis is competitive such that flow routes which achieve breakthrough first will become the dominant flow path (Ford et al., 2000). In contrast, hypogene settings favor non-competitive speleogenesis such that all bedrock heterogeneities in a cave-forming zone are exploited equally (Klimchouk, 2007).

Epigene karst is characterized by extensive epikarst that rapidly transmits recharge through solutional conduits that converge with depth (Palmer, 2007). As in eogenetic karst, organic acids associated with soils significantly increase dissolution at the surface. However, epigene epikarst drains to progressively larger solutional conduits, while eogenetic epikarst drains into highly porous and permeable bedrock where flow becomes diffuse (Taborosi et al., 2004). Epigene caves in alpine regions tend be vertically exaggerated with numerous vertical shafts as a result of the high gravitational potential (Ford and Williams, 2007). Because epigene karst can develop multiple levels in relation to base-level lowering, complex epigene systems can develop with multiple horizons that are hydrologically active and inactive. The longest cave documented in the world has formed this way in central Kentucky, U.S.A. Here, Mammoth Cave (Fig. VII.4c) formed with the regional lowering of the Green River, forming over 350 miles (560 km) of currently explored passages (Palmer, 2000). While epigene karst represents the longest

and deepest documented individual caves, most of the greatest caves by total volume and surveyed length in the world belong to hypogenic class.

GEOLOGIC SETTING

The Yates Field is located on the southeastern tip of the Central Basin Platform (Fig. VII.1) on a structural high where the San Andres Formation is at its highest elevation above sea-level in the region (Hills, 1970; Wessel, 1988). The Yates Field covers an area of ~41 square miles (~106 km^2) with production from Guadalupian strata, including the San Andres, Grayburg, Queen and Seven Rivers Formations (Fig. VII.3). The Yates Field is bounded on the east by the Midland Basin and the south by the Sheffield Channel, while the Central Basin Platform extends to the north and west (Fig. VII.1) (Hill, 1996).

During late Mississippian and early Pennsylvanian time, collision of the North American and South American Plates produced the Ouachita Orogeny and block faulting of the Tobosa Basin, which had formed in the late Precambrian (Horak, 1985). Block faulting created the initial Central Basin Platform, which divided the Midland and Delaware Basins, leaving the Sheffield Channel as a narrow seaway connection at the southern end of the Central Basin Platform (Horak, 1985). Block faulting continued through the early Permian, including Wolfcampian and early Leonardian time (Hill, 1996). Adjacent to the Central Basin Platform, the Delaware and Midland Basins subsided to reach their maximum depth in the Wolfcampian and early Leonardian. By the mid-Permian, the region was tectonically stable prior to deposition of the reservoir host rocks of the Yates Field. During the tectonically quiescent mid-Permian, deposition and subsidence dominated the Permian Basin region, ultimately resulting in total basin-

infilling by the late-Permian with evaporite sequences (Hill, 1996). In the latest Permian and early Triassic the region is believed to have been uplifted, but the exact tectonic mechanism is unclear (Hill, 1996).

Throughout the majority of the Mesozoic, the region was subaerially exposed and terrestrial erosion and sedimentation dominated (Dickenson, 1981). In the mid-Cretaceous, an episode of marine inundation covered the region briefly depositing basal sands and carbonate facies (Fig. VII.3) (Dickenson, 1981). Starting in the late Cretaceous, the Permian Basin region was subjected to tectonism. Within the Trans-Pecos region, two episodes of Laramide compression have been documented (Horak, 1985). The early compression phase was oriented northeast with associated northwest faulting and fracturing, while the later compression phase was oriented east-northeast with associated north-northwest oriented folds and fracturing (Horak, 1985). Intrusive dikes within the Delaware Basin suggest that compression was active until the middle Oligocene (Barker and Pawlewicz, 1987). In the late Oligocene through the middle Miocene, compression switched to Basin and Range extension with reactivation of previous compressional fractures, the development of northeast oriented faulting associated with northwest extension and geothermal gradients as high as 40-50°C/km (Barker and Pawlewicz, 1987). Currently, weak north-northeast to east-northeast extension continues. While no definitive evidence of the affects of Laramide and Basin and Range tectonism have been documented within the Midland Basin and Central Basin Platform, fractures oriented at N50°W and N40°E have been documented in the Yates Field (Craig, 1988; Tinker et al., 1995), which suggest that the affects of Cretaceous and Tertiary tectonism extended into the region. Additional evidence is suggested by uplift of the Fort Stockton Plateau and

entrenchment of the Pecos River, which has maintained its current position near the Yates Field (Fig. VII.1,2) since the early Tertiary (Thomas, 1972).

The highest oil production within the Yates Field is from the San Andres Formation, earlier termed the “Big Lime” (Fig. VII.3) (Levine et al., 2002). The San Andres Formation is primarily dolomite and is up to 750 feet (229 m) thick in the field area, which has been subdivided into two main depositional facies within the field area that separates the Yates Field into westside and eastside components (Craig, 1988). The west side (Fig. VII.2) is characterized as low-energy, restricted, subtidal, lime mudstone to wackestone facies, while the east side (Fig. VII.2) is characterized as higher-energy, subtidal, lime peloid/fusilinid packstone and grain-dominated packstone facies with a lesser grainstone facies component (Tinker and Mruk, 1995). The eastside and westside components form three to four high-frequency, prograding shoal sequences (Tinker and Mruk, 1995). The San Andres is unconformably overlain by the Grayburg Formation, which is composed of silty dolomite averaging 53 feet (16 m) thick, suggesting subtidal to peritidal deposition (Wessel, 2000a). Overlying the Grayburg, the Queen Formation has an average thickness of 47 feet (14 m), which consists of dolomite and subarkosic siltstone with thin interbeds of subarkosic sandstone (Wessel, 2000a). Unconformably overlying the Queen Formation is the Seven River Formation which averages 427 feet thick (130 m) and is primarily anhydrite / gypsum with minor interbeds of subarkosic fine grained sandstone and siltstone and silty dolomite deposited as sabka or salina facies (Wessel, 2000a).). The lower Seven Rivers is characterized by subarkosic sandstones units up to 20 feet which are proven oil reservoirs in the field. The deposition of the Seven Rivers Formation is believed to represent a transition to more restricted marine

circulation resulting from infilling and closing of the Sheffield Channel, which ultimately separated the Midland and Delaware Basins (Wessel, 2000a). Because the Seven Rivers Formation has been interpreted as being deposited in a broad, flat sabka environment, marker beds within the unit have been used to reconstruct paleotopography within the Yates Field area by evaluating the elevation of underlying strata in relation to marker beds, most commonly the dolomitic Seven Rivers "M" horizon (Craig, 1988).

The Yates Field is centered along a crescent-shaped structural high that is clearly visible at formational contacts of the San Andres, Grayburg, Queen and Seven Rivers Formations (Fig. VII.5a,b). The anticline dips more steeply (3-5°) on the eastern and southern sides of the Central Basin Platform, towards the Midland Basin and Sheffield Channel, with more gentle dips (0-1°) towards the interior of the Central Basin Platform (Tinker et al., 1995). Tinker and Mruk (1995) suggested that the anticlinal structure was the result of differential compaction of fine-grained and coarser-grained facies of the San Andres Formation. Although the anticlinal feature persists through strata overlying the San Andres Formation, thickening of overlying strata proximal to the eastside / westside Yates Field boundary suggests greater compaction of this region during subsequent Permian deposition. However, with only three wells within the field that penetrate strata underlying the San Andres Formation it is not possible to evaluate whether or not the same structural configuration exists at greater depths. If this structural configuration did persist beneath the San Andres Formation, then it would imply that Yates Field structure is not solely the result of differential compaction.

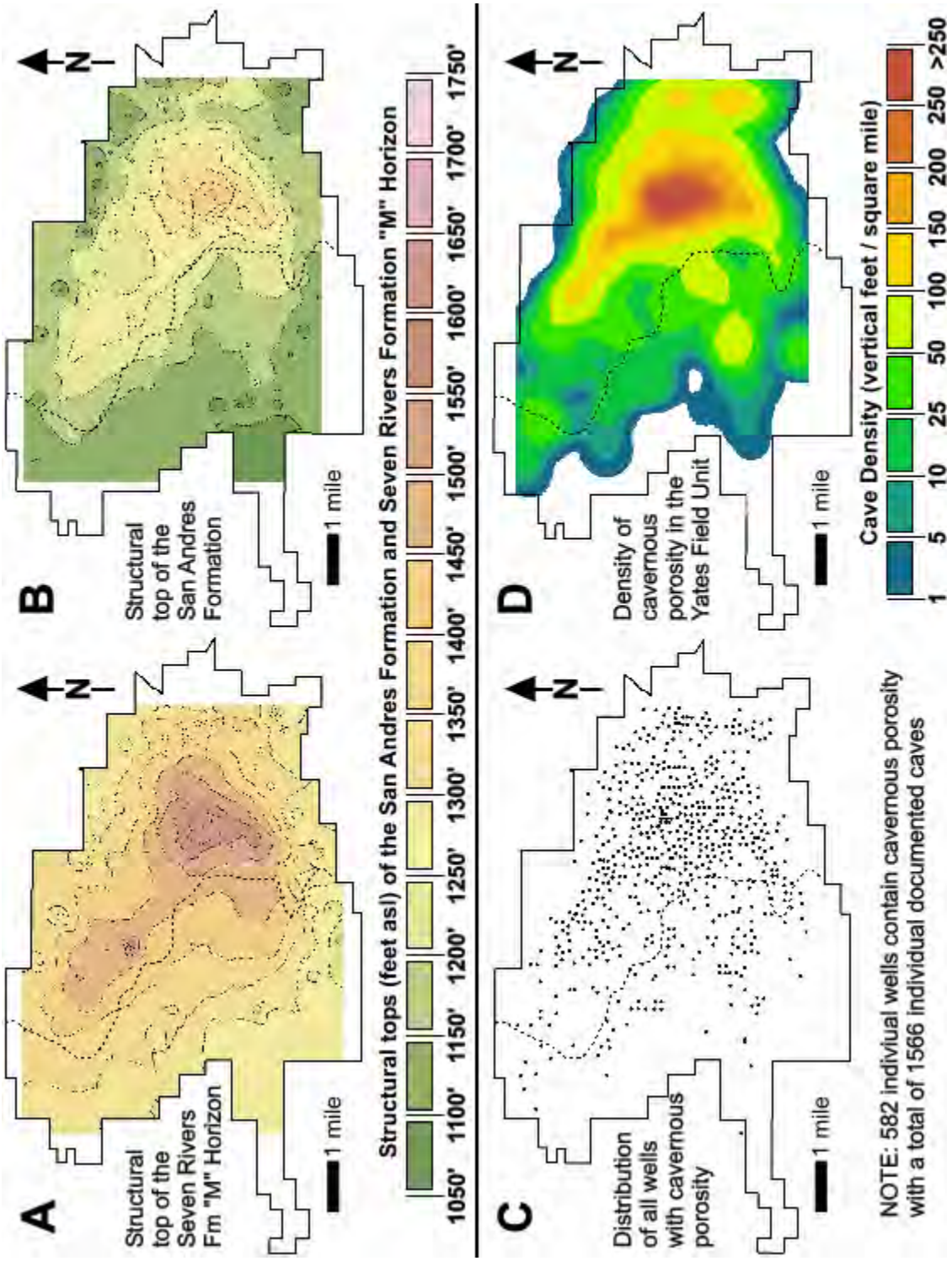

Fig. VII.5: Yates Field structure and karst development. a) structural top of the Seven rivers "M" horizon; b) structural top of the San Andres Formation; c) distribution of the wells that have intercepted caves within the Yates Field; d) density map of vertical feet of documented caves within the Yates Field.

KARST DEVELOPMENT: Regional and Local Karst Manifestations

Features consistent with karst development in lithified strata and characteristically observed in conventional core have been categorized into six key zones in paleocave systems: “(1) undisturbed-host rock, (2) disturbed-host rock, (3) collapsed roof and wall rock, (4) fine-chaotic breccia cavern fill (transported material), (5) coarse chaotic breccia cavern fill (collapsed material), and (6) cave-sediment cavern fill.” (Loucks and Mescher, 2001). Different and unique pore network types are associated with each paleocave zone and significantly control reservoir character (Loucks and Mescher, 2001).

Documented cave and karst development within the Permian Basin region is diverse and widespread. Many of the hydrocarbon reservoirs of the Permian Basin have zones of cavernous porosity; however, there is also an abundance of cave and karst features that are exposed at the surface which enable direct study of the speleogenetic processes that have contributed to karst development within the region. These surficial manifestations are widespread, including, but not limited to, development in: 1) Guadalupian backreef facies (Seven Rivers Formation) and reef facies (Capitan Formation) of the Guadalupe Mountains; 2) Ochoan basin-filling evaporite sequences of the Delaware and Midland Basins; 3) Guadalupian shelf and ramp shoal sequences of the Central Basin Platform; and 4) Cretaceous rocks of the Fort Stockton and Edwards Plateaus.

Within the Yates Field, karst development has been well-documented in the form of porosity development and secondary mineral deposition and alteration. Caves or cavernous porosity zones have been documented since the beginning of Yates Field production in the form of bit drops, as well as through petrophysical analyses. Secondary mineral deposition is diverse, including spar and speleothem void infillings, while

mineral alteration is widespread with field-wide dolomitization and zones of uranium enrichment. The distribution of karst within the Yates Field shows dominance towards the east, with over 1500 individual zones of cavernous porosity identified from petrophysical analyses alone (Fig. VII.5c,d). It is likely that some of this eastern dominance is the result of sampling bias because more wells have been drilled in this region. More intense drilling has been conducted in this area because this region has higher yields and flow rates, which indicates that greater permeability, generally attributed to karst porosity, exists within the production depths of eastside Yates Field.

Surficial Manifestations within the Permian Basin Region

The best documented and most extensive cave development within the Permian Basin occurs within the carbonate reef and back-reef facies exposed in the Guadalupe Mountains of southeastern New Mexico and far west Texas (Hose and Pisarowics, 2000), including world renowned Carlsbad Cavern and Lechuguilla Cave (Fig. VII.1; 4b). Traditionally, the speleogenetic origin of these caves has been attributed to sulfuric acid waters associated with a falling water table (Hill, 1990); however, no consistent levels of cave development have been documented throughout the caves of the Guadalupe Mountains or even within local regions of the Guadalupe Mountains, indicating that the majority of the cavernous porosity did not develop in association with specific water table horizons (Palmer, 2006; Klimchouk, 2007). The caves of the Guadalupe Mountains show direct evidence of confined speleogenesis driven by mixed convection dissolution (i.e. extensive morphologic evidence of confined dissolution including hypogene risers, wall channels, ceiling channels and ceiling cupolas), where fluids originating from depth

migrated through the Capitan reef and Artesia near-backreef facies (Klimchouk, 2007). In many of the caves, the result is a vertically exaggerated 3D pattern with maze clusters at various levels that shows multiple source locations of rising fluids within individual caves, where fluid has migrated both vertically and laterally exploiting all bedrock heterogeneities forming complex, morphological structures with hundreds of meters of vertical extent (Klimchouk, 2007).

While the carbonate caves of the Guadalupe Mountain are the most famous of the Permian Basin, abundant evaporite karst exists in the backreef and basin-filling facies. In the interbedded backreef facies of the Artesia Group, maze caves have been documented with multiple levels of development formed by dissolution of gypsum interbeds along fracture networks (e.g. Coffee Cave, Fig. VII.1) (Stafford et al., 2007a). The basic morphology of these caves have been shown to form through hypogene speleogenesis where ascending artesian fluids have migrated vertically and laterally in response to the eastward migration of the Pecos River (Stafford et al., 2007a). Because the caves have been breached by surficial processes, they commonly bear an overprint of surficial, epigene processes. Within the Delaware Basin, extensive evidence exists of hypogene speleogenesis. Most larger caves within the Castile Formation exhibit classic hypogene morphologies created by dissolution within a mixed convection system, although often overprinted by surficial, epigene processes as a result of surficial breaching (Stafford et al., 2007b). Extensive evaporite calcitization and associated native sulfur deposits within the Castile, Salado and Rustler formations indicate significant intrastratal dissolution and mineral alteration in the presence of ascending fluids and hydrocarbons (Kirkland and Evans, 1976). Scattered throughout the Delaware Basin, breccia pipes, blanket breccias

and solution subsidence troughs have been documented and attributed to confined dissolution driven by density convection. The warmer, rising, less dense and undersaturated fluids originated from the underlying siliciclastics of the Bell Canyon Formation while simultaneously more dense, saturated waters were returned to the lower transmissive zones through density convection (Anderson and Kirkland, 1980). The cave and karst development within the interior of the Delaware Basin clearly shows speleogenetic dominance by hypogene processes.

Since the Late Permian, the Permian Basin region has been largely subaerially exposed except during a phase of mid-Cretaceous marine deposition (Hill, 1996). Associated with the marine transgression, siliciclastic and carbonate sequences were deposited over much of the Permian Basin. Today, significant outcrops of the Cretaceous Fredricksburg Group occur throughout the Fort Stockton and Edwards Plateaus, forming resistant carbonate mesas within the Yates Field area (Wessel, 2000b). Abundant cave and karst development has been documented in the Fredricksburg Group (Fig. VII.3), including both epigene and hypogene karst (Elliott and Veni, 1994). Many of the individual caves clearly show hypogene origins based on diagnostic morphometric features and overall cave morphology, including some of the longest and most extensive caves documented within Texas (Elliott and Veni, 1994; Klimchouk, 2007). Although caves studied in the region show evidence of hypogene origins, many of them exhibit varying degrees of epigene overprinting, because hypogene processes are no longer active since these systems have become unconfined and breached by surface denudation. While documented caves are numerous throughout the region, caves developed in the overlying

Fredricksburg in the Yates Field and surrounding area illustrate well the importance of hypogene processes within the region (Fig. VII.6).

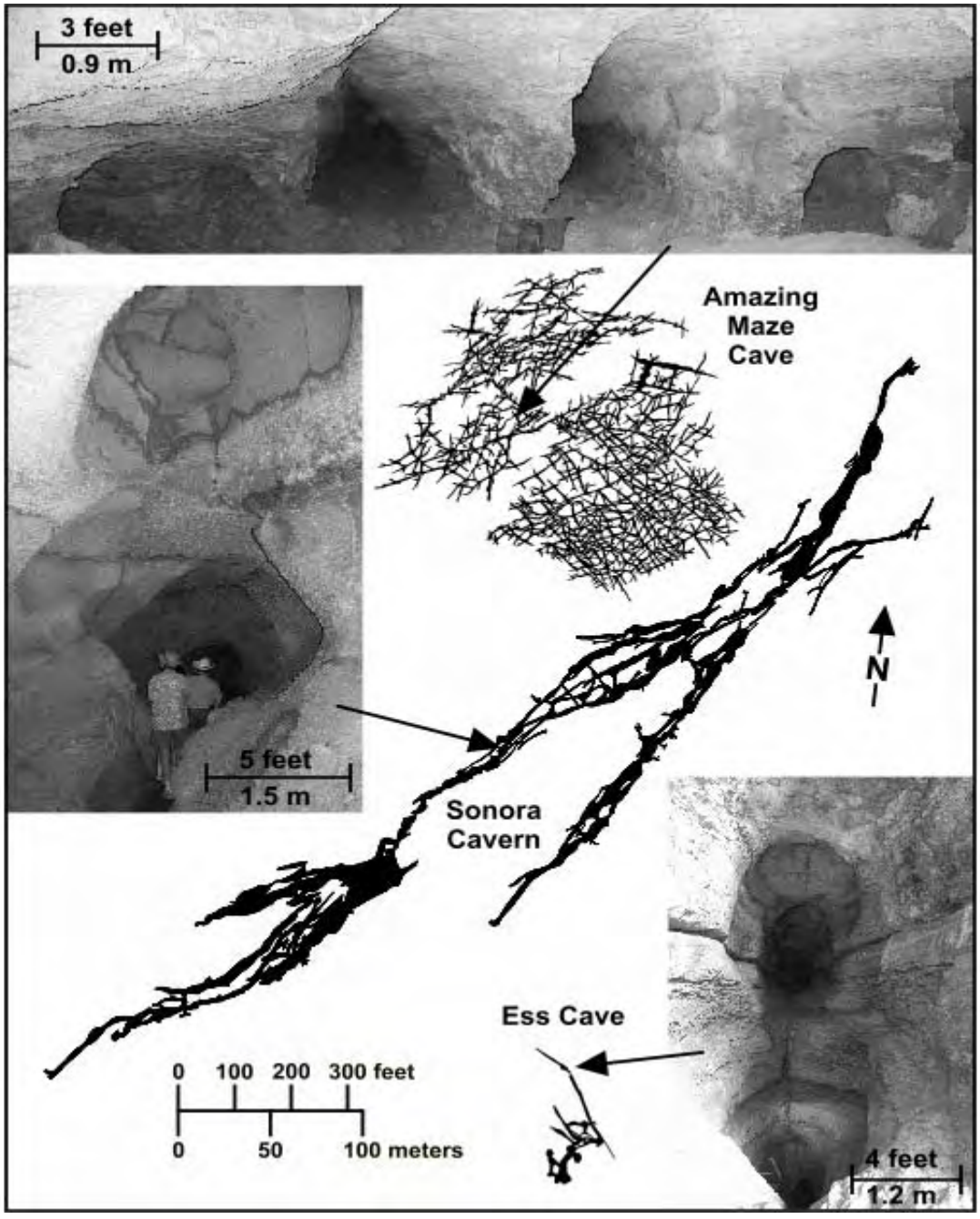

Fig. 6: Cretaceous hypogenic caves within near the Yates Field (see Fig. VII.1 for location of caves). Cave maps show classic hypogene maze patterns, while representative photos from each cave illustrate hypogene morphologies observed in all caves.

Sonora Cavern is located approximately 75 miles (120 km) east of the Yates Field near the town of Sonora (Fig. VII.1). The cave is a three dimensional maze formed along parallel fractures with over 3.8 miles (6.1 km) of mapped passages (Fig. VII.6) (Kastning, 1983; Veni, 1994). Although the cave is famous for its world class, epigene speleothems, solutional morphologies within the caves provide extensive evidence that the overall cave morphology was formed through hypogene speleogenesis (Klimchouk, 2007). This origin is also corroborated by the finding of metatyuyamunite, a uranium-vanadium mineral diagnostic of sulfuric acid dissolution (Onac et al, 2001). Amazing Maze Cave is located approximately 25 miles (40 km) west of the Yates Field between Bakersfield and Fort Stockton (Fig. VII.1). The cave has a surveyed length exceeding 4.7 miles (7.6 km) and forms a complex, multi-storey maze cave (Fig. VII.6) (Warton, 1994). Recent investigations (Klimchouk, 2007) have documented abundant hypogene morphologies throughout the cave, while extensive deposits of secondary gypsum and endellite indicate that hypogene dissolution was enhanced by sulfuric acid-rich waters. Ess Cave is located within the Yates Field boundary (Fig. VII.1), but is considerably smaller than Sonora Cavern and Amazing Maze Cave (Kunath and Smith, 1968). Investigations by the authors during this study found that Ess Cave is a three dimensional maze cave (Fig. VII.6) with abundant morphogenetic evidence of hypogene origins including risers, cupolas and multiple fluid entry points. All three caves exhibit these definitive features characteristic of hypogene speleogenesis within the Yates Field area. Because hypogene speleogenesis has been active in the past within the Fredricksburg Group of the Yates Field area, it is logical to assume that other, stratigraphically lower units within the region have also been

affected by hypogene processes. In contrast, no humanly explored caves in the area have been documented which show evidence of eogenetic origins.

Yates Field: Caves and Secondary Porosity

Cavernous porosity within the Yates Field has been characterized in various ways. Bit drops provide an obvious, direct indication of cavernous porosity that is still open; however, caliper and density logs, as well as unrecovered core intervals and core analyses provide additional identification of karstified zones, especially smaller caves that may not be detected or reported during drilling operations. Cavernous porosity that has not undergone more than approximately 6,560 ft (2,000 m) of burial will often have some karstic porosity that has not collapsed (Loucks and Mescher, 2001). Significant gauge divergence on caliper logs is used as an indication of cavernous porosity (Craig, 1988), which can be measured either subsequent to drilling or subsequent to acid washing when drilling mud introduced into porous zones is frequently removed. Similarly, low density wireline log measurements indicate regions of high porosity (Craig, 1988), while core analyses provide direct lithologic evidence of karstified horizons. Core analyses have identified rubble and brecciated zones believed to represent cave roof collapse of cavernous voids, as well as sediment fills and secondary speleothems and spar deposits (Tinker and Mruk, 1995; Tinker et al., 1995). The database of identified karst features and horizons within the Yates Field enables spatial characterization of karst development within the region (Fig. VII.5 c,d); however, this is largely limited to the upper San Andres Formation and to a varying degree the overlying Guadalupian units, because the cost of coring operations and petrophysical analyses have limited data collection to the primary

producing horizons. A major factor in limited wireline log (petrophysical data) is the difficulty in maintaining a fluid filled borehole during the logging process because of the high permeability and porosity in the San Andres.

Analyses of the spatial distribution of cavernous porosity in this study were limited to features identified by log analyses. Craig (1988) reported 285 caves identified by bit drops, ranging from 1 foot (0.3 m) to 21 feet (6.4 m) with and average height of 2.8 feet (0.6 m); however, bit drops were not incorporated in this study because of inconsistency in reporting by different drilling operations over the past 80 years. Core data were not used in the statistical analyses of cavernous porosity, but provides additional information on the characteristics and secondary mineralization associated with karst development. A total population of 1566 individual caves (Fig. VII.5c) with an average height of 3.9 feet (1.2 m) was identified in the present study through log analyses. The distribution of caves shows a distinct bias towards the eastern side of the Yates Field within the San Andres with the greatest density of caves showing significant correlation to the structural crest of the anticlinal structure that dominates the area (Fig. VII.5d), which is largely composed on dolomitized packstone facies. However, significant karst development also extends into the western portion of the San Andres in Yates Field (Fig. VII.5d), specifically into the region where the San Andres Formation is dominated by dolomitized mudstone and dolomitized wackestone facies. While karst development does appear to be most dense in the dolomitized grain-rich carbonate depositional facies, it does extend significantly into dolomitized, grain-poor carbonate depositional facies suggesting that karst development is not facies limited. Karsting is also observed less frequently in the superjacent Grayburg, Queen and Seven Rivers.

Karst development based on log analyses is normally distributed (Fig. VII.7) with maximum karst porosity at an elevation of approximately 1200 feet (366 m) above sea level (asl), which tapers off rapidly above 1300 feet asl (396 m) and below 1100 feet abs (335 m). Therefore, spatial analyses of karst distribution were conducted by looking at 4 intervals relative to modern sea level. Below 1100 feet abs (335 m) (Fig. VII.8a) karst development is highly clustered and does not show any distinct relationship to the structure or lithologic facies of the Yates Field area, but instead suggests that dissolution was focused at several distinct locations. From 1100 to 1200 feet abs (335 to 366 m) (Fig. VII.8b) karst development is widespread throughout the entire Yates Field with a distinct shift in greater abundance towards the northeastern portion of the field, suggesting higher abundance of grain-rich grained depositional facies; however, significant karst development is observed extending into grain-poor depositional facies towards the west. From 1200 to 1300 feet abs (366 to 396 m) (Fig. VII.8c) karst development tends to concentrate on the structural high of the Yates Field; however, a significant cluster of karst development still persists in westside Yates Field. Above 1300 feet abs (396 m) (Fig. VII.8d), karst development is primarily concentrated on the structural high of the Yates Field while less developed clusters of karst development remain around the periphery. The distribution of zones of cavernous porosity in relation to current elevation, suggests that karst development is not limited to packstone and grainstone facies of the Yates Field. Although the more permeable San Andres units of eastside Yates Field do appear to promote greater karst development, significant karst development does extend well into westside Yates Field. At elevations above 1100 feet abs (335 m) above sea

level, karst development appears to be strongly related to the structure of the Yates Field (Fig. VII.8).

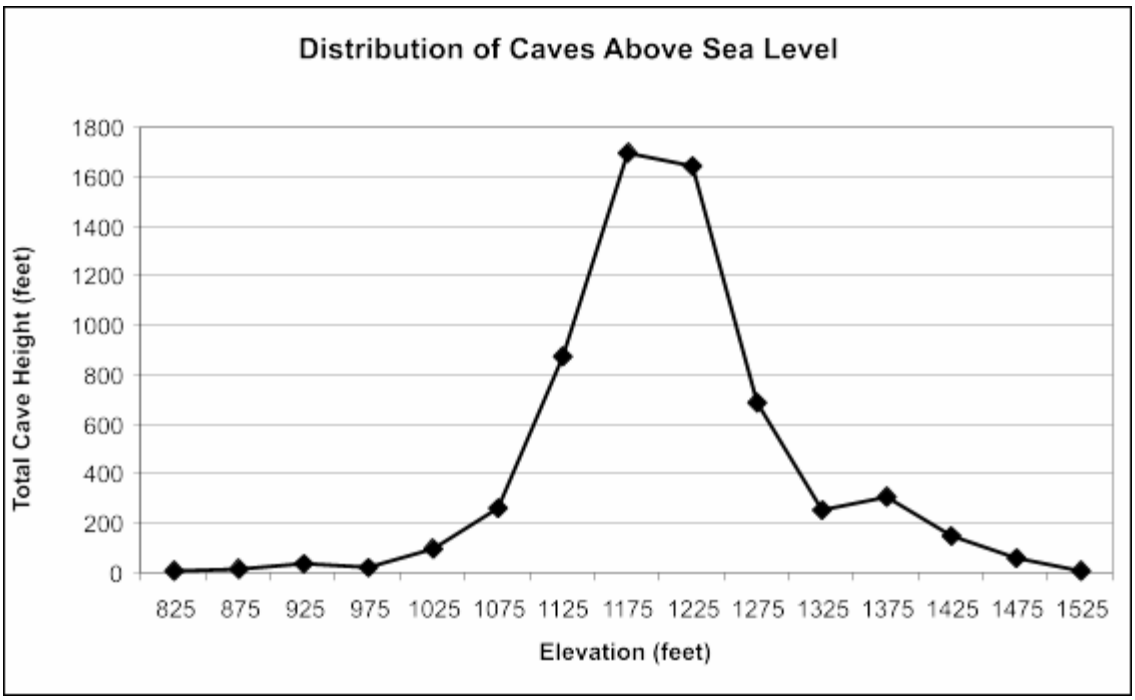

Fig. VII.7: Cavernous porosity within the Yates Field in relation to elevation shows a normal distribution with maximum development at approximately 1200 feet (366 m) asl.

While the greatest karst development within the Yates Field appears centered around the structural crest of the area (Fig. VII.8), the lateral shift towards the northeast is coincident with the location of the Toborg Field (Fig. VII.2). The Toborg Field is developed in Triassic sands and gravels and karstic Cretaceous carbonates (Fig. VII.3), generally from depths of 200 to 600 feet (61 to 183 m) (Franklin, 1966). While some of the oil in the Toborg Field has been shown to be associated with poor, nonstandard casing practices during the early development of the Yates Field long before unitization (Marathon, 1973), oil was observed seeping from surface exposures of Cenozoic sands

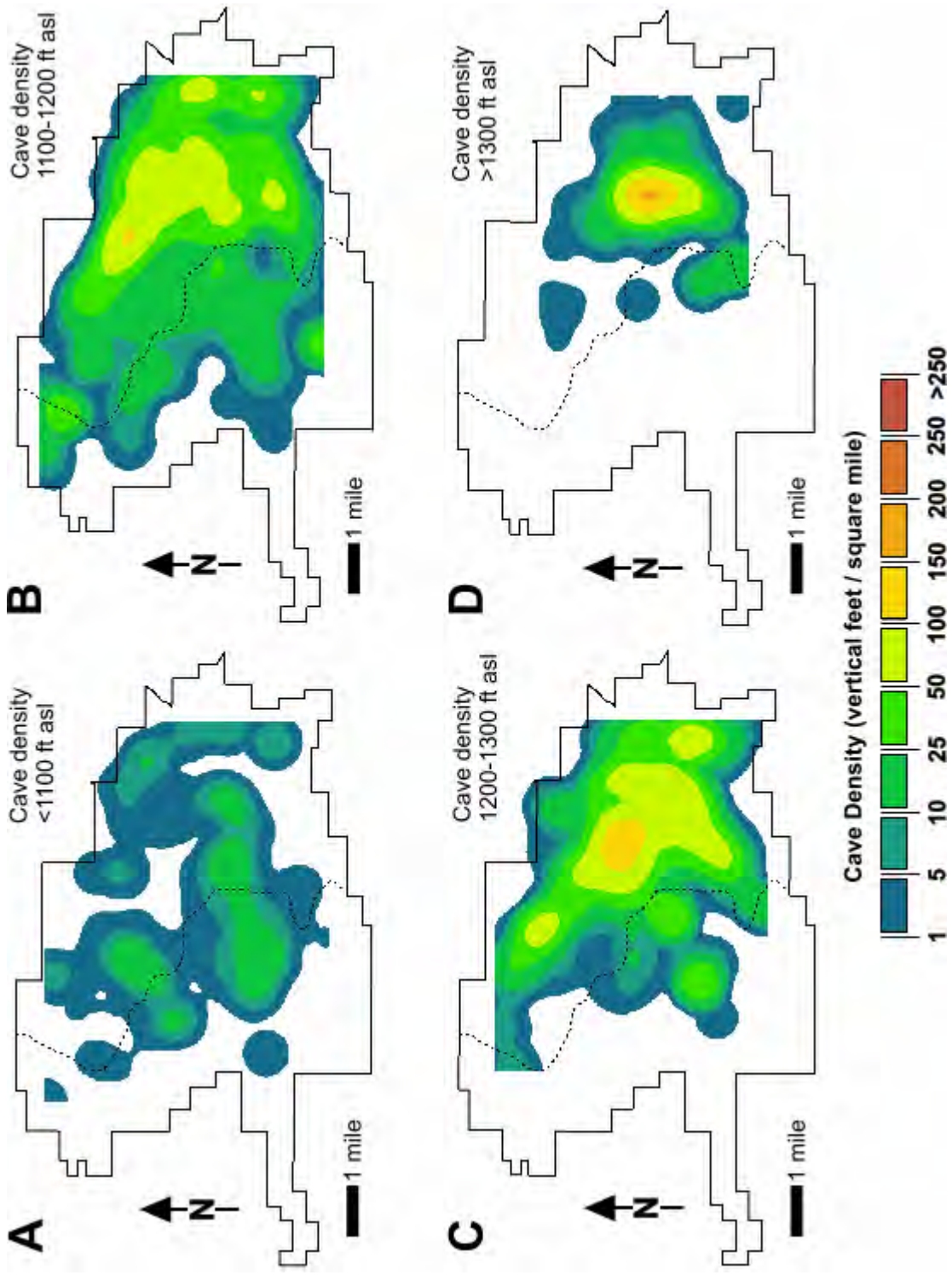

Fig. VII.8: Spatial distribution of Yates Field karst development in relation to sea level. a) karst density of features less than 1100 feet (335 m) asl; b) karst density of features between 1100 and 1200 feet (335 to 366 m) asl; c) karst density of features between 1200 and 1300 feet (366 to 396 m) asl; d) karst density of features above 1300 feet (396 m) asl.

into the Pecos River prior to development of the Yates Field (Franklin, 1966). The Toborg Field has since been shown to contain both indigenous oil and oil derived from the Yates Field (Marathon, 1973). While the Triassic siliciclastics of the Toborg reservoir do not contain karst development, cavernous porosity does exist within the Cretaceous carbonate rocks. Because the location of the Toborg Field overlaps both the northeastern margin of the Yates Field and the Pecos River, it is likely that the hydraulic potential created by the persistent down cutting of the Pecos River at this location (Fig. VII.2) since the early Tertiary has forced fluid migration and resulting reservoir development towards the northeastern margin of the Yates Field.

Yates Field: Secondary Mineralization

Over 22,000 feet (6,710 m) of conventional core have been collected within the Yates Field from 149 wells. Many of these cores provide lithologic evidence indicative of speleogenetic evolution of the San Andres and overlying Guadalupian strata. . Lithologic karst features include brecciation, void-filling clastic sediments, banded dolomite, and calcite spar lining pores, as well as unique mineralogies including zones of uranium enrichment. The carbonate sequences of the Yates Field were deposited as limestone facies that underwent multiple periods of dolomitization so that original limestone depositional fabrics often are not preserved by the sucrosic dolomite (Tinker and Mruk, 1995). Dolomitization is believed to have occurred widely in the subsurface of the Central Basin Platform through brine reflux of hypersaline, Guadalupian fluids (Leary and Vogt, 1986), most likely derived from compaction and dewatering during early burial.

Vuggy to cavernous porosity and solutionally enlarged fractures appear to be largely diagenetically related, attributable to karst processes, and have been correlated to lineament trends with the Yates Field area. Craig (1988) and Tinker and Mruk (1995) stated that karst porosity is developed along two dominant fracture orientations based on lineaments observed within the Yates Field and fluid-production trends. Although some variability exists within reported lineament orientations, interpreted fractures are oriented primarily at N50°W and N40°E within the Guadalupian units of the Yates Field, which corresponds well with deformation associated with Laramide compression and Basin and Range extension that have been well-documented in the Trans-Pecos region (Horak, 1985).

Karstic porosity commonly contains multiple generations of secondary infilling and cementation. While individual solutional features within the San Andres Formation contain varying degrees of secondary deposits, the most diagenetically complex solutional features contain fine-grained, clastic sediments that are covered by banded, dolomite with the remaining pore space filled by sparry calcite (Fig. VII.9). The fine-grained, clastic sediments lining and filling karst porosity are primarily dolomitic silt and mud with a small component of quartz silt and clay (Fig. VII.10a,b) (Craig et al., 1986). When found near the Grayburg contact, clastic sediments in the San Andres Formation are composed of clasts and quartz silt that have migrated downward along vertical solution enlarged fractures (Fig. VII.10d) (Craig, 1988; Tinker and Mruk, 1995). While this has been reported to be evidence of subaerial exposure of the San Andres Formation prior to Grayburg deposition (Craig, 1988; Tinker et al., 1995), no paleosols have been documented at the formational boundary to provide unequivocal proof of exposure, nor as

infiltrated terra rosa sediment within developed karst features below the contact as is common in other karsted terrains (Central Basin Platform, North Cowden Field; Northwestern Shelf, Dollarhide Field (Fusselman and Montoya formations); Ellenburger in various fields on Northwest Shelf, Central Basin Platform and Val Verde Basin, Behnken, personal communication, 2007). The Grayburg clasts may simply be the result of intrastratal piping of residual Grayburg strata along karst conduits into the underlying San Andres Formation.

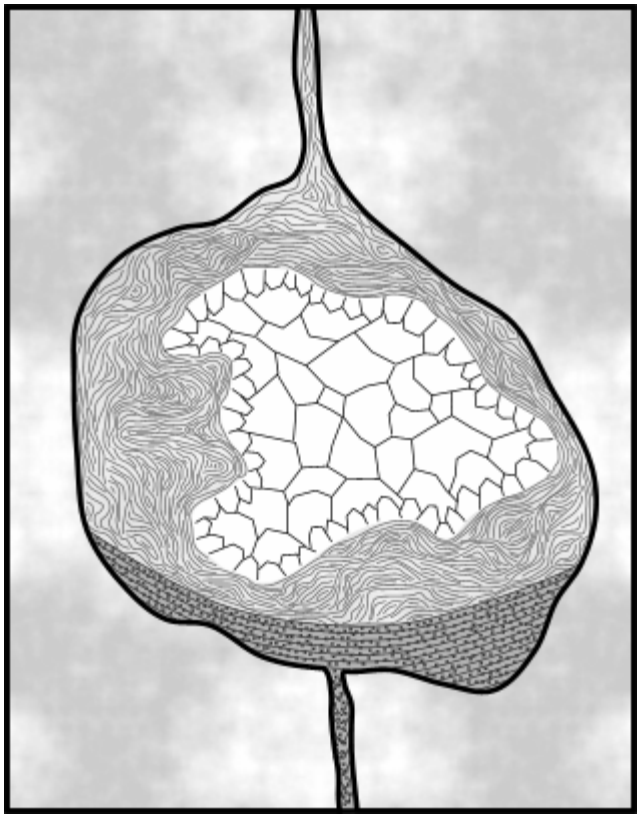

Fig. VII.9: Conceptual diagram showing the complex diagenesis associated with hypogene speleogenesis in the Yates Field, including vug development along a fracture (outlined in dark black), laminated clastic sedimentation (dark gray), banded dolomite (light gray) and calcite spar (white). Vugs, solutional fractures and caves within the Yates field commonly show one or more of the secondary deposits depicted in the figure. Conceptual diagram is approximately 1 inch (3.28 cm) wide.

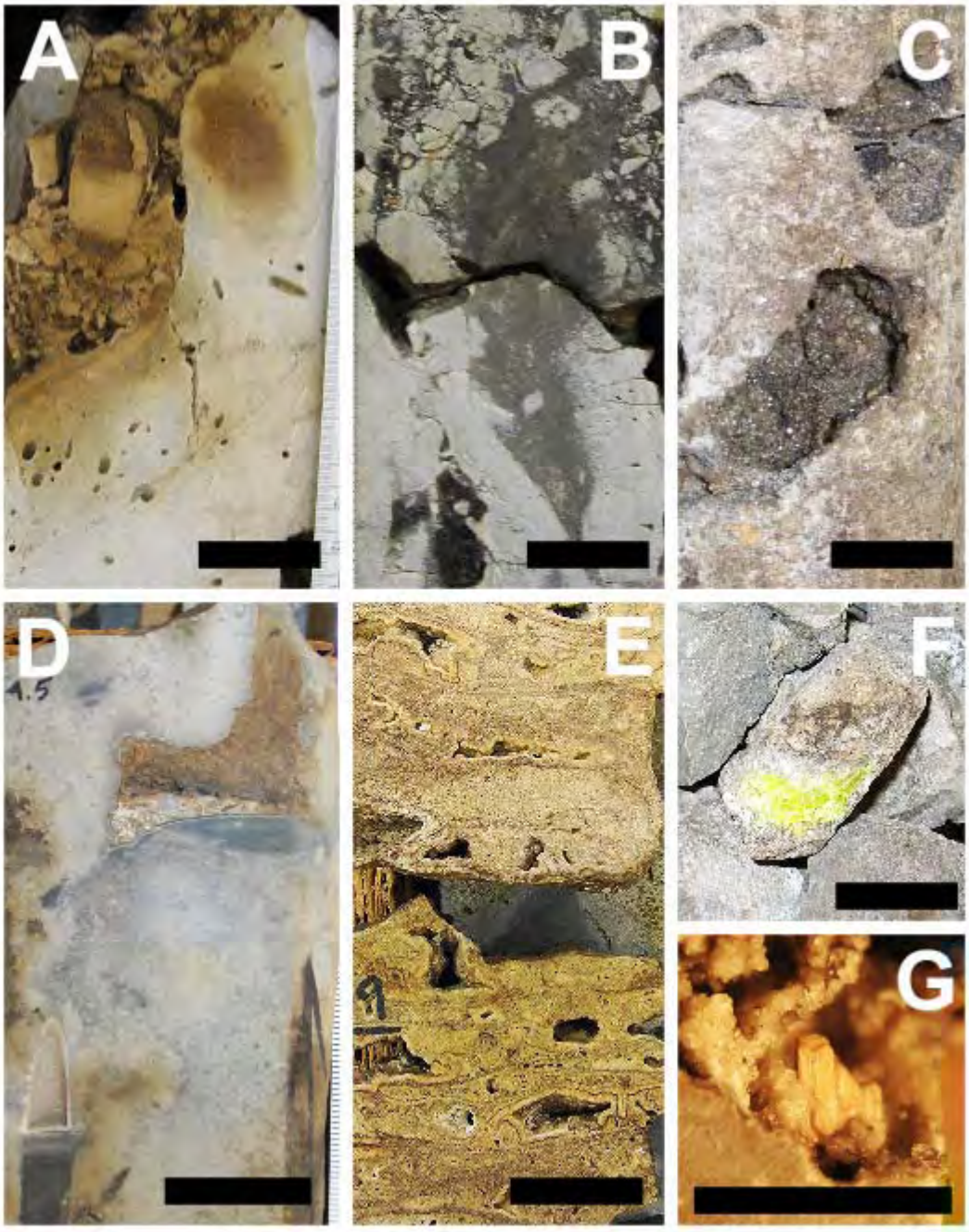

Fig. VII.10: Slabs of the San Andres Formation with direct evidence of karst development within the Yates Field. Black scale bars are 1 inch (3.28 cm) long. a) solutional void with intrastratal breccia showing significant oil staining within void fill and in the rock adjacent to the solutional void; b) typical reservoir breccia showing significant clast rotation and infilling with silt-sized residual grains; c) typical vugs with calcite spar lining; d) solutional voids with gravitational deposition of fine-grained residual clasts; e) banded dolomite fill within cored rubble zone which was interpreted by Tinker and Mruk (1995) as cave pearls; f) native sulfur within cored rubble zone; and g) diagenetic albite and calcite spar lining solutional vug.

While clastic sediments often preferentially fill the bottom of solutional features as result of gravity driven sedimentation, banded dolomite deposits generally coat the entire surface of vugs, caves and solutional fractures or entirely fill these solutional features (Fig. VII.10e) in the Yates Field, indicating that they were deposited subaqueously (Hill and Forti, 1997). Tinker et al. (1995) reported that cave pearls (Fig. VII.10e) were present as vug-filling structures within the San Andres Formation, which implies that speleothem deposition was subaqueous; however, review of the features previously identified as cave pearls found that these features do not exhibit the concentric, spheroidal morphology of true cave pearls (Hill and Forti, 1997). Instead, the structures identified as "cave pearls" are regions of extensive subaqueous speleothems deposition where the original solutional void is morphologically complex containing abundant matrix pendants (Fig. VII.10e). During this study, abundant subaqueous speleothem-like deposits were observed in cores; however, no banded secondary mineral deposits exhibited morphologies indicative of subaerial deposition. Similar to the banded dolomite that commonly lines the surface solutional features, calcite spar is frequently found either lining or completely filling vugs (Fig. VII.10c,g) and solutionally enlarged fractures within the Yates Field. Although the San Andres Formation is largely dolomitized, calcitic cement and spar are often disseminated throughout significant portions of the core representing a late generation of fluid migration and speleogenesis within the Yates Field (Leary and Vogt, 1986).

In addition to sediment fills, banded dolomite and calcite spar observed in association with solutional voids, several less common secondary minerals have been documented in cores. Native sulfur crystals over one centimeter in diameter have been found within cored rubble zones (Fig. VII.10f), suggesting sulfur mineralization within cavernous

voids, which is often associated with hypogenic, sulfuric-acid speleogenesis (Hill, 1990). Diagenetic albite crystals (Fig. VII.10g) over one centimeter in diameter along with calcite spar occur as partial vug-filling minerals in at least one section of core within the Yates Field. Pyrite and associated oxidation halos are commonly found in the dolomudstone facies with associated small-scale vuggy porosity. Rare occurrences of metal sulfides (e.g. galena and sphalerite) have also been reported from core in deeper wells within the study area (Mike Uland, 2006, personal communication), but no such occurrences were found in this study.

In order to evaluate the diagenetic relationship between dolomitized host rock, banded dolomite speleothems and calcite spar, isotopic analyses were conducted during this study on core samples from the San Andres Formation, which were compared with isotopic values for secondary calcite spar reported by Tinker and Mruk (1995). A total of 20 samples were collected from 9 different core locations. Two core sample locations contained banded dolomite, calcite spar and associated proximal host rock samples, while an additional four samples of calcite spar and three samples of banded dolomite were sampled with corresponding bedrock at other core locations. Samples were powdered and hydrocarbon staining grain surfaces were removed in solution using ethanol, in order to ensure isotopic analyses of bedrock and secondary deposits and not analyses of the hydrocarbons which coat the grains. Comparison of δ13C (PDB) and δ18O (PDB) indicates that the fluids associated with deposition of banded dolomite, calcite spar and original dolomitization of the host rock are all significantly different (Fig. VII.11). The isotopic values for San Andres bedrock samples are similar to dolomitization by brine reflux reported by Leary and Vogt (1986) for other portions of the San Andres Formation

within the Central Basin Platform. The isotopic values for calcite spar (Fig. VII.11) occur across a broad range of δ13C values, which places them in a transitional phase between thermal spar and hypogene spar formed through methane oxidation (Palmer, 2007). The banded dolomite speleothems have δ18O values similar to the dolomite host rock, but are significantly depleted with respect to δ13C (Fig. VII.11). This suggests that the speleothems are associated with the dissolution of the host rock and subsequent precipitation in the presence of light organic compounds, most likely hydrocarbons.

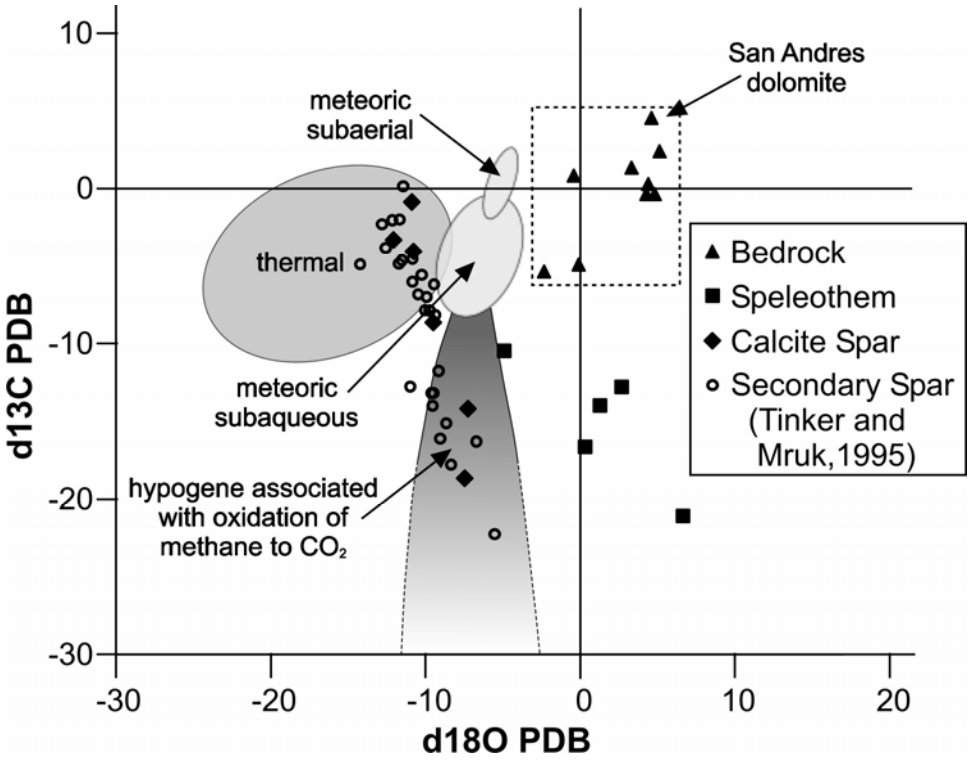

Fig. VII.11: δ13C (PDB) and δ18O (PDB) isotopic analyses of dolomite bedrock, banded dolomite "speleothems", calcite spar and secondary calcite spar reported by Tinker and Mruk (1995). Note that no secondary mineralization falls within the range of meteoric mineralization. Shaded regions represent secondary carbonate mineralization associated with speleogenesis as defined by Palmer (2007).

While solutional porosity and secondary mineralization occur throughout the Yates Field, zones of brecciation are extremely common (Fig. VII.10b) (Tinker and Mruk, 1995). Based on the classification of Kerans (1993), three types of brecciation occur in the Guadalupian strata of the Yates Field: 1) chaotic breccia; 2) mosaic breccia; and 3) fracture breccia. Brecciation within the Yates Field generally forms vertically transmissive structures that exhibit the classic pattern of a basal chaotic breccia often comprised of polymictic clast types with significant clast rotation which grades into a mosaic breccia with minor clast rotation that ultimately grades into a fracture breccia that is highly fractured with no significant clast rotation. This classic brecciation sequence has resulted from collapse of overlying strata into cavernous porosity within the solutionally enhanced horizons of the Yates Field (Fig. VII.12a). Although collapse of cavernous porosity can be induced by tectonics or increased overburden pressure, there are two primary mechanisms that form karstic brecciation. In epigenic and eogenetic settings, cavern collapse results from the lowering water tables and the associated loss of buoyant support, where the unsupported ceiling exceeds the tensile strength of the ceiling bedrock (Palmer, 2007). In hypogene settings, cavern collapse results from the continued dissolution along a soluble zone until the amount of rock removed exceeds the structural strength of overlying bedrock (Klimchouk, 2007).

Many features identified as “pits” within the San Andres Formation of the Yates field appear to be vertical, breccia pipes. These features can be traced through the San Andres, Grayburg, Queen and Seven Rivers Formations (Fig. VII.12a), indicating that the collapse features must post date Permian deposition. While uranium enrichment has been identified throughout the Yates Field, many of these breccia pipes exhibit the highest

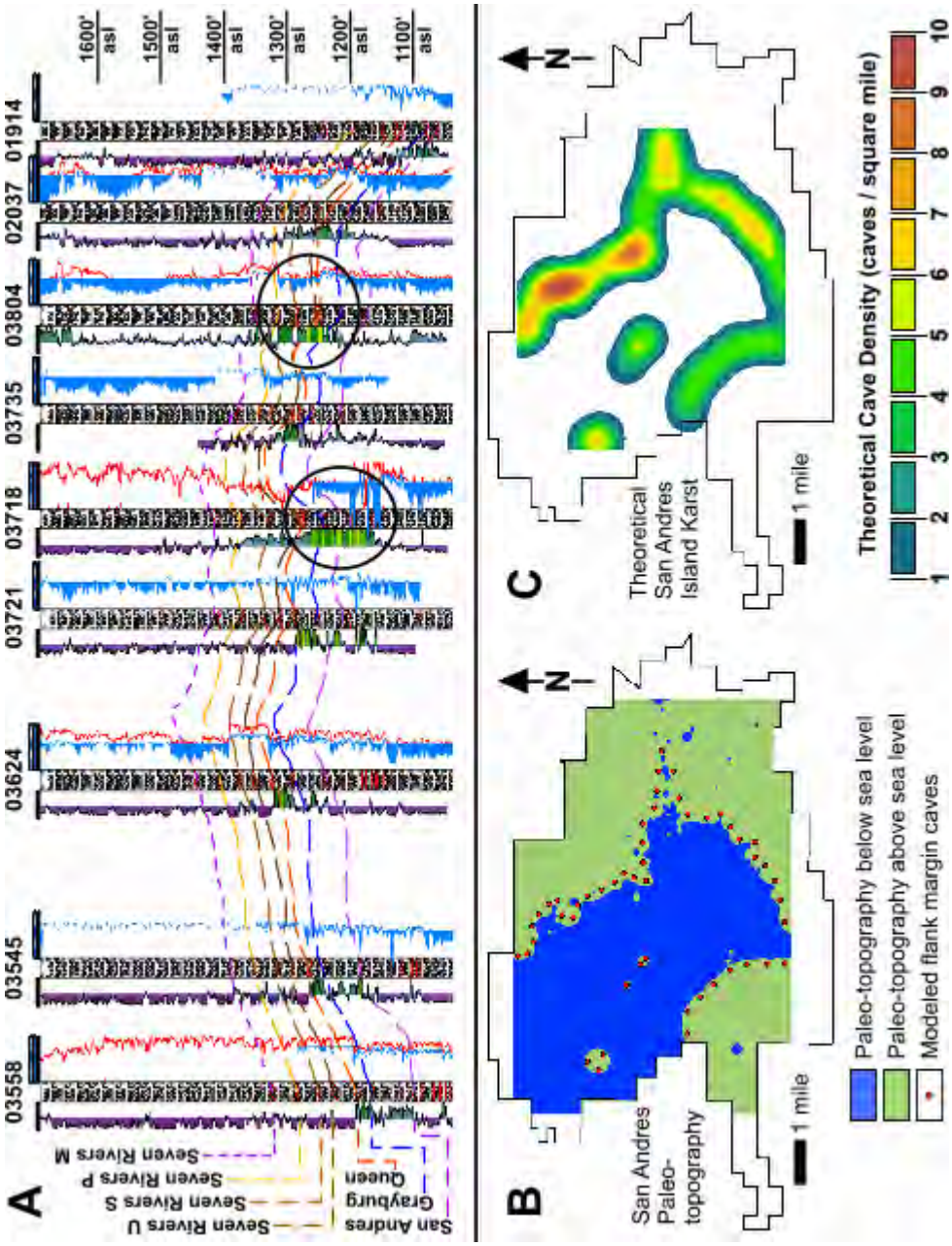

Fig. VII.12: Yates Field karst development. a) stratigraphic section through the Yates field showing formation tops identified through log analyses, including Gamma Ray (left side of individual well plots) and density logs (right side of individual well plots). Circled regions contain significant uranium enrichment (high GR) along vertical collapse structures; b) paleotopography reconstruction of the San Andres Formation based on a depth of 200 feet (61m) below the Seven Rivers "M" horizon; c) theoretical flank margin cave distribution modeled for subaerial exposure at a depth of 200 feet (61 m) below the Seven Rivers "M" horizon. Black dots represent individual flank margin caves evenly spaced along the paleocoastline for cave distribution modeling.

levels of enrichment observed on gamma ray logs within the region (Fig. VII.12a). This suggests that the same uranium-rich fluids that diagenetically altered the bedrock are likely the same fluids that facilitated or at least enhanced the development of these vertical, cross-formational collapsed breccia structures. The uranium enrichment …. Dana – can your fill in a few details on the uranium stuff you worked on.

SPELEOGENETIC MODELS FOR THE YATES FIELD

Karst science has made significant advances in recent decades towards understanding and characterizing speleogenetic processes with significant applications for reservoir characterization. Therefore, it is essential that old theories of karst porosity characterization be re-evaluated with respect to new advances in karst science in order to confirm existing theories or propose new ones such that petroleum reservoir management practices can be optimized. This is especially true for mature fields that are utilizing enhanced oil recovery techniques where proper characterization of reservoir heterogeneity may mean the difference for extending profitable production. In the sections below, past and current theories of Yates Field speleogenesis are outlined, with reference to specific characteristics of the Yates Field that support each interpretation. Following the convention of Craig (1988) and Tinker et al. (1995) caves are defined as voids greater than one foot (39 cm) in height or similar zones with bulk densities less than 1.75 gm/cm^3 which indicate significant porosity.

Island Karst Model: 20th Century Theory of Yates Field Speleogenesis

Extensive cavernous porosity has been recognized in the Yates Field since the early 20th century when the first wells were drilled, which experienced bit drops and yielded sustained high flow rates up to 200,000 bopd (Hennen and Metcalf, 1929). However, the first attempts to characterize the distribution and origin of cavernous porosity were conducted by Craig (1988) in the late 20th century, which was later expanded by Tinker et al. (1995). Their work on the speleogenesis of the Yates Field represented a crucial step forward in detailed karst reservoir characterization throughout the petroleum industry by attempting to evaluate karst porosity development and distribution more accurately for improved recovery and reservoir management practices, instead of treating fields as simple statistical plays where a specific percentage of wells drilled are expected to produce from porous, transmissive zones based on past drilling.

Craig (1998, 1990) proposed that the karst porosity of the Yates Field represented paleokarst that was developed as eogenetic, island karst during and / or immediately subsequent to the deposition of the San Andres Formation. While, Craig (1988) reported primarily on the extensive karst development within the San Andres Formation of the Yates Field, he also acknowledged additional karst development in the overlying Queen and Grayburg Formations, indicating that the karsting phenomenon was not limited to the San Andres Formation, but instead was developed throughout Guadalupian strata with features primarily oriented along major fracture sets. Craig (1988) provided several lines of evidence for eogenetic speleogenesis, including lithologic features observed in cores, petrophysical log data and distribution of caves. He reported that cores in the San Andres close to the Grayburg / San Andres contact commonly contain: 1) solutional voids with

complete or partial infilling by secondary, speleothem deposits, 2) solutionally widened fractures; 3) extensive breccia zones; and 4) partial infilling of solutional vugs and fractures by fine-grained clastics similar in composition to the Grayburg Formation. Craig (1988) suggests that these features indicate eogenetic, meteoric dissolution during Guadalupian subaerial exposure. However, as shown in previous sections, all of these features can be derived through other speleogenetic processes.

While the identification of cavernous porosity clearly shows that the Yates Field is a karsted reservoir, alone it does not prove what speleogenetic processes controlled the development of karst porosity. Therefore, Craig (1988) investigated the spatial distribution of cave development within the Yates Field. By using the Seven Rivers M horizon as a paleodatum, he attempted to reconstruct San Andres paleotopography. He restored the Seven Rivers M horizon to a horizontal plane and calculated the distance to underlying formational contacts in order to simulate depositional paleotopography. Using this reconstructed paleotopography, Craig (1988) theorized that a sea-level lowstand 200 feet (61 m) below the Seven Rivers M horizon represented subaerial exposure of a San Andres island complex prior to Grayburg deposition, which produced the extensive karst development observed at this boundary. Following, the work of Craig (1988), we reconstructed this same paleotopography surface 200 feet (61 m) below the Seven Rivers M horizon (Fig. VII.12b), but used the current reservoir database to more accurately define formation boundaries, which includes data collected in the past 20 years since the work of Craig (1988). Because flank margin caves are the dominant type of cave development on modern carbonate islands, we simulated flank margin cave development on this theoretical island complex by evenly spacing simulated caves along the

paleocoastline (Fig. VII.12b). The resulting pattern is shown in the Figure 12c, which indicates that eogenetic karst formed in relation to the interpreted paleotopography would produce a distribution pattern with minimum karst development in the far eastern portion of the Yates field. Yet the data show significant karst development extending into westside San Andres, which does not match Craig's (op. cit) patterns of cave development within the San Andres Formation in Yates Field (Fig. VII.5d; VII.8).

While Craig (1988) established this initial theory of eogenetic speleogenesis for the origin of Yates Field Porosity, Tinker et al. (1995) investigated sequence stratigraphy within the area and identified four prograding sequences. They suggested that each of these depositional sequences was capped by a subaerial exposure event, based on the presence of packstone to grainstone facies at the top of each sequence and more intense karst development along these boundaries. Based on their theory, four episodes of subaerial exposure existed during San Andres deposition as each shoal complex migrated eastward; therefore, three additional zones of island karst should exist beneath and to the west of the island complex that developed at the end of San Andres deposition. This indicates additional island karst should exist west of the theoretical distribution of flank margin caves modeled in Figure VII.12c. However, most of the actual karst development documented in the Yates field occurs to the east of this region.

To further evaluate the theory of eogenetic origins for Yates Field karst we analyzed the distribution of documented caves within the Yates Field relative to the top of the San Andres Formation in comparison to the reconstructed paleotopography of the area at the end of San Andres deposition (Fig. VII.13a). Assuming that the karst formed in relation to subaerial exposure, the distribution of documented karst should mimic the

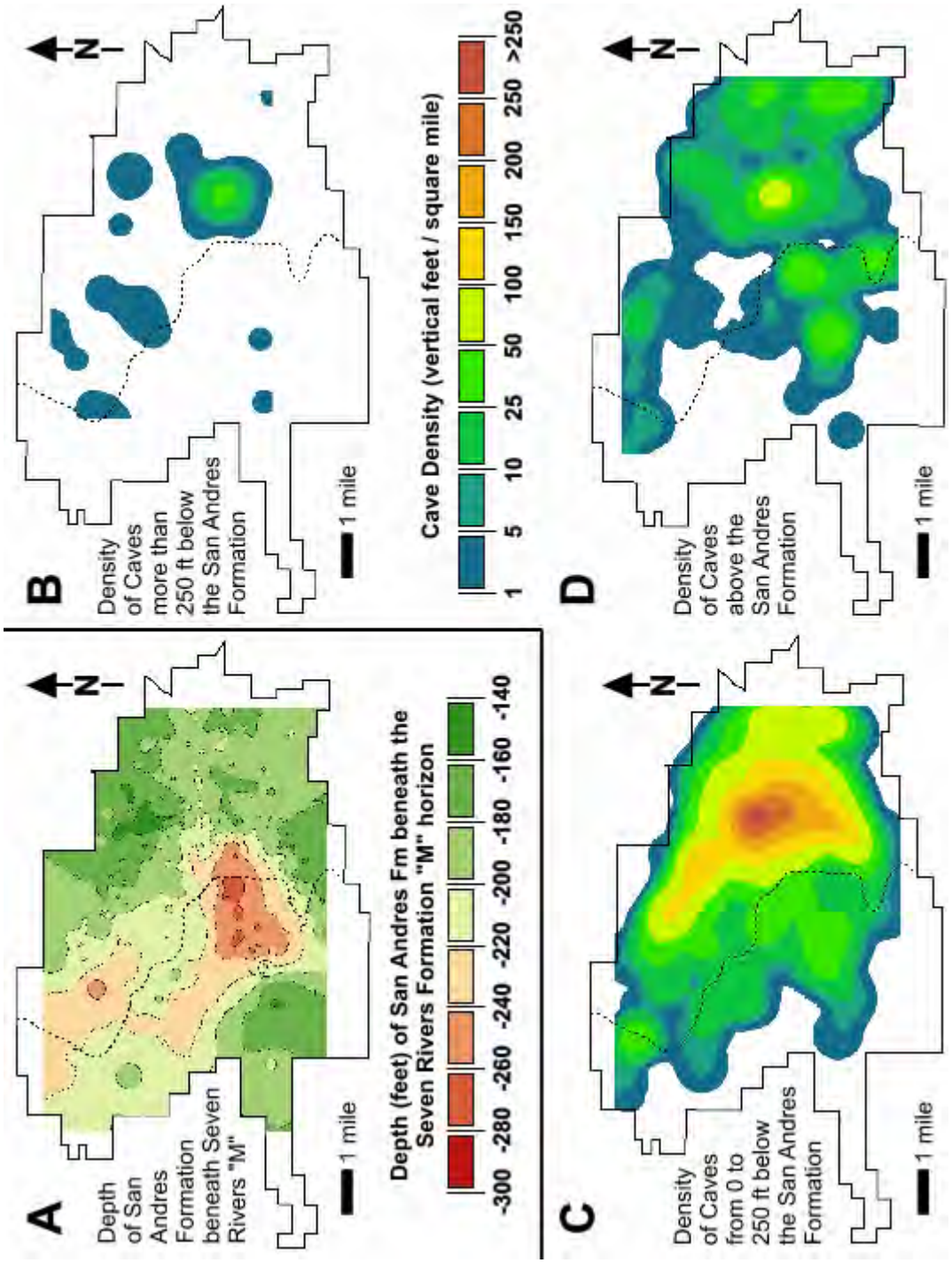

Fig. VII.13: Distribution of documented karst development within the Yates Field in relation to the San Andres / Grayburg contact. a) paleotopography reconstruction of the San Andres Formation with depth relative to the Seven Rivers “M” horizon; b) karst density of features more than 250 feet (76 m) below the formation contact; c) karst density of features up to 250 feet (76 m) below the formation contact; and d) karst density of features above the formation contact.

configuration of reconstructed island complexes. At depths greater than 250 feet (76 m) below the San Andres / Grayburg contact (Fig. VII.13b), several clusters of minor karst development are scattered throughout the Yates Field, with only one region of moderately dense karst development that is centered at the structural crest of the field. From the San Andres / Grayburg contact to a depth of 250 feet (76 m) below it (Fig. VII.13c), documented karst development is widespread, which includes significant karst developed that extends far into the westside Yates Field in what has been interpreted as the deepest portion of an inland lagoon in the paleotopography reconstruction (Tinker et al., 1995). While some of the documented karst development does crudely mimic the theoretical distribution of flank margin caves, the greatest density of karst development occurs along the structural crest of the Yates Field. A significant number of caves have been documented above the San Andres Formation (Fig. VII.12d), primarily in the Grayburg Formation but also the Queen and Seven Rivers Formations, which raises the necessity for other karst development processes or events. The distribution of caves above the San Andres Formation exhibits a highly clustered pattern with a slight shift in karst development towards the northeast, but the greatest density of karst development remains centered on the structural peak of the Yates Field.

While the work of Craig (1988) and Tinker et al. (1995) during the late 20th century was a significant advance in characterization of reservoir karst development using available karst process models, the distribution of cavernous porosity within the Yates Field does not correspond well with reconstructed San Andres islands (Fig. VII.12b,c;13a), which required the development of a fresh-water lens, an essential component of eogenetic, island karst dissolution. The sequence stratigraphy of the San

Andres Formation clearly shows at least four prograding facies suites, with the upper facies composed of a fusilinid / peloidal packstone to grainstone facies. However, this facies package only confirms that deposition occurred in shallow subtidal environments, but no definitive proof of subaerial exposure such as paleosols have been documented within the Yates Field area. nor as infiltrated terra rosa sediment within developed karst features below the contact as is common in other karsted terrains (Central Basin Platform, North Cowden Field; Northwestern Shelf, Dollarhide Field, Fusselman and Montoya formations; Ellenburger in various fields on Northwest Shelf, Central Basin Platform and Val Verde Basin, Behnken, personal communication, 2007).

The lithofacies defined from 118 wells with conventional core in the Yates Field have been compared to those of the Seminole San Andres Field in Andrews County, Texas. The principle reservoir lithofacies in Seminole are fusulinid dolowackestone, fusulinid-peloidal dolopackstone and coated-grain dolograinstone. (Sonnenfeld, et al, 2003; Meng, et al, 2003) The twelve depositional facies identified in the Seminole San Andres were utilized by iReservoirs to characterize core from 118 wells in Yates Field. Their comparison concluded that the Yates core facies demonstrate the absence of island shoal facies during deposition of the San Andres in the structurally high areas of maximum measured cave feet, where emergent island shoal facies should be highest. Their reconstruction takes into account post-depositional erosion and exposure of the San Andres during lowstand. Then islands were clearly present, but they were indurated carbonates. They comment that more grain-rich subtidal carbonate facies were probably concentrated along these deeper subtle highs, not as emergent island shoals. (iReservoir report to Marathon, 2003).

While it is possible that lithologic evidence of subaerial exposure surfaces is simply not preserved within the Yates Field, a definitive statement of Permian subaerial exposure cannot be made in its absence from over 100 conventional cores that penetrated the upper 250 ft of the San Andres Formation. . Because of this lack of definitive proof of subaerial exposure, Craig (1988) and Tinker et al. (1995) made the assumption that the presence of cavernous porosity close to formational contacts provided evidence of subaerial exposure, because their interpretations of karst development forming through eogenetic speleogenesis requires the presence of a freshwater lens. Therefore, through reciprocal reasoning the presence of karst implied that islands must have been subaerially exposed during deposition of the San Andres Formation.

Further complicating the proposed eogenetic speleogenesis model for the Yates Field is the recognition that karst development within the Yates is controlled by orthogonal fracturing within the field (Craig, 1988; Tinker et al., 1995). In modern carbonate island environments, fracturing most commonly occurs as erosion along coastlines creates coastal notches such that bank margin failures occur, thus creating long fractures parallel to coastlines and short fractures perpendicular to coastlines that enable block rotation associated with margin collapse (Stafford et al., 2005). This type of fracturing does not create consistent or coherent orientation of fracture sets throughout an entire island complex, as is observed in the Yates Field. If formed by bank margin failure as the emergent island hypothesis proposes we should see longer fracture sets parallel to the elongate island margins. In addition, bank margin failures generally only occur on steep coastlines developed by marine erosion of well-indurated sediment, none of which have been documented within the Yates Field. On tectonically active modern carbonate

islands, such as the Mariana Islands where basement rocks are volcanic peaks, differential uplift and subsidence has been shown to produce faults which effectively partition the freshwater lens (Stafford et al., 2005); however, this can be ruled out in the Yates Field because the Permian Basin was an enclosed inland basin, not a volcanic arc complex. Because the orthogonal fracturing pattern observed within the Yates Field is similar to that documented the Trans-Pecos region of Texas (Horak, 1985), it seems probable that the Yates Field fractures were also formed by Laramide compression and Basin and Range Extension. Craig (1988, 1998) indicated that tectonically generated fractures were formed by the Marathon-Ouachita compression in the latest Mississippian to lowermost Permian, significantly predating the deposition of the late Permian (Guadalupian) San Andres Formation. These fractures are, however, widely spaced (approximately 1500 ft (457 m). Reactivation and additional fracture stress patterns were introduced during Laramide and Basin and Range tectonism. Therefore, if karst development is focused along these fractures, then speleogenesis must postdate Laramide tectonism and could not have formed contemporaneous with San Andres deposition.

Hypogenic Karst Model: 21st Century Theory of Yates Field Speleogenesis

The Guadalupian strata of the Yates Field area have a stratigraphic cap of a late Permian (late Guadalupian) evaporites of the Seven Rivers Formation (i.e anhydrite) (Fig. VII.3), which provide a seal for the trapping and overpressure of the Yates Field reservoir, as evidenced by free-flowing wells early in the production history (Levine et al., 2002). There is no evidence that the Guadalupian strata have been exposed to epigene speleogenesis, because thick sequences of younger Ochoan evaporite rocks (e.g. Salado

and Rustler Formations) persist throughout the region (Wessel, 1988). Epigene speleogenesis requires that rocks be diagenetically mature and then exposed to the affects of near-surface, meteoric process as they are returned to the earth surface through tectonism and surface denudation (Ford and Williams, 2007; Palmer, 2007). Therefore, we would expect to see extensive karsting in the overlying evaporite sequences had the Guadalupian strata experienced a period of epigene speleogenesis. Although the Seven Rivers and younger Ochoan evaporites likely form a leaky seal within the Yates Field, epigene karsting in these rocks would have created significant cross formational flow paths between underlying reservoir host rock and overlying Triassic sands. This would have prevented the trapping and development of high reservoir pressure observed within the Yates Field, hence, we can rule out the possibility of karst development within the Yates Field by epigene processes. Therefore, hypogene speleogenetic origins remain as the only other alternative to syngenetic / eogenetic speleogenesis for creating karst porosity within the Yates Field.

As shown in the previous section, karst features observed in core samples and the distribution of documented caves within the Yates Field do not correspond well with patterns that have been documented in modern, eogenetic karst environments such as the Bahamas or Mariana Islands (e.g. Mylroie et al., 1995; Jenson et al., 2006). The internal sequence stratigraphy of the San Andres Formation clearly shows at least four prograding shoal sequences within the Yates Field (Tinker and Mruk, 1995); however, no cores have been drilled within the Yates Field that provide unequivocal proof that these shoals were subaerially exposed. It is obvious based on the presence of packstone to grain rich fusulinid-crinoid packstone and rare grainstone facies that the upper portions of each

shoal sequence were deposited within high-energy subtidal environments, but no paleosols or zones of complex paleo-epikarst have been documented which would definitively prove that San Andres island complexes were subaerially exposed. Small, but emergent islands form identified island complexes within the Leonardian Clearfork carbonates of the North Robertson Unit (Gaines County, TX, northern extent of the Central Basin Platform). These island deposits are characterized by adjacent lagoonal lime mudstones with intensive burrows. The emergent lithofacies contain root casts, paleosols, even thin (1-2 cm thick) coal seams with obvious terrestrial plant impressions in the lower energy dolomudstone lithofacies (DiMichelle, et al., 2000; Behnken, 2007, personal communication). While the development of paleosols are not required during subaerial exposure, the absence of definitive evidence of terrestrial exposure surfaces makes it impossible to clearly state that exposed islands existed during San Andres deposition. We must remember that coeval supratidal to intertidal environments could be present to the west of the Yates Field and the interior of the Central Basin Platform. Occasionally coaly fragments of vascular plants have been noted in very isolated instances in San Andres conventional core on the far southwest corner of the field in Tract. Based on sequence stratigraphy and lithology within the San Andres Formation, we can only state that deposition of the main reservoir lithofacies occurred within a high-energy, subtidal environment.

Craig (1988) and Tinker et al. (1995) both report more karst development in grain-rich facies of eastside Yates Field, which they imply represents an emergent island/shoal with the subsequent manifestation of a freshwater lens during San Andres time. The presence of greater karst development within these regions only shows that there was

preferential karst development within certain facies and that bedrock heterogeneity controlled the distribution of secondary porosity development. In hypogene settings, bedrock heterogeneity often results in complex three dimensional maze caves where all permeability differences are exploited equally in a confined system (Klimchouk, 2007). Because grain-rich carbonate facies are initially more permeable, intrastratal flow will be focused through these regions and dissolution is enhanced at permeability boundaries of different lithologies. In depositional packages like prograding shoal sequences of the San Andres Formation, hypogene speleogenesis is expected to form the greatest cavernous porosity at cycle boundaries where upward fluid migration is deflected laterally at the permeability boundary between more permeable, grain-rich or coarsely crystalline facies and less permeable, mud-rich, grain poor or finely crystalline facies. We also expect to see greater hypogene dissolution along formational boundaries, which would account for greater karst development along the San Andres / Grayburg contact. Similarly, focused dissolution along this boundary would result in the gravitational infiltration of clasts and residual quartz from the overlying Grayburg Formation into hypogene voids within the underlying San Andres Formation. Although, karstic brecciation can occur during any phase of speleogenesis, the most common and widespread occurrences of karstic brecciation have been associated with intrastratal dissolution of bedrock through hypogene speleogenesis (Klimchouk, 2007). Therefore, extensive brecciation within the Yates Field, greater solutional porosity development at lithologic boundaries and the introduction of overlying solutional clasts and residual grains into underlying solutional voids are all consistent features observed in hypogene speleogenetic systems.

One of the most compelling lines of evidence against the widespread development of eogenetic island karst within the Yates Field was provided by Craig (1988) and Tinker et al. (1995). They clearly documented that karst development within the Yates Field is developed along two primary fracture orientations, N50°W and N40°E. On modern carbonate islands fracturing is most often attributed to bank margin failures on steep coastlines (Stafford et al., 2005), which have not been interpreted in the Yates Field, or on carbonate islands formed on the tops of active volcanic peaks (Jenson et al., 2006), which never existed on the Central Basin Platform. Instead, the fracture pattern within the Yates Field mimics similar fracture patterns documented within the Trans-Pecos region that formed as a result of Laramide compression and Basin and Range extension (Horak, 1985). Passage orientations of regional hypogene caves (e.g. Amazing Maze Cave) show similar patterns of fracture control, indicating that patterns of hypogene dissolution in the Permian Basin are controlled by regional tectonism. Therefore, if karst development is focused along tectonic fractures formed during the Mesozoic and Cenozoic, then karst development clearly could not have formed contemporaneous to San Andres deposition and must at least post date the initiation of Laramide tectonism, implying that fracture dissolution is attributable to hypogene processes.

The presence of secondary mineralization also suggests that reservoir speleogenesis was driven by hypogene processes. No speleothem-like, banded dolomite deposits in the San Andres Formation exhibit morphologies indicative of deposition within air-filled / subaerial voids. Instead, these “cave formations” all exhibit morphologies that were consistent with those formed in water-filled / subaqueous environments (Hill and Forti, 1997). While “cave formation” morphology cannot be used to determine if the

"speleothems" were formed through eogenetic, hypogenic or epigenic speleogenesis, isotopic analyses of these deposits decisively demonstrates that it was impossible to have formed them by normal meteoric waters (Fig. VII.11). Therefore, if the speleothems were not formed by meteoric waters, then they could not have formed through eogenetic or epigenetic speleogenesis and must be the result of hypogene processes. Additionally, calcite spar found lining and/or filling many caves and vugs and greater uranium enrichment along vertical collapse structures suggest that a later stage of hypogene speleogenesis involving hydrothermal fluids occurred throughout the Yates Field area, which probable relates to the other unique minerals also seen within Yates Field core samples, such as diagenetic albite, galena, sphalerite and sulfur.

Because significant advances have been made in karst science and the identification of speleogenetic processes in recent decades (e.g. Ford and Williams, 2007; Klimchouk, 2007; Palmer, 2007), it is possible to re-interpret the origin of karst porosity in the Yates Field. While Craig (1988) and Tinker et al. (1995) provided an intriguing conceptual eogenetic karst model for porosity development within the Yates Field using karst models proposed and available at that time, their observations provided the basis for reinterpreting the Yates Field reservoir. Their recognition of solutional development focused along lithologic heterogeneities and orthogonal fracture patterns clearly identifies a system that is optimum for hypogene karst development. The presence of intrastratal sediments and subaqueous, non-meteoric mineral deposits only further confirms the dominance of hypogene processes. Therefore, we propose that the majority, if not all, of the cavernous porosity within the Yates Field is the result of confined dissolution driven

by hypogene speleogenesis, including the development of a new conceptual model, outlined below, for the Yates Field karst reservoir.

The Guadalupian strata of the Yates Field was deposited as high-energy subtidal deposits with minimal or no subaerial exposure, which did not enable the development of freshwater lenses capable of producing significant eogenetic cavernous porosity. Throughout the remaining Permian, diagenesis of Guadalupian strata was dominated by burial compaction and cementation associated with dewatering and subsidence as overlying strata were deposited. During this time, much of the Guadalupian strata were dolomitized through brine reflux processes and it is likely that some vuggy porosity was created through the formation of anhydrite nodules similar to that observed other portions of the Delaware Basin (Scholle et al., 1992).

Starting in the late Cretaceous, Laramide compression followed by Basin and Range extension created orthogonal fracturing within the Yates Field area, establishing preferential flow paths for vertical migration of hypogene fluids as evidenced by patterns of karst development. As hypogene fluids migrated vertically along fractures created by tectonism, flow extended laterally along lithologic boundaries resulting in increased dissolution at sequence and formational contacts. The greatest hypogene dissolution occurred along the crest of the Yates field as flow was focused not only along lithologic boundaries but also along the axis and peak of the anticline. It is likely that this initial episode of hypogene dissolution was the most intense as deeper basinal fluids were delivered to the Yates Field along vertical flow paths, creating much of the karstic porosity with contemporaneous introduction of clasts and residual grains from overlying strata into cavernous porosity developing in the San Andres Formation. Entrenchment of

the Pecos River along the northeastern edge of the Yates Field coupled with increased geothermal gradients associated with the initiation of Basin and Range extension provided the hydrodynamic activation of the hypogene speleogenesis within the Yates Field area. While fluid agressivity during this time was likely driven by a combination of hydrothermal and sulfuric acid rich fluids, which established steep density gradients for enhanced free convection dissolution. The deposition of banded dolomite within vugs, caves and solutionally enlarged fractures is likely contemporaneous with or immediately subsequent to this initial stage of intense hypogene dissolution, as hypogene fluids became saturated within the confined system.

As geothermal gradients in the region increased during Basin and Range extension, a second generation of hypogene speleogenesis resulted in solutional porosity enhancement, deposition of calcite spar and uranium enrichment, which have been interpreted as deposits formed in a mixed chemistry system containing both thermal and hydrocarbon-rich fluids. The dissolution of dolomite by rising, undersaturated, hypogene fluids would provide free cations of Ca^{++}, Mg^{++} and the anion HCO_3^-. As the waters cooled, they would then descend as part of a convection cell. The cooling and descending fluids could deposit the calcite as the relative concentrations rose as temperature declined. Descending plumes of hypogene fluids could deposit calcite spar relatively uniformly across a broad area of the San Andres and over considerable vertical ranges. The changes in calcite precipitation amounts reflected the vertical fluid changes in temperature and relative concentration. The presence of pore-filling calcite occluding reservoir permeability was noted by Tinker and Mruk (1995). The identification of native sulfur and calcite spar with an isotopic signature indicative of fluids enriched in carbon

dioxide from the oxidation of methane, suggests that this thermal phase of dissolution likely contained a sulfuric-acid component and may be associated with initial hydrocarbon maturation and emplacement with the Yates Field reservoir.

Ultimately, the general northeastward migration of hypogene porosity development with decreasing depth is probably the result of regional hydrologic potential created by persistent down cutting of the Pecos River at the same location on the northeastern margin of the Yates Field since the early Tertiary. While little data is available for characterizing the karst development within the strata overlying Guadalupian rocks of the Yates Field, development of karst porosity in the Toborg Field, as well as surface-breached, inactive hypogene caves (e.g. Ess Cave) within the Yates Field, provide additional support for the importance of Pecos River incision on regional, hypogene karst development.

CONCLUSIONS: Evolution of Speleogenetic Concepts

Karst science has made significant advances in recent decades (Ford and Williams, 2007; Palmer, 2007), specifically in the recognition of hypogene speleogenetic processes (Klimchouk, 2007). While hypogene speleogenetic processes have been long recognized as important in the formation of ore bodies (e.g. Mississippi Valley Type and native sulfur deposits), there has been reluctance in applying hypogene speleogenetic models to the origin of karsted hydrocarbon reservoirs and even humanly explored caves within North America, because of the dominance of karst research on more easily accessible eogenetic and epigenetic caves throughout the 20th century. While the work of Craig (1988), Tinker and Mruk (1995) and Tinker et al. (1995) was a substantial milestone in

the advancement of karst reservoir characterization, recent advances in the understanding of speleogenetic systems has promoted the development of a new conceptual model for the origin of karst porosity within the Yates Field area.

In contrast to the previously proposed eogenetic karst model of the late 20th century, we propose a new, 21st century model of hypogene speleogenesis for the karst development in the Yates Field reservoir. The distinct alignment of porosity development along tectonic fractures, permeability boundaries and the anticlinal crest of the Yates Field area forms classic patterns of three dimensional cavernous systems documented around the world in confined hydrologic systems where hypogene processes dominate. Extensive brecciation, intrastratal transport of residual clasts and sediments, and subaqueous, secondary mineralization with concomitant isotopic studies all provide compelling evidence supporting hypogene karst interpretations. Elevated regional geothermal gradients and the persistent down cutting of the nearby Pecos River at the same location since the early Tertiary provide powerful hydrologic drivers for intrastratal dissolution by ascending fluids. Therefore, it is expected that additional zones of extensive cavernous porosity exist to the west and south of the Yates field based on the northeastward migration of fluids towards the entrenching Pecos River. While no humanly explored caves in the west Texas region have been attributed to eogenetic speleogenetic origins, numerous caves and karst features throughout the entire Permian Basin region provide definitive proof of the importance of hypogene processes.

It is likely that many other hydrocarbon reservoirs within the region and around the world are the result of hypogene speleogenesis, suggesting that many of the fields that have been termed paleokarst reservoirs are not actually true paleokarst. Instead, the

emplacement of hydrocarbons simply represents a stage in the speleogenetic evolution of the reservoir where solutionally aggressive fluids have been displaced by hydrocarbons that now occupy the cavernous porosity. This suggests that we need to re-evaluate the currently accepted models for reservoir karst development throughout the greater Permian Basin. While it is possible that many current karst reservoir characterization models may be accurate, it is probable that at least some can be more easily and accurately explained through hypogene speleogenetic models.

Future work on the Yates Field karst characterization needs to focus on better characterization of the total distribution of the karst development within the region, not just the producing units. While bit drops may not be the most reliable source for characterizing the distribution of cavernous porosity because of variability in reporting, a comprehensive review of all bit drops and sudden rushes of fluids reported on scout tickets should provide substantial insight into regional patterns of karst development, not just karst development within producing horizons. While complete petrophyisical analyses of wells would be ideal for characterizing total karst distribution, it is not economically feasible; therefore, reports of bit drops, high fluid flow and documentation of the collapse cave fabrics from conventional core the only means of evaluating total spatial karst development with present information. By looking at total karst development in overlying units and producing units, delineation of hypogene karst patterns can be better evaluated. The acquisition of high resolution 3D seismic would permit continuous vertical and horizontal documentation of karstic processes within these carbonate reservoirs. This should provide crucial information on preferential flow paths for fluid migration that can be used to improve oil recovery techniques and reservoir management.

While both karst science and reservoir management continue to evolve and improve, it is crucial that reservoir characterization evolves accordingly. As with all geologic processes, our understanding of speleogenetic processes continues to advance such that it is important to constantly review and revise previous theories in order to advance our understanding of geologic systems. Implication of the hypogene speleogenesis theory to the interpretation of carbonate-hosted oil fields may improve prospecting approaches. Ultimately, continued advancement of reservoir characterization should lead to improved natural resource recovery and reservoir management.

ACKNOWLEDGEMENTS

The authors wish to thank the many people which made this project possible. Kinder Morgan Production Company LLC provided access to Yates Field reservoir data. The Texas Cave Management Association provided access to Amazing Maze Cave. The Permian Basin Grotto provided access to Ess Cave. Funding was partially provided through grants from the Geological Society of America and the American Association of Petroleum Geologists. Project support was provided by Kinder Morgan Production Company LLC, New Mexico Institute of Mining and Technology and the National Cave and Karst Research Institute. During a geologic internship by the senior author in the summer of 2006 with Kinder Morgan in Midland, Texas, the ideas behind this paper germinated. All of the Yates Field conventional core is now reposited at the Bureau of Economic Geology Core Research Facility in Midland, Texas.

CHAPTER VIII:
CONCLUSIONS AND IMPLICATIONS

Throughout this study, cave and karst development has been shown to be widespread within the evaporite facies of the greater Delaware Basin. Specifically, evaporite karst development within the Delaware Basin is far more common than previously recognized with a complex association of diagenetic mineral alternation. Spatial distribution and morphologic features observed in individual caves attest to evaporite systems that have been significantly affected by hypogene processes. Similarly, diagenetic characteristics of the Yates Field suggest that karst porosity within hydrocarbon reservoirs in the region is largely the result of confined dissolution. Therefore, it appears that hypogene processes dominate the speleogenetic evolution of the greater Delaware Basin region.

DELAWARE BASIN HYPOGENE SPELEOGENESIS

Evidence of hypogene speleogenesis is widespread throughout the Delaware Basin region in a range of lithologies. The caves of the Guadalupe Mountains have been associated with sulfuric acid processes, but original models could not explain the distribution and morphologies of these caves (Hill, 1990; Hose and Pisarowicz, 2000). However, recent investigations by Palmer (2006) and Klimchouk (2007) account for thes patterns of karst development inn the Guadalupe Mountains and have shown that hypogene speleogenesis dominated dissolution within these carbonate facies while

solutional agressivity was at least partially enhanced by the addition of sulfuric acid-rich fluids.

While karst in the carbonate reef facies of the Guadalupe Mountains has been well-studied, karst development in the evaporitic backreef and basin-filling facies were poorly studied. Land (2003, 2005) had shown that large sinkholes in the gypsum beds of the Seven Rivers Formation near Roswell, New Mexico had formed through intrastratal dissolution as rising fluids attempted to discharge to the Pecos River, but this was viewed as a local phenomenon. Throughout the evaporite facies of southeastern New Mexico and far west Texas, numerous individual caves had been documented (Belski, 1992; Easton, 1987; Lee, 1996) Most caves showed no significant genetic relationship to the surface geomorphology; therefore, many features were considered largely relict and had mainly developed in relation to previous climatic regime.

With the recent recognition of a definitive suite of morphological features (i.e. risers, wall channels, ceiling channels and cupolas) indicative of hypogene dissolution (Frumkin and Fischendler, 2005; Klimchouk, 2003, 2006, 2007), it became possible to reinterpret many of the previously documented cave and karst features within the region. Throughout all of the evaporite facies within the region, complete suites of hypogene features have now been documented in numerous caves, which show remarkably similar morphologic patterns to those recently attributed to hypogene processes within the carbonate facies of the Guadalupe Mountains.

In the evaporite shelf facies, hypogene speleogenesis is largely related to the entrenchment and eastward migration of the Pecos River (Chapter III - Stafford et al., 2007a). Water recharges to the west on the broad Pecos Slope, which extends into the

Sacramento Mountains, and is discharged as artesian springs along the Pecos River. Associated with artesian discharge is widespread development of hypogene cave systems, many of which exhibit multiple storeys of solutional development and complex morphologies (Chapter II - Stafford and Nance, 2009). Coffee Cave provides definitive evidence of complex cave networks forming within the Seven Rivers Formation as result of hypogene dissolution where semi-confined fluids migrated towards the Pecos River (Chapter III - Stafford et al., 2007a).

Within the Delaware Basin, the Castile Formation exhibits intense karst development (Chapters IV - Stafford et al., 2007b; Chapter V - 2008). Extensive field mapping coupled with GIS analyses has shown that approximately 10,000 individual karst features (e.g. sinkholes and caves) are surficially expressed within Castile outcrop region (Chapter IV - Stafford et al., 2007b). Many of these features are highly clustered indicating that fluid migration was focused in distinct regions. Within these focused regions, karst development is usually associated with occurrences of calcitized evaporites, secondary selenite and individual caves that contain extensive suites of hypogene features indicative of confined /semi-confined dissolution (Chapter V - Stafford et al., 2008).

Similar to the distribution of karst features, GIS analyses of the Castile outcrop region has shown that evaporite calcitization also shows a highly clustered pattern with more than 1000 individual occurrences documented (Chapter VI - Stafford et al., 200_a). The distribution of calcitized evaporites exhibits a similar pattern to that of the clustered distribution of karst features, suggesting a genetic relationship. Previous research on native sulfur occurrences within the Castile Formation (e.g. Wessel and Wiberly, 1992)) have shown that native sulfur deposits are a byproduct of evaporite calcitization in the

presence of ascending hydrocarbons along solutionally enhanced transmissive zones. This model for evaporite calcitization and associated with native sulfur emplacement is consistent with models for hypogene speleogenesis.

Sufficient evidence has shown that hypogene processes dominate speleogenesis and sulfate diagenesis within the Castile Formation. Solutionally aggressive fluids originating from the underlying Delaware Mountain Group siliciclastics rose through the Castile Formation resulting in widespread brecciation and the development of numerous solutional conduits (i.e. caves) (Chapter V – Stafford et al., 2008). Similarly, light hydrocarbons (e.g. methane) were delivered from the underlying Delaware Mountain Group, fueling sulfate reduction along solutionally enhanced pathways (Stafford et al., 200_a). Currently surface denudation within the Castile outcrop region is resulting in the epigenic overprinting of hypogene caves and the oxidation of native sulfur bodies as meteoric processes alter previously confined natural resources. Calcitized occurrences (e.g. castile buttes) stand in positive relief across the region, attesting to the dominance of hypogene processes in the regional diagenetic evolution.

The dominance of hypogene processes on speleogenesis within the evaporitic backreef, carbonate reef and evaporitic basin-filling facies in exposed Permian strata of the Delaware Basin suggests that hypogene processes are likely important in porosity development of strata still in the subsurface within the region. Previously, karst development within the Yates Field, on the southern tip of the Central Basin Platform and the far eastern edge of the Delaware Basin, had been attributed to syngenetic, mixing-zone dissolution (Craig, 1998, 1990). However, cross-formational breccias, spatial distribution of caves and the presence of unique mineralogies all suggest that karst

porosity within the Yates Field is the result of hypogene dissolution likely associated with higher geothermal gradients and the addition of sulfuric acid-rich fluids in the past (Stafford et al., 200_b). Further support for the dominance of hypogene processes within the Yates Field area comes from recognition of several exposed hypogene caves developed in Cretaceous strata that overly the Permian oil bearing strata.

Through this study, hypogene processes have been shown to dominate speleogenesis and solutional diagenesis of the Delaware Basin Region. The migration and entrenchment of the Pecos River has significantly controlled the distribution of hypogene karst by providing the hydrologic driving force for upward migration of fluids in many regions. Karst development within the Castile Formation has likely been heavily influenced by the Pecos River at depth, but within the outcrop region the interaction of meteoric water recharged in the Delaware Mountains and basinal, hydrocarbon-rich fluids migrating updip has resulted in complex diagenetic suites of sulfate alteration associated with confined, hypogene speleogenesis. Similarly hypogene processes have had significant effects on the diagenetic evolution of strata on the margins of the Delaware Basin, including development of karst porosity within the single largest oil field ever discovered in the Permian Basin (i.e. Yates Field Unit). Therefore, hypogene processes are clearly an integral part of the diagenesis of the entire Delaware Basin region and is not a phenomenon restricted to the world famous carbonate caves of the Guadalupe Mountains.

IMPLICATIONS FOR NATURAL RESOURCE MANAGEMENT

The recognition of the widespread occurrence of hypogene speleogenesis within the greater Delaware Basin has significant implications for natural resource management.

Karst conduits provide fast flow bypass features for rapid transfer of fluids and contaminants through the subsurface. Because hypogene karst does not form in direct relationship to the surficial processes, it generally forms poorly predictable patterns and occurrences that often undetectable prior to surficial breaching.

When caves are breached, the clustering nature of hypogene karst and associated porosity divergence with depth creates a situation where surface spills and contamination can be rapidly transmitted over large areas in the subsurface. While solutional conduits provide special environmental concerns in all karst terrains, the presence of hypogene karst within evaporite systems provides a unique environmental concern because these conduits provide direct fast flow routes for the transfer of contaminants into deep transmissive zones where fluids commonly have longer residence times. Because of the high solute load in evaporite aquifers, these deeper non-evaporite transmissive zones are often the primary zones of potable groundwater in evaporite terrains. In contrast, shallow epigene karst in evaporite settings generally does not connect to lower aquifers, but instead form shallow bypass features which provide fewer environmental concerns. Therefore, special care must be taken to avoid spills and breakage of fluid lines (e.g. wastewater, petroleum) within these evaporitic terrains, especially in proximity to known hypogene caves.

Similar to the unpredictability of hypogene karst for groundwater flow, hypogene caves create unique geohazards associated with land subsidence. Unbreached hypogene caves often collapse when overburden pressure is increased through construction of buildings or roads. Because of the low tensile strength of evaporite rocks and rapid rates of surface denudation due to high evaporite solubilities, hypogene evaporite caves will

commonly collapse with the addition of less overburden pressure than is expected for collapse of caves in traditional carbonate terrains. The recognition of the widespread occurrence of hypogene karst in the region suggests that greater care should be taken in site evaluation for construction of new buildings and infrastructure.

Recognition of complex diagenetic suites within the Castile Formation provides insight into the distribution of mineral resources within hypogene dominated speleogenetic systems. As with native sulfur occurrences in the Delaware Basin, other economic minerals in other settings have been associated with karst processes, including Mississippi Valley Deposits and breccia-hosted uranium deposits. These mineral resources are often associated with hydrothermal fluids, which simply represent a special subset of hypogene speleogenesis. Therefore, spatial analyses of the distribution of calcitization within the Castile Formation can be used as a proxy for investigating the spatial distribution and characteristics of other mineral resources associated with hypogene processes.

While most of this study focused on evaporite karst within the Delaware Basin region, identification of hypogene origins for karst porosity within the Yates oil field has significant implications for hydrocarbon reservoir characterization and management within the greater Permian Basin. It is likely that many other karst hosted hydrocarbon fields within the region are the result of hypogene processes, which can explain the occurrence of unique minerals, reservoir locations and reservoir characteristics. Recognition of hypogene origins of cavernous porosity within individual oil fields can have implications for increased recovery. A better understanding of porosity distribution

and connectivity can enable the development of management plans to maximize reservoir integrity, pressure stability and hydrocarbon extraction.

IMPLICATIONS FOR FUTURE RESEARCH

This study is the first to recognize the widespread occurrence of hypogene karst within evaporite facies of the Delaware Basin; therefore, it has opened the door to the possibility of numerous local studies to evaluate specific controls on local karst phenomenon. As with the study of Coffee Cave, it is likely a more accurate genetic evolution for local areas can be interpreted based on the regional recognition of hypogene processes. A better understanding of local karst phenomenon will inevitably improve natural resource management. Specifically, recognition of abundant hypogene caves within the Delaware Basin suggests that the region surrounding the Waste Isolation Pilot Plant (WIPP) should be reevaluated with respect to potential intrastratal dissolution within these deeper, basin-filling facies. Although currently no problems are suspected with hypogene karst near the WIPP site, it is logical that the local region should be reassessed with respect to our current knowledge of karst processes in the region.

Through the course of study of diagenetic mineral alterations within the Castile Formation, complex diagenetic zones have been identified in association with mineral alteration boundaries. Analyses of the association of hypogene karst, evaporite calcitization, secondary selenite emplacement and native sulfur occurrences will likely provid detailed information on the migration of different episodes of fluid migration through the Castile Formation. Detailed analyses of previously unreported alteration

boundary zones associated with evaporite calcitization will likely provide significant insight into the current understanding of sulfate reduction and evaporite diagenesis.

The recognition of hypogene origins of karst within the oil reservoirs of the Central Basin Platform will likely have significant affects on the future interpretation of cavernous porosity within the region. This will likely lead to the reinterpretation or reevaluation of many of the karsted carbonate reservoirs of the Permian Basin. Potentially this will enable the development of improved plans for reservoir management and pave the way for numerous new studies on the diagenetic evolution of individual fields.

Ultimately, recognition of the widespread occurrence of hypogene karst within the Delaware Basin will likely lead to the questioning of speleogenetic processes throughout southwestern United States and northeastern Mexico. In a broader sense, knowledge gained about regional speleogenesis through this study can be extrapolated to other continental basin settings that potentially behave in a similar hydrologic pattern. Even farther abroad, improved understanding of evaporite speleogenesis and the use of GIS-analyses in the interpretation of karst terrains can be used for current and future efforts to evaluate geomorphic landscapes not only on Earth but also on other planetary bodies (e.g. Mars). Therefore, it is expected that the results of this study will lead into a wide range of future research.

REFERENCES CITED

Adams, J.E., 1930. Origin of oil and its reservoir in Yates pool, Pecos County, Texas. AAPG Bulletin, v. 14, no. 6, p. 705-717.

Adams, J.E., 1944. Upper Permian Ochoa series of the Delaware Basin, west Texas and southeastern New Mexico. AAPG Bulletin, v. 28, p. 1596-1625.

Adams, J.E., 1972. Semi-cyclicity in the Castile anhydrite, in Elam, J.G. and Chuber, S. (eds), Cyclic Sedimentation in the Permian Basin. West Texas Geological Society, p. 196-202.

Alexander, J.I.D. and Watkinson, A.J., 1989. Microfolding in the Permian Castile Formation: an example of geometric systems in multilayer folding, Texas and New Mexico. GSA Bulletin, v. 101, p. 742-750.

Anderson, R.Y., 1982. Deformation-dissolution potential of bedded salt, Waste Isolation Pilot Plant site, Delaware Basin, New Mexico, in Lutze, W. (ed), Scientific Basis for Radioactive Waste Management, V, Elsevier Science Publishing Company New York, New York, p. 449-458.

Anderson, R.Y., Dean, W.E., Kirkland, D.W. and Snider, H.I., 1972. Permian Castile varved evaporite sequence. West Texas and New Mexico. GSA Bulletin, v. 83, p. 59-85.

Anderson, R.Y., Kietzke, K.K. and Rhodes, D.J., 1978. Development of dissolution breccias, northern Delaware Basin and adjacent areas. New Mexico Bureau of Mines and Mineral Resources, Bulletin 159, Socorro, NM, p. 47-52.

Anderson, R.Y. and Kirkland, D.W., 1966. Intrabasin varve correlation. GSA Bulletin, v. 77, p. 241-256.

Anderson, R.Y. and Kirkland, D.W., 1980. Dissolution of salt deposits by brine density flow. Geology, v. 8, p. 66-69.

Bachman, G.O., 1980. Regional geology and Cenozoic history of the Pecos Region, southeastern New Mexico. U.S. Geological Survey Open-File Report 80-1099, 116 p.

Bachman, G.O., 1984. Regional geology of Ochoan evaporites, northern part of Delaware Basin. New Mexico Bureau of Mines and Mineral Resources, Circular 184, 22 p.

Bachman, G.O., 1987. Karst in evaporites in southeastern New Mexico, Sandia National Laboratories, Contractor Report SAND86-7078. Albuquerque, New Mexico, 74 p.

Back, w., Hanshaw, B.B., Plummer, L.N., Rahn, P.H., Rightmire, G.T. and Rubin, M., 1983. Process and rate of dedolomitization: mass transfer and 14C dating in a regional carbonate aquifer. GSA Bulletin, v. 94, p. 1415-1429.

Back, W., Hanshaw, B.B. and Van Driel, J.N., 1984. Chapter 12, Role of groundwater in shaping the eastern coastline of the Yucatan Peninsula, Mexico. in LaFleur, R.G. (ed), Groundwater as a Geomorphic Agent. Allen and Unwin, Inc., Boston, MA, p. 281-293.

Barker, C.E. and Pawlewicz, M.J., 1987. The effects of igneous intrusions and higher heat flow on the thermal maturity of Leonardian and younger rocks, western Delaware Basin, Texas, in Mazzullo, L. and Cromwell, D. (eds), The Leonardian Facies in W. Texas and S.E. New Mexico and Guidebook to the Glass Mountains, West Texas. Permian Basin Section – SEPM, p. 69-84.

Barlow, C.A. and Ogden, A.E., 1992. A statistical comparison of joint, straight cave segment, and photo-lineament orientations. NSS Bulletin, 44: 107-110.

Barker, C.E. and Pawlewicz, M.J., 1987. The effects of igneous intrusions and higher heat flow on the thermal maturity of Leonardian and younger rocks, western Delaware Basin, Texas, in Mazzullo, L. and Cromwell, D. (eds), The Leonardian Facies in W. Texas and S.E. New Mexico and Guidebook to the Glass Mountains, West Texas. Permian Basin Section – SEPM, Midland, TX, p. 69-84.

Baumgardner, R.W., Hoadley, A.D. and Goldstein, A.G., 1982. Formation of the Wink Sink, a Salt Dissolution and Collapse Feature, Winkler County, Texas. Bureau of Economic Geology, University of Texas at Austin, Austin, TX, 38 p.

Belski, D., 1972. Coffee Cave: unpublished map.

Belski, D. (ed), 1992. GYPKAP Report Volume #2. Southwestern Region of the National Speleological Society, Albuquerque, NM, 57 p.

Bryfonki, D. (ed), 1985. Climate of the States, Volume 1. Gale Research Company, Detroit, Michigan.

Calaforra, J.M. and Forti, P., 1994. Two new types of gypsum speleothems from New Mexico: gypsum trays and gypsum dust. NSS Bulletin, v. 56, no. 1, p. 32-37.

Calaforra, J.M. and Pulido-Bosch, A., 1996. Some examples of gypsum karsts and the most important gypsum caves in Spain. Int. J. Speleology, v.25, no. 3-4, p. 225-238.

Calaforra, J.M. and Pulido-Bosch, A., 1999. Genesis and evolution of gypsum tumuli. Earth Surface Processes and Landforms, v. 24, p. 919-930.

Calaforra, J.M., Pulido-Bosch, A. and Lopes-Chicano, M., 2002. Gypsum karst of the Beltic Cordillera (south Spain). Carbonates and Evaporites, v. 17, no. 2, p. 131-141.

Calzia, J.P. and Hiss, W.L., 1978. Igneous rocks in northern Delaware Basin, New Mexico and Texas, in Austin, G.S. (ed), Geology and Mineral Deposits of Ochoan Rocks in Delaware Basin and Adjacent Areas. New Mexico Bureau of Mines and Mineral Resources, Circular 159, p. 39-45.

Cantón, Y., Sole-Benet, A. and Lazaro, R., 2003. Soil-geomorphology relations in gypsiferous materials of the Tabernas Desert (Almeria, SE Spain). Geoderma, v. 115, no. 3-4, p. 193-222.

Chapin, C.E. and Cather, S.M., 1994. Tectonic setting of the axial basins of the northern and central Rio Grande Rift, in Keller, G.R. and Cather, S.M. (eds), Structure, stratigraphy, and tectonic setting. GSA Special Paper 291, p. 5-25.

Choquette, P.W. and Pray, L.C., 1970. Geological nomenclature and classification of porosity in sedimentary carbonates. AAPG Bulletin, v. 54, p. 207-250.

Craig, D.H., 1988. Caves and other features of Permian karst in San Andres dolomite, Yates Field reservoir, west Texas, in James, N.P. and Choquette, P.W. (eds), Paleokarst. Springer, New York, NY, p. 342-363.

Craig, D.H., 1990. Yates and other Guadalupian (Kazanian) oil fields, U.S. Permian Basin, in Brooks, J. (ed), Classic Petroleum Provinces. Geological Society of London Special Publication No. 50, London, UK, p. 259-263.

Craig, D.H., Mruk, D.H., Heymans, M.J., Crevello, P.D. and Lanz, R.C., 1986. Stratigraphy and reservoir geology of the San Andres Dolomite – Yates Field, West Texas, in Bebout, D.G. and Harris, P.M. (eds), Hydrocarbon Reservoir Studies: San Andres / Grayburg Formations. Permian Basin. Permian Basin Section – SEPM, Midland, Texas, p. 139-143.

Cox, E.R., 1967. Geology and hydrology between Lake McMillan and Carlsbad Springs, Eddy Co., New Mexico. U.S. Geological Survey Water-Supply Paper 1828, 48 p.

Davis, G., 1965. Millrace Cave, unpublished sketch map.

Dean, W.E. and Anderson, R.Y., 1982. Continuous subaqueous deposition of the Permian Castile Evaporites, Delaware Basin, Texas and New Mexico, in Handford, C.R., Loucks, R.G. and Davies, G.R. (eds), Depositional and Diagenetic Spectra of Evaporites – A Core Workshop, SEPM, Tulsa, OK, p. 324-334.

Dean, W.E., Davies, G.R. and Anderson, R.Y., 1975. Sedimentological significance of nodular and laminated anhydrite. Geology, v. 3, p. 367-372.

Denizman, C., 2003. Morphometric and spatial distribution parameters of karstic depressions, lower Suwannee River basin, Florida. Journal of Cave and Karst Studies, v. 65, no. 1, p. 29-35.

Dickenson, W.R., 1981. Plate tectonic evolution of the southern Cordillera. Arizona Geological Society Digest, v. 14, p., 113-135.

Dickerson, P.W., 1985. Evidence for Late Cretaceous-early Tertiary transpression in Trans-Pecos Texas and adjacent Mexico, in Dickerson, P.W. and Muelberger, W.R. (eds), Structure and Tectonics of Trans-Pecos Texas. West Texas Geological Society, Midland, Texas, p. 285-294.

Dietrich, J.W., Owen, D.E., Shelby, C.A. and Barnes, V.E., 1995. Geologic Atlas of Texas: Van Horn-El Paso Sheet. University of Texas Bureau of Economic Geology, Austin, Texas, 1 sheet.

Demicco, R.V. and Hardie, R.Y., 1982. Continuous subaqueous deposition of the Permian Castile Evaporites, Delaware Basin, Texas and New Mexico, in Hadford, C.R., Loucks, R.G. and Davies, G.R. (eds), Depositional and Diagenetic Spectra of Evaporites – A Core Workshop. SEPM, Midland, TX, p. 324-334.

Doran, L.M. and Hill, C.A., 1998. Gypsum trays in Torgac Cave, New Mexico. Journal of Cave and Karst Studies, v. 60, no. 1, p. 39-43.

Drever, J.I., 1997, The Geochemistry of Natural Waters. Prentice Hall, Upper Saddle River, NJ, 436 p.

Dublyansky, Y.V., 2000. Hydrothermal speleogenesis – its settings and peculiar features, in Klimchouk, A., Ford, D.C., Palmer, A.N. and Dreybrodt, W. (eds), Speleogenesis: Evolution of Karst Aquifers. National Speleological Society, Inc., Huntsville, AL p. 292-297.

DuChene, H.R. and Belski, D.S., 1992. The San Andres Formation of the Pecos Slope gypsum, Southeastern New Mexico, in Belski, D.S. (ed), 1992, GYPKAP Report Volume #2. Southwestern Region of the National Speleological Society, Albuquerque, NM, p. 12-15.

Eaton, J. (ed), 1987. GYPKAP 1987 Annual Report. Southwestern Region of the National Speleological Society, Alamogordo, NM, 35 p.

Elliott, W.R. and Veni, G. (eds), 1994. The Caves and Karst of Texas. National Speleological Society of America, Huntsville, AL, 342 p.

Ehrlich, H.L., 1990. Geomicrobiology. Marcel Dekker, New York, NY, 646 p.

Fenneman, N.M., 1931. Physiography of Western United States. McGraw Hill Book Company, New York, NY.

Florea, L.J., Paylor, R.L., Simpson, L. and Gulley, J., 2002. Karst GIS advances in Kentucky. Journal of Cave and Karst Studies, v. 64, no. 1, p. 58-62.

Forbes, J. and Nance, R., 1997. Stratigraphy, sedimentology, and structural geology of gypsum caves in east central New Mexico. Carbonates and Evaporites, v. 12, no. 2, p. 64-72.

Forbes, J., 1998. Air temperature and relative humidity study: Torgac Cave, New Mexico. Journal of Cave and Karst Studies, v. 60, no. 1, p. 27-32.

Ford, D.C., 2006. Karst geomorphology, caves and cave deposits: a review of North American Contributions during the past half century, in Harmon, R.S. and Wicks, C.W. (eds), Perspectives on Karst Geomorphology, Hydrology and Geochemistry. GSA Special Paper 505, Boulder, CO, p. 1-14.

Ford, D., Lauritzen, S. and Ewers, R., 2006. Hardware and software modeling of initial conduit development in karst rocks, in Klimchouk, A., Ford, D.C., Palmer, A.N. and Dreybrodt, W. (eds), Speleogenesis: Evolution of Karst Aquifers. National Speleological Society, Inc., Huntsville, AL, p.175-183.

Ford, D.C and Williams, P.W., 1989. Karst Geomorphology and Hydrology. Unwin Hymam, London, UK, 601 p.

Ford, D.C. and Williams, P.W., 2007. Karst hydrogeology and geomorphology. John Wiley and Sons, London, UK, 562 p.

Franklin, D.W., 1966. Yates Field, Pecos County, Texas. Marathon Oil Company, Unpublished internal report, 18 p.

Friedman, G.M., 1966. Occurrence and origin of Quaternary dolomite of Salt Flat, West Texas. J. Sedimentary Petrography, v. 36, p. 263-267.

Frumkin, A. and Fischendler, I., 2005. Morphometery and distribution of isolated caves as a guide for phreatic and confined paleohydrological conditions. Geomorphology, v. 67, p. 457-471.

Garber, R.A., Grover, G.A. and Harris, P.M., 1989. Geology of the Capitan shelf margin – subsurface data from the northern Delaware Basin, in Harris, P.M. and Grover, G.A. (eds), Subsurface Outcrop Examination of the Capitan Shelf Margin, Northern Delaware Basin. SEPM Core Workshop no 13, San Antonio, TX, p. 3-269.

Guilinger, J.R. and Nestlerode, E., 1992. The geology and development of the Phillips Ranch Sulfur Deposit, , in Wessel, G.R. and Wimberly, B.H. (eds), Native Sulfur: Developments in Geology and Exploration. Society of Mining, Metallurgy, and Exploration, Inc., Littleton, CO, p. 125-134.

Harris, J.F., Mylroie, J.E. and Carew, J.L., 1995. Banana holes: unique karst features of the Bahamas. Carbonates and Evaporites, v. 10, no. 2, p. 215-224.

Havenor, K.C., 1968. Structure, stratigraphy, and hydrogeology of the northern Roswell Artesian Basin, Chaves County, New Mexico. New Mexico State Bureau Mines Mineral Resources, Circular 93, Socorro, NM, 30 p.

Hendrickson, G.E. and Jones, R.S., 1952. Geology and Ground-Water Resources of Eddy County, New Mexico. New Mexico Bureau of Mines and Mineral Resources, Socorro, NM, 189 p.

Hennen, R.V. and Metcalf, R.J., 1929. Yates oil pool, Pecos County, Texas. AAPG Bulletin, v. 13, no. 12, p. 1509-1556.

Hentz, T.F. and Henry, C.D., 1989. Evaporite-hosted native sulfur in Trans-Pecos Texas: relation to late-phase Basin and Range deformation. Geology, v. 17, p. 400-403.

Hill, C.A., 1990. Sulfuric acid speleogenesis of Carlsbad Caverns and its relationship to hydrocarbons, Delaware Basin, New Mexico, New Mexico and Texas. AAPG Bulletin, v. 74, no. 11, p. 1685-1694.

Hill, C.A., 1996. Geology of the Delaware Basin, Guadalupe, Apache and Glass Mountains: New Mexico and West Texas. Permian Basin Section – SEPM, Midland, TX, 480 p.

Hill, C. and Forti, P., 1997. Cave Minerals of the World, 2ed. National Speleological Society, Huntsville, AL, 463 p.

Hills, J.M., 1970. Late Paleozoic structural directions in southern Permian Basin, west Texas and southeastern New Mexico. AAPG Bulletin, v. 54, p. 1809-1827.

Horak, R.L., 1985. Trans-Pecos tectonism and its affects on the Permian Basin, in Dickerson, P.W. and Muelberger (eds), Structure and Tectonics of Trans-Pecos Texas. West Texas Geological Society, Midland, TX, p. 81-87.

Hose, L., 2000. Speleogenesis of Sistema Cheve, Oaxaca, Mexico, in Klimchouk, A., Ford, D.C., Palmer, A.N. and Dreybrodt, W. (eds), Speleogenesis: Evolution of Karst Aquifers. National Speleological Society, Inc., Huntsville, AL, p.358-361.

Hose, L.D. and Pisarowicz, J.A. (eds), 2000. The Caves of the Guadalupe Mountains. Journal of Cave and Karst Studies, v. 62, no. 2, 157 p.

Hung, L.Q., Dinh, N.Q., Batelaan, O., Tam, V.T. and Lagrou, D., 2002. Remote sensing and GIS-based analysis of cave development in the Suoimuoi Catchment (Son La – NW Vietnam). Journal of Cave and Karst Studies, v. 64, no. 1, p. 23-33.

iReservoir report to Marathon Oil Company, prepared by Gilman, J., Meng, H., Rothkopf, B., Sonnenfeld, M., and Uland, M. and Marathon Oil personnel, Ozcan J., and Stever, R., June 2003.

Jagnow, D.H., 1998. Bat usage and cave management of Torgac Cave, New Mexico. Journal of Cave and Karst Studies, v. 60, no. 1, p. 33-38.

James, A.N., 1992, Soluble Materials in Civil Engineering, Ellis Horwood, Chichester, UK.

Jenson, J.W., Keel, T.M., Mylroie, J.E., Mylroie, J.R, Stafford, K.W., Taborosi, D. and Wexel, C., 2006. Karst of the Mariana Islands: the interactions of tectonics, glacio-eustasy, and freshwater/seawater mixing in island carbonates, in Harmon, R.S. and Wicks, C.M. (eds), Perspectives on Karst Geomorphology, Hydrology, and Geochemistry: A Tribute Volume to Derek C. Ford and William B. White. Geological Society of America, Boulder, CO, p. 129-138.

Jeschke, A.A., Vosbeck, K. and Dreybrodt, W., 2001. Surface controlled dissolution rations of gypsum in aqueous solutions exhibit nonlinear dissolution kinetics. Geochimica et Cosmochimica Acta, v. 65, no. 1, p. 27-34.

Johnson, K.S., 2002. Karst in evaporite rocks of the United States. Carbonates and Evaporites, v. 17, no. 2, p. 90-97.

Johnson, K.S., Collins, E.W. and Seni, S.J., 2003. Sinkholes and land subsidence owing to salt dissolution near Wink Sink, West Texas, and other sites in western Texas and New Mexico, in Johnson, K.S. and Neal, J.T. (eds), Evaporite Karst and Engineering / Environmental Problems in the United States. Oklahoma Geological Survey, Norman, OK, p. 183-196.

Johnson, K.S. and Neal, J.T. (Eds.), 2003. Evaporite karst and engineering / environmental problems in the United States. Oklahoma Geological Survey, Norman, OK, 353 p.

Kasprzyk, A., 1995. Gypsum-to-anhydrite transition in the Miocene of southern Poland, J. Sedimentary Research, v. 65, no. 2, p. 348-357.

Kastning, E.H., 1983. Relict caves as evidence of landscape and aquifer evolution in a deeply dissected carbonate terrain: southwest Edwards Plateau, Texas, U.S.A. Journal of Hydrogeology, v. 61, p. 89-112.

Keller, G.R., Hills, J.M. and Djeddi, R., 1980. A regional geological and geophysical study of the Delaware Basin, New Mexico and west Texas, in Dickenson, P.W. and Hoffer, J.M. (eds), Trans-Pecos Region: New Mexico Geol. Soc., Guidebook, 31st Field Conf., SEPM-Permian Basin, Midland, TX, p. 105-111.

Kelley, V.C., 1971. Geology of the Pecos Country, Southeastern New Mexico. New Mexico Bureau of Mines and Mineral Resources, Socorro, NM, 78 p.

Kempe, S., 1996. Gypsum karst in Germany. Int. J. Speleology, v. 25, no. 3-4, p. 49-60.

Kendall, A.C. and Harwood, G.M., 1989. Shallow-water gypsum in the Castile Formation – significance and implications, in Harris, P.M. and Grover, G.A. (eds), Subsurface and Outcrop Examination of the Capitan Shelf Margin, Northern Delaware Basin. SEPM, Core Workshop No. 13, San Antonio, TX, p. 451-457.

Kerans, C., 1993. Description and interpretation of karst-related breccia fabrics, Ellenburger Group, west Texas, in Fritz, R.D., Wilson, J.L. and Yurewics, D.A. (eds), Paleokarst Related Hydrocarbon Reservoirs. SEPM Core Workshop No. 18, New Orleans, LA, p.181-200.

King, P.B., 1942. Permian of west Texas and southeastern New Mexico. AAPG Bulletin, v. 26, no. 4, p. 535-563

Kirkland, D.W. and Anderson, R.Y., 1970. Microfolding in the Castile and Todilto evaporites, Texas and New Mexico. GSA Bulletin, v. 81, p. 3259-3282.

Kirkland, D.W. and Evans, R., 1976. Origin of limestone buttes, Gypsum Plain, Culberson County, Texas. AAPG Bulletin, v. 60, p. 2005-2018.

Klemmick, G.F., 1992. Geology and mineralization of the Pokorny sulfur deposit, Culberson County, Texas, in Wessel, G.R. and Wimberly, B.H. (eds), Native Sulfur: Developments in Geology and Exploration. Society of Mining, Metallurgy, and Exploration, Inc., Littleton, CO, p. 109-124.

Klimchouk, A.B., 1991. Large maze caves in gypsum in the Western Ukraine: speleogenesis under artesian conditions. NSS Bulletin, v. 53, p. 71-82.

Klimchouk, A., 1996a. The typology of gypsum karst according to its geological and geomorphological evolution. International Journal of Speleology, v. 25, no. 3-4, p. 49-60.

Klimchouk, A., 1996b. Gypsum karst of the western Ukraine. Int. J. Speleology, v. 25, no. 3-4, p. 263-278.

Klimchouk, A., 1996. Dissolution and conversion of gypsum and anhydrite. Int. J. Speleology, v. 25, no. 3-4, p. 263-274.

Klimchouk, A., 1996b. Speleogenesis in gypsum. Int. J. Speleology, v. 25, no. 3-4, p. 61-82.

Klimchouk, A., 2000a. Speleogenesis of the great gypsum maze caves in the western Ukraine, in Klimchouk, A., Ford, D.C., Palmer, A.N. and Dreybrodt, W. (eds), Speleogenesis: Evolution of Karst Aquifers. National Speleological Society, Inc., Huntsville, AL, p. 431-442.

Klimchouk, A., 2000b. Speleogenesis under deep-seated and confined conditions, in Klimchouk, A., Ford, D.C., Palmer, A.N. and Dreybrodt, W. (eds), Speleogenesis: Evolution of Karst Aquifers. National Speleological Society, Inc., Huntsville, AL, p. 244-260.

Klimchouk, A., 2000c. Speleogenesis in gypsum, in Klimchouk, A., Ford, D.C., Palmer, A.N. and Dreybrodt, W. (eds), Speleogenesis: Evolution of Karst Aquifers. National Speleological Society, Inc., Huntsville, AL, p. 261-273.

Klimchouk, A., 2003. Conceptualization of speleogenesis in multi-story artesian systems: a model of transverse speleogenesis. Speleogenesis and Evolution of Karst Aquifers, v. 1, no. 2, p. 1-18.

Klimchouk, A., 2006. Unconfined versus confined speleogenetic settings: variations of solution porosity. Int. J. Speleology, v. 35, no. 1, p. 19-24.

Klimchouk, A., 2007. Hypogene Speleogenesis: Hydrogeological and Morphometric Perspective. National Cave and Karst Research Institute, Special Paper No. 1, Carlsbad, NM, 106 p.

Klimchouk, A. and Andrejchuk, V., 1996. Breakdown development in cover beds, and landscape features induced by intrastratal gypsum karst. Int. J. Speleology, v. 35, no. 1, p. 127-144.

Klimchouk, A.B. and Ford, D.C., 2000. Types of karst and evolution of hydrogeologic settings, in Klimchouk, A., Ford, D.C., Palmer, A.N. and Dreybrodt, W. (eds), Speleogenesis: Evolution of Karst Aquifers. National Speleological Society, Inc., Huntsville, AL, p. 45-53.

Klimchouk, A., Ford, D.C., Palmer, A.N. and Dreybrodt, W. (eds), 2000. Speleogenesis of Karst Aquifers. National Speleological Society, Inc., Huntsville, AL, 527 p.

Klimchouk, A., Lowe, D., Cooper, A., and Sauro, U. (eds.), 1996. Gypsum Karst of the World. Int. J. Speleology, v. 25, no. 3-4, 307 p.

Kohout, F. A., 1967.Ground-water flow and the geothermal regime of the Floridian Plateau. Transactions of the Gulf Coast Association of Geological Societies, v. 17, p. 339-354.

Kohout, F. A., Meisler, H., Meyer, F., Johnston, R., Leve, G., and Wait, R., 1988. Hydrogeology of the Atlantic Continental Margin, in Sheridan, R. and Grow, J. (eds.), The Geology of North America; the Atlantic Continental Margin, U.S. Boulder, Geological Society of America, v. I-2, p. 463-480.

Kunath, C.E. and Smith, A.R. (eds), 1968. The Caves of the Stockton Plateau. Texas Speleological Survey, Austin, TX, 111 p.

Land, L., 2003. Evaporite karst and regional ground water circulation in the lower Pecos Valley, in Johnson, K.S. and Neal, J.T. (eds), Evaporite Karst and Engineering and Environmental Problems in the United States. Oklahoma Geological Survey Circular 109, Norman, OK, p. 227-232.

Land**,** L., 2005. Evaluation of groundwater residence time in a karstic aquifer using environmental tracers: Roswell Artesian Basin, New Mexico, in Proceedings of the Tenth Multidisciplinary Conference on Sinkholes and the Engineering and Environmental Impacts of Karst, San Antonio, Texas, 2005. ASCE Geotechnical Special Publication no. 144, p. 432-440.

Land, L., 2006. Hydrogeology of Bottomless Lakes State Park, in Land, L., Lueth, V., Raatz, B., Boston, P. and Love, D. (eds), Caves and Karst of Southeastern New Mexico. New Mexico Geological Society, Guidebook 57, Albuquerque, NM, p. 95-96.

Land, L. and Newton, B. T., 2007. Seasonal and long-term variations in hydraulic head in a karstic aquifer: Roswell Artesian Basin, New Mexico. J. American Water Resources Association (in press).

Leary, D.A. and Vogt, J.N., 1986. Diagenesis of the Permian (Guadalupian) San Andres Formation, Central Basin Platform, West Texas, in Bebout, D.G. and Harris, P.M. (eds), Hydrocarbon Reservoir Studies: San Andres / Grayburg Formations, Permian Basin. Permian Basin Section – SEPM, Midland, TX, p. 67-68.

Lee, J. (ed), 1996. GYPKAP Report Volume 3. Southwestern Region of the National Speleological Society, Alamogordo, NM, 69 p.

Lee, M.K. and Williams, D.D., 2000. Paleohydrology of the Delaware Basin, western Texas: overpressure development, hydrocarbon migration, and ore genesis. AAPG Bulletin, v. 84, no. 7, p. 961-974.

Levine, S., Sigmon, R. and Douglas, S., 2002. Yates Field – super giant of the Permian Basin. Houston Geological Society Bulletin, v. 45, no. 3, p. 39-51.

Lock, B.E., Fife, A.W. and Anderson, E., 2004. Bacteria-petroleum reactions; salt dome cap rock genesis compared with similar processes from Permian outcrops in west Texas. Gulf Coast Association of Geological Societies Transactions, v. 54, p. 361-367.

Lorenz, J.C., 2006. Assessment of the Potential for Karst in the Rustler Formation at the WIPP Site. Sandia National Laboratories: Report, SAND 2005-7303, 102 p.

Lottes, A.L. and Rowley, D.B., 1990. Reconstruction of the Laurasian and Gondwanan segments of Permian Pangea. in McKerrow, W.S. and Scotese, C.R. (eds), Palaeozoic Palaeogeography and Biogeography. Memoirs of the Geological Society of London, v. 12, p. 383-395.

Loucks, R.G. and Mescher, P., 2001. Relationship between Paleocave Facies and Associated Pore Networks in Coalesced, Collapsed-Paleocave Systems. AAPG Bulletin., v. 85, no. 2, pp 384-391.

Lowe, D.J., Bottrell, S.H. and Gunn, J., 2000. Some case studies of speleogenesis by sulfuric acid, in Klimchouk, A., Ford, D.C., Palmer, A.N. and Dreybrodt, W. (eds), Speleogenesis: Evolution of Karst Aquifers. National Speleological Society, Inc., Huntsville, AL, p. 304-308

Macaluso, T. and Sauro, U., 1996. Weathering crust and karren on exposed gypsums surfaces. Int. J. Speleology, v. 25, no. 3-4, p. 115-126.

Machel, H.G., 1987. Saddle dolomite as a by-product of chemical compaction and thermochemical reduction. Geology, v. 15, p. 936-940.

Machel, H.G., 1992. Low-temperature and high-temperature origins of elemental sulfur in diagenetic environments, in Wessel, G.R. and Wimberly, B.H. (eds), Native Sulfur: Developments in Geology and Exploration. Society of Mining, Metallurgy, and Exploration, Inc., Littleton, CO, p. 3-22.

Machel, H.G., 1998. Gas souring by thermochemical sulfate reduction at 140°C: discussion. AAPG Bulletin, v. 82, p. 1870-1873.

Machel, H.G., 2001. Bacterial and thermochemical sulfate reduction in diagenetic settings – old and new insights. Sedimentary Geology, v. 140, p. 143-175.

Machel, H.G. and Burton, E.A., 1991. Burial-diagenetic sabkha-like gypsum and anhydrite nodules. Journal of Sedimentary Petrology, v. 61, no. 3, p. 394-405.

Maley, V.C. and Huggington, R.M., 1953. Cenozoic fill and evaporite solution in the Delaware Basin, Texas and New Mexico. GSA Bulletin, v. 64, p. 539-546.

Marathon Oil Company, 1973. Seepage Oil on Pecos River Near Iraan, Texas. Marathon Oil Company, Unpublished internal report, 17 p.

McDonnel, A., Loucks, R.G. and Dooley, T. 2007. Quantifying the origin and geometry of circular sag structures in northern Fort Worth Basin, Texas: Paleocave collapse, pull-apart fault systems, or hydrothermal alteration?, AAPG Bulletin. v. 91, no. 9: 1295-1318.

Moore, P.J., Martin, J.B. and Mylroie, J., 2007. Rapid development of secondary porosity within freshwater lenses of carbonate islands. GSA Abstracts with Programs, v. 39, no. 6, p. 467.

Murray, R.C., 1964. Origin and diagenesis of gypsum and anhydrite. J. Sedimentary Petrography, v. 34, p. 512-523.

Mylroie, J.E. and Carew, J.L., 1995. Karst development on carbonate Islands, in Budd, D.A., Harris, P.M. and Staller, A. (eds), Unconformities and Porosity in Carbonate Strata. AAPG, p. 55-76.

Mylroie, J.E., Carew, J.L. and Vacher, H.L., 1995. Karst development in the Bahamas and Bermuda, in Curran, H.A. and White, B. (eds), Terrestrial and Shallow Marine Geology of the Bahamas and Bermuda. San Salvador, Bahamas, p. 251-267.

Mylroie, J.E. and Jenson, J.W., 2002. Karst flow systems in young carbonate islands, in Martin, J.B., Wicks, C.M. and Sasowsky, I.D. (eds), Hydrogeology and Biology of Post-Paleozoic Carbonate Aquifers. Karst Waters Institute, Inc., p. 107-110

Nance, R., 1993. Application of the standard tablet method to a study of denudation in gypsum karst, Chosa Draw, southeastern New Mexico. MS Thesis, Univ. Northern Colorado, Greely, CO, 82p.

Nance, R., 1996, Montecito Cave, in Lee, J. (ed), 1996. GYPKAP Report Volume 3. Southwestern Region of the National Speleological Society, Alamogordo, NM, p. 22.

Nelson, J.W., 1991. Structural and geomorphic controls of the karst hydrogeology of Franklin County, Alabama. MS Thesis, Mississippi State, Mississippi State University, Mississippi State, MS, 165p.

Onac, B.P., Veni, G. and White, W.B., 2001. Depositional environment for metatyuyamunite and related minerals from Caverns of Sonora, TX (USA). European Journal of Mineralogy, v. 13, p. 135-143.

Orti, F. and Rosell, L., 2000. Evaporative systems and diagenetic patterns in the Calatayud Basin (Miocene, central Spain), Sedimentology, v. 47, p. 665-685.

Osborne, R.A.L., 2004. The troubles with cupolas. Acta Carsologica, v. 33, no. 2, p. 9-36.

Palmer, A.N., 1975. The origin of maze caves. NSS Bulletin, v. 37, no. 3, p. 56-76.

Palmer, A.N., 1991. Origin and morphology of limestone caves. GSA Bulletin, v. 103, p. 1-21.

Palmer, A.N., 2000. Maze origin by diffuse recharge through overlying formations, in Klimchouk, A., Ford, D.C., Palmer, A.N. and Dreybrodt, W. (eds), Speleogenesis: Evolution of Karst Aquifers. National Speleological Society, Inc., Huntsville, AL, p 387-390.

Palmer, A.N., 2000. Speleogenesis of Mammoth Cave System, Kentucky, U.S.A., in Klimchouk, A., Ford, D.C., Palmer, A.N. and Dreybrodt, W. (eds), Speleogenesis: Evolution of Karst Aquifers. National Speleological Society, Inc., Huntsville, AL, p. 367-377.

Palmer, A.N., 2006. Support for a sulphuric acid origin for caves in the Guadalupe Mountains, New Mexico. in Land, L., Lueth, V., Raatz, B., Boston, P. and Love, D. (eds), Caves and Karst of Southeastern New Mexico. New Mexico Geological Society, Socorro, NM, p. 195-202.

Palmer, A.N., 2007. Cave Geology. Cave Books, Dayton, OH, 454 p.

Pitt, W.D. and Scott, G.L., 1981. Porosity Zones of lower part of San Andres Formation, East-Central New Mexico. New Mexico State Bureau Mines Mineral Resources, Circular 179, Socorro, NM 20 p.

Phillips, W. B., 1917. The sulphur deposits of Culberson County, Texas. Dallas. Transactions of the Society of Mining Engineers of the American Institute of Mining, Metallurgical and Petroleum Engineers, p. 1449-1466.

Powers, D.W., 2003. Jal Sinkhole in southeastern New Mexico: evaporite dissolution, drill holes, and the potential for sinkhole development, in Johnson, K.S. and Neal, J.T. (eds), Evaporite Karst and Engineering / Environmental Problems in the United States. Oklahoma Geological Survey, Norman, OK, p. 227-232.

Polyak, V., 1992. Calcitic flowstone from Triple Engle Pit Cave, GYPKAP, in Belski, D.S. (ed), GYPKAP Report Volume #2. Southwestern Region of the National Speleological Society, Albuquerque, NM, p. 11.

Polyak, V. J. and Cokendolpher, J.C., 1996. Caves of Sinkhole Flat, Eddy County, New Mexico. Southwestern Caver, v. 34, no. 4, p. 61-64.

Quinlan, J.F., Smith, R.A. and Johnson, K.S., 1987. Gypsum karst and salt karst of the United States of America, in Atti symposio interntional sul carsimo nelle evaporiti, Le Grotte d'Italia. v. 4, no. XIII, p. 73-92.

Redell, J.R. and Fiesler, R.G., 1977. The Caves of Far West Texas. Texas Speleological Survey, Austin, TX, 103 p.

Richards, G.B., 1905. Native sulphur in El Paso County, Texas. U.S. Geological Survey, Bulletin 260, p. 589-592.

Ross, C.A., 1986. Paleozoic evolution of southern margin of Permian Basin. GSA Bulletin, v. 97, p. 536-554.

Sares, S.W., 1984. Hydrologic and Geomorphic Development of a Low Relief Evaporite Karst Drainage Basin, Southeastern New Mexico. MS Thesis, University of New Mexico, Albuquerque, NM, 123 p.

Sarg, J.F., 1981. Petrology of carbonate-evaporite facies transition of the Seven Rivers Formation (Guadalupian, Permian), Southeast New Mexico. J. Sedimentary Petrology, v. 51, p. 73-96.

Sauro, U., 1996. Gypsum karst of Italy. Int. J. Speleology, v. 35, no. 3-4, p. 239-250.

Selly, R.C., 1988. Applied Sedimentology, Academic Press, San Diego, CA, 446 p.

Scholle, P.A., Goldstein, R.H. and Ulmer-Scholle, D.S., 2004. Classic Upper Paleozoic Reefs and Bioherms of West Texas and New Mexico. New Mexico Institute of Mining and Technology, Socorro, NM, 166 p.

Scholle, P.A., Ulmer, D.S. and Melim, L.A., 1992. Late-stage calcites in the Permian Capitan Formation and its equivalents, Delaware Basin margin, west Texas and New Mexico: evidence for replacement of precursor evaporites. Sedimentology, v. 39, p. 207-234.

Schreiber, B.C., Roth, M.S. and Helman, M.L., 1982. Recognition of primary facies characteristics of evaporites and the differentiation of these forms from diagenetic overprints, in Handford, C.R., Loucks, R.G. and Davies, G.R. (eds), Depositional and Diagenetic Spectra of Evaporites – A Core Workshop, SEPM, Tulsa, OK.

Smith, A.R. and Elliot, W.R., 1994. Sulpheretted Hydrogen Cave, in: Elliott, W.R. and Veni., G. (Eds.), The caves and karst of Texas. National Speleological Society, Huntsville, AL, 316 p.

Sonnenfeld, P., 1984. Brines and Evaporites. Academic Press, London, UK.

Sonnenfeld, M.D., Wingate, T.P., Meng, H. Canter, L. and Zahm, L., 2003. Operational sequence stratigraphy for 3D reservoir modeling of Seminole San Andres Unit, Permian Basin, West Texas., (Poster), Am. Assoc. Petr. Geol., Bull. vol. Annual Convention, Salt Lake City, UT, www.irservoir.com.

Stafford, K.W., 2006. Gypsum karst of the Chosa Draw area, in Land, L., Lueth, V.W., Raatz, W., Boston, P. and Love, D. (eds), Caves and Karst of Southeastern New Mexico: New Mexico Geological Society Fifty-seventh Annual Field Conference. New Mexico Geological Society, Socorro, NM, p. 82-83.

Stafford, K.W., Behnken, F., Klimchouk, A., and Ulmer-Scholle, D., *200_b*. New insights into Yates Field reservoir characterization: Hypogenetic cavernous porosity instead of eogenetic cavernous porosity. AAPG Bulletin, submitted February 2008.

Stafford, K.W., Klimchouk, A. and Boston, P.J., 2006. Polygenetic evaporite karst of the Castile Formation of the western Delaware Basin. GSA Abstracts and Program, v. 38, no. 7, p. 289.

Stafford, K.W., Land, L. and Klimchouk, A., 2007a. Hypogenic speleogenesis within Seven Rivers evaporites: Coffee Cave, Eddy County, New Mexico. Journal of Cave and Karst Studies, v. 69, no. 3, in press.

Stafford, K.W., Mylroie, J.E., Taborosi, D., Jenson, J.W. and Myrloie, J.R., 2005. Karst development on Tinian, CNMI: controls on dissolution in relation to the Carbonate Island Karst Model. Journal of Cave and Karst Studies, v. 67, no. 1, p. 14-27.

Stafford, K.W. and Nance, R., 2009. Evaporite speleogenesis of the Gypsum Plain: New Mexico and far west Texas, in Palmer, A. and Palmer, M. (eds), The Caves and Karst of the USA, in press.

Stafford, K.W., Nance, R., Rosales-Lagarde, L. and Boston, P.J., 2008. Gypsum karst manifestations of the Castile Formation: Eddy County, New Mexico and Culberson County, Texas, USA. Int. J. Speleology, v. 37, no. 2, in press.

Stafford, K.W., Rosales-Lagarde, L. and Boston, P.J., 2007b. Castile evaporite karst potential map of the Gypsum Plain, Eddy County, New Mexico and Culberson County, Texas: a GIS methodological comparison. Journal of Cave and Karst Studies, v. 69, no. 3, in press.

Stafford, K.W., Ulmer-Scholle, D., and Rosales-Lagarde, L., *200_a*. Hypogene speleogenetic calcitization: Castile Buttes in the Western Delaware Basin. J. Sedimentary Research, submitted February 2008.

SWR, 1976. Mill Race Cave, unpublished cave map. Southwest Region of the National Speleological Society, Albuquerque, NM, 1 sheet.

Szukalski, B.W., Hose, L.D. and Pisarowicz, J.A. (eds), 2002. Cave and Karst GIS. Journal of Cave and Karst Studies, v. 64, no. 1, 93 p.

Taborosi, D., Jenson, J.W. and Mylroie, J.E., 2004. Karren features in island karst: Guam, Mariana Islands. Zeitschrifit fur Geomorphologie, v. 48, no. 3, p. 369-389.

Taylor, C.J., Nelson, H.L., Hileman, G. and Kaiser, W.P., 2005. Hydrogeologic-framework mapping of shallow, conduit-dominated karst – components of a regional GIS-based approach, in Kuniansky, E.L. (ed), U.S. Geological Survey Karst Interest Group Proceedings, Rapid City, South Dakota, September 12-15, 2005. U.S. Geological Survey Scientific Investigations Report 2005-5160, p. 103-113.

Thomas, R.G., 1972. The Geomorphic Evolution of the Pecos River System. Baylor Geological Studies, Bulletin No. 22, Waco, TX, 40 p.

Tinker, S.W., Ehret, J.R. and Brondos, M.D., 1995. Mulitple karst events related to stratigraphic cyclicity: San Andres Formation, Yates Field, west Texas, in Budd, D.A., Staller, A.H. and Harris, P.M. (eds), Unconformities and Porosity in Carbonate Strata. AAPG Memoir 63, Tulsa, OK, p. 213-237.

Tinker, S.C. and Mruk, D.H., 1995. Reservoir characterization of a Permian Giant: Yates Field, west Texas, in Stoudt, E.L. and Harris, P.M. (eds), Hydrocarbon Reservoir Characterization – Geologic Framework Flow Unit Modeling: SEPM Short Course No. 34. Tulsa, OK, p. 51-128.

Tóth, J., 1999. Groundwater as a geologic agent and overview of the causes, processes, and manifestations. Hydrogeology Journal, v. 7, p. 1-14.

Trzhtsinsky, Y.B., 2002. Human-induced activation of gypsum karst in Priangaria (east Siberia, Russia). Carbonates and Evaporites, v. 17, no. 2, p. 154-158.

U.S. Geological Survey, 2007. National Water Information System (NWIS): http://nwis.waterdata.usgs.gov.

Vacher, H.L. and Mylroie, J.E., 2002. Eogenetic karst from the perspective of an equivalent porous medium. Carbonates and Evaporites, v. 17, no. 2, p. 182-196.

Veni, G., 1994. Caverns of Sonora, in Elliott, W.R. and Veni, G. (eds), The Caves and Karst of Texas. National Speleological Society of America, Huntsville, AL, p. 138-139.

Veni, G., 2002. Revising the karst map of the United States. Journal of Cave and Karst Studies, v. 64, no. 1, p. 45-50.

Wallace, C.S.A. and Crawford, J.E., 1992. Geology of the Culberson ore body, in Wessel, G.R. and Wimberly, B.H. (eds), Native Sulfur: Developments in Geology and Exploration. Society of Mining, Metallurgy, and Exploration, Inc., Littleton, CO, p. 91-105.

Warren, J.K., 1989. Evaporite Sedimentology. Prentice-Hall, Englewood Cliffs, NJ, 285 p.

Warren, J.K. and Kendall, C.G., 1985. Comparison of sequences formed in marione sabkha (subaerial) and salina (subaqueous) settings – modern and ancient. AAPG Bulletin, v. 69, no. 6, p. 1013-1023.

Warton, M., 1994. Amazing Maze Cave, in Elliott, W.R. and Veni, G. (eds), The Caves and Karst of Texas. National Speleological Society of America, Huntsville, AL, p. 243-244.

Weber, R. H. and Kottlowski, F.E., 1959. Gypsum Resources of New Mexico: Bulletin 68. New Mexico Bureau of Mines and Mineral Resources, Socorro, NM, 68 p.

Welder, G.E., 1983. Geohydrologic framework of the Roswell ground-water basin, Chaves and Eddy Counties, New Mexico. New Mexico State Engineer Technical Report 42, Albuquerque, NM, 28 p.

Wessel, G.R., 1988. Shallow Stratigraphy, Structure, and Salt-Related Features, Yates Oil Field Area, Pecos and Crockett Counties, Texas. Ph.D. Thesis, Colorado School of Mines, Golden, CO, 144 p.

Wessel, G.R., 2000a. Stratigraphic relationships in the Yates Field area, Pecos and Crockett Counties, Texas – Part I. West Texas Geological Society Bulletin, v. 41, no. 7, p. 4-12.

Wessel, G.R., 2000b. Stratigraphic relationships in the Yates Field area, Pecos and Crockett Counties, Texas – Part II. West Texas Geological Society Bulletin, v. 41, no. 7, p. 4-8.

Wessel, G.R. and Wimberly, B.H. (eds), 1992. Native Sulfur: Developments in Geology and Exploration. Society of Mining, Metallurgy, and Exploration, Inc., Littleton, CO, 193p.

White, W.B., 1988. Geomorphology and Hydrology of Karst Terrains. Oxford Univ. Press, New York, NY, 464 p.

Welder, G. E., 1983. Geohydrologic framework of the Roswell Ground-Water Basin, Chaves and Eddy Counties, New Mexico. New Mexico State Engineer Technical Report 42, 28 p.

Worden, R.H. and Smalley, P.C., 1996. H_2S-producing reactions in deep carbonate gas reservoirs: Khuff Formation, Abu Dhabi. Chemical Geology, v. 133, p. 157-171.

Yauro, L. and Cooper, A., 2002. Evaporite karst and resultant geohazards in China. Carbonates and Evaporites, v. 17, no. 2, p. 159-165.

Zanbak, C. and Arthur, R.C., 1986. Geochemical and engineering aspects of anhydrite-gypsum phase transitions. Bulletin of the Association of Engineering Geologists, v. 23, no. 4, p. 419-433.

Zeigler, K.E., 2006. Stratigraphic chart, in Land, L., Lueth, V., Raatz, B., Boston, P. and Love, D. (eds), Caves and Karst of Southeastern New Mexico. New Mexico Geological Society, Albuquerque, NM, p. inside back cover.

Cross-Section ID NUMBER	Distance from Scarp (m)	Passage Width (m) Lower Level	Passage Width (m) Upper Level
1	32.08788	1.0989	
2	28.79118	0.76923	
3	63.40653	21.09888	
4	88.24167	10.65933	
5	88.57134	1.86813	
6	20.65932	5.60439	
7	1.64835	1.20879	
8	37.80216	1.0989	
9	40.43952	1.20879	
10	24.94503	3.73626	
11	46.1538	1.86813	
12	72.19773	4.72527	
13	54.61533	2.85714	
14	65.38455	2.30769	
15	69.34059	3.95604	
16	86.15376	7.14285	
17	95.16474	3.18681	
18	102.52737	1.75824	
19	18.6813		1.53846
20	13.95603		1.0989
21	6.26373		0.87912
22	32.08788		1.31868
23	10.989		0.87912
24	1.20879		0.43956
25	10.32966		2.1978
26	11.75823		1.97802
27	25.16481		8.68131
28	13.73625		0.98901
29	33.62634		5.05494
30	22.96701		0.76923
31	38.79117		0.54945
32	22.74723		0.98901
33	21.86811		0.65934
34	26.15382		0.54945
35	33.40656		1.31868
36	35.38458		2.52747

Table A.1. Comparison of passage width relative to distance from scarp in Coffee Cave. Note that "Lower Level" refers to passages that are currently flooded and measurements are from Belski (1972) and "Upper Level" refers to passage that were mapped during this study.

ID #	Type	Lithology	Width (m)	Length (m)	Depth (m)	Area (m^2)	Volume (m^3)
AA01	cave	sucrose	7.0	20.0	7.0	109.9	256.4
AA02	cave	gypsite	5.0	9.0	0.8	35.3	8.8
AA03	sink	gypsite	8.0	20.0	0.5	125.6	20.9
AA04	cave	sucrose	5.0	7.0	1.5	27.5	13.7
AA05	sink	gypsite	10.0	15.0	0.8	117.8	31.4
AA06	cave	sucrose	10.0	15.0	0.5	117.8	19.6
AA07	cave	sucrose	6.0	20.0	1.8	94.2	56.5
AA08	cave	sucrose	6.0	10.0	1.5	47.1	23.5
AA09	sink	gypsite	60.0	120.0	1.0	5652.0	1884.0
AB01	cave	gypsite	6.0	12.0	1.0	56.5	18.8
AB02	cave	gypsite	8.0	14.0	1.2	87.9	35.2
AB03	sink	gypsite	6.0	8.0	0.5	37.7	6.3
AB04	sink	gypsite	6.0	8.0	0.5	37.7	6.3
AB05	cave	gypsite	4.0	6.0	1.5	18.8	9.4
AB06	cave	gypsite	6.0	10.0	2.0	47.1	31.4
AB07	sink	gypsite	10.0	15.0	0.5	117.8	19.6
AB08	cave	gypsite	20.0	100.0	3.0	1570.0	1570.0
AB09	sink	gypsite	8.0	15.0	0.5	94.2	15.7
AB10	cave	gypsite	8.0	30.0	2.5	188.4	157.0
AB11	cave	gypsite	30.0	100.0	2.0	2355.0	1570.0
AB12	cave	gypsite	30.0	50.0	1.0	1177.5	392.5
AB13	sink	gypsite	5.0	20.0	0.8	78.5	20.9
AB14	sink	gypsite	6.0	30.0	1.5	141.3	70.6
AC01	sink	gypsite	30.0	100.0	2.0	2355.0	1570.0
AC02	sink	gypsite	30.0	60.0	0.5	1413.0	235.5
AC03	cave	laminated	8.0	10.0	1.5	62.8	31.4
AC04	sink	laminated	6.0	10.0	0.5	47.1	7.8
AC05	sink	laminated	8.0	15.0	0.5	94.2	15.7
AC06	cave	laminated	8.0	20.0	1.5	125.6	62.8
AC09	sink	gypsite	5.0	8.0	0.5	31.4	5.2
AC10	sink	gypsite	7.0	12.0	1.5	65.9	33.0
AC11	cave	sucrose	3.0	10.0	1.5	23.6	11.8
AC12	cave	laminated	70.0	100.0	2.5	5495.0	4579.2
AC13	cave	laminated	6.0	100.0	2.0	471.0	314.0
AC14	cave	laminated	40.0	7.0	1.5	219.8	109.9
AC15	cave	laminated	50.0	100.0	1.5	3925.0	1962.5
AC16	cave	laminated	8.0	40.0	3.5	251.2	293.1
AC17	cave	laminated	30.0	40.0	5.0	942.0	1570.0
AC18	sink	laminated	10.0	20.0	2.0	157.0	104.7
AC19	cave	laminated	40.0	20.0	1.5	628.0	314.0

Table A.2. Individual karst features documented during physical mapping within the Castile outcrop region. Width, Length, Depth, Area and Volume refer to sinkhole dimensions, where a “sink” is a filled sinkhole and a “cave” is an open sinkhole. Continued on next page.

ID #	Type	Lithology	Width (m)	Length (m)	Depth (m)	Area (m^2)	Volume (m^3)
AC20	sink	gypsite	10.0	15.0	1.0	117.8	39.2
AC21	sink	gypsite	8.0	12.0	0.5	75.4	12.6
AC22	sink	gypsite	20.0	40.0	4.0	628.0	837.3
AC23	cave	laminated	8.0	14.0	1.5	87.9	44.0
AC24	cave	gypsite	12.0	30.0	2.0	282.6	188.4
AD01	cave	sucrose	6.0	12.0	1.5	56.5	28.3
AD04	cave	sucrose	20.0	200.0	4.0	3140.0	4186.7
AD05	sink	gypsite	2.5	3.0	0.5	5.9	1.0
AD06	cave	sucrose	20.0	30.0	1.5	471.0	235.5
AD08	cave	sucrose	20.0	50.0	3.0	785.0	785.0
AD10	cave	sucrose	10.0	20.0	2.0	157.0	104.7
AE06	sink	soil	12.0	15.0	1.5	141.3	70.6
AE07	sink	soil	20.0	30.0	3.0	471.0	471.0
AE08	sink	soil	10.0	12.0	1.5	94.2	47.1
AE09	sink	soil	12.0	30.0	5.0	282.6	471.0
AG01	sink	gypsite	4.0	15.0	0.5	47.1	7.8
AG02	cave	sucrose	3.0	12.0	1.5	28.3	14.1
AG03	cave	gypsite	15.0	25.0	3.0	294.4	294.4
AH01	cave	sucrose	30.0	40.0	3.0	942.0	942.0
AH02	cave	sucrose	10.0	15.0	2.0	117.8	78.5
AH03	cave	sucrose	10.0	20.0	0.5	157.0	26.2
AH04	cave	sucrose	10.0	25.0	1.0	196.3	65.4
AH05	cave	sucrose	10.0	20.0	2.5	157.0	130.8
AH06	cave	sucrose	10.0	30.0	2.5	235.5	196.2
AH07	cave	sucrose	11.0	30.0	3.0	259.1	259.0
AH08	sink	sucrose	12.0	20.0	0.5	188.4	31.4
AH09	cave	sucrose	20.0	40.0	3.0	628.0	628.0
AH10	cave	sucrose	8.0	12.0	1.0	75.4	25.1
AH11	cave	gypsite	6.0	25.0	2.0	117.8	78.5
AH12	cave	sucrose	12.0	15.0	1.5	141.3	70.6
AH13	sink	sucrose	12.0	16.0	1.5	150.7	75.4
AH14	cave	sucrose	15.0	25.0	3.5	294.4	343.4
AH15	cave	sucrose	30.0	50.0	3.0	1177.5	1177.5
AH16	cave	sucrose	20.0	40.0	2.5	628.0	523.3
AH17	cave	sucrose	2.0	2.0	0.3	3.1	0.3
AH18	sink	gypsite	4.0	6.0	0.8	18.8	4.7
AH19	cave	sucrose	30.0	60.0	3.0	1413.0	1413.0
AH20	cave	sucrose	15.0	30.0	5.0	353.3	588.7
AH21	sink	gypsite	7.0	8.0	0.5	44.0	7.3
AH22	cave	sucrose	30.0	40.0	1.5	942.0	471.0

Table A.2. (cont.) Individual karst features documented during physical mapping within the Castile outcrop region. Width, Length, Depth, Area and Volume refer to sinkhole dimensions, where a “sink” is a filled sinkhole and a “cave” is an open sinkhole. Continued on next page.

ID #	Type	Lithology	Width (m)	Length (m)	Depth (m)	Area (m^2)	Volume (m^3)
AI01	sink	gypsite	12.0	14.0	0.5	131.9	22.0
AI02	sink	gypsite	30.0	50.0	1.5	1177.5	588.7
AI03	sink	soil	10.0	20.0	1.0	157.0	52.3
AI04	sink	gypsite	10.0	20.0	1.0	157.0	52.3
AI05	cave	gypsite	15.0	25.0	1.5	294.4	147.2
AI06	sink	gypsite	12.0	20.0	0.8	188.4	47.1
AI07	sink	gypsite	15.0	15.0	1.0	176.6	58.9
AI08	sink	gypsite	10.0	14.0	1.0	109.9	36.6
AI09	sink	gypsite	10.0	12.0	0.5	94.2	15.7
AI10	sink	gypsite	6.0	8.0	0.8	37.7	9.4
AI11	cave	gypsite	12.0	20.0	1.5	188.4	94.2
AI12	sink	gypsite	40.0	100.0	1.5	3140.0	1570.0
AI13	sink	gypsite	6.0	10.0	0.5	47.1	7.8
AJ01	cave	sucrose	50.0	100.0	3.5	3925.0	4579.2
AJ02	sink	sucrose	30.0	100.0	2.0	2355.0	1570.0
AJ03	sink	sucrose	20.0	25.0	1.5	392.5	196.2
AJ04	cave	mixed	15.0	25.0	5.0	294.4	490.6
AJ05	sink	gypsite	12.0	14.0	0.5	131.9	22.0
AJ06	sink	gypsite	14.0	18.0	1.0	197.8	65.9
AJ07	sink	sucrose	12.0	14.0	1.0	131.9	44.0
AJ08	sink	sucrose	6.0	8.0	0.5	37.7	6.3
AJ09	sink	sucrose	8.0	10.0	1.0	62.8	20.9
AJ10	cave	sucrose	10.0	14.0	2.0	109.9	73.3
AJ11	cave	sucrose	12.0	18.0	1.5	169.6	84.8
AJ12	sink	sucrose	14.0	18.0	0.5	197.8	33.0
AJ13	cave	sucrose	15.0	20.0	1.5	235.5	117.7
AJ14	sink	sucrose	12.0	15.0	1.0	141.3	47.1
AJ15	cave	sucrose	10.0	25.0	3.0	196.3	196.2
AJ16	sink	sucrose	20.0	100.0	5.0	1570.0	2616.7
AJ17	cave	sucrose	15.0	40.0	1.5	471.0	235.5
AJ18	cave	sucrose	25.0	60.0	2.0	1177.5	785.0
AJ19	cave	sucrose	50.0	100.0	3.0	3925.0	3925.0
AK01	cave	gypsite	15.0	30.0	1.0	353.3	117.7
AK02	cave	laminated	20.0	100.0	5.0	1570.0	2616.7
AK03	cave	calcitized	0.0	0.0	0.0	0.0	0.0
AK04	cave	laminated	15.0	30.0	4.0	353.3	471.0
AK05	cave	laminated	10.0	150.0	4.0	1177.5	1570.0
AK06	cave	laminated	100.0	100.0	8.0	7850.0	20933.3
AN01	sink	sucrose	40.0	60.0	1.0	1884.0	628.0
AN02	sink	laminated	40.0	80.0	1.0	2512.0	837.3

Table A.2. (cont.) Individual karst features documented during physical mapping within the Castile outcrop region. Width, Length, Depth, Area and Volume refer to sinkhole dimensions, where a “sink” is a filled sinkhole and a “cave” is an open sinkhole. Continued on next page.

ID #	Type	Lithology	Width (m)	Length (m)	Depth (m)	Area (m^2)	Volume (m^3)
AN03	cave	laminated	40.0	60.0	2.0	1884.0	1256.0
AN04	sink	laminated	30.0	40.0	0.5	942.0	157.0
AN05	cave	gypsite	30.0	100.0	4.0	2355.0	3140.0
AQ01	cave	gypsite	8.0	15.0	2.0	94.2	62.8
AR01	sink	gypsite	8.0	20.0	0.5	125.6	20.9
AR02	cave	gypsite	20.0	40.0	2.0	628.0	418.7
AR03	sink	gypsite	20.0	30.0	0.5	471.0	78.5
AR04	cave	gypsite	10.0	50.0	1.0	392.5	130.8
AR05	sink	gypsite	14.0	30.0	1.0	329.7	109.9
AR06	sink	gypsite	15.0	30.0	0.5	353.3	58.9
AR07	sink	gypsite	20.0	40.0	0.5	628.0	104.7
AR08	sink	gypsite	14.0	30.0	0.5	329.7	54.9
AR09	cave	laminated	5.0	40.0	2.0	157.0	104.7
AR10	sink	laminated	15.0	30.0	3.0	353.3	353.2
AR11	cave	gypsite	20.0	20.0	0.8	314.0	83.7
AR12	cave	gypsite	10.0	30.0	2.0	235.5	157.0
AR13	cave	gypsite	10.0	30.0	1.5	235.5	117.7
AR14	cave	laminated	4.0	10.0	1.5	31.4	15.7
AR15	sink	gypsite	25.0	30.0	1.0	588.8	196.2
AS01	sink	gypsite	20.0	30.0	0.5	471.0	78.5
AS02	sink	gypsite	20.0	40.0	1.0	628.0	209.3
AS03	sink	laminated	20.0	40.0	1.0	628.0	209.3
AS04	cave	gypsite	15.0	70.0	2.0	824.3	549.5
AS05	sink	gypsite	20.0	20.0	0.5	314.0	52.3
AU01	sink	laminated	50.0	60.0	2.0	2355.0	1570.0
AU02	cave	laminated	30.0	80.0	2.5	1884.0	1570.0
AU03	cave	laminated	8.0	20.0	3.0	125.6	125.6
AU04	sink	laminated	10.0	20.0	0.5	157.0	26.2
AU05	sink	gypsite	30.0	40.0	0.5	942.0	157.0
AV01	sink	gypsite	10.0	15.0	0.5	117.8	19.6
AV02	cave	gypsite	8.0	12.0	0.5	75.4	12.6
AV04	cave	gypsite	12.0	15.0	0.3	141.3	14.1
AV05	cave	gypsite	15.0	20.0	1.0	235.5	78.5
AV06	sink	gypsite	20.0	35.0	0.5	549.5	91.6
AV08	sink	gypsite	10.0	15.0	0.5	117.8	19.6
AV09	cave	gypsite	5.0	6.0	1.0	23.6	7.8
AV10	sink	gypsite	50.0	60.0	1.0	2355.0	785.0
AV11	cave	sucrose	10.0	100.0	0.5	785.0	130.8
AV12	sink	gypsite	40.0	50.0	0.5	1570.0	261.7
AV13	sink	gypsite	20.0	40.0	0.5	628.0	104.7

Table A.2. (cont.) Individual karst features documented during physical mapping within the Castile outcrop region. Width, Length, Depth, Area and Volume refer to sinkhole dimensions, where a “sink” is a filled sinkhole and a “cave” is an open sinkhole. Continued on next page.

ID #	Type	Lithology	Width (m)	Length (m)	Depth (m)	Area (m^2)	Volume (m^3)
AV14	sink	gypsite	30.0	100.0	0.5	2355.0	392.5
AW01	sink	gypsite	2.0	3.0	1.0	4.7	1.6
AY01	cave	sucrose	30.0	100.0	2.0	2355.0	1570.0
BA01	cave	laminated	20.0	40.0	1.5	628.0	314.0
BA03	cave	laminated	10.0	30.0	1.0	235.5	78.5
BA06	cave	sucrosic	10.0	>100	3.0	785.0	785.0
BA07	cave	sucrosic	10.0	10.0	1.5	78.5	39.2
BC01	cave	laminated	10.0	>50	4.0	392.5	523.3
BC02	cave	laminated	5.0	15.0	1.0	58.9	19.6
BC03	cave	laminated	>100	>100	1.5	7850.0	3925.0
BC04	cave	gypsite	5.0	20.0	3.0	78.5	78.5
BC05	cave	laminated	>100	>100	8.0	7850.0	20933.3
BC06	cave	laminated	10.0	>100	6.0	785.0	1570.0
BC07	cave	laminated	15.0	60.0	10.0	706.5	2355.0
BC08	cave	laminated	20.0	70.0	12.0	1099.0	4396.0
BC09	cave	laminated	10.0	40.0	8.0	314.0	837.3
BC10	sink	soil	7.0	9.0	0.5	49.5	8.2
BC11	cave	laminated	10.0	40.0	1.0	314.0	104.7
BC12	cave	laminated	10.0	40.0	1.0	314.0	104.7
BD01	sink	soil	100.0	>200	1.0	15700.0	5233.3
BD02	sink	gypsite	20.0	100.0	3.0	1570.0	1570.0
BD03	cave	laminated	15.0	20.0	3.5	235.5	274.7
BD04	cave	laminated	12.0	20.0	7.0	188.4	439.6
BD05	cave	laminated	10.0	5.0	4.0	39.3	52.3
BD06	cave	gypsite	15.0	50.0	3.0	588.8	588.7
BD07	cave	gypsite	20.0	40.0	4.5	628.0	942.0
BD08	cave	laminated	30.0	>200	1.5	4710.0	2355.0
BD09	sink	soil	3.0	5.0	0.5	11.8	2.0
BD10	sink	soil	3.0	5.0	4.0	11.8	15.7
BD11	sink	soil	2.0	3.0	0.3	4.7	0.5
BD12	sink	soil	6.0	10.0	1.0	47.1	15.7
BE01	cave	laminated	15.0	>100	3.0	1177.5	1177.5
BE02	cave	selenite	6.0	30.0	2.5	141.3	117.7
BE03	sink	selenite	8.0	12.0	1.0	75.4	25.1
BE04	cave	laminated	12.0	30.0	2.5	282.6	235.5
BE05	cave	laminated	10.0	20.0	2.0	157.0	104.7
BE06	cave	laminated	10.0	30.0	2.0	235.5	157.0
BG01	cave	gypsite	15.0	>100	2.0	1177.5	785.0
BG02	sink	laminated	4.0	12.0	1.0	37.7	12.6
BG03	cave	selenite	8.0	15.0	2.0	94.2	62.8

Table A.2. (cont.) Individual karst features documented during physical mapping within the Castile outcrop region. Width, Length, Depth, Area and Volume refer to sinkhole dimensions, where a “sink” is a filled sinkhole and a “cave” is an open sinkhole. Continued on next page.

ID #	Type	Lithology	Width (m)	Length (m)	Depth (m)	Area (m^2)	Volume (m^3)
BG04	cave	laminated	15.0	50.0	4.0	588.8	785.0
BG05	cave	gypsite	100.0	300.0	1.5	23550.0	11775.0
BG06	cave	gypsite	100.0	300.0	1.0	23550.0	7850.0
BG07	cave	gypsite	100.0	300.0	1.5	23550.0	11775.0
BG08	sink	gypsite	12.0	25.0	2.0	235.5	157.0
BG09	cave	gypsite	15.0	35.0	3.0	412.1	412.1
BG10	cave	gypsite	8.0	20.0	2.0	125.6	83.7
BG11	cave	gypsite	8.0	14.0	2.0	87.9	58.6
BH1	sink	gypsite	100.0	300.0	0.3	23550.0	2355.0
BH99	cave	gypsite	10.0	150.0	0.7	1177.5	274.7
BI01	cave	laminated	>100	>300	3.0	23550.0	23550.0
BI02	sink	Cox Lmst	70.0	100.0	1.0	5495.0	1831.7
BI03	cave	laminated	8.0	10.0	4.0	62.8	83.7
BI04	sink	gypsite	6.0	8.0	2.0	37.7	25.1
BI05	cave	laminated	>50	>200	4.0	7850.0	10466.7
BI06	cave	laminated	>50	>200	4.0	7850.0	10466.7
BI07	cave	laminated	50.0	100.0	4.0	3925.0	5233.3
BI08	sink	soil	50.0	100.0	2.0	3925.0	2616.7
BI8-5	cave	laminated	3.0	5.0	1.2	11.8	4.7
BI8-6	cave	laminated	25.0	50.0	0.5	981.3	163.5
BJ01	cave	laminated	30.0	>100	1.5	2355.0	1177.5
BJ02	cave	laminated	2.0	3.0	1.5	4.7	2.4
BJ03	cave	laminated	30.0	>100	1.0	2355.0	785.0
BJ04	sink	gypsite	6.0	8.0	0.6	37.7	7.5
BJ05	sink	soil	6.0	5.0	0.5	23.6	3.9
BJ06	cave	sucrosic	6.0	20.0	1.0	94.2	31.4
BJ07	cave	sucrosic	10.0	30.0	0.5	235.5	39.2
BJ08	cave	laminated	5.0	9.0	0.5	35.3	5.9
BJ09	cave	laminated	n/a	n/a	n/a	n/a	n/a
BJ10	cave	laminated	10.0	15.0	2.0	117.8	78.5
BJ11	cave	laminated	20.0	100.0	2.0	1570.0	1046.7
BJ12	cave	laminated	2.0	3.0	1.0	4.7	1.6
BJ13	cave	laminated	8.0	50.0	1.5	314.0	157.0
BJ14	cave	laminated	10.0	15.0	2.0	117.8	78.5
BJ15	cave	laminated	15.0	40.0	1.0	471.0	157.0
BJ16	cave	laminated	6.0	15.0	1.0	70.7	23.5
BJ17	sink	gypsite	6.0	8.0	0.5	37.7	6.3
BJ18	sink	soil	8.0	16.0	0.5	100.5	16.7
BJ19	cave	laminated	60.0	150.0	3.0	7065.0	7065.0
BJ20	sink	laminated	60.0	80.0	2.0	3768.0	2512.0

Table A.2. (cont.) Individual karst features documented during physical mapping within the Castile outcrop region. Width, Length, Depth, Area and Volume refer to sinkhole dimensions, where a “sink” is a filled sinkhole and a “cave” is an open sinkhole. Continued on next page.

ID #	Type	Lithology	Width (m)	Length (m)	Depth (m)	Area (m^2)	Volume (m^3)
BJ21	cave	laminated	10.0	20.0	1.5	157.0	78.5
BJ22	cave	laminated	40.0	60.0	1.5	1884.0	942.0
BJ23	sink	laminated	30.0	40.0	1.0	942.0	314.0
BJ25	cave	laminated	8.0	40.0	1.5	251.2	125.6
BJ26	cave	laminated	1.0	2.0	0.5	1.6	0.3
BJ27	cave	laminated	2.0	3.0	1.5	4.7	2.4
BJ28	cave	laminated	1.0	2.0	3.0	1.6	1.6
BJ29	cave	laminated	1.0	0.8	3.0	0.6	0.6
BJ30	cave	laminated	1.0	1.0	0.5	0.8	0.1
BJ31	cave	laminated	>100	>100	0.5	7850.0	1308.3
BJ32	sink	laminated	25.0	40.0	1.0	785.0	261.7
BJ33	cave	laminated	80.0	100.0	0.5	6280.0	1046.7
BJ34	cave	laminated	40.0	>100	1.0	3140.0	1046.7
BJ35	sink	laminated	1.0	2.5	1.5	2.0	1.0
BJ36	cave	laminated	0.5	0.7	2.0	0.3	0.2
BJ37	cave	laminated	1.0	2.0	0.5	1.6	0.3
BJ38	sink	laminated	0.3	0.3	0.7	0.1	0.0
BJ39	sink	laminated	0.2	0.2	0.5	0.0	0.0
BJ40	sink	laminated	1.0	1.5	0.4	1.2	0.2
BJ41	cave	laminated	30.0	>100	1.5	2355.0	1177.5
BJ42	cave	laminated	40.0	>100	1.0	3140.0	1046.7
BJ43	sink	soil	2.0	3.0	0.6	4.7	0.9
BJ9-2	cave	laminated	4.0	4.0	1.4	12.6	5.9
BJ9-3	cave	laminated	1.5	2.0	0.1	2.4	0.1
BJ9-5	cave	gypsite	25.0	30.0	0.4	588.8	78.5
BK1	cave	gypsite	100.0	200.0	3.0	15700.0	15700.0
BK2	sink	gypsite	20.0	50.0	0.4	785.0	104.7
BK3	sink	gypsite	25.0	100.0	0.4	1962.5	261.7
BN01	cave	sucrosic	40.0	60.0	9.0	1884.0	5652.0
BN02	sink	sucrosic	60.0	80.0	2.0	3768.0	2512.0
BN03	cave	sucrosic	30.0	60.0	2.0	1413.0	942.0
BN04	cave	sucrosic	40.0	60.0	0.5	1884.0	314.0
BN05	sink	sucrosic	30.0	60.0	1.0	1413.0	471.0
BN06	sink	sucrosic	30.0	40.0	0.5	942.0	157.0
BN07	sink	sucrosic	20.0	30.0	0.5	471.0	78.5
BN08	sink	sucrosic	10.0	15.0	0.5	117.8	19.6
BN09	sink	sucrosic	50.0	80.0	1.0	3140.0	1046.7
BN10	cave	sucrosic	30.0	70.0	2.0	1648.5	1099.0
BN11	cave	sucrosic	8.0	10.0	0.5	62.8	10.5
BN12	sink	gypsite	60.0	200.0	1.5	9420.0	4710.0

Table A.2. (cont.) Individual karst features documented during physical mapping within the Castile outcrop region. Width, Length, Depth, Area and Volume refer to sinkhole dimensions, where a “sink” is a filled sinkhole and a “cave” is an open sinkhole. Continued on next page.

ID #	Type	Lithology	Width (m)	Length (m)	Depth (m)	Area (m^2)	Volume (m^3)
BN13	cave	sucrosic	30.0	60.0	1.0	1413.0	471.0
BN14	cave	sucrosic	30.0	50.0	1.5	1177.5	588.7
BN15	sink	sucrosic	15.0	25.0	1.0	294.4	98.1
BN16	cave	sucrosic	30.0	80.0	3.0	1884.0	1884.0
BN17	cave	gypsite	10.0	30.0	3.0	235.5	235.5
BO01	sink	gypsite	20.0	40.0	2.0	628.0	418.7
BO02	sink	gypsite	40.0	7.0	2.0	219.8	146.5
BO03	sink	gypsite	10.0	>200	1.5	1570.0	785.0
BO04	sink	soil	15.0	50.0	1.0	588.8	196.2
BP01	cave	gypsite	1.5	2.5	1.0	2.9	1.0
BP02	cave	gypsite	80.0	>100	1.0	6280.0	2093.3
BP03	cave	gypsite	10.0	50.0	1.5	392.5	196.2
BP04	sink	gypsite	10.0	30.0	1.0	235.5	78.5
BP05	sink	gypsite	10.0	30.0	1.0	235.5	78.5
BP06	cave	gypsite	20.0	>100	2.5	1570.0	1308.3
BP07	sink	gypsite	8.0	20.0	0.5	125.6	20.9
BP08	sink	gypsite	8.0	15.0	0.5	94.2	15.7
BP09	cave	laminated	10.0	40.0	1.5	314.0	157.0
BP10	cave	gypsite	8.0	30.0	2.0	188.4	125.6
BP11	sink	gypsite	10.0	60.0	0.5	471.0	78.5
BP12	cave	gypsite	12.0	40.0	2.0	376.8	251.2
BP13	sink	gypsite	8.0	20.0	0.5	125.6	20.9
BP14	sink	gypsite	10.0	20.0	1.0	157.0	52.3
BP15	sink	gypsite	15.0	80.0	0.8	942.0	235.5
BQ01	sink	soil	10.0	15.0	1.0	117.8	39.2
BQ02	sink	soil	15.0	25.0	1.0	294.4	98.1
BQ03	sink	soil	10.0	15.0	0.8	117.8	29.4
BR1	cave	laminated	40.0	60.0	0.6	1884.0	376.8
BR4	sink	laminated	20.0	30.0	0.4	471.0	62.8
BR5	cave	gypsite	20.0	30.0	0.5	471.0	78.5
BR93	cave	laminated	20.0	>50	4.0	785.0	1046.7
BR94	cave	gypsite	30.0	30.0	1.5	706.5	353.2
BR95	sink	gypsite	10.0	15.0	0.5	117.8	19.6
BR96	cave	laminated	10.0	15.0	7.0	117.8	274.7
BR97	sink	laminated	20.0	40.0	0.5	628.0	104.7
BR98	sink	laminated	15.0	30.0	0.5	353.3	58.9
BR99	cave	laminated	15.0	40.0	5.0	471.0	785.0
BS99	sink	laminated	10.0	25.0	0.8	196.3	52.3
BU1	sink	laminated	20.0	25.0	0.2	392.5	26.2
BU2	cave	laminated	10.0	10.0	0.5	78.5	13.1

Table A.2. (cont.) Individual karst features documented during physical mapping within the Castile outcrop region. Width, Length, Depth, Area and Volume refer to sinkhole dimensions, where a “sink” is a filled sinkhole and a “cave” is an open sinkhole. Continued on next page.

ID #	Type	Lithology	Width (m)	Length (m)	Depth (m)	Area (m^2)	Volume (m^3)
BU3	cave	laminated	50.0	80.0	0.4	3140.0	418.7
BU4	cave	laminated	50.0	90.0	1.0	3532.5	1177.5
BU86	cave	gypsite	10.0	30.0	3.0	235.5	235.5
BU87	cave	gypsite	15.0	20.0	0.8	235.5	62.8
BU88	cave	gypsite	25.0	40.0	2.0	785.0	523.3
BU89	sink	gypsite	20.0	80.0	0.5	1256.0	209.3
BU90	sink	gypsite	5.0	8.0	0.3	31.4	3.1
BU91	sink	gypsite	10.0	15.0	0.4	117.8	15.7
BU92	sink	gypsite	10.0	15.0	0.4	117.8	15.7
BU93	sink	gypsite	4.0	20.0	0.3	62.8	6.3
BU94	cave	gypsite	2.0	4.0	1.0	6.3	2.1
BU95	sink	gypsite	20.0	>100	1.0	1570.0	523.3
BU98	cave	gypsite	10.0	>100	1.5	785.0	392.5
BU99	cave	gypsite	10.0	15.0	4.0	117.8	157.0
BV99	cave	gypsite	50.0	>100	2.5	3925.0	3270.8

Table A.2. (cont.) Individual karst features documented during physical mapping within the Castile outcrop region. Width, Length, Depth, Area and Volume refer to sinkhole dimensions, where a “sink” is a filled sinkhole and a “cave” is an open sinkhole.

Grid #	Field Mapping	DOQ Analyses
1	0	0
2	0	0
3	0	0
4	0	0
5	0	0
6	0	0
7	0	0
8	0	0
9	0	0
10	0	0
11	0	0
12	0	0
13	1	0
14	1	0
15	1	0
16	1	0
17	1	0
18	1	0
19	2	0
20	3	0
21	3	0
22	3	0
23	3	0
24	4	1
25	4	1

Grid #	Field Mapping	DOQ Analyses
26	4	1
27	5	1
28	5	1
29	5	2
30	6	2
31	6	2
32	6	2
33	9	2
34	9	2
35	10	2
36	10	3
37	11	3
38	11	3
39	12	3
40	12	5
41	12	5
42	14	5
43	15	6
44	15	7
45	16	8
46	17	9
47	17	9
48	20	11
49	31	12
50	48	35

Table A.3. Comparison of quantity of karst features identified within the Castile Formation during field mapping versus features identified through DOQ analyses.

Cave	Cross Section Area (m^2)	Distance from Entrance (m)
Bobcat	11.18	2.79
Bobcat	8.81	6.47
Bobcat	10.14	9.02
Bobcat	0.54	12.88
Bobcat	0.18	17.16
Bobcat	0.14	19.91
Bobcat	0.12	24.56
Dead East	1.45	1.44
Dead East	0.64	5.53
Dead East	0.55	9.95
Dead East	0.46	15.02
Dead East	0.49	19.72
Dead East	0.54	24.14
Dead East	0.50	28.28
Dead East	0.39	32.88
Dead East	0.57	38.98
Dead East	0.28	44.56
Exaggerated	1.33	0.74
Exaggerated	0.49	2.93
Exaggerated	0.12	3.86
Lightening	0.39	1.12
Lightening	0.17	4.05
Lightening	0.08	6.84
Room	3.36	1.40
Room	3.29	10.84
Room	1.45	18.60
Room	0.26	22.14
Turtle	0.95	0.70
Turtle	0.48	1.91
Turtle	0.99	4.23
Turtle	0.62	6.28
Turtle	1.04	8.19
Zombie	1.90	2.84
Zombie	2.01	8.79
Zombie	0.97	12.65
Zombie	0.73	19.67
Zombie	1.02	21.95
Zombie	0.77	28.93
Zombie	0.32	36.33
Zombie	0.24	42.09

Table A.4. Comparison of cross sectional area versus distance from insurgence for epigene caves surveyed in the Castile Formation during this study.

CAVE	LENGTH (m)	AZIMUTH
Bee Line	5.2	3.0
Bee Line	5.9	7.5
Bee Line	5.3	15.5
Bee Line	27.6	16.4
Bee Line	5.2	38.0
Bee Line	10.4	50.5
Bee Line	5.8	61.0
Bee Line	3.5	63.0
Bee Line	16.8	66.5
Bee Line	43.3	74.8
Bee Line	4.1	75.0
Bee Line	5.8	89.0
Bee Line	10.5	150.7
Bee Line	5.2	152.4
Bee Line	7.6	168.0
Birthday	20.1	15.7
Birthday	14.7	21.5
Birthday	8.9	33.7
Birthday	13.8	40.8
Birthday	20.1	60.0
Birthday	20.0	66.4
Birthday	9.0	66.6
Birthday	7.1	68.1
Birthday	5.4	68.7
Birthday	5.9	81.8
Birthday	8.7	87.0
Birthday	11.0	88.0
Birthday	11.3	100.1
Birthday	2.3	101.0
Birthday	4.6	101.0
Birthday	12.7	110.5
Birthday	21.4	124.4
Birthday	10.6	126.2
Birthday	4.9	135.0
Birthday	13.0	141.1
Birthday	9.6	145.5
Birthday	10.6	151.4
Blck Widow	12.3	85.0
Blck Widow	18.1	100.0
Bobcat	3.4	2.8

CAVE	LENGTH (m)	AZIMUTH
Bobcat	10.1	39.3
Bobcat	5.9	56.5
Bobcat	6.5	61.1
Bobcat	15.7	61.4
Bobcat	4.3	83.3
Bobcat	7.0	115.3
Bobcat	3.5	127.1
Bobcat	10.1	140.1
Bobcat	14.2	169.7
Bobcat	23.4	179.8
Brantley	1.6	2.2
Brantley	2.7	6.1
Brantley	5.1	8.5
Brantley	9.6	10.6
Brantley	23.0	28.5
Brantley	0.8	31.9
Brantley	7.0	36.8
Brantley	4.6	39.5
Brantley	13.3	45.0
Brantley	15.7	53.7
Brantley	13.3	62.5
Brantley	9.0	62.8
Brantley	6.0	77.3
Brantley	10.4	89.0
Brantley	9.7	100.5
Brantley	8.1	105.0
Brantley	3.3	110.1
Brantley	12.0	119.3
Brantley	11.4	122.1
Brantley	3.7	123.0
Brantley	2.1	133.0
Brantley	49.2	135.9
Brantley	11.4	143.9
Brantley	4.8	144.2
Brantley	9.0	145.1
Brantley	12.2	162.7
Brantley	7.2	162.9
Brantley	2.1	173.1
Room	2.5	54.5
Room	1.5	72.8

Table A.5. Length and orientation of individual passages in caves surveyed during this study. Continued on next page.

CAVE	LENGTH (m)	AZIMUTH
Room	8.7	87.1
Room	5.3	93.8
Room	7.8	113.2
Room	10.2	164.2
Room	1.0	164.3
Chamber	2.0	38.4
Chamber	2.2	50.5
Chamber	2.3	82.0
Chamber	0.7	85.6
Chamber	1.1	116.2
Complex	9.2	9.4
Complex	5.0	17.5
Complex	4.2	39.2
Complex	3.5	54.5
Complex	10.0	56.8
Complex	5.5	74.9
Complex	7.3	84.8
Complex	3.2	88.0
Complex	5.5	93.5
Complex	7.5	94.8
Complex	11.7	107.2
Complex	12.6	131.1
Complex	3.6	142.3
Complex	5.2	153.4
Complex	5.3	155.2
Complex	3.0	162.7
Complex	12.6	168.4
Complex	4.9	178.7
Contortion	3.0	43.2
Contortion	5.1	43.7
Contortion	6.6	49.8
Contortion	10.0	49.9
Contortion	8.2	56.2
Contortion	14.0	72.0
Contortion	13.9	78.5
Contortion	18.4	96.6
Contortion	20.9	102.5
Contortion	5.9	109.4
Contortion	7.9	130.0
Contortion	5.5	135.2

CAVE	LENGTH (m)	AZIMUTH
Contortion	5.6	139.5
Contortion	3.0	143.3
Contortion	13.7	145.3
Contortion	5.1	159.3
Contortion	7.5	169.5
Crystal	2.0	0.0
Crystal	2.2	0.0
Crystal	5.9	1.5
Crystal	1.9	12.0
Crystal	11.7	13.0
Crystal	1.5	17.5
Crystal	5.9	20.5
Crystal	4.5	24.5
Crystal	7.3	24.5
Crystal	2.7	24.7
Crystal	2.0	30.0
Crystal	3.9	31.0
Crystal	9.4	31.7
Crystal	5.5	33.0
Crystal	4.3	33.1
Crystal	7.6	37.2
Crystal	5.7	40.4
Crystal	3.3	42.0
Crystal	21.3	44.6
Crystal	3.5	45.0
Crystal	2.2	46.4
Crystal	4.5	52.0
Crystal	10.3	54.3
Crystal	2.9	55.6
Crystal	1.3	55.8
Crystal	4.2	56.3
Crystal	6.4	57.0
Crystal	16.0	57.3
Crystal	5.2	59.2
Crystal	11.6	59.2
Crystal	2.1	59.6
Crystal	3.7	59.7
Crystal	2.4	60.0
Crystal	3.5	60.8
Crystal	0.9	61.2

Table A.5. (cont.) Length and orientation of individual passages in caves surveyed during this study. Continued on next page.

CAVE	LENGTH (m)	AZIMUTH
Crystal	3.4	62.0
Crystal	5.0	62.4
Crystal	9.5	63.5
Crystal	5.0	64.3
Crystal	3.3	67.1
Crystal	2.5	68.2
Crystal	3.5	69.5
Crystal	4.6	75.1
Crystal	4.3	76.7
Crystal	7.6	77.3
Crystal	2.4	78.5
Crystal	5.7	89.2
Crystal	9.1	91.0
Crystal	4.2	91.1
Crystal	2.2	92.1
Crystal	2.9	92.3
Crystal	3.7	93.7
Crystal	2.5	95.4
Crystal	3.7	95.5
Crystal	2.1	96.3
Crystal	5.2	97.9
Crystal	2.1	98.7
Crystal	8.1	99.9
Crystal	17.1	100.8
Crystal	3.1	104.2
Crystal	10.3	104.6
Crystal	2.9	104.8
Crystal	3.3	107.8
Crystal	2.8	108.4
Crystal	2.4	109.6
Crystal	2.2	112.4
Crystal	1.6	115.3
Crystal	2.9	116.9
Crystal	11.7	117.7
Crystal	4.0	117.8
Crystal	2.7	118.1
Crystal	5.6	118.2
Crystal	1.5	121.2
Crystal	12.6	122.7
Crystal	3.7	126.7
Crystal	7.2	128.7
Crystal	1.1	130.4
Crystal	6.0	130.5
Crystal	5.9	132.3
Crystal	3.9	134.6
Crystal	2.6	135.0
Crystal	2.0	136.6
Crystal	7.2	136.8
Crystal	4.0	138.6
Crystal	5.9	139.6
Crystal	4.2	144.1
Crystal	5.0	144.1
Crystal	8.7	145.0
Crystal	5.9	145.1
Crystal	4.3	145.7
Crystal	6.4	147.4
Crystal	9.6	149.2
Crystal	4.0	150.0
Crystal	1.1	150.5
Crystal	10.7	151.2
Crystal	4.4	151.4
Crystal	8.1	153.7
Crystal	6.9	154.3
Crystal	2.0	155.9
Crystal	1.0	156.5
Crystal	3.1	158.1
Crystal	5.0	158.9
Crystal	12.6	161.0
Crystal	3.6	163.4
Crystal	5.7	164.3
Crystal	10.4	165.2
Crystal	1.4	166.8
Crystal	2.9	170.5
Crystal	5.5	171.4
Crystal	5.6	171.9
Crystal	6.7	174.2
Crystal	3.8	174.6
Crystal	8.9	177.2
Crystal	3.5	179.3
D. Bunny	8.0	5.1

Table A.5. (cont.) Length and orientation of individual passages in caves surveyed during this study. Continued on next page.

CAVE	LENGTH (m)	AZIMUTH
D. Bunny	6.2	5.3
D. Bunny	4.8	25.2
D. Bunny	9.9	26.4
D. Bunny	2.8	29.5
D. Bunny	3.9	32.7
D. Bunny	18.7	34.2
D. Bunny	5.3	40.6
D. Bunny	3.9	41.3
D. Bunny	8.6	43.3
D. Bunny	8.3	46.8
D. Bunny	5.8	47.3
D. Bunny	11.2	49.2
D. Bunny	4.3	50.4
D. Bunny	7.7	50.7
D. Bunny	11.4	51.2
D. Bunny	7.7	52.3
D. Bunny	3.5	56.2
D. Bunny	2.5	56.8
D. Bunny	20.6	57.5
D. Bunny	7.9	57.6
D. Bunny	5.9	59.0
D. Bunny	14.5	71.2
D. Bunny	15.4	84.7
D. Bunny	15.1	85.7
D. Bunny	13.4	86.9
D. Bunny	4.2	89.0
D. Bunny	12.2	91.5
D. Bunny	5.1	94.1
D. Bunny	11.5	94.8
D. Bunny	9.3	102.4
D. Bunny	8.8	114.5
D. Bunny	7.9	114.5
D. Bunny	12.5	114.9
D. Bunny	8.0	121.3
D. Bunny	5.6	121.9
D. Bunny	3.3	122.8
D. Bunny	5.5	126.6
D. Bunny	10.4	126.6
D. Bunny	6.6	127.3
D. Bunny	9.2	127.7

CAVE	LENGTH (m)	AZIMUTH
D. Bunny	9.5	130.5
D. Bunny	16.0	132.2
D. Bunny	8.0	134.5
D. Bunny	6.5	135.0
D. Bunny	8.7	140.3
D. Bunny	3.9	142.7
D. Bunny	9.7	144.0
D. Bunny	8.5	145.4
D. Bunny	13.2	145.4
D. Bunny	12.9	149.2
D. Bunny	11.2	151.6
D. Bunny	8.2	154.3
D. Bunny	3.8	155.4
D. Bunny	3.7	155.6
D. Bunny	4.1	157.2
D. Bunny	4.1	157.3
D. Bunny	6.3	163.2
D. Bunny	10.9	172.2
D. Bunny	2.2	176.3
D. Bunny	4.5	177.3
D. Bunny	4.8	177.9
Dead East	35.2	91.0
Dead East	12.9	92.7
Delayed	1.7	24.5
Delayed	2.2	81.8
Delayed	1.0	162.4
Exaggerated	2.0	2.0
Exaggerated	2.0	158.1
Hassle Hole	9.9	29.4
Hassle Hole	5.3	34.0
Hassle Hole	2.7	41.5
Hassle Hole	1.4	44.0
Hassle Hole	6.8	50.3
Hassle Hole	6.2	51.7
Hassle Hole	13.6	54.9
Hassle Hole	12.1	60.0
Hassle Hole	3.9	66.9
Hassle Hole	12.0	70.2
Hassle Hole	2.7	74.5
Hassle Hole	3.8	79.1

Table A.5. (cont.) Length and orientation of individual passages in caves surveyed during this study. Continued on next page.

CAVE	LENGTH (m)	AZIMUTH
Hassle Hole	3.8	80.5
Hassle Hole	3.3	83.1
Hassle Hole	3.4	83.4
Hassle Hole	5.1	87.4
Hassle Hole	9.8	88.7
Hassle Hole	6.6	89.1
Hassle Hole	3.2	105.8
Hassle Hole	13.3	107.1
Hassle Hole	2.8	111.8
Hassle Hole	7.2	113.8
Hassle Hole	3.3	117.6
Hassle Hole	8.0	128.4
Hassle Hole	1.3	134.0
Hassle Hole	1.2	147.2
Hassle Hole	4.8	170.5
Lightening	2.3	21.1
Lightening	3.4	36.3
Lightening	0.8	142.3
Lightening	0.9	148.7
Lightening	3.0	152.5
Pokey	3.5	68.7
Pokey	4.2	81.8
Pokey	7.0	105.3
Tick Crawl	1.8	15.6
Tick Crawl	2.4	28.0
Tick Crawl	7.1	69.5
Tick Crawl	2.7	93.4
Tick Crawl	3.0	106.9
Tick Crawl	4.3	120.3
Tick Crawl	4.7	121.0
Tick Crawl	3.6	144.7
Tick Crawl	6.4	153.3
Tick Crawl	3.0	155.7
Tiger	3.3	6.2
Tiger	15.5	23.5
Tiger	6.9	70.8
Tiger	3.8	80.4
Tiger	5.4	141.7
Tortoise	4.8	19.2
Tortoise	5.8	95.8

CAVE	LENGTH (m)	AZIMUTH
Worthwhile	5.7	13.9
Worthwhile	3.3	55.7
Worthwhile	4.1	67.1
Worthwhile	8.0	102.3
Zombie	11.4	25.5
Zombie	3.0	29.1
Zombie	7.0	30.2
Zombie	7.1	113.3
Zombie	9.5	113.8
Zombie	3.1	115.4
Zombie	5.0	121.9
Zombie	7.3	139.3
Zombie	4.6	141.3

Table A.5. (cont.) Length and orientation of individual passages in caves surveyed during this study.

API #	Cave Height (ft)	Cave Elevation (ft asl)
423710060100	2	1354
423710060100	1	1348.5
423710060100	5	1324.5
423710060100	10	1299
423710060100	4	1290
423710060100	2	1285
423710060100	1	1216.5
423710060100	1	1195.5
423710060300	2	1138
423710060300	3	1130.5
423710086700	2	1272
423710086700	10	1248
423710094600	1	1161.5
423710094600	3	1269.5
423710098100	4	1207
423710098100	1	1343.5
423710216400	2	1115
423710216400	3	1228.5
423710216400	2	1221
423710216400	3	1178.5
423710216400	2	1162
423710216400	2	1157
423710216600	2	1304
423710216600	2	1300
423710216600	1	1197.5
423710216600	6	1190
423710216600	1	1175.5
423710216600	1	1170.5
423710216600	2	1125
423710216600	3	1120.5
423710216600	3	1111.5
423710217000	3	1315.5
423710217000	5	1270.5
423710217100	4	1265
423710217100	2	1127
423710217100	4	1120
423710217100	2	1108
423710217100	1	1096.5
423710217100	1	1087.5
423710217100	2	1077

API #	Cave Height (ft)	Cave Elevation (ft asl)
423710217200	2	1218
423710217400	2	1219
423710217800	4	1200
423710221000	27	1147.5
423710221400	7	1173.5
423710221500	2	1238
423710221500	3	1226.5
423710221700	4	1201
423710221800	2	1200
423710222000	1	1227.5
423710222000	10	1210
423710222100	12	1190
423710222200	8	1214
423710222400	4	1185
423710222500	6	1244
423710222600	18	1229
423710245000	4	1029
423710245000	1	1008.5
423710245000	1	1173.5
423710245000	1	1165.5
423710245000	4	1149
423710245000	1	1110.5
423710246600	68	1295
423710246600	1	1242.5
423710246600	2	1154
423710246600	4	1132
423710246600	6	1120
423710246600	2	1102
423710246700	2	1188
423710246700	2	1182
423710246700	1	1116.5
423710246700	3	1112.5
423710246800	2	1052
423710246800	1	930.5
423710246800	2	1141
423710246800	3	1220.5
423710246800	1	1194.5
423710246800	1	1181.5
423710246800	2	1156
423710246800	1	1150.5

Table A.6. Location of caves within the Yates Field Unit based on petrophysical analyses of wireline logs. API # is the unique well identifier. Continued on next page.

API #	Cave Height (ft)	Cave Elevation (ft asl)
423710246800	1	1112.5
423710246900	6	1135
423710246900	1	1178.5
423710247000	5	1243.5
423710247000	2	1153
423710247300	1	1235.5
423710247400	2	1168
423710247400	1	1148.5
423710247400	3	1103.5
423710247400	2	1096
423710247500	6	1145
423710247800	5	1218.5
423710285400	2	1169
423710301100	1	1222.5
423710301100	1	1087.5
423710301300	2	1297
423710312000	2	1173
423710312000	2	1199
423710312000	1	1190.5
423710314800	3	1188.5
423710379400	1	1129.5
423710396700	2	1104
423710400800	1	1101.5
423710420900	4	1214
423710420900	4	1192
423710421000	17	1231.5
423710421000	4	1218
423710421000	3	1209.5
423710421100	4	1205
423710421100	6	1195
423710421100	3	1183.5
423710421200	2	1180
423710421200	3	1167.5
423710421300	2	1224
423710421300	3	1217.5
423710421300	2	1297
423710421400	6	1217
423710421400	1	1210.5
423710421400	16	1199
423710421400	4	1187
423710421400	3	1176.5
423710427600	12	1246
423710428000	2	1117
423710428000	2	1097
423710429000	2	1083
423710429000	3	1066.5
423710430500	6	1152
423710430500	1	1145.5
423710430500	3	1084.5
423710430600	6	1259
423710430600	4	1149
423710430600	4	1142
423710430600	4	1094
423710430800	1	1121.5
423710430800	2	1084
423710431000	5	1142.5
423710431100	7	1262.5
423710431400	5	1152.5
423710431400	3	1099.5
423710431500	1	1157.5
423710431500	2	1149
423710431500	3	1143.5
423710431500	2	1129
423710431500	1	1097.5
423710431500	1	996.5
423710432100	14	1181
423710432300	2	1272
423710444800	3	1156.5
423710555800	4	1202
423710556000	3	1143.5
423710560800	2	1079
423710560800	11	1132.5
423710570700	3	1239.5
423710570700	5	1232.5
423710570700	1	1223.5
423710570700	3	1217.5
423710570700	15	1198.5
423710570900	1	1198.5
423710571100	4	1108
423710571100	3	1082.5

Table A.6. (cont.) Location of caves within the Yates Field Unit based on petrophysical analyses of wireline logs. API # is the unique well identifier. Continued on next page.

API #	Cave Height (ft)	Cave Elevation (ft asl)
423710571700	10	1150
423710571800	7	1215.5
423710572600	12	1195
423710573300	5	1130.5
423710573300	3	1117.5
423710573500	5	1102.5
423710573700	3	1148.5
423710573700	4	1132
423710573700	4	1283
423710573700	7	1274.5
423710573700	3	1266.5
423710575300	2	1233
423710575300	2	1193
423710575500	6	1147
423710576500	3	1133.5
423710576500	1	1096.5
423710576500	3	1089.5
423710576500	4	1237
423710576500	45	1210.5
423710605000	4	1229
423710605000	26	1180
423710605000	7	1149.5
423710605200	2	1115
423710605300	2	1387
423710605300	2	1370
423710605300	2	1363
423710605400	3	1155.5
423710605400	2	1150
423710605400	1	1109.5
423710605400	3	1243.5
423710605400	3	1222.5
423710605500	3	1259.5
423710605500	2	1249
423710605500	1	1237.5
423710605600	2	1205
423710605800	1	842.5
423710605900	2	1050
423710606000	2	1308
423710606100	4	1133
423710606100	4	1161
423710606200	3	1137.5
423710606300	6	1266
423710606300	2	1257
423710606300	3	1252.5
423710606300	3	1229.5
423710606300	1	1433.5
423710606300	1	1430.5
423710606300	1	1382.5
423710606300	1	1362.5
423710606300	1	1351.5
423710606600	5	1304.5
423710606600	2	1222
423710606800	1	1304.5
423710606800	3	1295.5
423710606900	2	1327
423710606900	2	1321
423710606900	6	1287
423710606900	1	1272.5
423710606900	2	1256
423710606900	5	1158.5
423710606900	2	1450
423710607000	1	1280.5
423710607100	2	1158
423710607100	1	1152.5
423710607100	2	1148
423710607300	3	1148.5
423710607400	3	1080.5
423710607400	1	1265.5
423710607400	2	1259
423710607500	2	1107
423710607500	3	1233.5
423710607500	7	1222.5
423710607500	12	1211
423710607600	8	1186
423710607800	2	1109
423710607800	4	1225
423710607800	11	1212.5
423710607800	9	1196.5
423710607900	1	1178.5
423710607900	4	1150

Table A.6. (cont.) Location of caves within the Yates Field Unit based on petrophysical analyses of wireline logs. API # is the unique well identifier. Continued on next page.

API #	Cave Height (ft)	Cave Elevation (ft asl)
423710608200	2	1135
423710608200	1	1071.5
423710608300	3	1181.5
423710608300	3	1168.5
423710608300	7	1152.5
423710608601	1	1139.5
423710608601	5	1121.5
423710608601	2	1304
423710609100	5	1265.5
423710609100	3	1180.5
423710609100	3	1174.5
423710609400	1	1240.5
423710609400	18	1207
423710609400	1	1195.5
423710609400	2	1192
423710609500	2	1220
423710609500	2	1143
423710609800	3	1353.5
423710609800	2	1327
423710609800	1	1217.5
423710610200	6	1231
423710610200	2	1219
423710610200	1	1213.5
423710610200	2	1155
423710610200	3	1405.5
423710610200	2	1296
423710610300	3	1336.5
423710610300	2	1331
423710610400	9	1223.5
423710610400	4	1178
423710610600	4	1256
423710610800	3	1114.5
423710610800	2	1108
423710611100	4	1243
423710611100	3	1229.5
423710611100	2	1200
423710611100	3	1093.5
423710611100	2	1085
423710611100	2	1322
423710611100	2	1305

API #	Cave Height (ft)	Cave Elevation (ft asl)
423710611400	1	1005.5
423710611400	2	1131
423710611400	2	1125
423710611500	9	1215.5
423710611500	5	1179.5
423710611500	2	1317
423710611700	3	1153.5
423710611700	2	1380
423710611800	3	1163.5
423710611800	1	1301.5
423710611800	3	1264.5
423710611800	8	1257
423710611800	4	1245
423710611900	7	1300.5
423710611900	2	1293
423710611900	4	1282
423710611900	5	1178.5
423710611900	7	1170.5
423710611900	13	1093.5
423710612400	4	1056
423710612400	1	1180.5
423710612400	1	1174.5
423710612400	3	1138.5
423710612400	3	1132.5
423710612500	2	1179
423710612500	6	1147
423710612600	6	1135
423710612800	1	1082.5
423710612900	9	1310.5
423710612900	2	1281
423710612900	2	1157
423710613300	1	1236.5
423710613300	2	1185
423710613300	7	1164.5
423710613300	3	1157.5
423710613300	2	1145
423710613400	13	1321.5
423710613500	2	1245
423710613500	15	1227.5
423710613500	3	1133.5

Table A.6. (cont.) Location of caves within the Yates Field Unit based on petrophysical analyses of wireline logs. API # is the unique well identifier. Continued on next page.

API #	Cave Height (ft)	Cave Elevation (ft asl)
423710613700	11	1154.5
423710613700	4	1137
423710613900	3	1180.5
423710614000	3	1392.5
423710614000	3	1381.5
423710640500	9	1225.5
423710640500	7	1189.5
423710640500	4	1280
423710640700	4	1160
423710640700	2	1150
423710640800	2	1244
423710640800	2	1222
423710640800	4	1469
423710640800	2	1433
423710640800	2	1170
423710641400	1	1191.5
423710641400	2	1225
423710641400	7	1298.5
423710641400	2	1257
423710641400	2	1056
423710641600	1	1182.5
423710652000	5	1244.5
423710652000	3	1235.5
423710652000	2	1193
423710652000	3	1412.5
423710652000	2	1379
423710652200	3	1211.5
423710652200	2	1163
423710652700	6	1218
423710652700	2	1211
423710652700	4	1204
423710652700	2	1194
423710652700	2	1173
423710652700	2	1153
423710652700	2	1139
423710652800	6	1285
423710652800	1	1169.5
423710652800	10	1151
423710652800	2	1132
423710652800	2	1073

API #	Cave Height (ft)	Cave Elevation (ft asl)
423710653000	5	1235.5
423710653000	2	1403
423710653200	8	1356
423710653200	1	1349.5
423710653200	3	1336.5
423710653200	4	1232
423710653200	3	1215.5
423710653200	2	1206
423710653200	2	1153
423710653300	2	1159
423710653400	4	1111
423710653400	2	1412
423710653400	7	1163.5
423710653400	4	1155
423710653800	1	1157.5
423710653800	2	1224
423710653800	3	1149.5
423710654500	1	1092.5
423710654500	4	1324
423710654500	3	1317.5
423710654500	3	1308.5
423710654500	2	1370
423710654900	2	1026
423710654900	2	1072
423710654900	2	1015
423710654900	9	1272.5
423710654900	3	1261.5
423710654900	3	1137.5
423710654900	2	1114
423710655000	16	1370
423710655000	2	1465
423710655100	4	1073
423710655100	2	1056
423710655100	3	1158.5
423710655100	2	1150
423710655200	1	1092.5
423710655200	3	1354.5
423710655200	1	1198.5
423710655200	7	1170.5
423710655200	2	1119

Table A.6. (cont.) Location of caves within the Yates Field Unit based on petrophysical analyses of wireline logs. API # is the unique well identifier. Continued on next page.

API #	Cave Height (ft)	Cave Elevation (ft asl)
423710655300	3	1188.5
423710655400	4	1325
423710655500	3	1267.5
423710655500	3	1146.5
423710655500	2	1134
423710655500	2	1115
423710655500	2	1220
423710655500	3	1151.5
423710655800	1	1348.5
423710655800	4	1153
423710655800	2	1099
423710655800	2	1049
423710656400	10	1140
423710656500	2	1301
423710656500	2	1266
423710656500	17	1224.5
423710656500	2	1208
423710656500	3	1160.5
423710656600	3	1227.5
423710656600	3	1201.5
423710656700	5	1218.5
423710656800	4	1373
423710656800	3	1181.5
423710656800	2	1159
423710656900	1	1192.5
423710657000	1	913.5
423710657000	1	883.5
423710657000	1	864.5
423710657000	2	1342
423710657000	2	1335
423710657000	2	1269
423710657200	4	1168
423710657200	3	1237.5
423710657400	1	1067.5
423710657400	1	1247.5
423710657400	3	1205.5
423710657500	5	1242.5
423710657500	12	1226
423710658000	5	1192.5
423710658000	5	1181.5
423710658300	5	1239.5
423710658300	10	1197
423710658300	4	1188
423710658300	11	1178.5
423710658300	7	1168.5
423710658300	3	1109.5
423710658300	7	1067.5
423710659100	7	1208.5
423710659100	4	1199
423710659100	2	1177
423710659200	3	1205.5
423710659200	4	1198
423710659200	3	1168.5
423710659200	4	1156
423710659200	4	1146
423710659200	3	1135.5
423710659200	4	1108
423710668400	4	1201
423710668400	4	1169
423710668700	13	1187.5
423710668700	10	1166
423710668900	2	1090
423710668900	2	1210
423710676600	4	1192
423710676600	2	1160
423710676600	1	1155.5
423710676600	2	1152
423710676600	30	1128
423710676600	14	1104
423710680200	2	1198
423710680700	1	1315.5
423710680700	5	1237.5
423710680700	3	1220.5
423710680700	2	1213
423710680700	4	1201
423710680700	2	1424
423710682300	4	1186
423710682300	1	1177.5
423710682300	4	1152
423710682300	2	1121

Table A.6. (cont.) Location of caves within the Yates Field Unit based on petrophysical analyses of wireline logs. API # is the unique well identifier. Continued on next page.

API #	Cave Height (ft)	Cave Elevation (ft asl)
423710682800	3	1161.5
423710685500	2	1140
423710685500	3	1135.5
423710685500	2	1110
423710685500	6	1088
423710685900	2	1209
423710685900	2	1204
423710685900	2	1198
423710686600	9	1232.5
423710686600	2	1192
423710686600	3	1180.5
423710686600	2	1155
423710686700	8	1241
423710686700	2	1115
423710687100	3	1151.5
423710687100	2	1146
423710687100	2	1133
423710687100	1	1104.5
423710687100	1	1092.5
423710687200	3	1107.5
423710687200	2	1091
423710687200	3	1073.5
423710687200	2	1067
423710687400	2	1217
423710687400	6	1191
423710687400	2	1138
423710687400	2	1427
423710687400	2	1419
423710687400	1	1272.5
423710687500	1	1176.5
423710687500	32	1298
423710687500	3	1441.5
423710687600	2	1275
423710687600	5	1267.5
423710687600	4	1247
423710687600	3	1241.5
423710687600	3	1202.5
423710687600	4	1167
423710687600	1	1484.5
423710687700	6	1229

API #	Cave Height (ft)	Cave Elevation (ft asl)
423710687700	3	1217.5
423710687700	2	1210
423710687700	2	1205
423710687700	2	1199
423710687700	2	1188
423710687700	4	1174
423710698400	3	1271.5
423710698400	2	1254
423710698400	2	1163
423710698400	3	1151.5
423710698500	3	1283.5
423710698500	9	1276.5
423710698500	1	1269.5
423710698500	4	1264
423710698500	1	1254.5
423710698500	2	1252
423710698500	6	1246
423710698500	1	1209.5
423710698500	2	1442
423710698500	1	1397.5
423710698600	11	1229.5
423710698800	3	1237.5
423710699000	11	1229.5
423710699000	3	1220.5
423710702700	2	1144
423710705100	2	1131
423710705100	2	1125
423710705100	1	1190.5
423710705100	1	1151.5
423710705100	1	1111.5
423710705300	5	1152.5
423710706100	3	1095.5
423710706100	2	1207
423710706100	3	1192.5
423710706500	14	1203
423710706500	1	1142.5
423710706500	3	1135.5
423710706700	3	1430.5
423710706700	3	1421.5
423710707200	5	1315.5

Table A.6. (cont.) Location of caves within the Yates Field Unit based on petrophysical analyses of wireline logs. API # is the unique well identifier. Continued on next page.

API #	Cave Height (ft)	Cave Elevation (ft asl)
423710707200	2	1258
423710707200	2	1248
423710707200	3	1245.5
423710707200	7	1235.5
423710707200	2	1229
423710707200	1	1223.5
423710707200	8	1152
423710707200	1	1432.5
423710707400	2	1336
423710707500	3	1201.5
423710707500	5	1265.5
423710707500	2	1252
423710707500	27	1232.5
423710707500	2	1214
423710707500	10	1180
423710707800	2	890
423710707800	3	859.5
423710707800	2	1121
423710708100	3	1221.5
423710708100	9	1205.5
423710708600	3	1289.5
423710708600	7	1281.5
423710708700	12	1151
423710708700	9	1269.5
423710708900	4	1293
423710708900	2	1273
423710708900	8	1266
423710708900	10	1255
423710708900	5	1241.5
423710708900	5	1230.5
423710708900	3	1193.5
423710708900	2	1183
423710708900	19	1143.5
423710708900	1	1110.5
423710709000	9	1373.5
423710709000	2	1362
423710709000	4	1219
423710709000	4	1206
423710709000	3	1186.5
423710709000	2	1171

API #	Cave Height (ft)	Cave Elevation (ft asl)
423710709200	3	1306.5
423710709300	6	1244
423710709300	2	1199
423710709300	5	1194.5
423710709300	2	1189
423710709300	4	1180
423710709300	3	1167.5
423710709300	3	1146.5
423710709400	1	1113.5
423710709400	4	1107
423710709400	2	1101
423710709400	1	1096.5
423710709400	4	1196
423710709700	2	1249
423710709700	2	1243
423710709700	2	1240
423710709700	2	1157
423710709800	2	1312
423710709800	3	1285.5
423710709800	2	1262
423710710000	4	1243
423710710200	3	1146.5
423710710200	8	1135
423710710200	4	1269
423710710200	4	1262
423710710200	2	1160
423710710400	4	1161
423710710800	13	1160.5
423710710900	4	1209
423710710900	1	1201.5
423710710900	11	1190.5
423710710900	12	1177
423710710900	2	1146
423710711100	5	1398.5
423710711100	2	1391
423710711100	1	1188.5
423710711100	1	1169.5
423710711100	1	1156.5
423710711100	2	1140
423710711300	1	1149.5

Table A.6. (cont.) Location of caves within the Yates Field Unit based on petrophysical analyses of wireline logs. API # is the unique well identifier. Continued on next page.

API #	Cave Height (ft)	Cave Elevation (ft asl)
423710711300	2	1140
423710712100	3	1216.5
423710712100	1	1141.5
423710712100	1	1089.5
423710712100	3	1226.5
423710712100	2	1086
423710712100	7	1243.5
423710712300	2	1248
423710713300	4	1358
423710713300	2	1344
423710713300	1	1336.5
423710713300	1	1326.5
423710713300	3	1217.5
423710713300	2	1212
423710713300	1	1183.5
423710713400	1	1022.5
423710713600	3	1113.5
423710713700	6	1101
423710713700	4	1173
423710713700	2	1130
423710713700	2	1076
423710713800	3	1197.5
423710714000	6	1325
423710714700	1	1085.5
423710714700	4	1117
423710714700	2	1100
423710714700	1	1226.5
423710714800	2	1216
423710714800	5	1144.5
423710714900	2	1252
423710714900	4	1291
423710715000	3	1219.5
423710715000	3	1199.5
423710715100	4	1227
423710715200	3	1236.5
423710715200	2	1206
423710715800	9	1206.5
423710715800	30	1178
423710715800	2	1120
423710715800	2	1115
423710715800	6	1100
423710715900	3	1186.5
423710715900	2	1183
423710715900	2	1362
423710716000	2	1294
423710716000	2	1262
423710716000	1	1258.5
423710716000	1	1254.5
423710716000	2	1248
423710716000	6	1410
423710716000	2	1394
423710716000	2	1384
423710716100	4	1200
423710717300	3	1405.5
423710717300	2	1401
423710717300	4	1366
423710717300	2	1357
423710717300	2	1246
423710717300	2	1228
423710717300	6	1222
423710717300	2	1213
423710717300	3	1139.5
423710717300	2	1465
423710717300	10	1414
423710717900	2	1359
423710717900	1	1323.5
423710717900	2	1219
423710717900	1	1178.5
423710717900	3	1170.5
423710717900	2	1124
423710717900	11	1402.5
423710718400	3	1137.5
423710718400	2	1109
423710718400	3	1159.5
423710718400	2	1152
423710718500	1	1160.5
423710718700	4	1235
423710718700	6	1180
423710718700	2	1167
423710718900	3	1182.5

Table A.6. (cont.) Location of caves within the Yates Field Unit based on petrophysical analyses of wireline logs. API # is the unique well identifier. Continued on next page.

API #	Cave Height (ft)	Cave Elevation (ft asl)
423710718900	1	1141.5
423710719100	2	1211
423710719100	2	1200
423710719100	2	1186
423710719100	2	1178
423710719300	2	1091
423710719500	1	1256.5
423710719500	6	1083
423710719600	7	1189.5
423710719600	3	1170.5
423710721600	2	1167
423710721600	4	1103
423710721600	6	1074
423710727500	2	1231
423710727700	3	1143.5
423710728200	3	1134.5
423710728500	3	1354.5
423710737500	7	1221.5
423710737500	2	1216
423710737800	4	1150
423710738600	3	1254.5
423710738600	2	1216
423710738600	5	1158.5
423710738900	2	1367
423710738900	2	1256
423710738900	3	1213.5
423710738900	2	1182
423710739100	13	1187.5
423710741200	2	1067
423710741200	2	1213
423710741500	2	1140
423710741500	1	1136.5
423710741500	2	1131
423710742100	3	1121.5
423710742100	6	1102
423710749300	2	1151
423710749300	3	1089.5
423710749300	3	1077.5
423710750900	2	1115
423710752100	2	1167
423710752300	4	1246
423710752300	2	1170
423710752700	2	1107
423710770200	40	1241
423710770200	14	1187
423710770200	5	1172.5
423710770200	4	1152
423710770200	3	1134.5
423710770200	3	1277.5
423710775600	2	1298
423710775600	2	1286
423710775600	18	1259
423710775600	1	1171.5
423710775600	1	1415.5
423710775600	1	1402.5
423710775600	2	1336
423710775800	3	1147.5
423710775800	9	1132.5
423710776100	10	1310
423710776100	3	1188.5
423710776100	6	1182
423710776100	1	1177.5
423710776100	2	1171
423710776100	1	1342.5
423710776700	8	1168
423710776700	2	1122
423710776700	4	1106
423710779600	2	1097
423713014600	2	983
423713014600	2	924
423713014600	13	1024.5
423713014600	5	1127.5
423713014600	2	1115
423713231300	2	1194
423713231300	1	1189.5
423713231300	4	1181
423713231300	7	1172.5
423713231300	2	1154
423713231800	9	1211.5
423713231900	2	1255

Table A.6. (cont.) Location of caves within the Yates Field Unit based on petrophysical analyses of wireline logs. API # is the unique well identifier. Continued on next page.

API #	Cave Height (ft)	Cave Elevation (ft asl)
423713232000	2	1245
423713232000	2	1224
423713232100	3	1238.5
423713232100	2	1187
423713232100	11	1177.5
423713235500	2	1216
423713235700	5	1241.5
423713235700	3	1220.5
423713235700	2	1164
423713235800	3	1218.5
423713235800	3	1150.5
423713235800	3	1047.5
423713236900	3	1195.5
423713236900	2	1189
423713237000	3	911.5
423713237000	15	1272.5
423713237100	5	1244.5
423713237100	2	1237
423713237100	1	1214.5
423713237100	3	1207.5
423713237100	12	1177
423713237100	6	1165
423713237100	2	1155
423713238000	2	1173
423713238200	1	1332.5
423713238200	4	1277
423713238200	3	1268.5
423713238200	2	1228
423713238200	13	1158.5
423713238200	7	1146.5
423713238200	11	1134.5
423713238200	3	1120.5
423713238800	2	1208
423713238900	1	1228.5
423713239000	3	1025.5
423713239000	1	990.5
423713239000	3	1205.5
423713239000	2	1154
423713239000	3	1132.5
423713239100	7	1186.5
423713239100	2	1169
423713239200	4	1226
423713254600	4	1046
423713262800	5	1168.5
423713262800	2	1161
423713262800	2	1155
423713262900	2	1191
423713263600	2	949
423713263700	1	1050.5
423713263800	1	1316.5
423713263900	2	1257
423713263900	4	1215
423713264300	3	1222.5
423713264300	2	1207
423713264400	10	1205
423713264400	3	1116.5
423713264400	1	1058.5
423713264400	1	1007.5
423713264400	1	834.5
423713264500	8	1178
423713264600	4	1151
423713264600	6	1142
423713264700	3	1173.5
423713264700	5	1162.5
423713264700	5	1126.5
423713265600	3	1415.5
423713265600	7	1399.5
423713265600	1	1225.5
423713265600	3	1120.5
423713265600	2	1410
423713265700	2	1251
423713265800	11	1238.5
423713265900	10	1211
423713265900	10	1172
423713265900	2	1153
423713266500	2	1056
423713273700	19	1234.5
423713273700	1	1211.5
423713273700	2	1189
423713273700	3	1184.5

Table A.6. (cont.) Location of caves within the Yates Field Unit based on petrophysical analyses of wireline logs. API # is the unique well identifier. Continued on next page.

API #	Cave Height (ft)	Cave Elevation (ft asl)
423713273700	2	1176
423713273800	2	1148
423713273800	2	1044
423713273800	2	1210
423713273800	2	1248
423713273800	3	1242.5
423713273900	3	1339.5
423713273900	3	1275.5
423713273900	12	1238
423713273900	2	1221
423713273900	2	1214
423713274000	7	1205.5
423713274000	3	1159.5
423713274000	5	1236.5
423713274400	2	1350
423713274400	18	1318
423713274400	2	1306
423713274400	4	1301
423713274400	1	1297.5
423713274400	3	1294.5
423713274400	2	1284
423713274400	1	1280.5
423713274400	1	1277.5
423713274400	1	1270.5
423713274400	8	1253
423713274400	2	1244
423713274400	2	1225
423713274400	2	1180
423713274400	5	1173.5
423713274600	2	1215
423713274800	6	1202
423713276000	2	1201
423713276500	3	1248.5
423713276500	2	1220
423713276600	2	1240
423713276600	7	1188.5
423713276800	26	1244
423713276800	4	1224
423713276800	3	1167.5
423713276800	2	1163
423713276800	1	1378.5
423713276800	1	1373.5
423713276800	3	1335.5
423713276900	9	1040.5
423713276900	1	1272.5
423713276900	3	1156.5
423713279500	1	1150.5
423713279500	3	1132.5
423713279600	4	1206
423713279700	4	1158
423713279700	3	1152.5
423713280700	2	1222
423713280700	2	1125
423713280800	2	1226
423713281400	2	1224
423713281400	1	1200.5
423713281400	1	1184.5
423713281400	3	1179.5
423713281800	1	1169.5
423713282600	2	1158
423713283000	1	1302.5
423713283000	3	1241.5
423713283100	2	1207
423713283100	2	1202
423713283100	2	1197
423713283100	3	1387.5
423713283100	2	1382
423713283100	2	1361
423713283200	2	1216
423713283200	24	1177
423713284600	4	1263
423713284800	2	1172
423713284800	2	1136
423713285000	2	1206
423713285700	2	1256
423713285700	3	1180.5
423713285800	2	1156
423713285800	3	1359.5
423713285800	2	1341
423713285800	1	1275.5

Table A.6. (cont.) Location of caves within the Yates Field Unit based on petrophysical analyses of wireline logs. API # is the unique well identifier. Continued on next page.

API #	Cave Height (ft)	Cave Elevation (ft asl)
423713286400	10	1471
423713286400	3	1362.5
423713286500	4	1222
423713286500	2	1159
423713286500	4	1148
423713286600	3	1193.5
423713286600	4	1189
423713286600	4	1181
423713286600	3	1176.5
423713286600	2	1170
423713286600	2	1154
423713286600	3	1139.5
423713286600	2	1315
423713301000	2	1099
423713301000	2	1088
423713301100	1	1091.5
423713301900	2	1070
423713302300	2	1077
423713302300	2	1056
423713303200	1	1018.5
423713303500	2	1050
423713339700	3	1147.5
423713339700	2	1400
423713341500	3	1248.5
423713341800	3	1223.5
423713341800	3	1209.5
423713341901	14	1190
423713341901	2	1171
423713341901	3	1159.5
423713342000	1	1054.5
423713342200	2	1228
423713342200	10	1214
423713342200	5	1205.5
423713342300	1	1217.5
423713342300	4	1200
423713344900	2	1120
423713344900	2	1104
423713345000	2	1128
423713345400	2	1225
423713345500	16	1282
423713345500	4	1264
423713345600	4	1172
423713348600	6	1230
423713348600	1	1251.5
423713348700	6	1382
423713348700	7	1288.5
423713348700	5	1278.5
423713348700	6	1268
423713348700	5	1254.5
423713348700	2	1230
423713348700	1	1174.5
423713348800	4	1203
423713349500	2	1194
423713349500	3	1168.5
423713349700	2	1074
423713349800	33	1213.5
423713349800	16	1186
423713350000	6	1174
423713350100	4	1165
423713357700	2	1214
423713357700	2	1200
423713357700	3	1195.5
423713357700	3	1186.5
423713357700	3	1158.5
423713358000	1	1110.5
423713358000	13	1181.5
423713358400	6	1150
423713358500	2	1234
423713358500	4	1205
423713358500	8	1194
423713360000	2	1168
423713360000	5	1159.5
423713360000	6	1150
423713360100	4	1238
423713360100	6	1229
423713360100	4	1216
423713360200	4	1217
423713360300	2	1240
423713361200	1	1047.5
423713363600	6	1223

Table A.6. (cont.) Location of caves within the Yates Field Unit based on petrophysical analyses of wireline logs. API # is the unique well identifier. Continued on next page.

API #	Cave Height (ft)	Cave Elevation (ft asl)
423713363800	5	1143.5
423713364800	17	1191.5
423713364900	13	1240.5
423713365000	2	1336
423713365000	16	1260
423713365000	6	1247
423713365000	1	1238.5
423713365000	1	1127.5
423713365100	4	1207
423713365100	2	1190
423713365100	1	1173.5
423713365100	2	1299
423713365200	11	1158.5
423713365300	10	1171
423713365400	2	1197
423713365400	10	1161
423713365400	3	1145.5
423713365600	2	1118
423713365600	1	1275.5
423713365600	1	1244.5
423713365600	1	1235.5
423713365600	3	1221.5
423713365600	12	1207
423713365600	6	1190
423713365600	1	1183.5
423713365600	6	1168
423713365600	1	1158.5
423713365600	1	1155.5
423713365600	1	1151.5
423713365600	1	1147.5
423713365600	1	1136.5
423713368700	2	894
423713371700	1	1059.5
423713372200	4	1044
423713378200	3	1187.5
423713378200	3	1167.5
423713378200	3	1130.5
423713378200	1	1279.5
423713378300	2	1184
423713378300	9	1172.5

API #	Cave Height (ft)	Cave Elevation (ft asl)
423713378500	6	1155
423713378900	2	1371
423713378900	3	1249.5
423713378900	2	1245
423713378900	7	1239.5
423713378900	2	1234
423713378900	2	1214
423713378900	4	1194
423713378900	6	1170
423713378900	1	1143.5
423713379100	4	1164
423713379200	2	1239
423713380400	2	1174
423713380400	14	1164
423713380500	3	1221.5
423713380600	2	1114
423713380700	18	1443
423713380700	1	1375.5
423713380700	3	1370.5
423713380700	2	1167
423713380900	2	1224
423713381000	2	1477
423713381000	1	1309.5
423713381000	1	1294.5
423713381000	2	1227
423713381000	2	1218
423713381000	2	1129
423713381100	1	1334.5
423713381100	3	1327.5
423713381100	1	1320.5
423713381100	14	1306
423713381100	4	1201
423713381100	7	1179.5
423713381100	33	1389.5
423713381100	27	1356.5
423713381200	1	1350.5
423713381200	2	1346
423713381200	1	1338.5
423713381200	2	1328
423713381200	3	1322.5

Table A.6. (cont.) Location of caves within the Yates Field Unit based on petrophysical analyses of wireline logs. API # is the unique well identifier. Continued on next page.

API #	Cave Height (ft)	Cave Elevation (ft asl)
423713381400	6	1180
423713381400	5	1171.5
423713381400	4	1146
423713381400	6	1137
423713381400	3	1129.5
423713381500	4	1224
423713381500	6	1142
423713381600	3	1090.5
423713381600	2	1079
423713381600	1	1073.5
423713381700	9	1255.5
423713381700	10	1232
423713381700	4	1195
423713381700	1	1155.5
423713381700	1	1308.5
423713383300	8	1141
423713384100	4	1240
423713384600	2	1190
423713384600	1	1184.5
423713384700	12	1246
423713384700	2	1201
423713384700	1	1164.5
423713384800	3	1303.5
423713384800	2	1269
423713384800	2	1209
423713384800	10	1200
423713384800	2	1191
423713384800	2	1183
423713384800	5	1177.5
423713384800	2	1157
423713385000	16	1238
423713385000	8	1212
423713385000	2	1201
423713385000	2	1191
423713385000	1	1166.5
423713385100	1	1251.5
423713385100	3	1181.5
423713385100	1	1176.5
423713385200	1	1318.5
423713385200	16	1293

API #	Cave Height (ft)	Cave Elevation (ft asl)
423713385200	3	1277.5
423713385200	2	1272
423713385200	2	1264
423713385200	2	1215
423713385200	4	1209
423713385200	1	1159.5
423713385800	12	1220
423713385800	3	1191.5
423713385800	14	1165
423713386500	2	977
423713386500	1	1136.5
423713386700	3	1222.5
423713386800	2	1154
423713388700	1	1078.5
423713388700	3	1223.5
423713388900	3	1263.5
423713389000	5	1191.5
423713389000	2	1174
423713390000	2	1219
423713390000	1	1213.5
423713390000	2	1186
423713391300	2	1145
423713413000	4	1204
423713413400	2	1152
423713414100	8	1229
423713414100	9	1216.5
423713414200	4	1249
423713414200	6	1241
423713414200	3	1206.5
423713414300	3	1244.5
423713414300	1	1137.5
423713414400	3	1129.5
423713414500	2	1200
423713414500	2	1165
423713414500	2	1155
423713414500	2	1151
423713414600	8	1359
423713414700	2	1158
423713414700	2	1154
423713414900	2	1253

Table A.6. (cont.) Location of caves within the Yates Field Unit based on petrophysical analyses of wireline logs. API # is the unique well identifier. Continued on next page.

API #	Cave Height (ft)	Cave Elevation (ft asl)
423713415800	3	1121.5
423713415900	29	1424.5
423713415900	3	1402.5
423713415900	12	1393
423713415900	2	1353
423713415900	4	1172
423713415900	2	1155
423713415900	2	1472
423713415900	24	1455
423713416000	4	959
423713416000	4	951
423713416000	2	940
423713416000	2	835
423713416200	4	1244
423713416200	2	1235
423713416200	2	1218
423713416200	4	1166
423713416200	4	1137
423713416200	4	1130
423713416400	1	1138.5
423713417200	3	1288.5
423713417200	6	1232
423713417200	2	1226
423713417200	5	1201.5
423713417200	4	1187
423713417600	2	1215
423713417600	2	1183
423713417600	2	1165
423713417700	3	1176.5
423713418000	5	1174.5
423713418100	4	1176
423713418100	10	1141
423713418200	2	1225
423713418200	1	1211.5
423713418200	2	1187
423713418200	1	1210.5
423713418200	12	1155
423713418300	4	1189
423713418300	5	1179.5
423713418300	2	1172
423713418300	2	1158
423713419500	11	1161.5
423713419500	4	1150
423713419600	3	1206.5
423713419600	2	1199
423713419600	3	1189.5
423713420000	2	1275
423713420000	1	1177.5
423713420200	2	1151
423713420200	1	1055.5
423713420200	3	1047.5
423713420600	2	1173
423713420600	1	1389.5
423713420700	2	1026
423713427100	3	1267.5
423713427100	2	1252
423713427100	1	1245.5
423713427100	3	1240.5
423713427100	4	1233
423713427200	5	1287.5
423713427300	3	1302.5
423713428500	2	851
423713432900	2	935
423713433400	2	1051
423713433400	2	1038
423713433800	3	1171.5
423713439000	13	1043.5
423713440500	2	1192
423713441200	2	1235
423713441900	2	1074
423713441900	1	1058.5
423713444700	6	1092
423713445300	1	1176.5
423713445300	4	1154
423713445300	1	1148.5
423713445600	2	1248
423713445900	2	1153
423713446500	2	1047
423713446700	7	1179.5
423713447000	9	1210.5

Table A.6. (cont.) Location of caves within the Yates Field Unit based on petrophysical analyses of wireline logs. API # is the unique well identifier. Continued on next page.

API #	Cave Height (ft)	Cave Elevation (ft asl)
423713447000	2	1194
423713450100	3	1044.5
423713464400	1	1394.5
423713465200	3	1122.5
423713478400	4	1178
423713484200	1	1137.5
423713493200	3	1112.5
423713493200	5	1107.5
423713493200	1	1102.5
423713494200	8	1098
423713495100	1	952.5
423713495100	10	931
423713495200	3	1307.5
423713495200	5	1249.5
423713495300	4	1212
423713495400	9	1185.5
423713497400	3	1091.5
423713500000	1	1060.5
423713500400	2	1176
423713500400	2	1073
423713501000	2	1246
423713501000	1	1154.5
423713503000	2	1257
423713503100	5	1242.5
423713503200	2	1479
423713503200	3	1463.5
423713503200	1	1293.5
423713503400	2	1045
423713518200	4	1072
423713518200	2	889
423713518300	3	1035.5
423713526200	6	1131
423713526200	6	1117
423713526200	5	1084.5
423713526400	1	977.5
423713526400	3	972.5
423713526400	1	953.5
423713530300	2	1186
423713531400	3	1081.5
423713531500	2	1129

API #	Cave Height (ft)	Cave Elevation (ft asl)
423713538200	1	1085.5
423713538500	1	1175.5
423713540100	7	1248.5
423713540100	2	1414
423713540700	1	1242.5
423713540700	2	1229
423713540700	2	1224
423713541000	3	1185.5
423713541000	4	1167
423713541900	2	1337
423713541900	2	1200
423713542500	3	1089.5
423713545900	4	1171
423713546400	8	1171
423713546400	3	1185.5
423713546700	5	1248.5
423713546700	20	1228
423713546700	7	1213.5
423713546700	3	1203.5
423713546700	3	1192.5
423713546700	1	1448.5
423713547000	5	1263.5
423713547000	6	1252
423713547000	4	1243
423713547000	1	1234.5
423713547000	4	1219
423713547000	4	1203
423713547000	3	1196.5
423713547000	2	1190
423713547000	1	1185.5
423713547000	13	1174.5
423713547000	3	1160.5
423713547000	1	1147.5
423713551800	4	1251
423713551800	2	1246
423713551800	2	1238
423713559900	4	1200
423713559900	2	1191
423713560800	1	1385.5
423713560800	2	1333

Table A.6. (cont.) Location of caves within the Yates Field Unit based on petrophysical analyses of wireline logs. API # is the unique well identifier. Continued on next page.

API #	Cave Height (ft)	Cave Elevation (ft asl)
423713563400	2	1282
423713563400	11	1158.5
423713563400	2	1327
423713563500	22	1229
423713563500	1	1359.5
423713563600	1	1343.5
423713568400	3	1391.5
423713568600	1	1281.5
423713568600	4	1277
423713568700	2	1230
423713568700	2	1294
423713569000	27	1398.5
423713569100	7	1377.5
423713569100	11	1363.5
423713569100	7	1348.5
423713569100	3	1332.5
423713569400	2	826
423713569400	1	814.5
423713569400	8	1043
423713569800	1	1333.5
423713569800	7	1120.5
423713570200	4	1174
423713570200	5	1162.5
423713570200	4	1152
423713570200	3	1353.5
423713570700	3	1202.5
423713571500	2	1158
423713571600	2	1279
423713571900	4	1305
423713572100	2	1359
423713572100	6	1231
423713572100	3	1206.5
423713572100	9	1173.5
423713572500	2	1160
423713572600	5	1381.5
423713572800	1	1386.5
423713572800	1	1338.5
423713572800	3	1198.5
423713572800	7	1184.5
423713572800	2	1178

API #	Cave Height (ft)	Cave Elevation (ft asl)
423713572900	1	1106.5
423713573000	1	1185.5
423713573200	6	1224
423713573200	3	1149.5
423713573200	5	1143.5
423713573200	2	1137
423713574600	21	1405.5
423713575300	3	1167.5
423713576200	1	1084.5
423713576200	1	1059.5
423713578900	2	871
423713585300	2	1459
423713585300	1	1387.5
423713585300	2	1306
423713585300	1	1298.5
423713585300	4	1233
423713585300	1	1228.5
423713585300	2	1157
423713591500	13	1139.5
423713591800	1	1072.5
423713594900	2	1214
423713594900	2	1453
423713595100	3	1176.5
423713595200	2	1227
423713596000	6	934
423713596200	1	1202.5
423713596400	3	1232.5
423713596400	4	1223
423713596400	3	1184.5
423713596600	7	1135.5
423713596600	3	1128.5
423713596600	3	1270.5
423713596700	5	1234.5
423713596700	7	1227.5
423713596700	3	1209.5
423713596700	2	1204
423713596700	2	1193
423713601600	3	852.5
423713601600	1	841.5
423713601800	3	1240.5

Table A.6. (cont.) Location of caves within the Yates Field Unit based on petrophysical analyses of wireline logs. API # is the unique well identifier. Continued on next page.

API #	Cave Height (ft)	Cave Elevation (ft asl)
423713602000	2	1179
423713605800	3	1224.5
423713605900	1	1175.5
423713609900	3	1153.5
423713610000	6	1282
423713610000	2	1277
423713610000	5	1253.5
423713610000	3	1177.5
423713610100	4	1056
423713610100	2	1051
423713610300	5	1297.5
423713610300	6	1275
423713610300	6	1258
423718000000	2	1062
423718000000	1	1383.5
423718000100	3	1405.5
423718000100	7	1376.5
423718000100	1	1372.5
423718000100	1	1351.5
423718000100	1	1313.5
423718000100	2	1304
423718000100	3	902.5
423718000100	6	1515
423718000100	3	1502.5
423718000100	1	1498.5
423718000100	1	1489.5
423718114300	1	1188.5
423718115000	6	1236
423718115000	1	1144.5
423718115000	2	1054
423718118100	1	1378.5
423718118100	3	1328.5
423718118100	2	1324
423718118100	4	1307
423718118400	2	1376
423718118400	3	1202.5
423718118400	2	1147
423718118400	2	1126
423718123800	8	1149
423718123800	2	1264

API #	Cave Height (ft)	Cave Elevation (ft asl)
423718123800	3	1258.5
423718123800	2	1250
423718123800	2	1236
423718132800	5	1201.5
423718142200	1	1159.5
423718142200	6	1095
423718148700	4	1215
423718148700	2	1208
423718148700	3	1145.5
423718236000	2	1118
423718236100	1	1107.5
423718236500	58	1136
423718238900	2	922
423718238900	2	1261
423718238900	2	1254
423718238900	4	1201
423718238900	2	1196
423718238900	3	1192.5
423718238900	3	1184.5
423718239100	8	1163
423718239100	9	1152.5
423718239100	1	1322.5
423718243600	3	821.5
423718243600	6	1162
423718246100	1	1142.5
423718246100	2	1103
423718246900	3	1122.5
423718246900	5	1068.5
423718247200	3	1070.5
423718247200	2	1058
423718249600	1	1157.5
423718249600	2	1154
423718249600	2	1128
423718249600	2	1450
423718249600	2	1325
423718249600	8	1288
423718249600	5	1278.5
423718262600	3	1082.5
423718267900	2	1226
423718268100	3	1368.5

Table A.6. (cont.) Location of caves within the Yates Field Unit based on petrophysical analyses of wireline logs. API # is the unique well identifier. Continued on next page.

API #	Cave Height (ft)	Cave Elevation (ft asl)
423718268100	1	1188.5
423718269600	4	1291
423718269600	5	1197.5
423718269600	2	1171
423718269600	1	1126.5
423718269900	1	1126.5
423718269900	2	1013
423718273400	3	1154.5
423718273400	3	1140.5
423718274700	3	1113.5
423718278100	5	1151.5
423718278800	1	1093.5
423718279100	23	1237.5
423718281300	3	1359.5
423718281300	2	1351
423718281300	2	1341
423718281300	3	1312.5
423718281400	2	1245
423718281400	1	1235.5
423718281400	2	1231
423718281400	1	1228.5
423718281400	1	1224.5
423718281400	1	1204.5
423718281400	2	1201
423718281400	1	1198.5
423718281400	3	1189.5
423718281700	8	1235
423718281700	8	1150
423718281700	1	1102.5
423718281700	1	1085.5
423718281700	1	1073.5
423718282000	3	1172.5
423718282000	2	1167
423718282000	8	1242
423718282700	2	1070
423718282700	15	1255.5
423718284200	2	950
423718285400	12	1182
423718285400	3	1169.5
423718286000	1	1138.5
423718286000	1	1099.5
423718286000	2	1093
423718286000	3	1071.5
423718286000	1	1063.5
423718286800	3	1130.5
423718348400	7	1116.5

Table A.6. (cont.) Location of caves within the Yates Field Unit based on petrophysical analyses of wireline logs. API # is the unique well identifier.

ID #	Formation	Lithology	d13C PDB	d34S CDT	d18O PDB
C1	Castile	Gypsum		11.98	-20.52
C2	Castile	Calcitized	-35.41		-6.72
C3	Castile	Selenite		46.69	-6.03
C4	Castile	Sulfur		2.51	
C5	Castile	Gypsum		11.89	-21.22
C6	Castile	Calcitized	-24.20		-5.07
C7	Castile	Selenite		16.54	-17.99
C8	Castile	Sulfur		5.06	
C9	Castile	Gypsum		11.62	-21.42
C10	Castile	Calcitized	-6.64		-4.08
C11	Castile	Selenite		17.53	-17.25
C12	Castile	Sulfur		3.69	
C13	Castile	Gypsum		11.69	-21.96
C14	Castile	Calcitized	-7.90		-4.06
C15	Castile	Selenite		13.65	-18.03
C16	Castile	Gypsum		11.71	-21.39
C17	Castile	Calcitized	2.44		-3.19
C18	Castile	Selenite		14.37	-18.65
C19	Castile	Gypsum		11.48	-21.56
C20	Castile	Calcitized	7.09		3.07
C21	Castile	Selenite		13.79	-16.43
C22	Castile	Gypsum		11.78	-21.77
C23	Castile	Calcitized	-19.46		-7.99
C24	Castile	Selenite		11.59	-20.06
C25	Castile	Gypsum		12.19	-20.28
C26	Castile	Calcitized	-16.86		-2.14
C27	Castile	Selenite		12.45	-20.06
C28	Castile	Gypsum		11.36	-20.73
C29	Castile	Calcitized	6.22		0.97
C30	Castile	Selenite		20.18	-12.03
C31	Castile	Gypsum		11.56	-21.33
C32	Castile	Calcitized	4.43		-0.41
C33	Castile	Selenite		13.96	-16.91
C34	Castile	Gypsum		11.19	-20.09
C35	Castile	Calcitized	3.88		-1.14
C36	Castile	Selenite		15.50	-15.31
C37	Castile	Gypsum		11.32	-19.70
C38	Castile	Calcitized	3.91		-0.99
C39	Castile	Selenite		11.36	-20.16
C40	Castile	Gypsum		11.34	-19.11

Table A.7. Isotopic analyses of samples from Castile and San Andres Formations, including δ13C (PDB), δ34S (CDT) and δ18O (PDB). Continued on next page.

ID #	Formation	Lithology	d13C PDB	d34S CDT	d18O PDB
C41	Castile	Calcitized	-39.05		-4.62
C42	Castile	Selenite		14.24	-16.15
C43	Castile	Gypsum		11.74	-20.50
C44	Castile	Calcitized	1.72		-0.67
C45	Castile	Selenite		16.47	-14.41
C46	Castile	Gypsum		11.43	-19.16
C47	Castile	Calcitized	0.58		-5.39
C48	Castile	Selenite		13.38	-18.37
Y1	San Andres	Dolomite	0.12		4.14
Y2	San Andres	Speleothem	-21.28		6.40
Y3	San Andres	Dolomite	-0.51		4.57
Y4	San Andres	Speleothem	-10.60		-5.19
Y5	San Andres	Dolomite	-0.53		3.97
Y6	San Andres	Speleothem	-16.76		0.07
Y7	San Andres	Speleothem	-14.18		0.99
Y8	San Andres	Dolomite	-5.12		-0.39
Y9	San Andres	Speleothem	-12.95		2.40
Y10	San Andres	Calcite Spar	-1.06		-11.11
Y11	San Andres	Dolomite	4.41		4.34
Y12	San Andres	Calcite Spar	-8.82		-9.79
Y13	San Andres	Dolomite	-5.50		-2.59
Y14	San Andres	Calcite Spar	-14.32		-7.47
Y15	San Andres	Dolomite	2.19		4.84
Y16	San Andres	Calcite Spar	-3.55		-12.25
Y17	San Andres	Dolomite	0.66		-0.64
Y18	San Andres	Calcite Spar	-4.22		-11.06
Y19	San Andres	Dolomite	1.19		3.08
Y20	San Andres	Calcite Spar	-18.78		-7.70

Table A.7. (cont.) Isotopic analyses of samples from Castile and San Andres Formations, including δ13C (PDB), δ34S (CDT) and δ18O (PDB).